Polymer-Based Nanodiscs for Structural and Functional Analyses of Bacterial and Mammalian Membrane Proteins

By

Mansoore Esmaili

A thesis submitted in partial fulfillment of the requirement for the degree of

Doctor of Philosophy

Department of Biochemistry

University of Alberta

Abstract

Unlike cytosolic proteins, membrane proteins (MPs) are embedded within the plasma membrane and the lipid bilayer of intracellular organelles. MPs serve in various cellular processes such as ion and metabolite transports, bioenergetic processes, signal transductions, and cell-cell communications. Making up nearly 25% of the human proteome, MPs account for over 65% of the current drug targets.

The structural integrity and functional dynamics of MPs have been evolved in the lipophilic membrane bilayers. However, the reconstitution and *in vitro* characterization of MPs in their native lipid bilayers remain challenging.

Since the revelation of the first structure of a membrane protein in the 1970s, small molecule detergents have been used for the purification of MPs from their lipid bilayer into lipid-like artificial assemblies of detergent micelles. However, detergents remove the native lipid molecules away and, consequently, compromise the activity and stability of MPs. As such, lipid-dependent conformational studies of MPs and structural analysis of membrane-embedded enzymes with lipid substrates are incredibly demanding. The development of other membrane mimetic systems (such as bicelles, short synthetic polymers or amphipols, and protein-based discoidal nanodiscs) has facilitated the accommodation of synthetic lipids to stabilize MPs. Yet, the preparation of these membrane mimetics still relies on the use of detergents.

Synthetic amphipathic polymers present an invaluable tool for truly detergent-free excision and liberation of superstructures of MPs and their surrounding annular membrane bilayer in donut-shaped nanoparticles or discs. Among all, styrene-*co*-maleic

acid polymers (SMAs) are the most well-studied amphipathic polymers with the highest yield for purification of MPs. Some drawbacks such as sensitivity to acidic pH and high concentration of divalent cations, interference with the spectroscopic analysis of proteins, high polydispersity index (PDI) and nonspecific interaction with protein surfaces have hindered the ultimate optimal utilization of SMA polymers for structural characterization of MPs in membrane bilayer and hence for drug discovery purposes.

In this thesis, I discuss synthesis, chemical modifications, and biophysical characterization of multiple series of novel non-RAFT amphipathic polymers that demonstrate improved behaviors at acidic pH and high concentration of calcium. Some of these unique amphipathic polymers (such as methyl stilbene-*alt*-maleic acid copolymers) show very low polydispersity (PDI ~1) and strict alternation in sequence (a well-defined sequence of co-monomers), and some exhibit distinct spectrophotometric profiles. Furthermore, I address the application of these novel polymeric detergents for the purification and functional analysis of a lipid A palmitoyl transferase, PagP, from the outer membrane of *E. coli*, as well as for detergent-free purification and lipid analysis of the infectious mammalian prion protein (PrP^{Sc}) directly from the brains of infected rodents.

Preface

This thesis is the original work by Mansoore Esmaili (M.E.), who is the primary author of the following manuscripts:

1. A version of Chapter 2 will be submitted for publication soon.

M.E. conceptualized the formulations of polymers, performed the experiments, analyzed data and wrote the first draft. M.E., Dr. Michael Overduin (M.O.) and Dr. Holger Wille (H.W.) edited the manuscript.

2. A version of Chapter 3 has been submitted for publication.

ME conceptualized the formulations of polymers. M.E. performed the experiments, analyzed data and wrote the first draft. M.E. and M.O. edited the manuscript. Polymers were synthesized in 2010 by a graduate student who was supervised by Dr. Richard Turner (Virginia Tech). The Turner lab shared the polymers with M.E. and M.O. in 2018.

3. A version of Chapter 4 has been submitted for publication.

M.E. and M.O. conceptualized the formulations of polymers. M.E. performed the experiments, analyzed data and wrote the first draft of the manuscript. M.E. and M.O. edited the manuscript.

In chapters 2, 3 and 4:

M.E. has prepared the EM grids, and the electron micrographs were taken by Dr. Claudia Acevado under the supervision of H.W.

M.E. has prepared the samples for ^{31}P NMR, ^{1}H NMR and ^{13}C NMR experiments, and Dr. Rustem Shaykhutdinov collected data and analyzed the spectra.

4. A version of Chapter 6 has been submitted for publication.

M.O. and H. W. conceptualized the project. M.E. has performed the experiments. Brian Taconomy (supervised by H.W.) carried out the bioassay experiments. M.E. prepared the EM grids and Dr. Xiongyao Wang (supervised by H.W.) took EM images. Audric Moses performed lipid analysis experiment. H.W., M.E., and M.O. analyzed data. M.E. wrote the first draft. M.E. and M.O. edited the manuscript.

5. Appendix 2 contains original, unpublished data produced in collaboration with Dr. John Klassen's research group (Department of Chemistry), with 50% of M.E.'s contribution. A related manuscript is under preparation.

All experiments in mice and Syrian hamsters were performed in accordance with guidelines set by the Canadian Council on Animal Care and approved by the animal care use committee for Health Sciences at the University of Alberta (protocol AUP00000884).

M.E. has prepared all the figures using Adobe Illustrator, Adobe Photoshop, PyMOL, ChemDraw and Prism. For those stated otherwise in figure captions, the copyright permissions have been acquired from the publishers.

6. M.E. and M.O. (co-inventors) have filed a provisional patent entitled "functional derivatives of maleimide copolymers for nanodisc production" (EFS ID: 37543271, Application #: US 62/925,086) on novel amphipathic polymers disclosed in this thesis (filing date October 23, 2019).

Acknowledgments

I dedicate this work to Mehri, Mojtaba and my grandparents for their unconditional love and support throughout my life.

I would like to express my gratitude to Dr. Michael Overduin for his excellent supervision, profound scientific vision, and endless support that he has been providing for me.

I would also like to express my sincere appreciation to Drs. Holger Wille and John Klassen for their continuous guidance and tremendous support as my supervisory committee members.

I am genuinely thankful to the collaborators, Drs. Bert Klumperman, John Klassen, Holger Wille, Paul Jorasz, Richard Turner, Russell Bishop. I truly appreciate your ideas, feedback, and incredible collaborative environment you provided during our joint projects.

I am incredibly grateful to Drs. Dennis Vance and Hans Vogel for kindly accepting our invitation to be the examiners of my Ph.D. exam, and for generously offering their time reading this thesis.

I am thankful to those who work with me closely and patiently: Brian Taconomy, Chanelle Brown, Christopher Jay, Claudia Acevado, Debajyotti Dutta, Jun Li, Mark Soh, Mohamed Vakili, Rustem Shaykhutdinov, Valentina Back, Valerie Sim, Xinli (Lili) Tang, Xiongyao Wang, Yilin Wang.

I am thankful to my labmates, friends, colleagues, and staff at the Prion center and the Medical Sciences Building (MSB) for their tremendous assistance.

My special thanks to my best friend, Mohamedali, for his friendship, support, and encouragement.

Contents

Chapter 3; Nanodiscs of Native Membrane generated by Methyl-Substituted Stilbene-Maleic Acid Copolymers with Minimal Polydispersity and Dynamics

List of Figures

List of Tables

List of abbreviations

ABC transporter:	ATP-binding cassette transporter
ABCA1:	ATP-binding cassette transporter
ACIII:	Alternative complex III
AFM:	Atomic force microscopy
AO:	Amine oxide
ApoA1:	Apolipoprotein A-I
AP:	Alkaline phosphatase
APP:	Amyloid precursor protein
ATR-FTIR:	Attenuated total reflectance- FTIR
BR:	Bacteriorhodopsin
BRET:	Bioluminescence resonance energy transfer
BSE:	Bovine spongiform encephalopathy
BSA:	Bovine serum albumin
CD:	Circular dichroism
CE:	Cholesterol esters
CERP:	Cholesterol efflux regulatory protein
CG:	Coarse-grained
CID:	Collision-induced dissociation

CJD: Creutzfeldt–Jakob disease

CNS: Central nervous system

CNT: Classical nucleation theory

Cryo-EM: Cryo electron microscopy

CWD: Chronic wasting disease

^{Cyt}PrP: Cytoplasmic PrP

DDM: *N*-dodecyl-*β*-*D*-maltoside

Di16pg: Dipalmitoyl phosphatidylglycerol

DIBMA: Diisobutylene-*alt*-maleic acid

DIBMALP: DIBMA-base nanodiscs

DLS: Dynamic light scattering

DMF: Dimethylformamide

DMPC: 1,2-dimyristoyl-*sn*-glycerol-3-phosphocholine

doMe: di-*ortho*-methyl

DPPC: 1,2-dipalmitoyl-*sn*-glycerol-3-phosphocholine

DSC: Differential scanning calorimetry

DTT: Dithiothreitol

DXMS: Deuterium exchange mass spectrometry

EA:	Ethylamine
E. coli:	*Escherichia coli*
EPR:	Electron paramagnetic resonance spectroscopy
ER:	Endoplasmic reticulum
ERK:	Extracellular-regulated kinases
ELSD:	Evaporative light scattering detector
ESI-MS:	Electrospray ionization mass spectrometry
F.I:	Fluorescence intensity
FC:	Free cholesterol
FRET:	Fluorescence resonance energy transfer
FT:	Flow through
FT-IR:	Fourier transform infrared spectroscopy
FVB:	Friend leukemia virus B
GPCR:	G-protein-coupled receptors
GPI:	Glycosyl-phosphatidylinositol
HD:	Hydrophobic domain
His:	Histidine
His-SMA:	Histamine-SMA

HPLC:	High-performance liquid chromatography
HRP:	Horse radish peroxidase
HY:	Hyper
IMS:	Ion mobility separation
IP:	Immunoprecipitation
LCP:	Lipidic cubic phase
LDAO:	Lauryldimethylamine N-oxide
LPS:	Lipopolysaccharides
LRP:	Laminin receptor precursor
LUV:	Large unilamellar vesicles
LysoPE:	Lysophosphatidylethanolamine
LysoPG:	Lysophosphatidylglycerol
MA:	Methylamine
MAn:	Maleic anhydride
MD:	Molecular dynamics
MLV:	Multilamellar vesicle
MP:	Membrane protein
MS:	Mass spectrometry

MSP:	Membrane scaffold protein
NADPH:	Nicotinamide adenine dinucleotide phosphate
Ni-NTA:	Nickel-nitrilotriacetic acid
NMR:	Nuclear magnetic resonance spectroscopy
NPC:	Niemann Pick Type C disease
NRAGE:	Neurotrophin receptor-interacting MAGE homolog
OD:	Optical density
oaTOF	Orthogonal acceleration time of flight
OM:	Outer membrane
oMe	*Ortho*-methyl
PA	Propylamine
PAA:	polyacrylic acid
PC:	Phosphatidylcholine
PDB:	Protein data bank
PDI:	Polydispersity index
PE:	Phosphatidylethanolamine
PG:	Phosphatidylglycerol
PI:	Phosphatidyl inositol

PIRIBS:	Parallel-in-register-β-sheet
PK:	ProteinaseK
PMA:	Polymethacrylate copolymer
PMCA:	Protein misfolding cyclic amplification
pMe:	*Para*-methyl
PMSF:	Phenylmethylsulfonyl fluoride
POPG:	1-palmitoyl-2-oleoyl-*sn*-glycerol-3-phospho-glycerol
PrP:	Prion protein
PrP^c:	Cellular prion protein
PrP^{Sc}:	Infectious isoform of the prion protein (named after scrapie prions)
PS:	Phosphatidyl serine
PTA:	Phosphotungstic acid
PVDF:	Polyvinylidene difluoride
QS:	Quinin sulfate
QY:	Quantum yield
RAFT:	Reversible addition−fragmentation chain-transfer polymerization
Rec-PrP:	Recombinant prion protein
RML:	Rocky Mountain Laboratory

ROS: Reactive oxygen species

SANS: Small-angle neutron scattering

SAXS: Small-angle X-ray scattering

SCA: Statistical coupling analysis

SEC: Size exclusion chromatography

SLS: Static light scattering

SM: Sphingomyelin

SMA: Styrene-*co*-maleic acid

SMALP: Styrene-maleic acid lipid particle

SMAn: Styrene-maleic anhydride

SPR: Surface plasmon resonance

STMA: Stilbene-*alt*-maleic acid

TBS: Tris buffer saline

TEM: Transmission electron microscopy

TG: Triglycerides

TME: Transmissible mink encephalopathy

TOF: Time of flight

TRAM: Translocating chain associating membrane protein

TRAP: Translocon-associated protein complex

TSE: Transmissible spongiform encephalopathies

UPS: Unfolded protein response

UV-vis: Ultraviolet–visible spectrophotometry

ZSMA: Zwitterionic SMA

βS: β-solenoid

Chapter 1

Introduction to Polymer-Based

Purification of Membrane Proteins

The membrane bilayer is composed of a heterogeneous and dynamic population of different classes of membrane proteins and lipids, and it operates as a critical regulator of cellular function in all kingdoms of life. Thus, deciphering the molecular structure, function, and interaction dynamics of the biological membrane is a vital step toward breakthroughs in drug discovery.

Despite the diversity of membrane proteins and the extensive variation in lipid species, as well as the tightly-coherent interrelation among lipids and proteins, biochemical and biophysical analyses have been mainly focused upon the individual components of the membrane bilayer in isolation. Since the first publication of a membrane protein's atomic structure in the 1970s [1], many high-resolution structures of membrane proteins have been investigated and resolved in different membrane mimetic systems.

All model membrane systems such as micelles, bicelles, polyions, monolayers, bilayers, microemulsions, and vesicles show an amphiphilic property, which under designated conditions helps maintain the proper structure of integral membrane proteins in aqueous solution rather than in lipophilic surfaces. Hence, appropriate conformation and function of the protein are not necessarily guaranteed. Herein, I review the distinguishable differences between these membrane-like systems:

1.1. Micelles

Micelles are aggregates of small amphipathic molecules called detergents. Given the equilibrium between monomers and micelles of detergents in aqueous solution, the structure of micelles relies on the chemistry (hydrophilic head and hydrophobic tail) of

each monomer and the experimental buffer condition. Of note, peptide and lipid-peptide surfactants with more uniform lateral pressure and interior packing (like of native membranes) are classified as high-performance detergents. Despite being the most popular membrane mimics, detergents markedly interrupt intra- and inter-protein interactions, including interactions with ligands and lipid molecules, which may lead to changes in sub-conformational kinetics, aggregation, and inactivation of proteins [2, 3].

1.2. Lipid- detergent mixtures

Lipid/detergent mixtures contain a binary assembly of each component. The presence of lipids improves the thermal stability of membrane proteins and, in some cases, significantly enhances their activity. Increasing the concentration of lipid molecules in such mixtures (particularly under certain conditions such as temperature and buffer composition) results in the formation of isotropic (small) and anisotropic (large) planar bilayers, or bicelles. The former of which may be utilized for high-resolution structural methods such as crystallography and solution nuclear magnetic resonance (NMR), while the latter is useful for solid-state NMR spectroscopy [3]. Although the lipid component makes this system much similar to the native membrane, detergent molecules can diffuse into the lipid phase. This compromises the stability of the lipid phase, which in turn leads to the destabilization of the encapsulated protein. Moreover, practically, preserving the assembly of lipid-detergent in solution is quite challenging, considering the need to concentrate samples, to exchange buffers, or even upon transient changes in temperature [2].

1.3. Amphipols

Short synthetic amphipathic polymers (amphipols) are comprised of hydrophobic (short alkyls C8–C10) and hydrophilic (charged groups, hydroxyl, glucose) moieties along the polymer chain and display a higher affinity for irreversible interaction with transmembrane proteins than with small hydrophobic molecules such as lipids or ligands. Limited self-assembly (as defined by critical aggregation concentration) of amphipols into globular particles with a well-defined diameter may create a hydrophobic inner core suitable for the incorporation of membrane proteins. The hydrophobic core does not resemble the lipid bilayer; unlike detergent, it limits the release of lipids.

Amphipols are not adequately effective in liberating lipid-protein assemblies spontaneously. The preparation of the protein/amphipol complex is a multistep, detergent-dependent procedure in which detergent is exchanged out and desired lipids plus amphipols are added to the naked membrane protein (devoid from natural lipids), which may have undergone some conformation changes by this stage. However, amphipols offer advantageous thermal stability to proteins and, due to their low aggregation concentration, are cost-effective [4].

1.4. Nanodiscs

1.4.1. Helical Membrane Scaffold Proteins (MSPs)

The nanometric discoidal membrane bilayer, or nanodisc, was first replicated from full-length amphipathic apolipoprotein A-I (apoA1), the main constituent (~70%) of high-density lipoprotein (HLD) particles, which involve a soluble, polydisperse population of lipid-protein complexes in the body, responsible for the transport of specific lipids such as

cholesterol ester and other small molecule metabolites [5, 6]. The engineering of apoA1 proteins made possible the production of a library of amphipathic protein "belts" of various sizes, which may be mixed with detergent-solubilized lipid-protein complexes. In the production process, upon the removal of detergents from the mixture, the self-assembly process begins, and protein-lipid natural tendency brings them together into highly-uniform, nano-sized lipid bilayer architecture. Finally, two copies of apoA1 proteins (helical membrane scaffold proteins (MSPs)) encircle the entire complex [7].

The availability of MSPs (some tagged with hexahistidine or FLAG tags) in various sizes and the feasibility of manipulating the lipid-protein ratio enables scientists to design and build nanodiscs within a range of ~10 –17 nm. Medium-sized MSP nanodiscs (formed of MSP1D1 and MSP1E3) can accommodate 140–340 lipid molecules, while large ones (*e.g.*, those composed of MSP2N2 with 16 helices) can accommodate up to ~ 650 lipids (Fig 1.1).
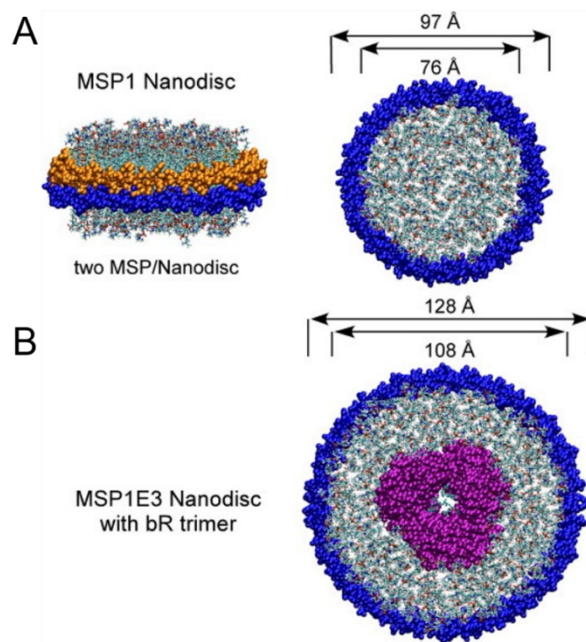
Figure 1.1. MSP Nanodiscs. Genetically engineered MSP1D1 and MSP1E3D1 can form nanodiscs of different sizes. A. Side and top views of MSP Nanodiscs (10 nm) composed of two MSP1D1 (navy blue and orange space-filling models) and phospholipids. B. Nanodisc composed of MSP1E3D1 (12.8 nm, navy blue), phospholipid and bacteriorhodopsin (bR) trimer (purple space-filling model) with 21 transmembrane helices. Arrows indicate the diameter of discs. Figure adapted with permission from ref [8].

The thermal phase transition of the lipid bilayer differs slightly between small and large discs, affecting the respective lipid packing (elasticity/flexibility in lateral movements) and the possibility of expansion in discs of different sizes. However, small-angle X-ray scattering (SAXS) and differential scanning calorimetry (DSC) analyses suggest that the phase transition of lipids in MSP nanodiscs is significantly higher than that reported for multilamellar lipid vesicles (MLV) and unilamellar vesicles (liposomes) [9-15].

An unprecedented range of membrane proteins (with up to 24 transmembrane helices) from various sources have been reconstituted into MSP discs, and their conformational dynamics and interactions have been studied by cryo-electron microscopy (cryo-EM), solution-state nuclear magnetic resonance spectroscopy (ss-NMR), and X-ray crystallography. MSP nanodiscs provide a superior system for *in vitro* reconstitution of membrane proteins to examine the role of lipid microdomain and to observe the conformational changes of membrane proteins. Despite all the advantages of MSPs and their substantial impact on the field of membrane biology. This procedure is detergent-dependent; hence natural lipids may be lost during the initial purification steps [7].

Collectively, the preparation of all membrane mimics described above (Fig 1.2) is undesirably relied on the use of detergents. The uniquely resourceful tool for truly

detergent-free excision of parts of the cellular membrane is, thus far, synthetic styrene-maleic acid copolymers (SMA), with their full characteristics described in the following section.
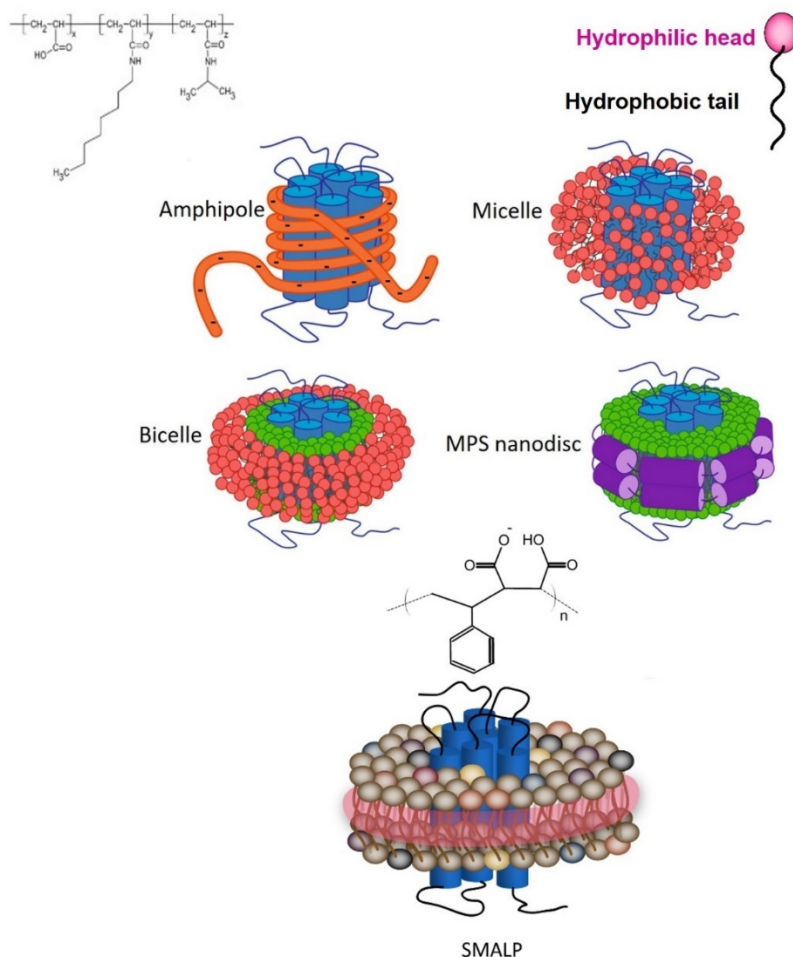
Figure 1.2. Schematics of the most popular membrane mimetics that have been utilized for purification and structural analyses of integral membrane proteins. General schematic structure of small molecule detergents with hydrophobic tail and hydrophilic heads, as well as chemical structures of amphipole and SMA polymer are shown above respective supermolecular structures.

1.4.2. SMA copolymers

Unlike bio-polymers, synthetic polymers are synthesized chemically by polymerization of synthetic co-monomers through either chain-growth or step-growth mechanisms. During chain-growth polymerization, an initiator triggers the formation of radical or ionized forms of each unsaturated monomer that then leads to chain propagation step in which monomers polymerize and repeatedly add to the length of polymers, finally upon addition of terminator, chain growth ends. The step-growth mechanism, however, does not require any initiator or/and terminator since each monomer contains an active reaction site, and the condensation between monomers follows by an elimination reaction in which another molecule, namely water, is released [16].

Synthetic polymers are incomparable to well-sequenced biopolymers (DNA, protein, peptides). In fact, since the invention of synthetic rubber back in the 1930s, different categories of copolymers, including alternating, random, block, grafted, periodic, gradient, and aperiodic copolymers have been developed [17].

Styrene and maleic anhydride (MAn) are the two hydrophobic building blocks of SMAn polymers, and the initial molar ratio of these two co-monomers in polymerization batch determines the final ratio of styrene: maleic anhydride in final polymer chain (Fig. 1.3a). The anhydride form of SMA polymer (also known as XIRAN resin) (SMAn) is heat and chemical resistant plastic with wide application range for the synthesis of automobile parts, plastic appliances, industrial dyes, and pigments. Historically, TOTAL Cray Valley (Exton, PA, USA) and Polyscope (Geleen, Netherlands) were the two primary (yet not

sole) suppliers of SMA copolymers, which respectively use SMA and SZ prefixes in their catalogs. Malvern Cosmeceuticals. Ltd. supplies SMA2000 under the commercial name of Lipodisq®.

Maleic anhydride is the only monomer that can be modified post-polymerization, and this has expanded the application of SMAn polymers to biomedical sciences. Polymeric drug delivery has benefited from non-covalent interaction of hydrophobic small molecule drug candidates (such as zinc protoporphyrin, doxorubicin and pirarubicin) to styrene-maleic acid polymers to encapsulate these drugs into micellar constructions with styrene moieties and drug molecules in interior and maleic acid pendant chains in exterior [18-21]. The segmental reorientation of styrene and polyanionic maleic acids in SMA copolymer is crucial for its adsorption to hydrophobic ligands while the particle remains soluble in buffer. Such formulations could improve the ultimate bioavailability and bioefficacy of drug candidates and decrease their gastrointestinal toxicity. The SMA micellar platform has transformed the field of membrane structural biology [22].

In the absence of hydrophobic ligands, amphipathic SMA copolymer displays hyper coiling behavior so that styrene groups engaged in water-insoluble core and carboxylic acids stay on the surface. This increases the viscosity of solution in salt and pH-dependent manner [19, 23]. Notably, the flexibility of the backbone bonds determines the orientation of styrene groups and favors hydrophobic interactions. The dynamic secondary structures in SMA polymer result in formation of two hydrophobic and hydrophilic active surfaces (which highly resemble amphipathic helices of Apo-I proteins) that can associate with lipid films and form nanometer-sized doughnut-shape particles

9

dubbed Lipodisq [24]. Small-beta barrel protein, PagP, and bacteriorhodopsin (bR) were the first proteins reconstituted and characterized in nanodiscs of DMPC lipids and SMA polymers (also termed SMALP particles) with a diameter of 10-20 nm [25]. This discovery broke fresh ground in membrane biology. However, until recently, the specific biophysical behavior of SMA polymers in the interface of membranes was not fully understood. *In silico* approaches have already been utilized to simulate the behavior of dendrimers [26], polymer- mediated fusion, micelle-lipid interfaces [27] and lipoprotein complexes [28]; therefore molecular dynamic (MD) simulations have proved to be useful to shed light on molecular-scale interaction of SMA and solubilization of biomembrane [29, 30]. Atomistic models are currently not optimal for large system sizes and simulation timescales. Conversely, coarse-grained (CG) field molecular dynamics modelings are used to simulate the behavior of complex biological systems (through their coarse-grained representation) [26]. As a result, the self-aggregation of polyanionic SMA copolymers in solution was confirmed using the coarse-grained (CG) approach. Due to considerable affinity of polymer molecules to the membrane (DDPC lipid molecules), that is driven by primary interaction of styrene groups with hydrophobic acyl chains, SMA polymers spontaneously (within 20 msec of simulation) and cooperatively insert into adjacent lipid bilayer, bend the membrane at the site of adsorption, then slowly penetrate to the lipid bilayer and localize in the acyl chains of lipids apart from phosphate headgroups, hence leaving styrene groups in a perpendicular orientation to lipid acyl chains. While surrounding the lipid bilayer, interestingly, SMA polymer is more stretched (showing higher gyration radius) than free polymers in solution [27].

On the other hand, the encapsulation event perturbs the membrane curvature (by forming a bulge) and planarity, allowing water molecules to permeate inside. Intriguingly, the distribution of Na^+ ions undergo remarkable changes after encapsulation, as well, and that compensates the repulsion between anionic carboxyl moieties in the lipid-water interface.

Furthermore, MD models suggest that relative abundance and the sequence of maleic acid and styrene moieties in the polymer chains may slightly change the behavior of polymers in interaction with model DMPC lipid membrane. For instance, polymers with 2:1 ratio of styrene (S) to maleic acid (MA) completely disaggregate once they integrate with bilayer, whereas SMA polymer with 3:1 ratio of S: MA (comprising a highly ordered sequence of SSS-MA) show a higher number of adsorption sites with membrane and maintain their tangled configuration upon insertion into the lipid bilayer. Polymers' net charge (one charge per MA), length (≥1.4 kDa), and sequential polydispersity (SSS≥3) are among the crucial factors that influence the formation and stability of nanodiscs [30] (Fig. 1.3c).

A relatively universal protocol has been established for SMA-based purification of membrane proteins that are mainly overexpressed in various host organisms and often contain different purification tags (Fig. 1.3b) [31]. This procedure involves the isolation of membranes and their incubation with SMA polymers in neutral and preferably alkaline buffers. Based upon the biophysical and biochemical properties of individual proteins, experimental conditions such as temperature, pH, ionic strength, concentration (and type) of SMA polymer and the purification tag should be finely optimized. These factors,

collectively, influence polymer-polymer, polymer-lipid, protein-polymer interactions, which may compromise the yield, purity, activity of final purified target protein, and thus the downstream analyses. Notably, as demonstrated by multiple research groups, the lipid composition of nanodiscs is inevitably susceptible to change through inter-particle collision. Variations in ionic strength, the mass ratio of lipid to polymer and the type of amphipathic polymers, together, control the collision rate and may limit the kinetics of lipid exchange.

Experimental data shows that SMA2:1 (SMA2000) and 3:1 (SMA3000, SZ25010) with an average molecular mass of 7.5-10 kDa can be equally effective in direct purification of membrane proteins from bacterial membrane and spinach chloroplast thylakoids [32, 33]. On the contrary, SMA 1:1 (SMA1000), SMA2021, SMA10235, SMA17352, and SZ09008, SZ09006, SZ40005, SZ42010, SZ33030, SZ28065, SZ28110 and SZ2625 were not as useful. Unexpectedly, SMA1440 (1.4:1) displays a remarkable potential for the solubilization of the thylakoid membrane. This could potentially challenge the notions that MD simulation models present and call for more pragmatic approaches to opt for the most proper choice of SMA for each target membrane protein.

Despite all the advantages that SMALP technology has offered, there are paramount drawbacks that hinder the application of this technique for the full spectrum of membrane proteins.
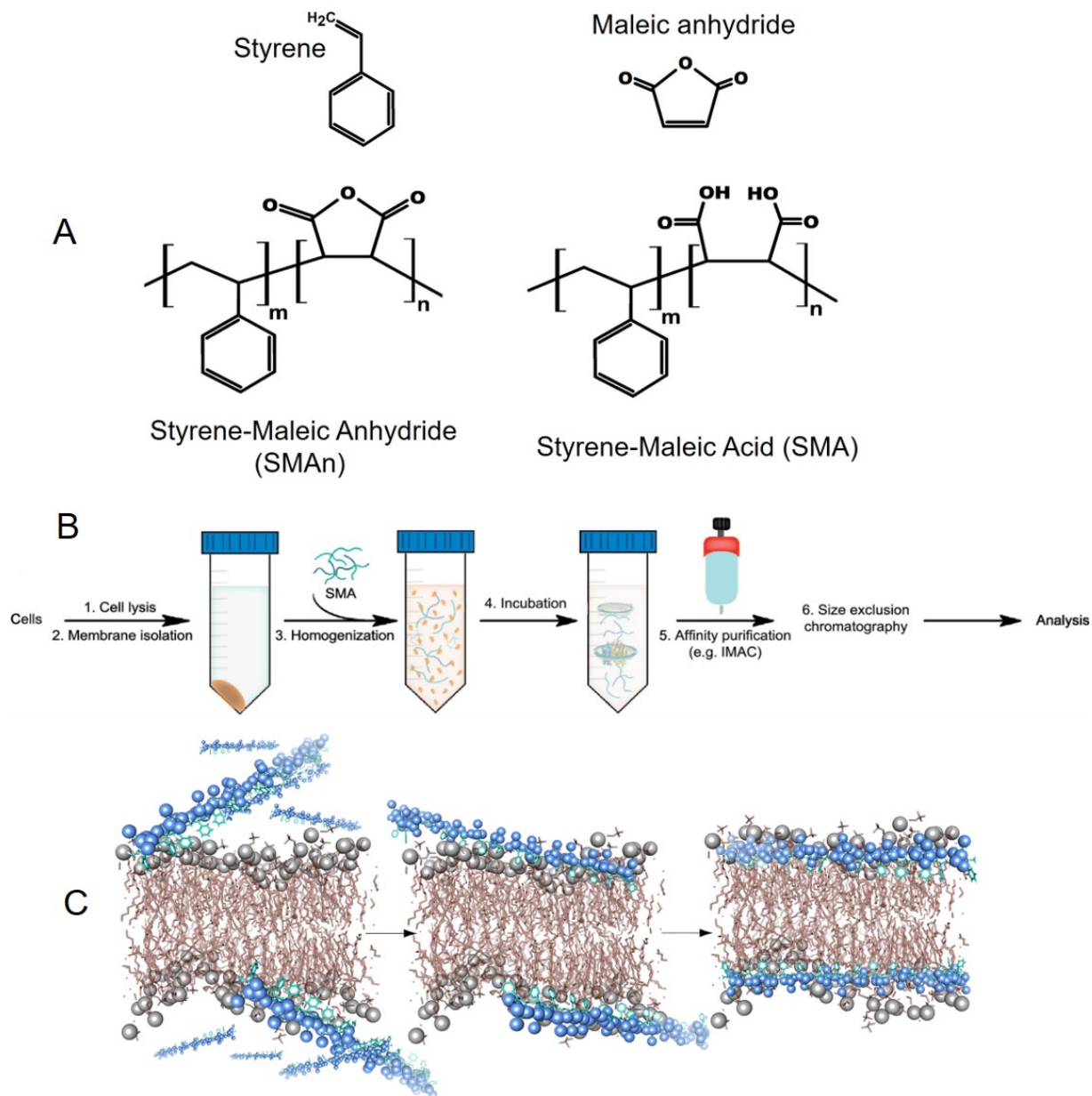
Figure 1.3. A. Chemical structures of styrene, maleic anhydride, styrene-maleic anhydride and styrene-maleic acid copolymers. m and n indicate, respectively, number of repeating units of styrene and maleic anhydride (or acid) in a polymer chain. B. Schematic diagram of the SMALP protocol. Cells are broken open and membrane fractions are suspended in buffer before the addition of SMA. After incubation, the membrane solution with SMA at first appears cloudy and then clarifies. The protein-

containing SMALPs can be purified by immobilized metal affinity and size exclusion chromatography and be analyzed by a variety of biochemical and structural assays. C. Schematic model showing interactions between SMA polymers (blue) and a membrane bilayer (grey phosphate headgroups and red acyl chains).

Ionic strength and pH (external factors) and abundance of carboxyl groups of MA monomers (pk_{a1} ~ 4 and pK_{a2} ~ 9) regulate the overall charge of SMA polymers. These factors are detrimental to the formation of secondary structures along the polymer chain and so to polymer solubility in solution and solubilization of lipid membrane by SMA [34]. In line with this, polyvalent cations (such as magnesium and calcium) and acidic pH compromise the solubility of SMA and limit the utilization of SMA polymers for purification of metal-dependent membrane proteins (*e.g.,* ABC (ATP-binding cassette) transporter and ATPases) and those which required acidic pH (≤ 6) for their optimal function (*e.g.,* KcsA potassium channel and lysosomal membrane proteins) [35]. On the other hand, since hydrophobic interactions and self-assembling processes are the driving force for the formation of SMALP nanoparticles, it is not surprising that polymers can nonspecifically adsorb to hydrophobic patches of proteins (instead of acyl chains of lipids). Likewise, electrostatic interactions with positively charged surfaces of proteins and polyanionic SMA polymers could negatively impact the folding and function of target proteins. Reportedly, improving batch polydispersity and sequential randomness of SMA polymer could enhance the yield of purification and facilitate the downstream application of isolated nanodiscs via high-resolution techniques such as cryo-EM. Not to mention that aromatic phenyl groups of styrene interfere with far-ultraviolet (UV) spectroscopic analysis of membrane proteins [36]. As such, SMA-based nanodisc technology has undergone many developments to optimize the chemical formulation of SMA. New

formulations of SMA interact with membrane bilayers through the same mechanism as SMA2000 (standard SMA).

Most of the chemical variations in styrene-maleic anhydride polymers came possible through maleic anhydride residues that offer an excellent nucleophilic center. A list of chemicals can be utilized to convert MAn moieties to their maleamic acid form. This approach will reduce the number of carboxylic acids, hence may shift the pK_a of polymer macromolecules. Chemicals like Ethanolamine [37], quaternary amines [38], tertiary amines [39], diamines (*e.g.,* diamino ethyl) [40] (Fig. 1.4) have been used for this purpose. Dehydration reaction, on the other hand, adds even more opportunities to increase the variation of active SMA polymers. It is worth mentioning that none of these reactions should neither compromise the solubility of resulting SMA polymers nor slow down their ability to solubilize lipid bilayer. The final products of each synthesis reaction should be verified by analytical methods such as ^{13}C NMR, FT-IR, mass spectrometry (MS), and the ability to form nanodiscs of lipid-proteins as well as size distribution of these particles should be examined by transmission electron microscopy, light scattering (dynamic light scattering (DLS), static light scattering (SLS)). Generally, the new variants of SMA tend to form larger particles and, due to low abundance of carboxylic groups, have a wider range of pH tolerance and lower sensitivity to divalent cations (*e.g.,* calcium). However, regardless of the type of polymerization reaction utilized for the synthesis of parent polymer and the nature of sidechains, the backbone to which such modifications are applied makes a dramatic difference in the results. For instance, the use of low molecular weight parent SMAn polymers (1.6 kDa random copolymer and 1.3 kDa RAFT (reversible addition-fragmentation chain transfer) polymer)) invariably leads to the most optimal

products. Small polymers possibly show detergent-like behavior than long polymers [35, 38].

Further, some chemical modifications could expand the application of nanodiscs for drug discovery; one intriguing example is SMA-SH, which is originated from the reactivity of cysteamine with maleic anhydride groups of SMA2000 (Fig. 1.5) and contains free thiol groups that can consequently receive thiol-reactive fluorescent probes such as A487 and Atto647N [41]. Some of the sidechain modifications are indeed inspirations of natural phospholipid headgroups, zSMA contains zwitterionic phosphatidylcholine (PC) groups grafted to low molecular weight RAFT-polymerized SMAn [35]. The undesired nonspecific interaction between styrenes and protein targets as well as its interference with spectrophotometric techniques (CD, UV-Vis, fluorescence) could be alleviated mainly by some chemical modifications, yet this process is so challenging that in many cases, one chooses to build a new polymer by starting a new polymerization reaction using modified styrene residues (see chapter 7).

In some cases, even non-styrene (aliphatic) amphipathic polymers have shown to be remarkably effective alternatives for aromatic SMA. Poly diIsoButylene-*alt*-maleic Acid (DIBMA, negative net charge) [42] and polymethacrylate (PMA, positive net charge) [43] random copolymer are, respectively, formed by polymerization of diIsobutylene and maleic anhydride co-monomers, and butyl methacrylate and cationic methacroylcholine chloride co-monomers (Fig. 1.4). DIBMA and PMA polymers can solubilize lipid membranes and are resistant to changes in pH. These two polymers are reasonably tolerant to higher concentrations of Ca^{+2} cations and show an insignificant

effect on lipid packing order. As demonstrated by the Keller group, DIBMA-base nanodiscs (DIBMALPs) show the least collisional lipid transfer [44]. The major pitfall with non-aromatic amphiphilic polymers involves the significantly low yield of purification of membrane proteins directly extracted from native membranes.

In summary, a brief look at the current publications on polymer-based nanodiscs made from native membrane suggests the superior applicability of SMA (particularly SMA2:1 and SMA3:1) in addressing fundamental biological questions.
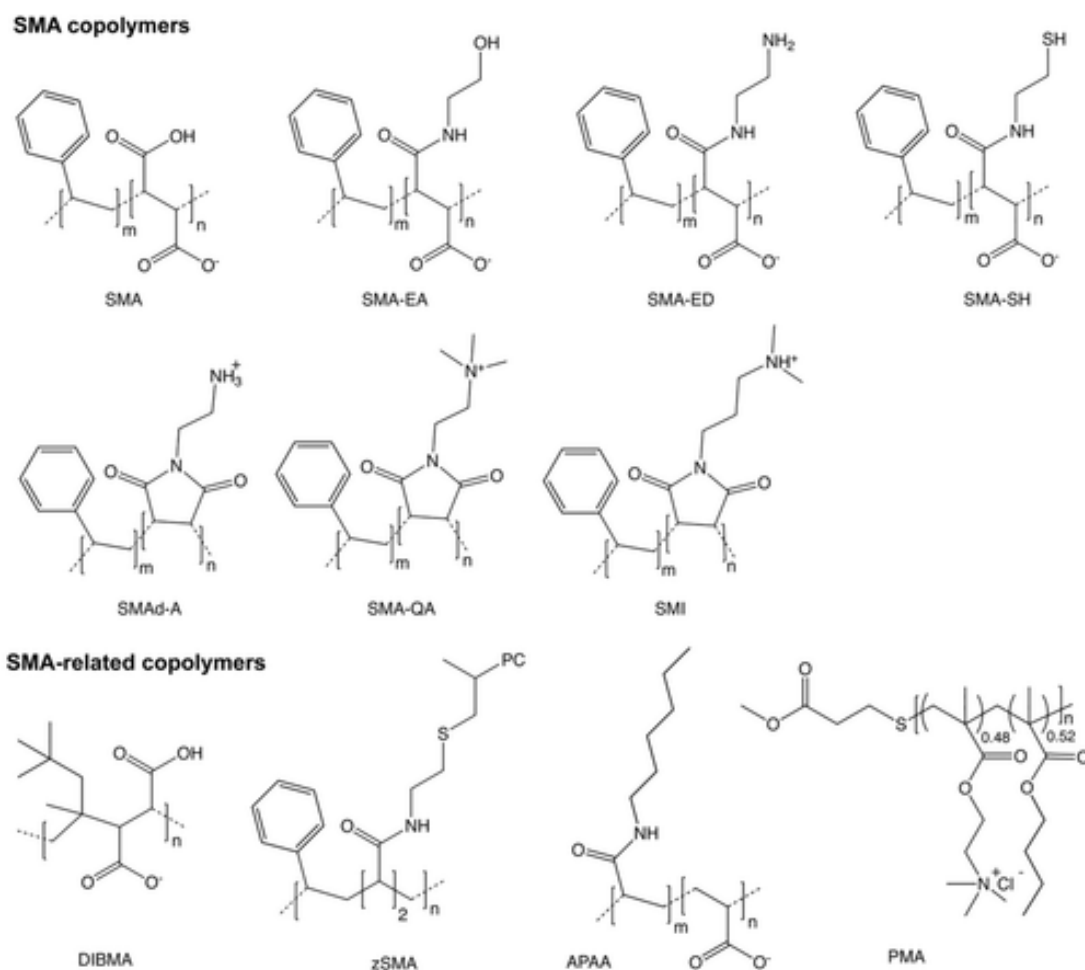
Figure 1.4. The chemical structures of aliphatic and aromatic amphipathic copolymers used to produce native nanodiscs. Figure adapted with permission from ref [36].

The SMALP-based purification preserves native lipid molecules that surround membrane proteins, offering tremendous opportunity to not only study the lipid composition around a target membrane protein yet also addressing the pivotal roles of lipids in conformational and functional cycles via biophysical tools such as high-resolution X-ray crystallography (especially lipid cubic phase, LCP), cryo-electron microscopy (EM), and low-resolution SAXS and SANS, Electron paramagnetic resonance spectroscopy (EPR), and FRET. Previous reports convey considerable underlying efforts to obtain atomic-resolution structures of membrane proteins in nanodiscs for the rational design of novel therapeutics, for instance, G-protein-coupled receptors (GPCR) family [45], which account for over 30% of the human proteome (some involve in lipid transport) and represent the most challenging drug discovery targets [46]. Some promising examples of such efforts are as follows:

Using lipid cubic phase crystallography (LCP or *in meso*), the Ernest lab resolved the crystal structure of SMA- solubilized bacteriorhodopsin at 3.2 Å resolution in synthetic monoolein lipids [47, 48]. Neutral synthetic lipids such a monoacylglycerol (mesophase) substitute the complex natural lipids during reconstitution steps. Although *in meso* crystallography is not specifically designed for membrane proteins, it provides snapshots of crystal structures of target membrane protein in a hydrophobic (oily) matrix that assembles into lamellar and reverse hexagonal phases. (Fig.1.5a). The most popular lipid used for this approach is monoolein and its temperature- composition phase behavior has been well-characterized in the literature. The presence of lipid bilayer may prevent impurities from interfering with crystal growth and crystallization

process; therefore, LCP crystallography does not require very pure protein samples [49, 50].

Electron microscopy of membrane protein-lipid complexes in SMALP nanodiscs displays the most exciting tool for observing the natural lipid bilayer around and buried inside the protein core. Further, the electron density of regulatory and structural lipids can be detected and modeled into the high-resolution EM map of the structure.

Alternative complex III (ACIII) involves a multi-subunit complex of membrane proteins and plays critical roles in the respiratory and photosynthetic chains of many bacteria. Despite functional analogy with their counterpart cytochrome *bc1* complex, the ACIII and bc1 complexes do not share any structural similarity. The crystal structure of bc1 complex (from bovine heart mitochondria) was first resolved in the 1990s at 2.3 Å resolution in detergent micelles and depleted from their natural lipid molecules [51]. The Gennis lab in 2018 purified and resolved the structure of a functionally active ACIII complex bound to cytochrome c from Flavobacterium Johnsonian [52]. The complex contains all 10 subunits (ActA, ActB, ActC, ActD, ActE and ActF) and associated cofactors (*i.e.,* [3Fe–4S] cluster, a [4Fe–4S] cluster and six haem c units) in SMALP nanodisc made from SZ25010 and SZ30010 polymers. The EM map shows an unprecedentedly interesting arrangement of subunits. For instance, two subunits bind to lipid bilayer through post-translational modification (N-terminal triacylation of cysteine residues). Also, it displays a thin density of lipid and SMA polymer around a complex. This density was further used to model phosphatidylethanolamine (PE) lipid molecules to the structure. The catalytic cycle of the complex has been attributed to a

core assembly of ActC and ActB that is involved in oxidation of quinol, a haem c assembly consisting of ActA and ActE that directs electrons from ActB to the terminal electron acceptor. The role of transmembrane ActD and ActF subunits remains to be unveiled (Fig. 1.6b).

Another example of a high-resolution image of a multimeric membrane protein embedded within lipid molecules comes from SMA2000-solubilized multidrug efflux protein, AcrB, which contains a hydrophobic core that binds to dyes, and lipophilic antibiotics and even commercial detergents. AcrB protects Gram-negative bacteria against these hazards and therefore causes antimicrobial resistance [53]. AcrB has been an attractive target for biochemists since 2002 when its first asymmetric trimer structure was resolved in n-Dodecyl-B-D-Maltoside (DDM) micelles [54-59]. SMA-solubilized AcrB particles have a diameter of 12 nm, of which 9 nm accounts for the width of trimeric protein itself. The cryo-EM density map shows that the central cavity of the trimer is occupied with 21 low-density lipid molecules (packed in a two layer-triangle) as well as seven annular less-ordered "belt" lipids representing the upper and lower leaflets of the bilayer.

Interestingly, due to 3.2 Å resolution of the structure, the thickness of lipid phase (the Z coordinates of phosphate headgroups) and the contact points (through hydrogen bonds) between lipid headgroups and amino acids of each subunit (for instance sidechain of arginine and backbone nitrogen of glycine) were quite distinguishable, and that revealed the strikingly asymmetric nature of these interactions, which, in turn, can be attributed to the regulatory role of lipids in functional cycles of AcrB. Notably, the

architecture and orientation of lipids toward periplasmic (outer leaflet) and cytosolic face appear differently, *i.e.,* outer leaflet lipids shape a loosely packed with curved-shape alkyl chain while those in the inner surface are straight and relatively densely-packed. This observation could imply the regulatory role of lipids in conformational changes associated with trimer in order to keep the central hydrophobic pore in open or closed states. Such high-resolution images of the intimate interaction between a membrane protein and lipid bilayer were also reported in 2005 for two-dimensional (2D) crystals of aquaporin in DMPC synthetic lipids [60, 61]. The SMALP platform enables us to obtain equally informative snapshots from the surroundings of membrane proteins; however, it requires more improvement to a need for engineering the amphipathic polymers for formation of larger nanodiscs.
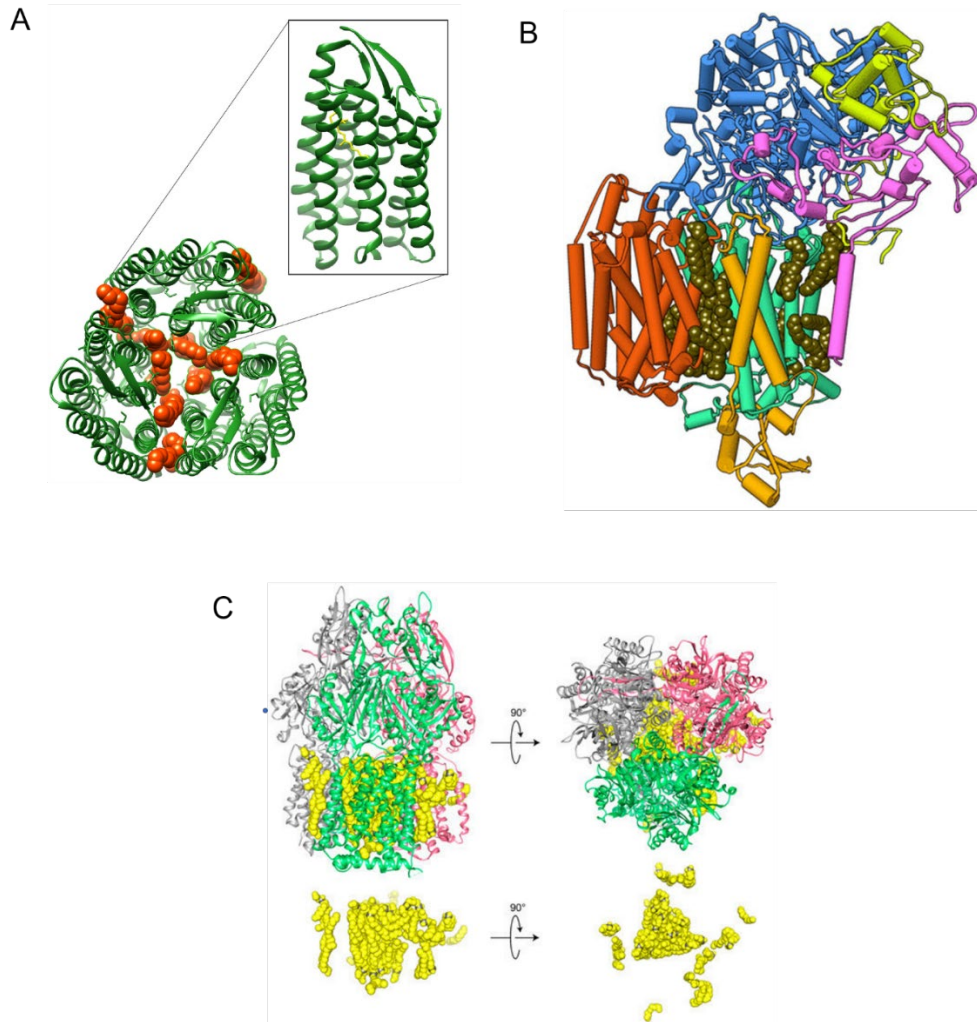
Figure 1.5. A. The *in meso* crystal structure of a rhodopsin trimer bound to monooleins after solubilization with SMA. The three subunits of the trimer (green) are shown with nine monoolein lipids (red) within the interfaces and three retinal molecules (yellow) (PDB 5ITC). B. The cryo-EM structure of the ACIII photosystem complex after solubilization with SMA(2:1) polymer. The color-coded ActA (purple), ActB (blue), ActC (magenta), ActD (orange), ActE (yellow), and ActF (red) subunits and phospholipids (space-filling in brown) are shown (EMD-7286, EMD-7448). C.The cryo-EM structure of trimeric wild-type AcrB. The protein solubilized intact with SMA(2:1) retains its membrane microenvironment, as seen from the top and side perspectives, with subunits colored green, gray, and pink, and 24 hexagonally arrayed phospholipids in the central bilayer colored yellow shown in two perspectives (EMD-7074, PDB 6BAJ).

Other analytical approaches such as EPR [62], Fluorescence-based methods (FRET/BRET) [63], surface plasmon resonance (SPR) [64], SAXS, NMR have been utilized to shed light on lipid dependent protein-protein interaction in the lipid bilayer, receptor oligomerizations/regulation and lipid-dependent oligomerization of essential peripheral membrane proteins (such as α-synuclein and amyloid precursor protein (APP) peptides) [43, 47], in polymer-based nanodiscs. The size and lipid composition of nanodiscs are well-controlled during the preparation of LUV vesicles. Moreover, both protein or lipid molecules can be labeled either before or after encapsulation into nanodiscs using antibodies or proper synthetic labels. Since nonspecific interaction between SMA polymers and proteins remains a primary concern, the full activity of post-assembled nanodiscs must be confirmed.

In principle, polymer-based nanodiscs have a broad range of applicability for virtually any biomedically-relevant membrane protein targets in human physiology and pathology.

In this thesis, I utilized a series of detergent-free methodologies to shed light on the structure and functional mechanism of two membrane proteins, (i) the infectious mammalian prion protein (PrP^{Sc}) and (ii) an *E. coli* outer membrane enzyme, PagP.

The infectious mammalian prion (PrP^{Sc}) is a GPI-anchored peripheral membrane protein responsible for transmissible spongiform encephalopathies (TSEs) or prion diseases. In Chapter 5, I review the history of prion diseases and the current literature on physiological cofactors (such as lipids and nucleic acids) involved in the structural and conformational transition of the cellular PrP to the infectious isoform

(PrP^{Sc}). In Chapter 6, I exclusively discuss how the substitution of small-molecule detergents (such as sarkosyl) with polymer-based nanodiscs would 1. reduce the excessive fibrillization of PrP^{Sc}, 2. facilitate the isolation of *in vivo,* highly infectious, oligomeric PrP^{Sc}, and 3. allow the lipidomic studies of prion diseases.

PagP is a palmitoyl transferase in the outer membrane of *E. coli* that folds into a small β-barrel structure with eight antiparallel β strands (Fig. 1.6) [65]. In chapters 2, 3 and 4, the solubilization of PagP from the outer membrane (OM) of *E. coli* was used to examine how efficiently the novel polymers could solubilize complex native biological membranes and form native discs.

The enzymatic function of PagP remains enigmatic. Using a hydrocarbon ruler inside the central hydrophobic cavity, PagP distinguished only C16 acyl chains (C16:0) and catalyzes the transfer of palmitoyl chain from *sn*-1 position of a phospholipid (from the inner leaflet of the OM) to lipid A of lipopolysaccharide (LPS) on the outer leaflet of the OM [66]. Many virulent Gram-negative bacteria such as *Legionella pneumophila*, *Bordetella bronchiseptica,* and *Yersinia pseudotuberculosis* use this LPS remodeling mechanism to develop resistance to cationic antibacterial peptides and antibiotics [67]. Generally, a variety of outer membrane enzymes (some with unknow structures) take part in LPS remodeling (Fig. 1.7) of Gram-negative bacteria [68].

Generally, the purification of the outer membrane proteins from their native lipid environment is laborious with insufficiently low yield (1 mg/ 1 liter of *E. coli* culture) [69]. Therefore, it is much preferred to overexpress PagP in cytosolic inclusion bodies and to refold it either in detergent micelles or in synthetic liposomes. Interestingly, the high-

resolution X-ray structures of refolded PagP in LDAO and many NMR structures of detergent-refolded PagP confirmed that some detergents such as DPC and LDAO [65] occupy the central hydrophobic cavity, and inhibit PagP activity, whereas those (dodecyl-β-D-maltoside (DDM) and CYFOS-7) that cannot fit in the barrel core show no inhibitory effect [70].

A series of unpublished biochemical data suggest that PagP contains two putative catalytic triads (amino acids that form the active sites and are involved in catalytic activity); His33, Asp76, Ser77 at outside of the outer leaflet of OM and Tyr87, Asp61, His67 triad in proximity to the inner leaflet. In a collaborative project (see Appendix 2), we utilized a combination of detergent-free purification and soft electrospray ionization mass spectrometry (native ESI-MS) [71] to identify native lipid molecules in nanometer proximity of folded wild type (active) and mutants (inactive) of PagP.
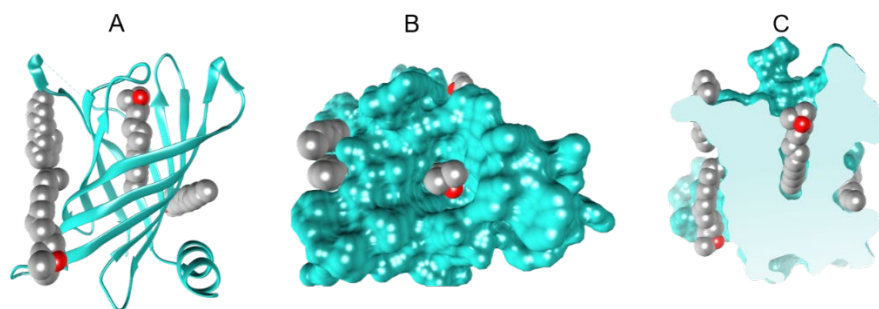
Figure 1.6. A. Ribbon structure of PagP (PDB 1THQ) and four detergent (LDAO, gray spheres) molecules used in the crystallization protocol. (B, C) The top and clipped side views of the space-filling model of PagP display a single LDAO bound to the hydrophobic interior cavity with the phosphate headgroup exposed outside.
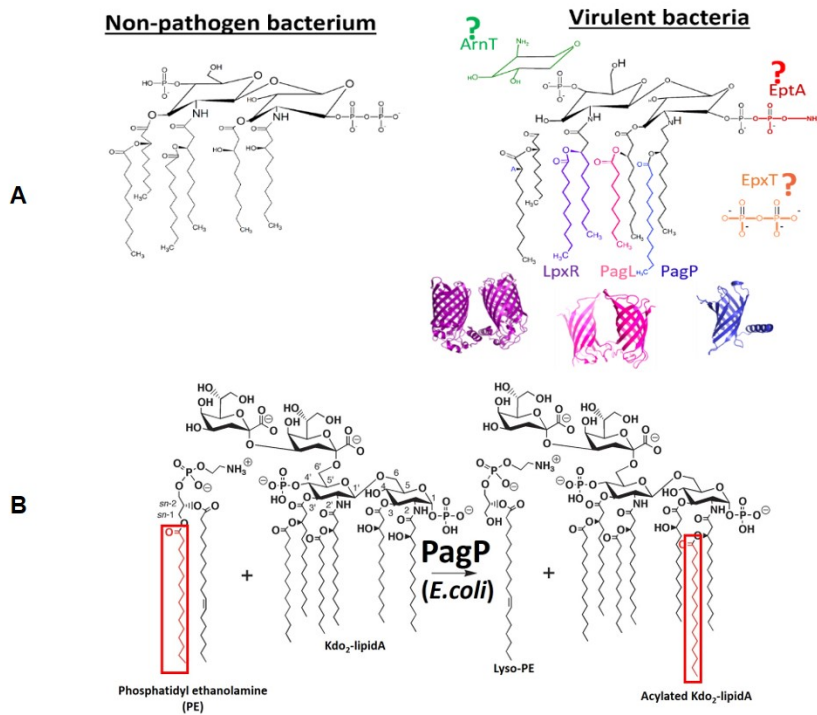
Figure 1.7. A. LPS in non-pathogenic bacteria consists of phosphorylated glucosamine disaccharide with multiple fatty acids. Whereas in different pathogenic Gram-negative bacteria, various outer membrane β-barrel enzymes modify LPS. The catalytic mechanism of some of these enzymes are still unknown. B. Palmitoyltransferase activity of PagP in *E. coli (*figure adapted with permission from ref [72])*.*

1.5. References

[1] R. Henderson, P.N. Unwin, Three-dimensional model of purple membrane obtained by electron microscopy, Nature, 257 (1975) 28-32.

[2] L. Frey, N.A. Lakomek, R. Riek, S. Bibow, Micelles, Bicelles, and Nanodiscs: Comparing the Impact of Membrane Mimetics on Membrane Protein Backbone Dynamics, Angew Chem Int Edit, 56 (2017) 380-383.

[3] P.J. Loll, Membrane proteins, detergents and crystals: what is the state of the art?, Acta Crystallogr F Struct Biol Commun, 70 (2014) 1576-1583.

[4] J.L. Popot, T. Althoff, D. Bagnard, J.L. Baneres, P. Bazzacco, E. Billon-Denis, L.J. Catoire, P. Champeil, D. Charvolin, M.J. Cocco, G. Cremel, T. Dahmane, L.M. de la Maza, C. Ebel, F. Gabel, F. Giusti, Y. Gohon, E. Goormaghtigh, E. Guittet, J.H. Kleinschmidt, W. Kuhlbrandt, C. Le Bon, K.L. Martinez, M. Picard, B. Pucci, J.N. Sachs, C. Tribet, C. van Heijenoort, F. Wien, F. Zito, M. Zoonens, Amphipols from A to Z, Annu Rev Biophys, 40 (2011) 379-408.

[5] M.A. McLean, M.C. Gregory, S.G. Sligar, Nanodiscs: A Controlled Bilayer Surface for the Study of Membrane Proteins, Annu Rev Biophys, 47(2018)107-124.

[6] D.J. Rader, Molecular regulation of HDL metabolism and function: implications for novel therapies, J Clin Invest, 116 (2006) 3090-3100.

[7] M.A. Schuler, I.G. Denisov, S.G. Sligar, Nanodiscs as a new tool to examine lipid-protein interactions, Methods Mol Biol, 974 (2013) 415-433.

[8] T.H. Bayburt, S.G. Sligar, Membrane protein assembly into Nanodiscs, FEBS Lett, 584 (2010) 1721-1727.

[9] M. Alami, K. Dalal, B. Lelj-Garolla, S.G. Sligar, F. Duong, Nanodiscs unravel the interaction between the SecYEG channel and its cytosolic partner SecA, EMBO J, 26 (2007) 1995-2004.

[10] T.H. Bayburt, Y.V. Grinkova, S.G. Sligar, Assembly of single bacteriorhodopsin trimers in bilayer nanodiscs, Arch Biochem Biophys, 450 (2006) 215-222.

[11] T. Boldog, S. Grimme, M.S. Li, S.G. Sligar, G.L. Hazelbauer, Nanodiscs separate chemoreceptor oligomeric states and reveal their signaling properties, Proc Natl Acad Sci USA, 103 (2006) 11509-11514.

[12] C.E. Carney, I.L. Lenov, C.J. Baker, K.W. MacRenaris, A.L. Eckermann, S.G. Sligar, T.J. Meade, Nanodiscs as a Modular Platform for Multimodal MR-Optical Imaging, Bioconjugate Chem, 26 (2015) 899-905.

[13] A. Das, J. Zhao, G.C. Schatz, S.G. Sligar, R.P. Van Duyne, Screening of Type I and II Drug Binding to Human Cytochrome P450-3A4 in Nanodiscs by Localized Surface Plasmon Resonance Spectroscopy, Anal Chem, 81 (2009) 3754-3759.

[14] I.G. Denisov, Y.V. Grinkova, T.H. Bayburt, S.G. Sligar, Small-angle X-ray scattering study of monodisperse lipid-protein nanodiscs as nanoscale fragments of biological membrane, Biophys J, 86 (2004) 437–447.

[15] I.G. Denisov, Y.V. Grinkova, A.A. Lazarides, S.G. Sligar, Directed self-assembly of monodisperse phospholipid bilayer nanodiscs with controlled size, J Am Chem Soc, 126 (2004) 3477-3487.

[16] J. Huang, S.R. Turner, Recent advances in alternating copolymers: The synthesis, modification, and applications of precision polymers, Polymer, 116 (2017) 572-586.

[17] R. Friedel, Polymer Pioneers - a Popular History of the Science and Technology of Large Molecules - Morris, ISIS, 78 (1987) 275-276.

[18] A.K. Iyer, K. Greish, J. Fang, R. Murakami, H. Maeda, High-loading nanosized micelles of copoly(styrene-maleic acid)-zinc protoporphyrin for targeted delivery of a potent heme oxygenase inhibitor, Biomaterials, 28 (2007) 1871-1881.

[19] S.R. Tonge, B.J. Tighe, Responsive hydrophobically associating polymers: A review of structure and properties, Adv. Drug Deliv. Rev, 53(2001)109-122.

[20] K. Greish, A. Nagamitsu, J. Fang, H. Maeda, Copoly(styrene-maleic acid) - Pirarubicin micelles: High tumor-targeting efficiency with little toxicity, Bioconjugate Chem, 16 (2005) 230-236.

[21] K. Greish, T. Sawa, J. Fang, T. Akaike, H. Maeda, SMA-doxorubicin, a new polymeric micellar drug for effective targeting to solid tumours, J Control Release, 97 (2004) 219-230.

[22] W.B. Liechty, D.R. Kryscio, B.V. Slaughter, N.A. Peppas, Polymers for Drug Delivery Systems, Annu Rev Chem Biomol, 1 (2010) 149-173.

[23] W. Dannhauser, W.H. Glaze, R.L. Dueltgen, K. Ninomiya, Evidence from Intrinsic Viscosity and Sedimentation for Hypercoiled Configurations of Styrene-Maleic Acid Copolymer, J Phys Chem, 64 (1960) 954-955.

[24] M.C. Orwick, P.J. Judge, J. Procek, L. Lindholm, A. Graziadei, A. Engel, G. Grobner, A. Watts, Detergent-free formation and physicochemical characterization of nanosized lipid-polymer complexes: Lipodisq, Angew Chem Int Ed, 51 (2012) 4653-4657.

[25] T.J. Knowles, R. Finka, C. Smith, Y.-P. Lin, T. Dafforn, M. Overduin, Membrane proteins solubilized intact in lipid containing nanoparticles bounded by styrene-maleic acid copolymer, J. Am. Chem. Soc, 131 (2009) 7484-7485.

[26] H. Lee, R.G. Larson, Coarse-grained molecular dynamics studies of the concentration and size dependence of fifth- and seventh-generation PAMAM dendrimers on pore formation in DMPC bilayer, J Phys Chem B, 112 (2008) 7778-7784.

[27] U. Adhikari, A. Goliaei, L. Tsereteli, M.L. Berkowitz, Properties of Poloxamer Molecules and Poloxamer Micelles Dissolved in Water and Next to Lipid Bilayers: Results from Computer Simulations, J Phys Chem B, 120 (2016) 5823-5830.

[28] A.Y. Shih, P.L. Freddolino, A. Arkhipov, K. Schulten, Assembly of lipoprotein particles revealed by coarse-grained molecular dynamics simulations, J Struct Biol, 157 (2007) 579-592.

[29] M.M. Xue, L.S. Cheng, I. Faustino, W.L. Guo, S.J. Marrink, Molecular Mechanism of Lipid Nanodisk Formation by Styrene-Maleic Acid Copolymers, Biophys J, 115 (2018) 494-502.

[30] P.S. Orekhov, M.E. Bozdaganyan, N. Voskoboynikova, A.Y. Mulkidjanian, H.J. Steinhoff, K.V. Shaitan, Styrene/Maleic Acid Copolymers Form SMALPs by Pulling Lipid Patches out of the Lipid Bilayer, Langmuir, 35 (2019) 3748-3758.

[31] S.C. Lee, T.J. Knowles, V.L.G. Postis, M. Jamshad, R.A. Parslow, Y.-p. Lin, A. Goldman, P. Sridhar, M. Overduin, S.P. Muench, T.R. Dafforn, A method for detergent-free isolation of membrane proteins in their local lipid environment, Nat Protoc, 11 (2016) 1149-1162.

[32] K.A. Morrison, A. Akram, A. Mathews, Z.A. Khan, J.H. Patel, C.M. Zhou, D.J. Hardy, C. Moore-Kelly, R. Patel, V. Odiba, T.J. Knowles, M.U.H. Javed, N.P. Chmel, T.R. Dafforn, A.J. Rothnie, Membrane protein extraction and purification using styrene-maleic acid (SMA) copolymer: effect of variations in polymer structure, Biochem J, 473 (2016) 4349-4360.

[33] O. Korotych, J. Mondal, K.M. Gattas-Asfura, J. Hendricks, B.D. Bruce, Evaluation of commercially available styrene-co-maleic acid polymers for the extraction of membrane proteins from spinach chloroplast thylakoids, Eur Polym J, 114 (2019) 485-500.

[34] S. Scheidelaar, M.C. Koorengevel, C.A. van Walree, J.J. Dominguez, J.M. Dorr, J.A. Killian, Effect of Polymer Composition and pH on Membrane Solubilization by Styrene-Maleic Acid Copolymers, Biophys J, 111 (2016) 1974-1986.

[35] M.C. Fiori, Y. Jiang, G.A. Altenberg, H. Liang, Polymer-encased nanodiscs with improved buffer compatibility, Sci Rep, 7 (2017) 1-10.

[36] M. Overduin, M. Esmaili, Memtein: The fundamental unit of membrane-protein structure and function, Chem Phys Lipids, 218 (2019) 73-84.

[37] T. Ravula, S.K. Ramadugu, G. Di Mauro, A. Ramamoorthy, Bioinspired, Size-Tunable Self-Assembly of Polymer-Lipid Bilayer Nanodiscs, Angew Chem Int Ed, 56 (2017) 11466-11470.

[38] T. Ravula, N.Z. Hardin, S.K. Ramadugu, S.J. Cox, A. Ramamoorthy, Formation of pH-Resistant Monodispersed Polymer-Lipid Nanodiscs, Angew Chem Int Ed, 57 (2018) 1342-1345.

[39] S.C.L. Hall, C. Tognoloni, J. Charlton, E.C. Bragginton, A.J. Rothnie, P. Sridhar, M. Wheatley, T.J. Knowles, T. Arnold, K.J. Edler, T.R. Dafforn, An acid-compatible co-polymer for the solubilization of membranes and proteins into lipid bilayer-containing nanoparticles, Nanoscale, 10 (2018) 10609-10619.

[40] T. Ravula, N.Z. Hardin, S.K. Ramadugu, A. Ramamoorthy, pH Tunable and Divalent Metal Ion Tolerant Polymer Lipid Nanodiscs, Langmuir, 33 (2017) 10655-10662.

[41] S. Lindhoud, V. Carvalho, J.W. Pronk, M.E. Aubin-Tam, SMA-SH: Modified Styrene-Maleic Acid Copolymer for Functionalization of Lipid Nanodiscs, Biomacromolecules, 17 (2016) 1516-1522.

[42] A.O. Oluwole, B. Danielczak, A. Meister, J.O. Babalola, C. Vargas, S. Keller, Solubilization of Membrane Proteins into Functional Lipid-Bilayer Nanodiscs Using a Diisobutylene/Maleic Acid Copolymer, Angew Chem Int Edit, 56 (2017) 1919-1924.

[43] K. Yasuhara, J. Arakida, T. Ravula, S.K. Ramadugu, B. Sahoo, J. Kikuchi, A. Ramamoorthy, Spontaneous Lipid Nanodisc Fomation by Amphiphilic Polymethacrylate Copolymers, J Am Chem Soc, 139 (2017) 18657-18663.

[44] B. Danielczak, S. Keller, Collisional lipid exchange among DIBMA-encapsulated nanodiscs (DIBMALPs), Eur Polym J, 109 (2018) 206-213.

[45] A.S. Hauser, M.M. Attwood, M. Rask-Andersen, H.B. Schioth, D.E. Gloriam, Trends in GPCR drug discovery: new agents, targets and indications, Nat Rev Drug Discov, 16 (2017) 829-842.

[46] C. Southan, J.L. Sharman, H.E. Benson, E. Faccenda, A.J. Pawson, S.P.H. Alexander, O.P. Buneman, A.P. Davenport, J.C. McGrath, J.A. Peters, M. Spedding, W.A. Catterall, D. Fabbro, J.A. Davies, Nc-Iuphar, The IUPHAR/BPS Guide to pharmacology in 2016: towards curated quantitative interactions between 1300 protein targets and 6000 ligands, Nucleic Acids Res, 44 (2016) 1054-1068.

[47] J.S. McDowall, I. Ntai, J. Hake, P.R. Whitley, J.M. Mason, C.R. Pudney, D.R. Brown, Steady-State Kinetics of a-synuclein Ferrireductase Activity Identifies the Catalytically Competent Species, Biochemistry, 56 (2017) 2497-2505.

[48] J. Broecker, B.T. Eger, O.P. Ernst, Crystallogenesis of Membrane Proteins Mediated by Polymer-Bounded Lipid Nanodiscs, Structure, 25 (2017) 384-392.

[49] M. Caffrey, A comprehensive review of the lipid cubic phase or in meso method for crystallizing membrane and soluble proteins and complexes, Acta Crystallogr F, 71 (2015) 3-18.

[50] D. Li, V.E. Pye, M. Caffrey, Experimental phasing for structure determination using membrane-protein crystals grown by the lipid cubic phase method, Acta Crystallogr D Biol Crystallogr, 71 (2015) 104-122.

[51] D. Xia, C.A. Yu, H. Kim, J.Z. Xia, A.M. Kachurin, L. Zhang, L. Yu, J. Deisenhofer, Crystal structure of the cytochrome bc1 complex from bovine heart mitochondria, Science, 277 (1997) 60-66.

[52] C. Sun, S. Benlekbir, P. Venkatakrishnan, Y. Wang, S. Hong, J. Hosler, E. Tajkhorshid, J.L. Rubinstein, R.B. Gennis, Structure of the alternative complex III in a supercomplex with cytochrome oxidase, Nature, 557 (2018) 123-126.

[53] W. Qiu, Z. Fu, G.G. Xu, R.A. Grassucci, Y. Zhang, J. Frank, W.A. Hendrickson, Y. Guo, Structure and activity of lipid bilayer within a membrane-protein transporter, Proc Natl Acad Sci USA, 115 (2018)12985-12990.

[54] S. Murakami, R. Nakashima, E. Yamashita, A. Yamaguchi, Crystal structure of bacterial multidrug efflux transporter AcrB, Nature, 419 (2002) 587-593.

[55] K.M. Pos, A. Schiefner, M.A. Seeger, K. Diederichs, Crystallographic analysis of AcrB, FEBS Lett, 564 (2004) 333-339.

[56] E.W. Yu, G. McDermott, H.I. Zgurskaya, H. Nikaido, D.E. Koshland, Jr., Structural basis of multiple drug-binding capacity of the AcrB multidrug efflux pump, Science, 300 (2003) 976-980.

[57] S. Murakami, R. Nakashima, E. Yamashita, T. Matsumoto, A. Yamaguchi, Crystal structures of a multidrug transporter reveal a functionally rotating mechanism, Nature, 443 (2006) 173-179.

[58] M.A. Seeger, A. Schiefner, T. Eicher, F. Verrey, K. Diederichs, K.M. Pos, Structural asymmetry of AcrB trimer suggests a peristaltic pump mechanism, Science, 313 (2006) 1295-1298.

[59] T. Eicher, H.J. Cha, M.A. Seeger, L. Brandstatter, J. El-Delik, J.A. Bohnert, W.V. Kern, F. Verrey, M.G. Grutter, K. Diederichs, K.M. Pos, Transport of drugs by the multidrug transporter AcrB involves an access and a deep binding pocket that are separated by a switch-loop, Proc Natl Acad Sci USA, 109 (2012) 5687-5692.

[60] R.K. Hite, Z. Li, T. Walz, Principles of membrane protein interactions with annular lipids deduced from aquaporin-0 2D crystals, EMBO J, 29 (2010) 1652-1658.

[61] T. Gonen, Y. Cheng, P. Sliz, Y. Hiroaki, Y. Fujiyoshi, S.C. Harrison, T. Walz, Lipid-protein interactions in double-layered two-dimensional AQP0 crystals, Nature, 438 (2005) 633-638.

[62] A.P. Bali, I.D. Sahu, A.F. Craig, E.E. Clark, K.M. Burridge, M.T. Dolan, C. Dabney-Smith, D. Konkolewicz, G.A. Lorigan, Structural characterization of styrene-maleic acid copolymer-lipid nanoparticles (SMALPs) using EPR spectroscopy, Chem Phys Lipids, 220 (2019) 6-13.

[63] A. Dathe, T. Heitkamp, I. Perez, H. Sielaff, A. Westphal, S. Reuter, R. Mrowka, M. Borsch, Observing monomer- transitions of neurotensin receptors 1 in single SMALPs by homoFRET and in an ABELtrap, Proc Spie, 10884 (2019)1-12.

[64] E.B. Martin Jakubec, Samuel Furse, Morten L. Govasli, Vinnit George, Diana Turcu, Igor Iashchishyn, Ludmilla Morozova-Roche, Øyvind Halskau, Cholesterol is a strong promotor of an α-Synuclein membrane binding mode that accelerates oligomerization, bioRxiv DOI: 10.1101/725762, (2019).

[65] V.E. Ahn, E.I. Lo, C.K. Engel, L. Chen, P.M. Hwang, L.E. Kay, R.E. Bishop, G.G. Prive, A hydrocarbon ruler measures palmitate in the enzymatic acylation of endotoxin, EMBO J, 23 (2004) 2931-2941.

[66] P.M. Hwang, W.Y. Choy, E.I. Lo, L. Chen, J.D. Forman-Kay, C.R. Raetz, G.G. Prive, R.E. Bishop, L.E. Kay, Solution structure and dynamics of the outer membrane enzyme PagP by NMR, Proc Natl Acad Sci USA, 99 (2002) 13560-13565.

[67] C.R. Raetz, C.M. Reynolds, M.S. Trent, R.E. Bishop, Lipid A modification systems in gram-negative bacteria, Annu Rev Biochem, 76 (2007) 295-329.

[68] R.E. Bishop, Structural biology of membrane-intrinsic beta-barrel enzymes: sentinels of the bacterial outer membrane, Biochim Biophys Acta, 1778 (2008) 1881-1896.

[69] K. Kanonenberg, J. Royes, A. Kedrov, G. Poschmann, F. Angius, A. Solgadi, O. Spitz, D. Kleinschrodt, K. Stuhler, B. Miroux, L. Schmitt, Shaping the lipid composition of bacterial membranes for membrane protein production, Microb Cell Fact, 18 (2019) 131.

[70] G.H.M. Huysmans, S.E. Radford, D.J. Brockwell, S.A. Baldwin, The N-terminal helix is a post-assembly clamp in the bacterial outer membrane protein PagP, J Mol Biol, 373 (2007) 529-540.

[71] C.V. Robinson, Mass spectrometry: From plasma proteins to mitochondrial membranes, Proc Natl Acad Sci USA, 116 (2019) 2814-2820.

[72] R.E. Bishop, The lipid A palmitoyltransferase PagP: molecular mechanisms and role in bacterial pathogenesis, Mol Microbiol, 57 (2005) 900-912.

Chapter 2

Native Nanodiscs Formed by Imidazole and Amineoxide conjugated Styrene-Maleamic acid Copolymers

2.1. Significance

Copolymers formed by random distributions of styrene and maleic acid monomers directly solubilize intact membranes into 10 nm discs. However, these polymers are inherently polydisperse, difficult to detect, tend to precipitate with cations and have limited pH ranges due to their charges. Here, we report that when derivatized with biocompatible amine oxide (AO) and histamine (His) moieties, alternating and intrinsically fluorescent styrene-maleic anhydride copolymers spontaneously convert biological membranes into nanodiscs with diameters of 15-25 nm that can be resolved by dynamic light scattering and electron microscopy. Their fluorescence signals allow monitoring under diverse solution conditions, whether free or lipid bilayer-bound. These polymers are useful in a broad range of pH and divalent cation levels and designed to reduce undesirable nonspecific interactions. Fluorescent nanoparticles composed of styrene-maleic anhydride (SMA) derivatized with histamine allow membrane complexes to be purified and assayed using immobilized metal affinity resins. The native nanodiscs can accommodate PagP palmitoyltransferase from outer bacterial membranes or potentially megadalton assemblies. Thus, the exposed polar sidechain of nanodisc-forming polymers provides a unique handle for integrating critical features for facile solubilization, purification, detection, and resolution of various membrane protein complexes directly from any biological material.

2.2. Introduction

Membrane: protein complexes represent critical sensors, transducers and signaling enzymes as well as being valuable targets for drug discovery. Transferring such assemblies intact into soluble nanodiscs for structure-function studies without exposure

to detergents, which tend to strip away associated biological lipids, remains an ongoing challenge that is being addressed by amphipathic polymer design [1]. We previously showed that native nanodiscs could be spontaneously generated by adding non-alternating styrene-maleic acid copolymers to biological membranes [2]. Although these synthetic polymers have been used to determine high-resolution structures of multiple endogenous membrane proteins [3, 4], their utility is blunted by several issues. The random alternation of monomers smears polymer signals and blurs resolution of how proteins specifically recognized lipid molecules. Hence resolving atomic details within crystals, NMR spectra, or cryo-electron microscopy maps of native protein: lipid complexes remains challenging.

Moreover, the negatively charged groups attract cations and alkaline protein surfaces, potentially causing precipitation and nonspecific deactivation. The obligate charge of water-soluble SMA restricts the operational pH range to around neutrality, precluding direct solubilization of acidophile, lysosomal, or endocytic membranes in their natural low pH contexts. Non-alternating SMA sequences possess styrene clusters, which can promote aggregation and nonspecific protein association with potentially deleterious consequences. Finally, the capacities of current discs, which have diameters of around 10 nm, are stretched by integration of large assemblies like metabolons (the temporary complex of enzymes in a metabolic pathway) [5] or photosystems [3].

Polymer space is being explored in order to discover new features that expand functionality and utility [6]. Inclusion of functional groups such as ethylenediamine [7], tertiary [8], quaternary amines [9], or alcohol amine [10] is known to alter polymer

solubility. Phosphocholine sidechains enhance buffer compatibility [11]. Thiol groups can be linked to affinity or fluorescent tags [12]. Replacing the aromatic styrene with aliphatic groups eliminates spectral absorbance [13]. Each of these developments has illuminated useful features. However, a single polymer type that integrates desired features and facilitates simple detection, enhanced resolution and efficient direct incorporation of diverse membrane types for convenient purification and high-resolution analysis of lipid-bound protein multimers remain elusive.

Here, a family of SMA copolymers with alternating hydrophobic and polar monomers in a ratio of 1:1 are designed and shown to turn biological membranes into native nanodiscs. Grafting amphoteric AO and imidazole sidechains yielded a series of fluorescent polymers (Scheme 2.1) that show broad solubility profiles and contain affinity tags. They are chemically distinct from non-alternating SMA polymers, which are inherently more polydisperse due to their random sequence patterns. Alternating SMA copolymers were previously shown to be ineffective at solubilizing lipid vesicles [14], spinach chloroplast thylakoids [15] and *E. coli*, insect and mammalian cells [16]. However, these polymers they were not derivatized to optimize the balance of hydrophobicity and polarity. The incorporation of these unique zwitterionic sidechains led to sufficient net hydrophobicity that enables the spontaneous formation of native nanodiscs from synthetic and biological membranes. Unlike SMA2000, the polymers reported here display stable fluorescence from pH values between 5-10, higher polycation conditions and potentially diverse membrane types. This paves the way for purifying, tracking and resolving many currently elusive membrane: protein structures from in vivo sources.

2.3. Results and discussion

2.3.1.Synthesis of SMA polymer derivatives

Compact sidechains were attached to the SMA to enable metal ion affinity resin-based purification and broaden solubility profiles. This series involved grafting a histamine group onto SMA polymer (through covalent interaction between primary amine of histamine and anhydride groups of SMAn) with alternating styrene-maleic anhydride monomers (SMA(1:1)) to form His-SMA polymers [17]. The initial maleamic acid product (**1**) includes a negative charge for enhanced water solubility (Scheme. 2.1a).

Due to their zwitterionic properties, lack of negative effects on protein functions and low ecotoxicity, AO moieties are valuable features of widely used surfactants such as lauryldimethylamine N-oxide (LDAO) [22]. Both ethyl and propyl dimethyl AO groups contain primary amine groups that covalently interact (through SN2 nucleaophilic attack) with maleic anhydride of SMAn(1:1) polymer and form AO2-SMA (**2**) and AO3-SMA (**3**) derivatives, respectively, with open ring maleamic acid (Scheme 2.1b).

The open ring formulations of AO-SMA polymers (**2** and **3**) were heated for 4 hours at 135 °C to generate formulations with closed maleimide rings. However, this reaction was not complete and the majority of maleamic acid rings still maintained in open configurations. The resulting polymers are designated as AO2-SMA (**4**) and AO3-SMA (**5**) and contain mainly open maleamic acid rings and a small percentage of maleimide groups. Since a mixture of maleamic acid and maleimide moieties exist in AO2-SMA (**4**) and AO3-SMA (**5**) polymers, we refer to **4** and **5** formulations as polymers with partially closed maleimide rings (Fig. 2.1b). Further studies are required to set up a protocol to achieve complete

and uniform closure of maleamic acid rings in AO-SMA **4** and **5** polymers throughout the polymer chains. Also we need to determine the percentage of ring closure in AO-SMA polymers **4** and **5** and fully characterize the purity and chemical composition of AO-SMA polymers **4** and **5**.
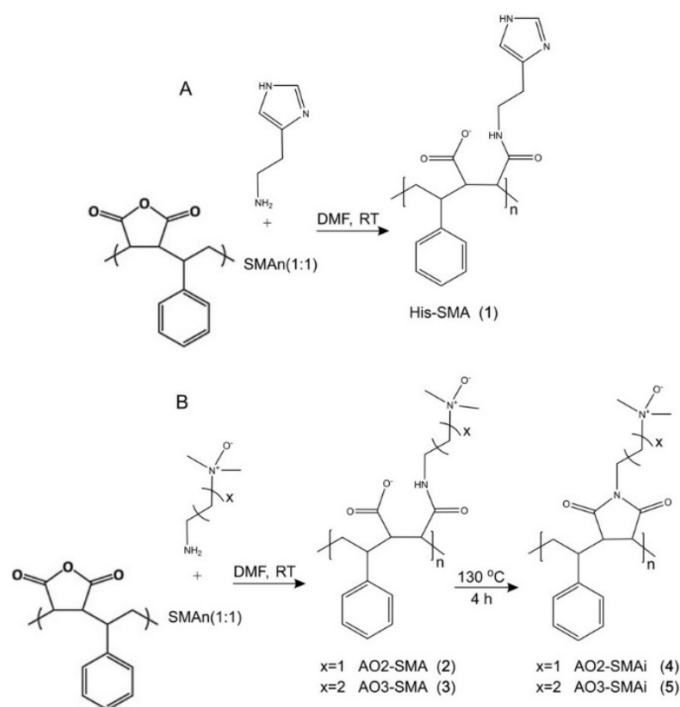
Figure 2.1. Schematic outlining the copolymer synthesis. A. Grafting of histamine onto SMA(1:1) leads to His-SMA polymer (**1**) with an open ring configuration. B. Partial oxidation of the tertiary amine-containing ethyl (x=2) or propyl (x=3) alkyl groups in H_2O_2 yields the AO products [18], the identity of which was confirmed by ESI-MS (Fig. 2.3). Alkyl diamine, N, N dimethyl n-oxide sidechains were grafted to SMAn(1:1) and AO-SMA polymers (**2** and **3**) were synthesized in open ring configurations. Heating AO-SMA polymers **2** and **3** for 4 hours at 135 °C led to the formation of AO-SMA **4** and **5**, respectively, with partially closed maleimide ring. The chemical structures of polymers **1**, **4** and **5** were further confirmed by ^{13}C NMR in water (see Appendix 3).

The attenuated total reflection-Fourier transform infrared (ATR-FTIR) spectra of His-SMA (**1**) show bands at 1380, 1577-1600 and 1668 cm^{-1} (Fig. 2.2), which represent expected vibrations of the aromatic imidazole group [19-21]. The 1700-1714 cm^{-1} bands represent the amide stretch vibrations of opened maleamic acid ring configurations in His-SMA, AO2-SMA (**2**) and AO3-SMA (**3**) and . The band at ~1780 cm$^{-1,}$ which are indicative of the C=O bonds of the maleic anhydride residues are absent, confirming the completion of the reaction (Fig 2.2a,b) .Heating led to the partial closure of maleamic ring in AO2-SMA **4** and AO3-SMA **5** as verified by FT-IR. In both spectra, a small band at 1770 cm^{-1} indicates the formation of imide C=O (Fig 2.2c)

The FT-IR spectra of AO2 and AO3 compounds showed weak bands at 965 cm^{-1}, which corresponds to stretching vibrations of the N-O group (Fig. 2.3a) and 1100 cm^{-1} band, which is absent in the SMAn(1:1) reactant [23]. Furthermore, mass to charge (m/z) of the ESI-MS profiles of AO compounds confirmed the conversion of amine compounds to their corresponding amine oxide derivatives (Fig. 2.3b).
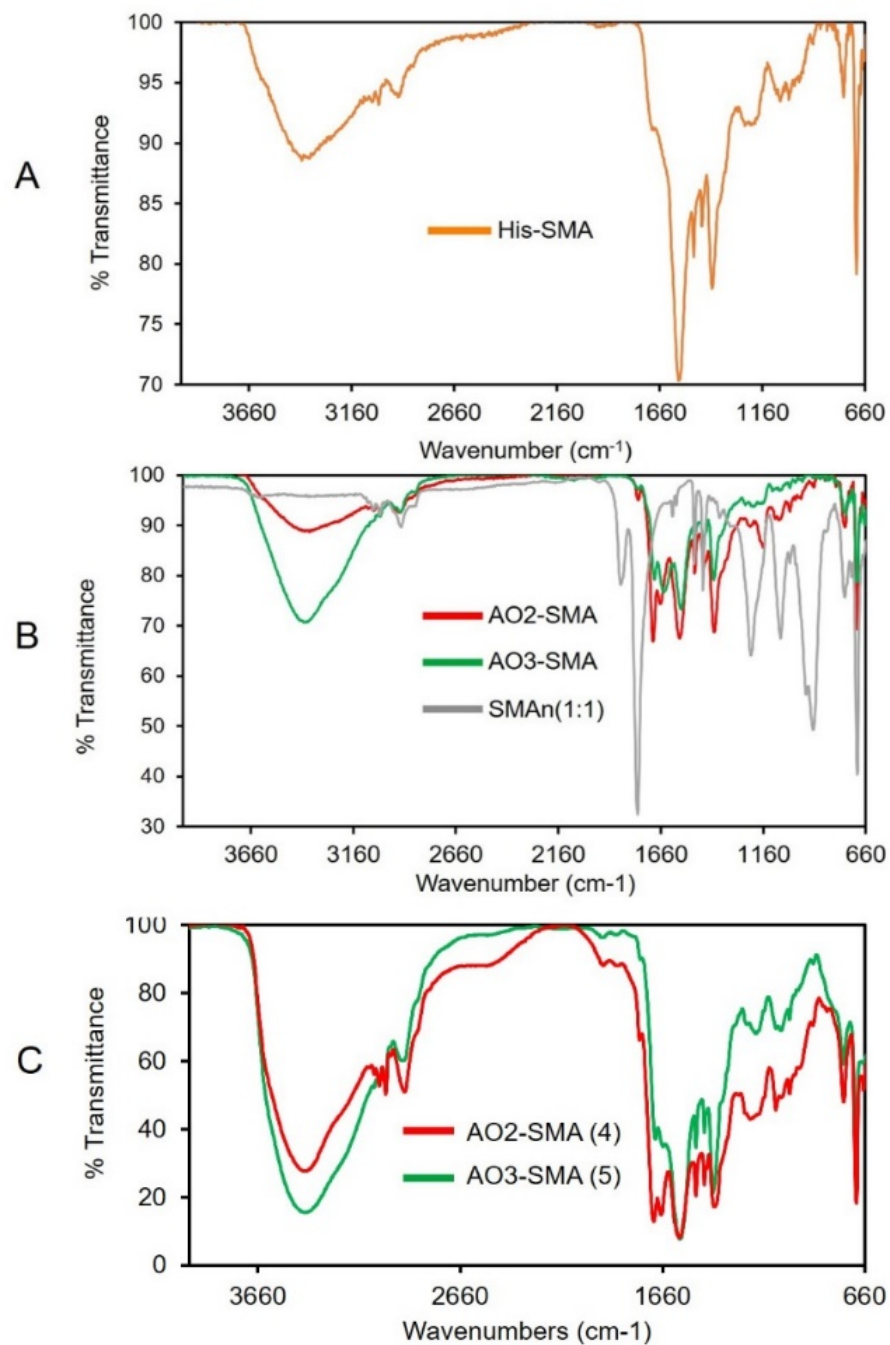
Figure 2.2. ATR-FTIR spectra of (A) His-SMA (**1**), (B) and AO2-SMA (**2**), AO3-SMA (**3**), and (C) AO2-SMA (**4**) and AO3-SMA (**5**) (heated) and contain partially closed maleimide rings.
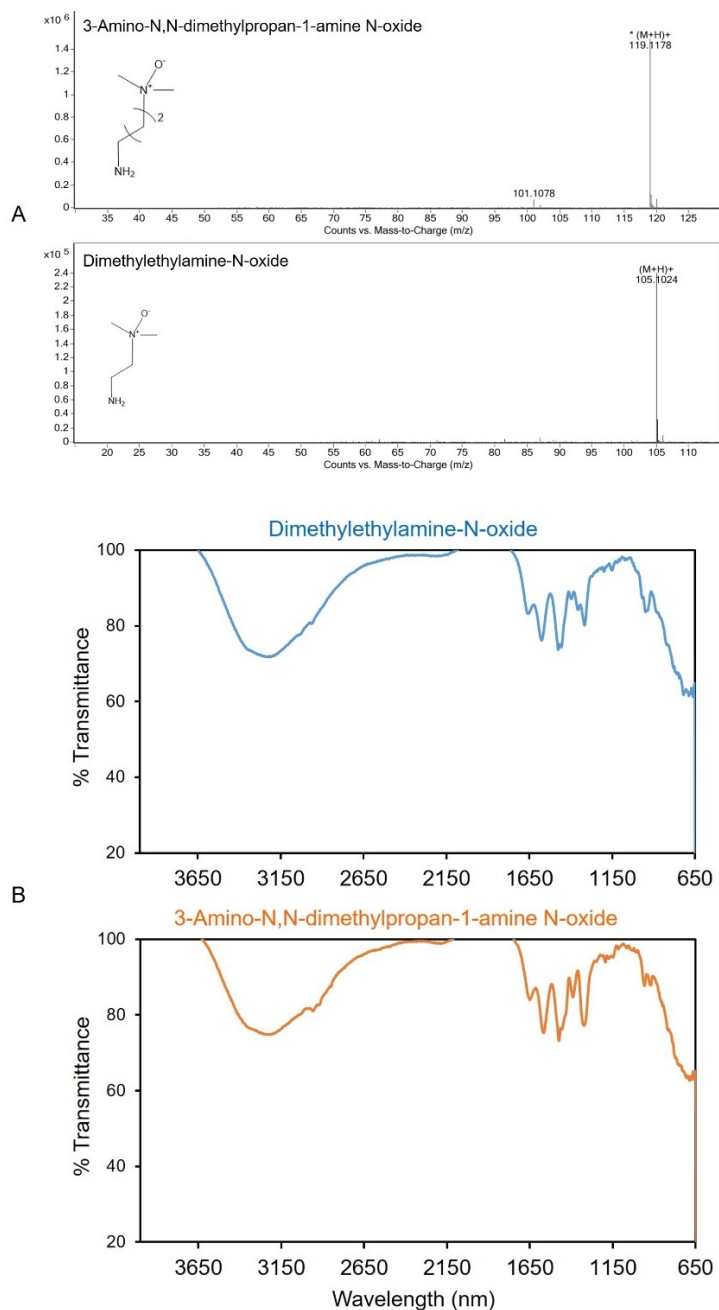
Figure 2.3. A. ESI-MS spectra of amine oxide reagents used for the synthesis of AO-SMA polymers. Samples were dissolved in methanol and analyzed using full scan high resolution (with continuous monitoring of two lock mass as references) in positive ion mode electrospray, via direct flow injection into methanol as the carrier solvent. The instrument used was Agilent Technologies 6220 Accurate Mass oaTOF. B. ATR-FTIR spectra of AO2 (top) and AO3 (bottom) compounds.

2.3.2. Solution behavior of SMA derivatives.

The aqueous solubility and compatibility of the His and AO modified polymers were investigated to define their biochemical utility. Divalent cation and pH levels in the physiological ranges were explored, with membrane proteins normally operating at calcium concentrations range up to ~4 mM and intracellular pH from ~5 to 8. Based on optical density measurements, compounds 1 remain soluble at Ca^{2+} concentrations of up to 7 mM, respectively, while above this value, they precipitate and yield turbid solutions (Fig. 2.3). The open-ring form 1 is soluble from pH 4-10, reflecting the latter polymer's additional polarity and effect on its pK_a and amphoteric capacity. Likewise, 2 and 3 are soluble at pH 5-10 in water (Fig. 2.4b), and in the presence of up to 8 and 6 mM $CaCl_2$ (the turning points of graphs in Fig. 2.4a), respectively, consistent with their zwitterionic character.

His-SMA(1:1) and AO-SMA(1:1) (**4, 5**) polymers were tested for direct, spontaneous solubilization of lipid vesicles composed of dimyristoylphosphatidylcholine (DMPC). Products **1, 4, 5**, all clarified the cloudy vesicle suspensions at room temperature within minutes at pH 5-10 (Fig. 2.4). This out-performs other SMA copolymers having similar molecular weights but relatively more styrene (*e.g.,* SMA2000, SZ30010), which precipitate once exposed to divalent cation concentrations over 2.5 mM or at pH values under 7.0, thus limiting utility [16]. Hence, SMA(1:1) derivatized with AO and His moieties possess broader solubility profiles and cationic compatibility than SMA(2:1) polymer, presumably due to its higher hydrophobicity and charge.
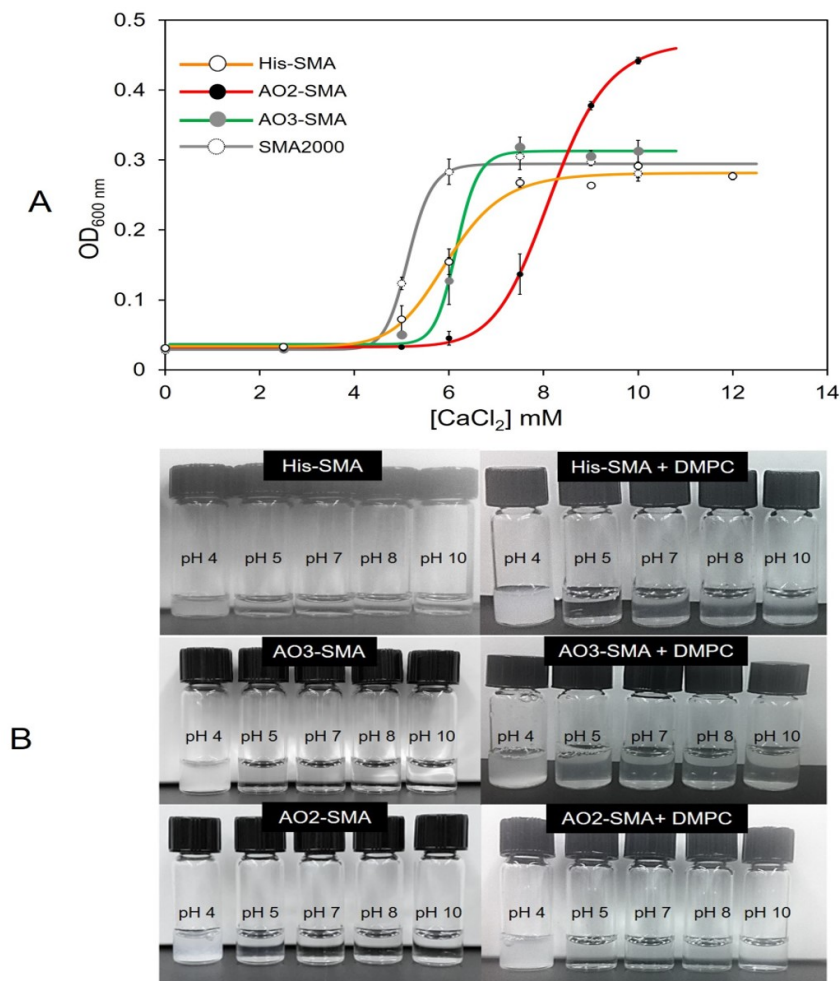
Figure 2.4. A. Calcium tolerance of AO2-SMA (**4**), AO3-SMA (**5**) and His-SMA (**1**) polymers was quantified by optical densities at 600 nm of 1% (w/v) solutions and compared with SMA2000 which has a 2:1 styrene to maleic acid ratio. B. The solubilities of each polymer (0.5% w/v) at different pH levels from 5 to 10 are shown, as are their abilities to clarify suspensions of vesicles formed by DMPC.

2.3.3. Fluorescence of SMA(1:1) derivatives.

Being able to track and monitor polymers and resultant nanodiscs is explicitly highly desirable. While SMA polymers can be detected by UV absorbance of their styrene groups, these signals are obscured by overlapping protein absorbance. Unlike SMA2000, SMA1000 is indeed intrinsically fluorescent (Fig. 2.6a). This can be attributed to the

regular alternation of emissive styrene groups and the various electron-withdrawing maleamic moieties could induce fluorescence. Indeed, fluorescence signals were observed with maximum excitation wavelengths of His-SMA at 320 nm and maximum emission wavelengths of 421-424 nm (Fig. 2.5). Differently, both AO products share similar excitation profiles (λ_{max} exci 350 nm) with maximum emissions of ~ 423 nm. Worth noting that, amine-oxide reagents are not fluorescent (λ_{exci} 350 nm), while histamine displays fluorescence with a maximum emission at 400 nm (λ_{exci} 320 nm, Fig. 2.5). Either can be incorporated as zwitterionic sidechains to generate a diversity of fluorescent SMA(1:1) polymer types. This obviates the need to attach large fluorophores as these alternating SMA derivatives possess repeated subunits that are intrinsically and distinctively fluorescent.
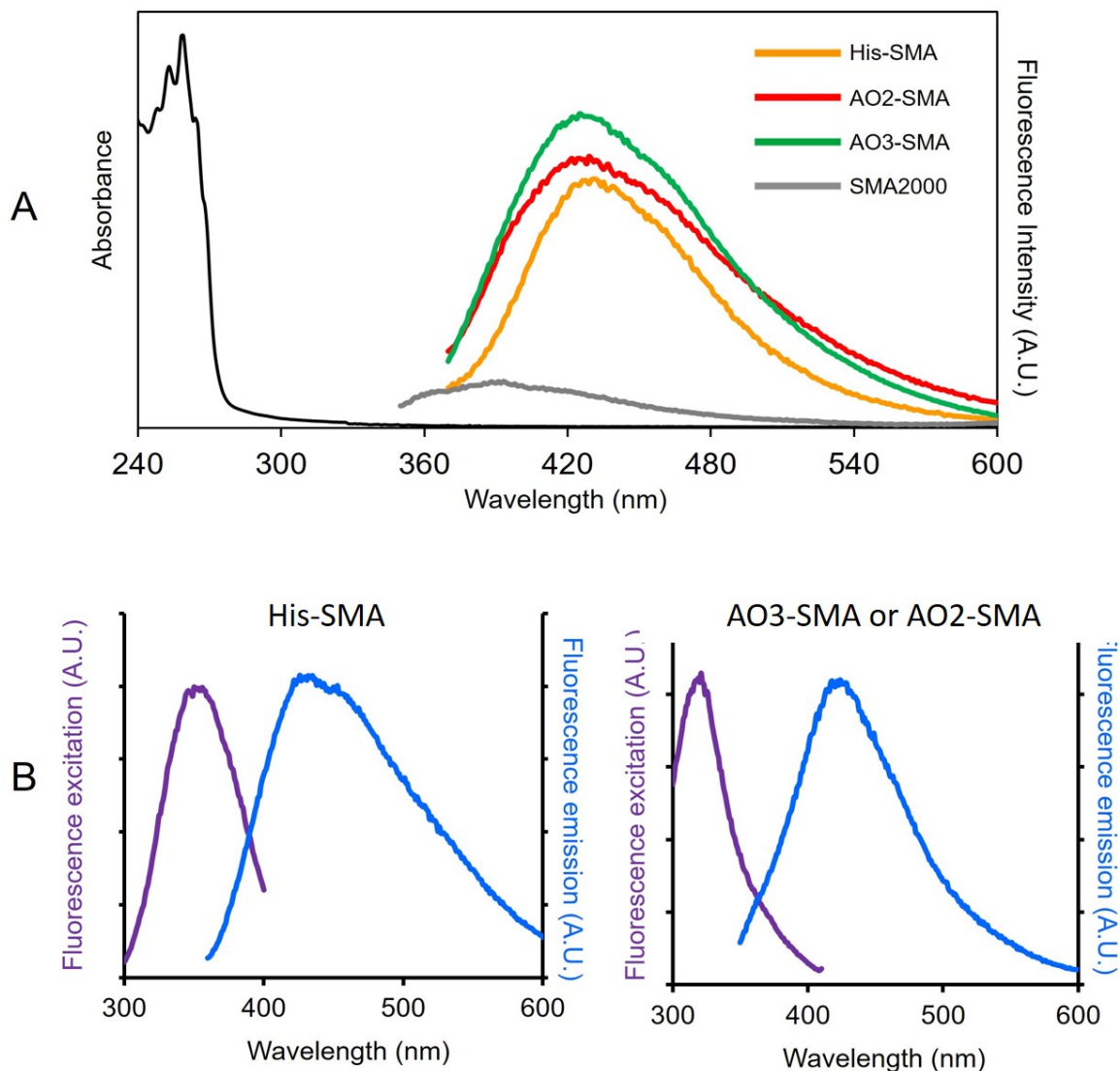
Figure 2.5. A. UV-Vis absorption (left axis) and fluorescence emission spectra (right axis) of modified SMA polymers (1% w/v) in Tris buffer, pH 8.0 upon irradiation of His and AO-SMA copolymers with 320 and 350 nm UV light, respectively, exhibiting an average Stoke's shift of ~140nm. The spectrum of SMA2000 is shown upon excitation at 320 nm. Given the maximum absorbance of these polymers (between 260-280 nm) [24], the Stokes shifts of the modified polymers were estimated to be approximately 146 nm. B. Excitation and emission spectra of each AO2-SMA (**4**), AO3-SMA (**5**) and His-SMA (**1**) polymers.
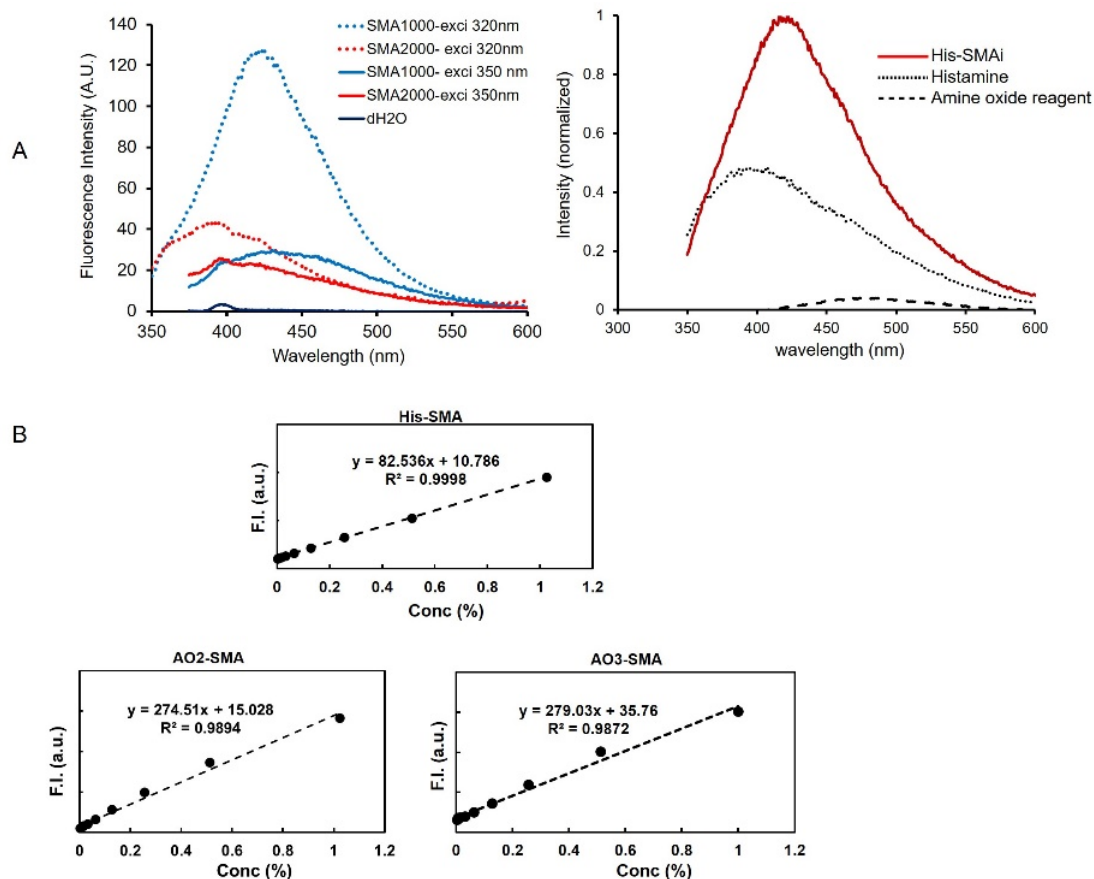
Figure 2.6. A. A comparison of intrinsic fluorescence of SMA1000 and SMA2000 (maleic acid forms, 1% w/v, in water), histamine (1 mg/mL in water) and AO-3 (10 mg/mL) compound in water. B. The fluorescence intensity of different variants of His-SMA (**1**) and AO-SMA copolymers (**4**, **5**) show linear relationships with their concentrations.

The quantum yields (QY) of the modified polymers were calculated using quinine sulfate as a standard [25, 26]. The QY values of AO2-SMA (**4**) and AO3-SMA (**5**) (λ_{exci} 350 nm) are 1.900 (± 0.080)% and 2.000 (± 0.020)%, respectively, while the QY values of His-SMA polymer (λ_{exci} 320 nm) is 1.000 (±0.03)%. Thus, each product type has a consistent QY, and the AO forms appear to have two times brighter fluorescence than the His products.
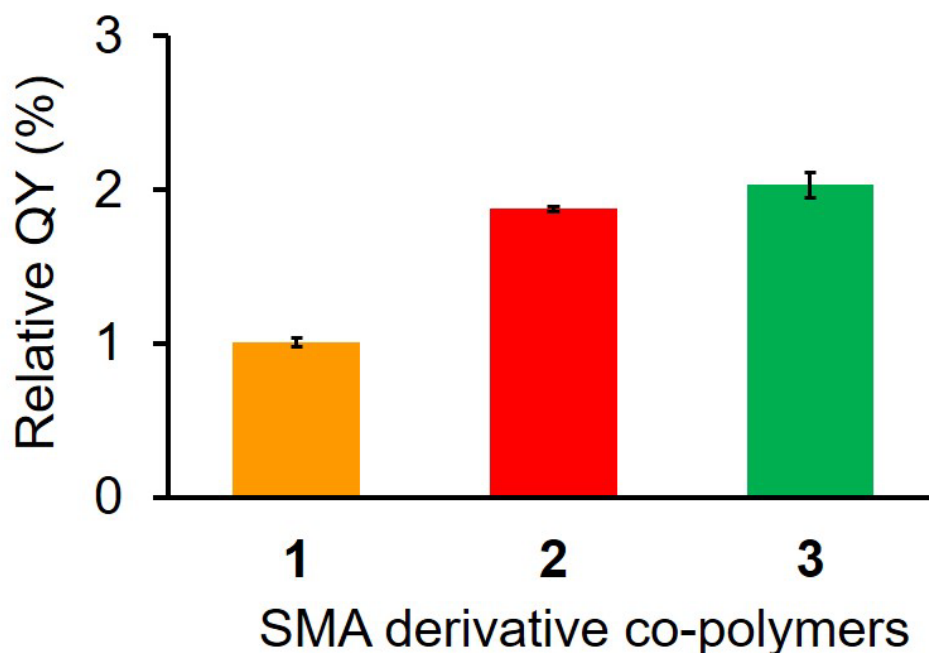
Figure 2.7. A comparison between the relative fluorescence quantum yields of AO-SMA (**4, 5**) and His-SMA (**1**) in water.

The robustness of fluorescence was assayed over the variety of conditions under which the copolymers are typically used to form native nanodiscs. The fluorescent emissions are linearly related to the polymer concentration (Figs. 2.6 and 2.7). Besides, the signals are maintained in the presence of DMPC vesicles over a range of pH values. The maximum fluorescence wavelength is consistent, although the intensity is increased as the pH is reduced from 10 to 5. The titration with $CaCl_2$ has little effect on the fluorescence signal of the soluble polymer (Fig. 2.8). Hence, fluorescence signals of the new copolymers allow their concentrations to be readily quantified in free and membrane-bound states under a variety of solution conditions. His derivatized SMA(1:1) copolymer can also be recognized using an anti-histamine antibody, which was used to demonstrate that these polymers interact preferentially with Ni -NTA resins and can be eluted with

imidazole buffer (50 mM) (Fig. 2.9) while AO-SMA displays almost no interaction. Hence these multifunctional substituents can be used as both affinity tags, fluorescent signals and antibody epitopes.
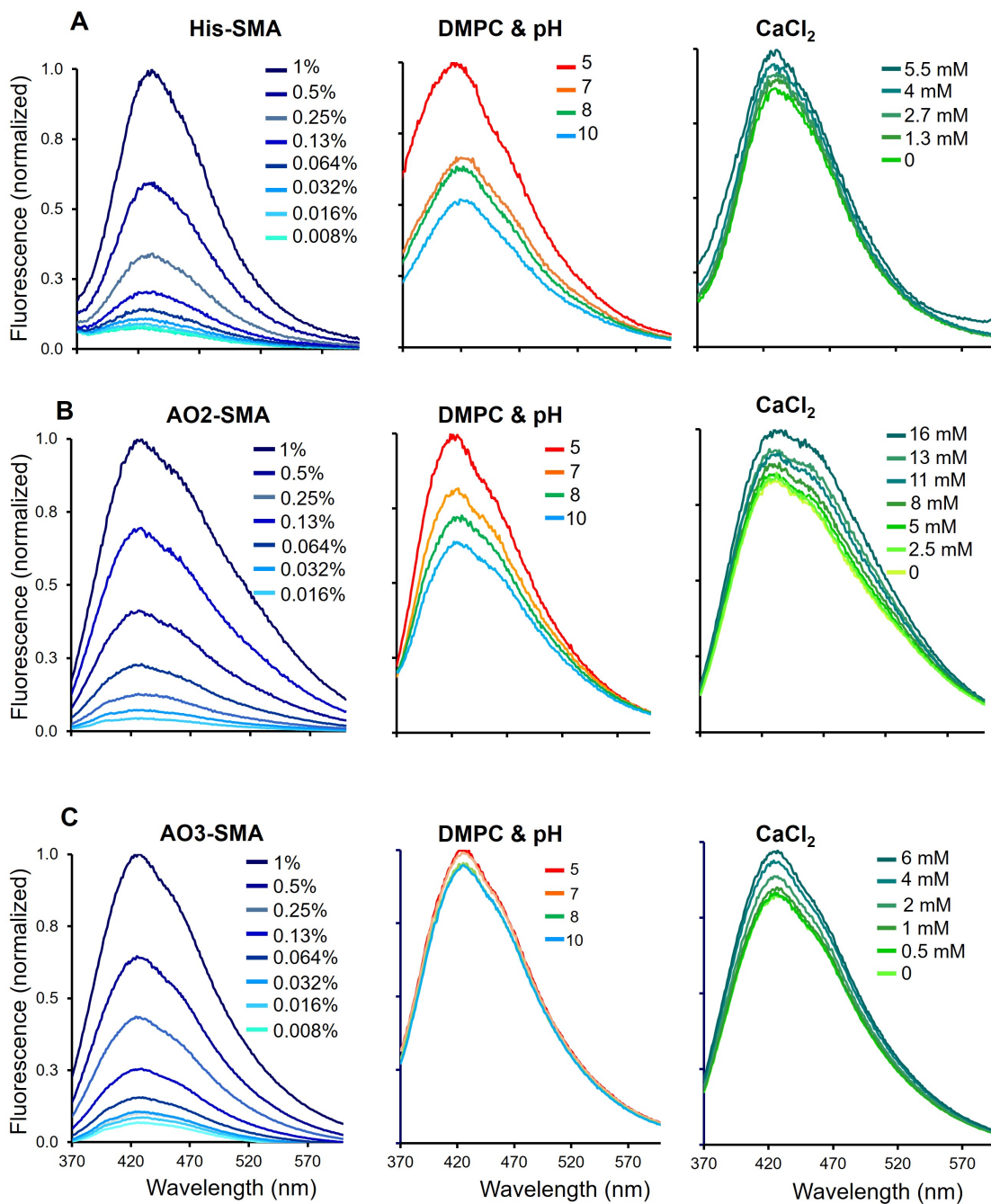
Figure 2.8. Fluorescence spectra of His-SMA (**1**) (A), AO2-SMA (**4**) (B) and AO3-SMA (**5**) (C) polymers under different polymer concentrations (left panels), pH ranges from 5-10 and lipid vesicles composed of 3 mM DMPC (middle panels) and increasing $CaCl_2$ levels (right panels).
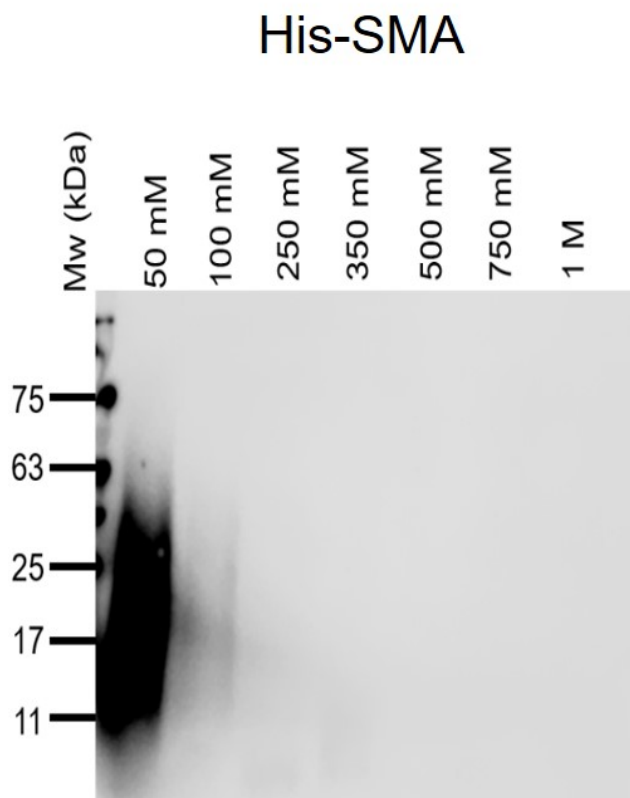
His-SMA

Figure 2.9. Interaction between His-SMA with nickel-NTA resins. His-SMA binds to Ni-NTA column. The bound polymers can be eluted using different concentrations of imidazole and detected on immunoblots via anti-histamine antibody. The majority of His-SMA are eluted at 50 mM imidazole, thus demonstrating a low affinity to Ni-NTA resin. Under the same condition, SMA2000 and AO-SMA do not bind to Ni-NTA resins.

2.3.4. Sizes of fluorescent nanodiscs.

The dispersal of lipid vesicles into rapidly tumbling nanodiscs can be observed by ^{31}P NMR. The transition of imperceptibly broad ^{31}P resonances of DMPC into sharper

signals indicates critical polymer concentrations for 1, 2, and 3 of between 1 and 2% w/v (Fig. 2.10). This is the concentration range at which the copolymers clarify otherwise turbid solutions of lipids or membrane fractions.
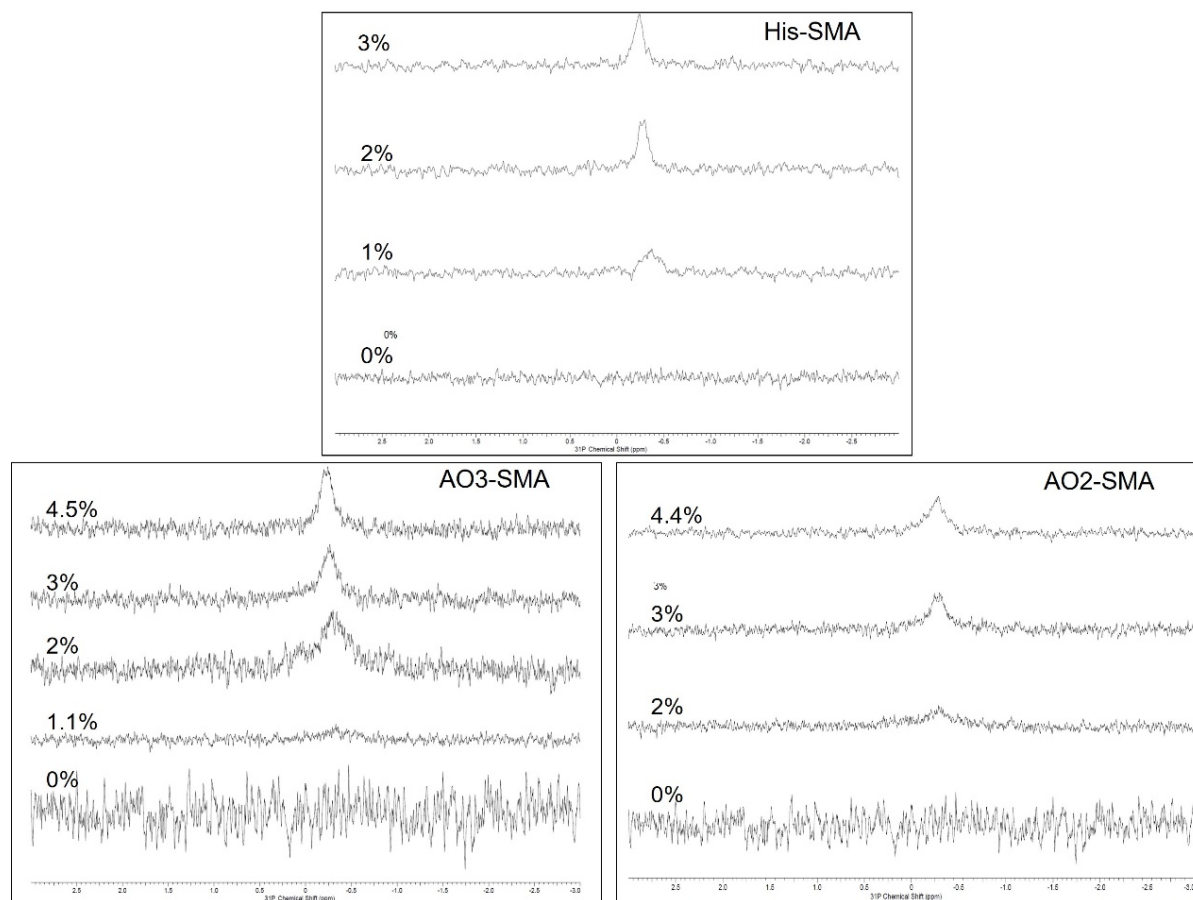
Figure 2.10. The ^{31}P NMR spectra show the interaction between AO2-SMA (**4**), AO3-SMA (**5**) and His-SMA (**1**) polymers with DMPC lipid vesicles. The ^{31}P NMR signals of lipid sharpen upon increasing the concentration of SMA polymers.

Although conventional SMALPs form 10 nm in diameter [2], many membrane assemblies exceed this size [3-5]. The fluorescent discs were predicted to be larger due to the reduction of net charge on the AO and His-modified polymers. The dimensions of discs solubilized from DMPC vesicles by **1**, **4**, **5** (1% w/v) were found to be about 24, 16,

21 nm, respectively, by dynamic light scattering (DLS) experiments (Fig. 2.11). As such, they are approximately twice the size of discs typically reported for SMA(2:1) and SMA(3:1) series, and could more readily accommodate larger memteins (native assemblies of membrane proteins) [3, 5] as would other SMA variants [9, 10], although not with the low sequential polydispersity of SMA(1:1) derivatives. The average particle size can be adjusted by altering the ratio of polymer to lipid (Table. 2.1), although broader size distributions are evident at low and high copolymer concentrations (Fig. 2.12). This could reflect partial membrane fragmentation and larger aggregates, consistent with other reports [27], and emphasizes the importance of using a sufficient amount of the novel polymer (typically 1-2%) for complete membrane fragmentation but not so much that large aggregates form.
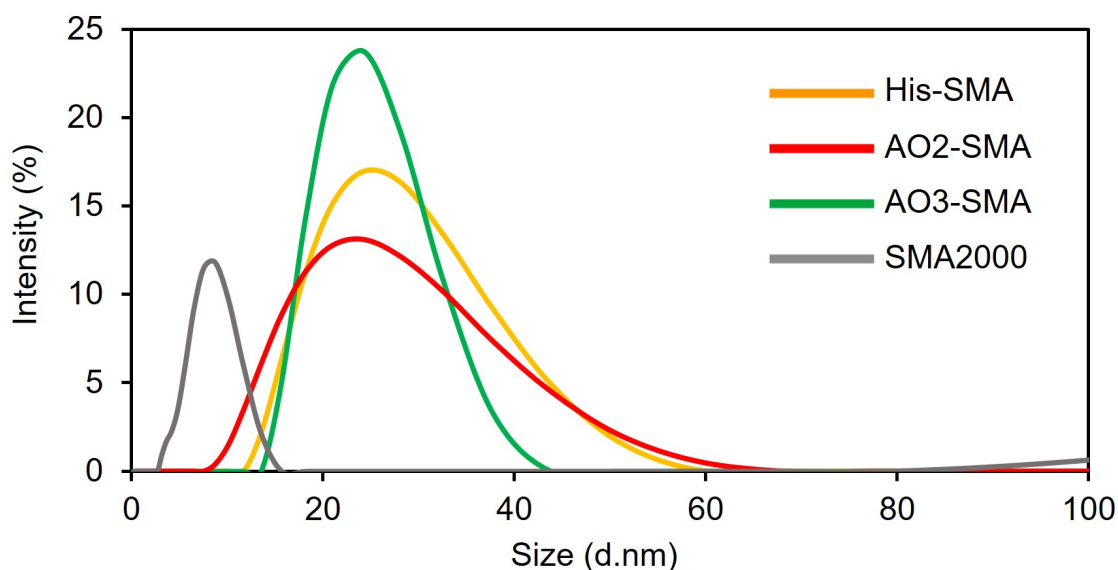
Figure 2.11. Diameters of nanodiscs formed from DMPC vesicles solubilized by AO2-SMA (**4**), AO3-SMA (**5**) and His-modified SMA (**1**) copolymers (1% w/v, Tris 10 mM, pH 8.0, 100 mM NaCl) based on DLS measurements. SMA2000 was used as a control and generated the expected 10 nm discs.
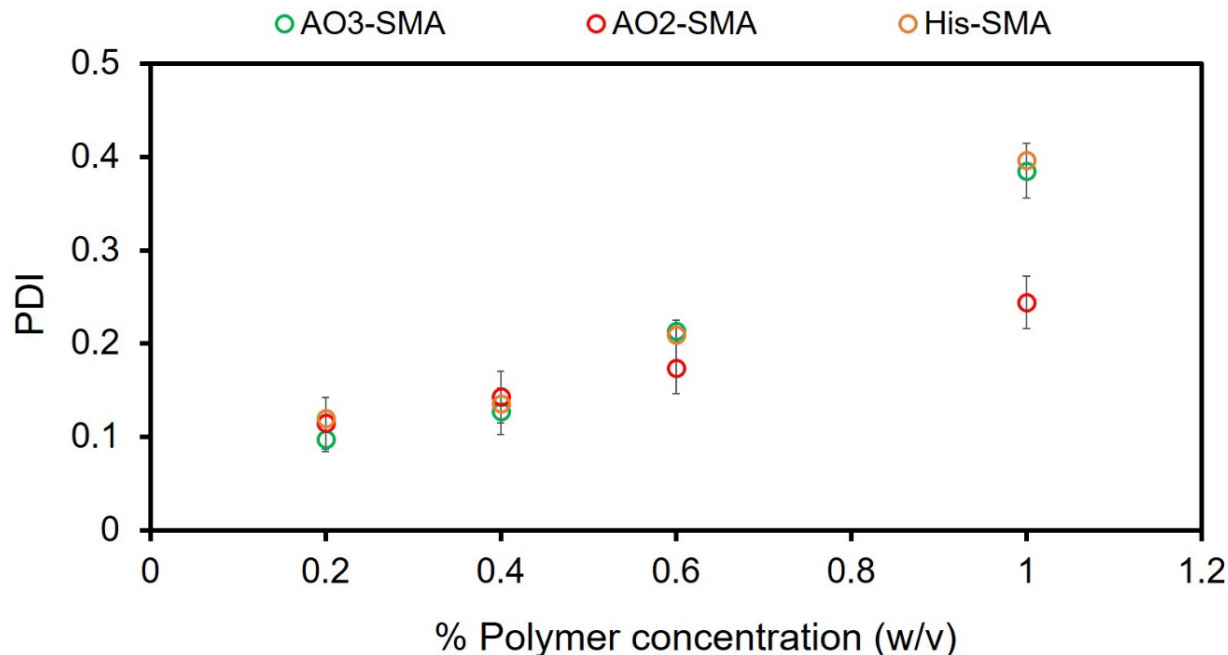
Figure 2.12. The change in polydispersity index (PDI) was monitored upon increasing the concentration of AO2-SMA (**4**), AO3-SMA (**5**) and His-SMA (**1**) in DMPC lipid samples (as specified in Table. 2.1).

Polymer	SMA concentration (w/v)			
	0.2%	**0.4%**	**0.6%**	**1%**
His-SMA (**1**)	28.9±0.3	25.6±0.35	24.4±0.52	24.5±0.17
AO2-SMA (**4**)	28.7±0.5	25.5±0.06	25.9±0.4	21.3±0.2
AO3-SMA (**5**)	72±0.3	55±0.3	32.8±0.15	28.2±0.1

Table 2.1. The average size (in nanometer) of nanodiscs formed of DMPC lipid vesicles containing different amounts (% w/v) of AO-SMA (**4, 5**) and His-SMA (**1**) was measured using DLS.

2.3.5. Native nanodisc formed by AO- and His- SMA(1:1) polymers.

Biological membranes present ordered bilayers packed with glycolipids, phospholipids, sterols, and proteins; hence they are more challenging for SMA to penetrate. The AO- and His-modified SMA polymers (**1**, **4**, **5**, 2% w/v) efficiently solubilize *E. coli* membranes at levels comparable to SMA2000 and SZ30010, which have styrene to maleic acid ratios of 2:1 and 2.3:1, respectively. The AO2 derivatives of the latter alternating SMAs are also similarly effective, while unmodified SMA(1:1) offers slightly lower total protein yields (Fig. 2.13).

The purification of an *E. coli* outer membrane protein PagP was tested using the panel of SMA copolymers. PagP, a transmembrane β-barrel enzyme, modifies lipopolysaccharide, functions as a monomer and has been structurally characterized [28, 29]. The PagP protein was overexpressed in *E. coli* with an N-terminal signal sequence for specific delivery into the outer membrane as well as a C-terminal His6 tag to aid in purification. The outer membrane was isolated by sucrose density gradients [30], solubilized using the various copolymers followed by purification by Ni-NTA resins and gel filtration chromatography (Fig. 2.14). PagP, 20 kDa protein band, appeared principally as a monomer after purification with His-SMA 1. The AO2 and AO3 derivatives of SMA1000 (**4** and **5** yielded less protein, while the AO2 derivative of SMA2000 produced the most combination of PagP oligomers. The conventional SMA varieties, including SMA2000 and SZ30010, as well as an AO2 derivative of the latter, yielded a ladder of additional multimeric states. Detergent-solubilized PagP, reportedly, displays similar aggregation behavior in SDS-PAGE. Thus His substituted SMA appears to act as state-specific solubilizers while AO modifications enhance total protein yield. We, however, were not

able to purify any of the oligomeric states of PagP using affinity purification and SEC chromatography.

Native nanodisc dimensions: The AO-SMALP-PagP and His-SMALP-PagP nanodiscs were further used for TEM imaging and revealed a relatively large and homogeneous population of discs with diameters of around 20 nm (Fig. 2.15), which is in alignment with our DLS data (Fig. 2.11).
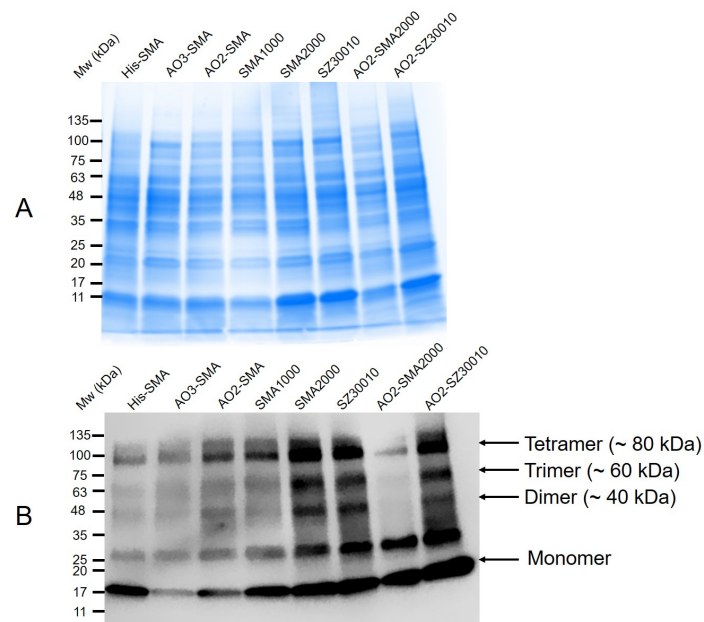
Figure 2.13. The efficiency of different SMA polymers (2% w/v) in solubilizing biological membranes were compared. A. The SDS-PAGE gel shows total crude proteins extracted from *E. coli* outer membrane by different copolymers before purification. B. The immunoblot (probed for His tags) indicates the amount of PagP protein monomer and multimer states solubilized directly from the outer membranes using each polymer. All samples were heated in sample buffer before running on SDS-PAGE. The band at 25 kDa may represent dimer PagP that is not fully unfolded after heating, hence shows different electrophoretic mobility than both fully folded dimeric PagP and fully unfolded monomeric PagP.
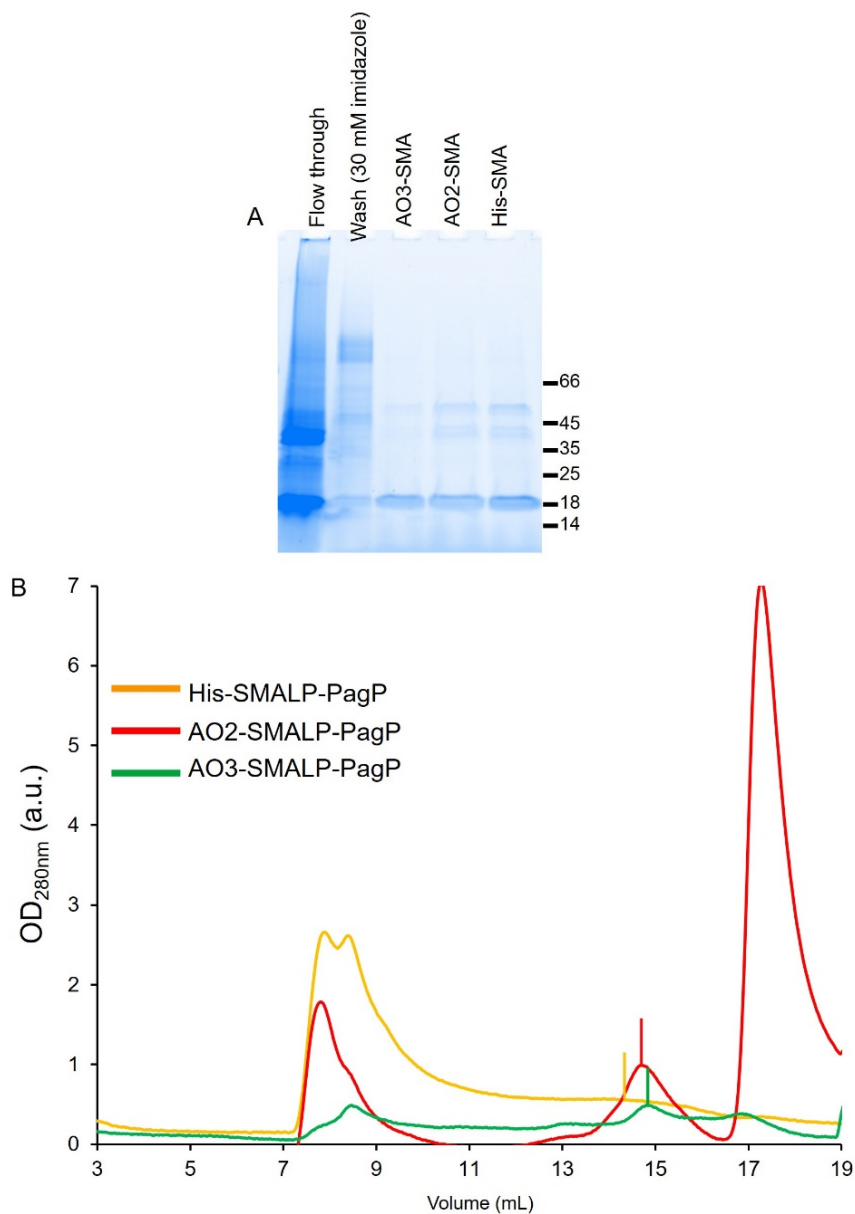
Figure 2.14. A. Detergent-free affinity purification of His-tagged PagP from the outer membrane of *E. coli* using AO-SMA (**4, 5**) and His-SMA (**1**). SMALP-PagP discs were eluted with 250 mM imidazole and visualized on stain-free gels. B. SEC profiles of PagP native nanodiscs composed of different newly developed polymers. Lines indicate the fractions that contain His-tagged PagP nanodiscs.
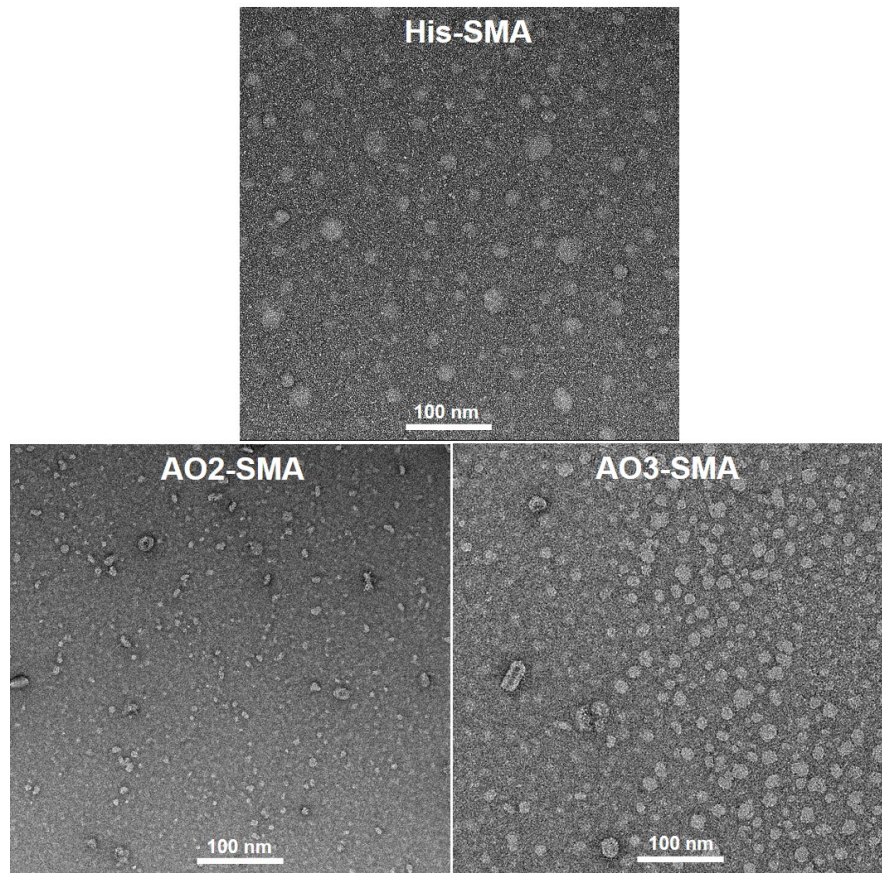
Figure. 2.15. Negative stain electron micrographs of nanodiscs of PagP- containing *E. coli* outer membrane solubilized in 1.5% (w/v) AO2-SMA (**4**), AO3-SMA (**5**) and His-SMA (**1**) polymers. The diameters of discs are between 15-25 nm. The scale bar is 100 nm. The concentration of PagP nanodiscs made by AO2-SMA were less concentrated than those formed by either AO3-SMA or His-SMA; hence fewer nanodiscs are imaged in PagP-AO2-SMA micrograph. This observation may imply that AO2-SMA can not solubilize biomembrane as efficiently as the other two polymers.

In summary, a family of novel copolymers has been designed by derivatizing SMA with AO and His groups in order to integrate multiple advantageous features in a single formulation. This solves three major issues which were limiting the utility of nanodisc technology. The incorporation of AO and His sidechains during SMA activation endows the polymers with intrinsic fluorescence without needing to add labels retrospectively. This

60

ensures that the low polydispersity of AO and His modified SMA(1:1) copolymers is maintained, while also allowing incorporation of these multifunctional sidechains into potentially any SMA copolymer that allows efficient membrane solubilization. These sidechains could be applied to other native nanodisc-forming polymers, including DIBMA [13], which have different hydrophobic groups but retain the maleic anhydride handle. The presence of readily detectable SMA variants provides an avenue for developing arrays of nanosensors and screening platforms for memteins of diverse sizes and activities.

2.4. Conclusions

We synthesized two novel series of SMA polymers through conjugation of small amphoteric side chains to maleic anhydride co-monomers. We showed that these functionalized AO and His variants of SMA exhibit improved buffer capacity and enhanced tolerance to divalent cations, and they form relatively larger lipid nanodiscs in solution. The novel SMA formulations can readily be used for purification of membrane proteins into native nanodiscs, as we examined the purification and characterization of a bacterial outer membrane enzyme, PagP, using these modified polymers. In terms of their optical properties, AO and His grafted SMA(1:1) polymers display useful fluorescence emissions with maxima at 425 nm and quantum yields of 2% and 1%, respectively.

Since His-SMA(1:1) and SMA(1:1) have the same excitation and emission profiles (λ_{max} excitation 320 nm, λ_{max} emission 420 nm), we conclude that incorporation of imidazole side chains has the least effect on the fluorescence originated from the backbone. In other words, the fluorescence of His-SMA is due to the backbone phenyl group. In contrast, the fluorescence properties (QY, $\lambda_{max,}$ excitation 350 nm and $\lambda_{max,}$

emission 450 nm) of AO2 and AO3-SMA polymers (**4, 5**) is distinguished from both

SMA(1:1) and His-SMA, suggesting that fluorescence property of AO-SMA polymers (**4, 5**) stems from the AO-side chains. It seems that heating (130 °C, 4 hours) affects the

fluorescence property of AO-SMA. Further exploration is needed to fully characterize the

closure state of maleamic acid groups in AO-SMA (**4,5**) polymers and to determine the

origin of fluorescence in these two polymers.

The AO and His moieties can be similarly incorporated into non-alternating SMA

polymers. Moreover, the fluorescence output is independent of the closure state of

maleimide ring, is stable over time, and persistent over diverse solution conditions and

upon interaction with lipid vesicles.

2.5. Experimental section

2.5.1. Polymer synthesis

His-SMA polymer product 1 was synthesized by slowly adding 9 mmol of

histamine (dissolved in water) to SMAn(1:1) in DMF for 10 hours at room temperature.

The product was precipitated with diethyl ether/water, dissolved in 1 M NaOH, pH

adjusted to 8 and lyophilized. (Scheme 2.1). The AO reagents, 1,3-propanediamine, N,

N-dimethyl, N-oxide and N,N-dimethyl ethyl, were synthesized by oxidation of their

corresponding tertiary amines N, N-dimethyl,1,3-propanediamine and N,N-over time

(Sigma-Aldrich) [18]. The products were dried and stored under vacuum. The AO

structures were confirmed by electrospray ionization mass spectrometry (ESI-MS) and

ATR-FTIR. The AO compounds were grafted onto SMAn(1:1) in dimethylformamide

(DMF). The polymers were precipitated first by diethyl ether, and then by HCl (pH < 3).

Pellets were solubilized in NaOH (0.5 M), the pH was adjusted to 8, and polymers were dried under vacuum.

Preparation of SMALPs. Multilayer vesicles (MLV) solutions of 5 mM DMPC (Avanti Polar Lipid) were prepared in 100 mM NaCl, Tris 10 mM, pH 8.0. Stock solutions of polymers (10% w/v, filtered) were prepared in 10 mM Tris, pH 8.0 and were added to the lipid vesicles and incubated at room temperature (23-25 °C) until clarification. Fresh solutions of unilamellar DMPC vesicles were prepared before each experiment, as described [31]. Briefly, the MLV vesicles were prepared in a sonicator (Branson) on ice for 4 min at 45% W, in 5 sec on, 5 sec off cycles. The resulting MLVs (average diameter of 135 nm) were then mixed with different concentrations of polymers and incubated for eleven hours at room temperature.

2.5.2. Dynamic light scattering

The DLS measurements of the SMALPs were performed at 25 °C using a Zetasizer Nano ZSP (Malvern Panalytical) with 3 mm cuvettes. All experiments were repeated three independent times, each with a 12 scan average. Data was analyzed using a Zetasizer software version 7.12.

2.5.3 Calcium and pH sensitivity of SMA(1:1) derivatives

Buffers at different pH and $CaCl_2$ levels were prepared [32], polymer (2% w/v stock solution in water) was added to each sample (final concentration of polymer 0.5 % w/v) and optical density (OD) of solutions was monitored at 600 nm with three replicates.

2.5.4. NMR spectroscopy

The ^{31}P NMR spectra of lipids were acquired using a Varian VNMRS 600 MHz NMR spectrometer and 5 mm indirect detection broadband z-PFG probe. Experiments were performed with a 20 ms 90º pulse, broadband ^{1}H WALTZ decoupling, 1024 scans, and 1 s repetition delay. NMR spectra were referenced by setting the H_3PO_4 (100%) signal to 0 ppm. The standard ^{31}P observation pulse sequence, which includes ^{1}H WALTZ decoupling sequence, was used to detect any ^{31}P signals from both protonated and non-protonated ^{31}P nuclei.

2.5.5. Fluorescence spectrophotometry

Stock solutions of polymers were prepared in deionized water and diluted to desired concentrations. Emission fluorescence spectra (bandwidth 10 nm) were monitored at excitation wavelengths 350 nm and 320 nm (bandwidth 5 nm) on a Varian Cary Eclipse and ATR-FTIR (Nicolet 8700) spectrophotometers. The effects of titrating in stock solutions of NaOH/HCl (1 M), $CaCl_2$ (20 mM) and DMPC (10 mM) followed by 1 min incubation at room temperature on the emission spectra of each sample were examined after correction for dilution.

2.5.6. Quantum yield (QY) calculations

The QY of each polymer was calculated relative to quinine bisulfate (QS) at their maximum excitation wavelengths. In brief, a solution of QS ($A_{320nm} = 0.01$) in 0.1 N sulfuric acid was used as a reference standard. The absorbance versus integrated fluorescence intensity (F.I.) plots with zero intercept show that this concentration of QS fits well in the linear part of plots. Stock solutions of polymers were prepared in dH_2O (pH 7.0) and

diluted to an OD320nm or $OD_{350\ nm}$ of 0.2-0.3. The emission spectra were collected in triplicate between 350-600 nm and 375-600 nm, respectively. Data were analyzed in GraphPad Prism8 software [33] using:

$$\frac{F_{polymer}}{A_{polymer}\ \phi_{polymer}} = \frac{F_S}{\phi_S\ A_S} \qquad\qquad \text{Equation.1}$$

Where $F_{polymer}$ is the integrated fluorescent intensity of polymers, $A_{polymer}$ is the absorption of polymers and $\phi_{polymer}$ defines the quantum yield of polymers. F_S, A_S and ϕ_S are integrated fluorescent intensity, absorbance and quantum yield of quinine sulfate.

Purification of PagP from *E. coli* outer membrane. The plasmid pETCrcAH expresses a C-terminal His6 tagged PagP, which encodes the native 22 residue signal peptide that is cleaved during targeting to the outer membrane, after induction with isopropyl-β-D-thiogalactopyranoside in *E. coli* BL21(DE3)*pLysE* grown in broth at 37 °C (30). The outer membranes from French Press lysates of bacterial cells were isolated by ultracentrifugation of the crude membrane fraction at 195,000×g (Ti45 rotor, Beckman) in 55% (w/v) sucrose (in Tris 10 mM, pH 8.0). The outer membranes were then incubated with 2% (w/v) of each polymer in Tris 10 mM pH 8.0, 100 mM NaCl, 5% (v/v) glycerol for 30 min at 37 °C followed by overnight incubation at 4 °C. The suspension was centrifuged at 58,000×g and the soluble PagP discs were purified using HisPur Ni-NTA resins (Thermo Scientific™) [34]. Fractions containing PagP were eluted with 250 mM imidazole, pooled, and separated over a Sephadex® 200 10/300 GL column (GE).

2.5.7. SDS-PAGE electrophoresis and Western blotting

Total membrane lysates and purified PagP samples were mixed in 2X sample buffer (Bio-Rad) and boiled for 10 mins at 95 °C. Samples were next loaded on 10% precast stain-free SDS-PAGE gels (Bio-Rad) [35]. The resolved proteins were transferred to polyvinylidene difluoride (PVDF) membrane (Bio-Rad) for blotting. The membrane was blocked in fish gelatin (2% w/v) in Tris Buffer Saline (TBS) + 0.1% (v/v) Tween20. His-tagged PagP was detected using HisProbe™-HRP conjugate (1:6000, Pierce). The fluorescence was detected using Clarity™- ECL substrate (Bio-Rad) on a Li-Cor Odyssey image system, and the intensity of bands was estimated using Li-Cor software. Polyclonal rabbit anti-histamine antibody (Sigma-Aldrich) was (diluted 1:13,000) in fish gelatin (2% w/v) in TBS and incubated for one hour at room temperature. After three washes with TBS and Tween20 (0.1% v/v), the membrane was incubated with HRP conjugated goat anti-rabbit secondary antibody for one hour.

2.5.8. Transmission electron microscopy (TEM) of PagP SMALPs

Carbon-coated copper grids with a 400 nm-mesh (Electron Microscopy Science, USA) were glow charged using an Pelco Easy Glow 100 x glow discharge unit (Ted Pella Inc, USA) for 30 seconds. Microliter amounts of either the NTA-column-purified PagP or fractions from size exclusion chromatography were adsorbed on the grids for 1 min. The grids were washed three times (3×50 µL) with filtered deionized water and stained with filtered 2% (w/v) uranyl acetate. Excess stain was removed using a filter paper and the grids were air-dried for at least two hours before TEM imaging. EM micrographs were collected using a Tecnai G20 transmission electron microscope (FEI Eindhoven, NL; an

acceleration voltage of 200 kV), which is equipped with an Eagle 4 k × 4 k CCD camera (FEI company).

2.6. References

[1] M. Overduin, M. Esmaili, Memtein: The fundamental unit of membrane-protein structure and function, Chem Phys Lipids, 218 (2019) 73-84.

[2] T.J. Knowles, R. Finka, C. Smith, Y.P. Lin, T. Dafforn, M. Overduin, Membrane proteins solubilized intact in lipid containing nanoparticles bounded by styrene-maleic acid copolymer, J Am Chem Soc, 131 (2009) 7484-7485.

[3] C. Sun, S. Benlekbir, P. Venkatakrishnan, Y. Wang, S. Hong, J. Hosler, E. Tajkhorshid, J.L. Rubinstein, R.B. Gennis, Structure of the alternative complex III in a supercomplex with cytochrome oxidase, Nature, 557 (2018) 123-126.

[4] W. Qiu, Z. Fu, G.G. Xu, R.A. Grassucci, Y. Zhang, J. Frank, W.A. Hendrickson, Y. Guo, Structure and activity of lipid bilayer within a membrane-protein transporter, Proc Natl Acad Sci USA, 115 (2018)12985-12990.

[5] T. Laursen, J. Borch, C. Knudsen, K. Bavishi, F. Torta, H.J. Martens, D. Silvestro, N.S. Hatzakis, M.R. Wenk, T.R. Dafforn, C.E. Olsen, M.S. Motawia, B. Hamberger, B.L. Møller, J.E. Bassard, Characterization of a dynamic metabolon producing the defense compound dhurrin in sorghum, Science, 354 (2016) 890-893.

[6] M. Overduin, B. Klumperman, Advancing membrane biology with poly(styrene-co-maleic acid)-based native nanodiscs., Eur Polymer J., 110 (2018) 63-68.

[7] T. Ravula, N.Z. Hardin, S.K. Ramadugu, A. Ramamoorthy, PH Tunable and Divalent Metal Ion Tolerant Polymer Lipid Nanodiscs, Langmuir, 33 (2017) 10655-10662.

[8] S. Hall, C. Tognoloni, J. Charlton, É. Bragginton, A. Rothnie, P. Sridhar, M. Wheatley, T. Knowles, T. Arnold, K. Edler, D. TR., An acid-compatible co-polymer for the solubilization of membranes and proteins into lipid bilayer-containing nanoparticles., Nanoscale, 10 (2018) 10609-10619.

[9] T. Ravula, N.Z. Hardin, S.K. Ramadugu, S.J. Cox, A. Ramamoorthy, Formation of pH-Resistant Monodispersed Polymer-Lipid Nanodiscs, Angew Chem Int Ed, 57 (2018) 1342-1345.

[10] T. Ravula, S.K. Ramadugu, G. Di Mauro, A. Ramamoorthy, Bioinspired, Size-Tunable Self-Assembly of Polymer–Lipid Bilayer Nanodiscs, Angew Chem Int Ed, 56 (2017) 11466-11470.

[11] M.C. Fiori, Y. Jiang, G.A. Altenberg, H. Liang, Polymer-encased nanodiscs with improved buffer compatibility, Sci Rep, 7 (2017) 7432.

[12] S. Lindhoud, V. Carvalho, J.W. Pronk, M.E. Aubin-Tam, SMA-SH: Modified Styrene-Maleic Acid Copolymer for Functionalization of Lipid Nanodiscs, Biomacromolecules, 17 (2016) 1516-1522.

[13] A.O. Oluwole, J. Klingler, B. Danielczak, J.O. Babalola, C. Vargas, G. Pabst, S. Keller, Formation of Lipid-Bilayer Nanodiscs by Diisobutylene/Maleic Acid (DIBMA) Copolymer, Langmuir, 33 (2017) 14378-14388.

[14] A. Grethen, A.O. Oluwole, B. Danielczak, C. Vargas, S. Keller, Thermodynamics of nanodisc formation mediated by styrene/maleic acid (2:1) copolymer, Sci Rep, 7 (2017) 11517-11531.

[15] O. Korotych, J. Mondal, K.M. Gattás-Asfura, J. Hendricks, B.D. Bruce, Evaluation of commercially available styrene-co-maleic acid polymers for the extraction

of membrane proteins from spinach chloroplast thylakoids, Eur Polymer J., 114 (2019) 485-500.

[16] K.A. Morrison, A. Akram, A. Mathews, Z.A. Khan, J.H. Patel, C. Zhou, D.J. Hardy, C. Moore-Kelly, R. Patel, V. Odiba, T.J. Knowles, M.U. Javed, N.P. Chmel, T.R. Dafforn, A.J. Rothnie, Membrane protein extraction and purification using styrene-maleic acid (SMA) copolymer: effect of variations in polymer structure, Biochem J, 473 (2016) 4349-4360.

[17] N. Kielland, M. Vendrell, R. Lavilla, Y.T. Chang, Imaging histamine in live basophils and macrophages with a fluorescent mesoionic acid fluoride, Chem Commun, 48 (2012) 7401-7403.

[18] G.L.K. Hoh, D.O. Barlow, A.F. Chadwick, D.B. Lake, S.R. Sheeran, Hydrogen Peroxide Oxidation of Tertiary Amines, J Am Oil Chem Soc, 40 (1963) 268-271.

[19] M.K. Trivedi, A.B. Dahryn Trivedi, G.N. Gunin Saikia, Physical and Structural Characterization of Biofield Treated Imidazole Derivatives, Nat Prod Res, 3 (2015)1-8.

[20] C.P. Wong, P.J. Miller, Vibrational spectroscopic studies of alane, J Energ Mater, 23 (2005) 169-181.

[21] J. Coates, Interpretation of infrared spectra, a practical approach, Encyclopedia of analytical chemistry: applications, theory and instrumentation, (2006) 1-23.

[22] L. Conley, Y. Tao, A. Henry, E. Koepf, D. Cecchini, J. Pieracci, S. Ghose, Evaluation of eco-friendly zwitterionic detergents for enveloped virus inactivation, Biotechnol Bioeng, 114 (2017) 813-820.

[23] L. Hou, H. Zhang, H. Chen, Q. Xia, D. Huang, L. Meng, X. Liu, Synthesis and surface properties of N, N-dimethyl-N-dodecyl polyoxyethylene amine-based surfactants: Amine oxide, betaine and sulfobetaine, J Surfactants Deterg, 17 (2014) 403-408.

[24] A.O. Oluwole, A. Meister, J.O. Babalola, C. Vargas, S. Keller, Membrane Proteins Solubilization of Membrane Proteins into Functional Lipid-Bilayer Nanodiscs Using a Diisobutylene / Maleic Acid Copolymer, Angew.chem.Int.Ed 56 (2017) 1919-1924.

[25] C. Wurth, M. Grabolle, J. Pauli, M. Spieles, U. Resch-Genger, Relative and absolute determination of fluorescence quantum yields of transparent samples, Nat Protoc, 8 (2013) 1535-1550.

[26] J. Yang, C.-C. Dong, X.-L. Chen, X. Sun, J.-Y. Wei, J.-F. Xiang, J.L. Sessler, H.-Y. Gong, Excimer Disaggregation Enhanced Emission: A Fluorescence "Turn-On" Approach to Oxoanion Recognition, J. Am. Chem. Soc, 141(2019) 4597-4612.

[27] S.C.L. Hall, C. Tognoloni, G.J. Price, B. Klumperman, K.J. Edler, T.R. Dafforn, T. Arnold, Influence of Poly(styrene- co-maleic acid) Copolymer Structure on the Properties and Self-Assembly of SMALP Nanodiscs, Biomacromolecules, 19 (2018) 761-772.

[28] R.E. Bishop, The lipid A palmitoyltransferase PagP: molecular mechanisms and role in bacterial pathogenesis, Mol Microbiol, 57 (2005) 900-912.

[29] G.H.M. Huysmans, S.E. Radford, D.J. Brockwell, S.A. Baldwin, The N-terminal helix is a post-assembly clamp in the bacterial outer membrane protein PagP, J Mol Biol, 373 (2007) 529-540.

[30] R.E. Bishop, H.S. Gibbons, T. Guina, M.S. Trent, S.I. Miller, C.R.H. Raetz, Transfer of palmitate from phospholipids to lipid A in outer membranes of Gram-negative bacteria, EMBO J, 19 (2000) 5071-80.

[31] N.J. Cho, L.Y. Hwang, J.J.R. Solandt, C.W. Frank, Comparison of Extruded and Sonicated Vesicles for Planar Bilayer Self-Assembly, Materials, 6 (2013) 3294-3308.

[32] M.C. Fiori, Y. Jiang, G.A. Altenberg, H. Liang, Polymer-encased nanodiscs with improved buffer compatibility, Sci Rep, 7 (2017) 1-10.

[33] G.L.K. Hoh, D.O. Barlow, A.F. Chadwick, D.B. Lake, S.R. Sheeran, Hydrogen peroxide oxidation of tertiary amines, J Am Oil Chem Soc, 40 (1963) 268-271.

[34] S.C. Lee, T.J. Knowles, V.L.G. Postis, M. Jamshad, R.A. Parslow, Y.-p. Lin, A. Goldman, P. Sridhar, M. Overduin, S.P. Muench, T.R. Dafforn, A method for detergent-free isolation of membrane proteins in their local lipid environment, Nat Protoc, 11 (2016) 1149-1162.

[35] K.J. Laurie, A. Dave, T. Straga, E. Souzeau, T. Chataway, M.J. Sykes, T. Casey, T. Teo, J. Pater, J.E. Craig, S. Sharma, K.P. Burdon, Identification of a novel oligomerization disrupting mutation in CRYAlphaA associated with congenital cataract in a South Australian family, Hum Mutat, 34 (2013) 435-438.

Chapter 3

Nanodiscs of Native Membrane Generated by Methyl-Substituted Stilbene-*alt*-Maleic Acid Copolymers with Minimal Polydispersity and Dynamics

3.1. Significance

The ability of synthetic polymers to spontaneously convert biological membranes into native nanodiscs has introduced a turning point in structural biology. However, the commonly used styrene-*co*-maleic acid (SMA) polymers exhibit relatively high polydispersity, backbone mobility, and semi-random sidechain distributions that limit nanodisc homogeneity and the resolution of protein: lipid complexes in SMA lipid particles (SMALPs). Herein we show that certain stilbene-*alt*-maleic acid (STMA) copolymer derivatives offer an improved system for forming native nanodiscs that are relatively monodispersed and have broader utility in a range of physiological solutions. Methyl-substituted STMA copolymers spontaneously solubilize vesicles across a wide pH range and obviate any need for conventional detergents, which typically strip away biological lipids. Moreover, these STMA derivatives convert raw bacterial outer membranes into homogeneous nanodiscs that can be used to purify the outer membrane protein assemblies such as the PagP palmitoyltransferase. STMA derivatives form regular nanodiscs that can be readily resolved by negative stain electron microscopy (EM). Methyl-substituted STMA derivatives have sterically restricted backbone, contain strictly alternating sidechains, and can effectively solubilize lipid bilayers to form ~20 nm membrane protein-containing nanodiscs for high-resolution structural analysis. Moreover, their maleimide groups offer convenient handles for further derivation with functional groups such as affinity labels and fluorophores.

3.2. Introduction

The development of native nanodiscs [1] that solubilize membrane: protein assemblies within SMA polymers [2] has stimulated researchers to synthesize various polymers [3] to expand the applications of this technology further. Many of these polymers contain random sequence distributions of hydrophilic and hydrophobic sidechains and size ranges of 5-10 kDa. The homopolymerization of either or both monomer building blocks contribute to sequential polydispersity and can lead to undesirable nonspecific interactions with proteins or polycations rather than lipids in a bilayer. The homopolymerization of styrene [4] in styrene-*co*-maleic acid (SMA) copolymers results in statistically random distributions of polystyrene dyads and triads, therefore sequential heterogeneity along the polymer chains. On the other hand, the rate of homopolymerization of maleic anhydride (MAn) and the chance of formation of MAn-MAn dyads is lower [5]. As a result, SMA polymers generally lack a well-defined, regular chain architecture. Besides, high backbone flexibility and irregularity also contribute, yielding polymers that are prone to aggregation in aqueous solution and exhibit batch variability. This prevents their efficient application in biological and medical applications that depend on chemically well-defined compositions.

It remains a critical challenge to overcome the heterogeneity problems of SMA copolymers that are most widely used to form native nanodiscs. This would reduce the formation of large aggregates and improve purification of specific membrane protein states. Once in stable and homogenous nanodiscs, the memteins would be better suited for downstream functional and structural characterization using methods including cryo-electron microscopy (cryo-EM), which can provide near-atomic resolution of memteins [6, 7].

Here, we investigated whether an alternating stilbene monomer could replace the conventional non-alternating styrene monomers. The stilbene subunit also contains phenyl moieties but form more structurally restrained polymers [8] that could further stabilize and regularize nanodiscs. Synthesis and derivatization of STMA copolymers can occur either using *cis* (using *Z*-stilbene) or *trans* (using *E*-stilbene) configurations [5], with the latter reacting more readily with maleic anhydride units and resulting in more stable products (Fig. 3.1) [9]. Semi-rigid and strictly alternating unsubstituted STMA and a set of derivatives were synthesized *via* radical polymerization. These copolymers mimic the chemical composition of the most effective SMA polymers that offer a 2:1 styrene to maleic acid ratio. However, the STMA polymers differ in terms of steric hindrance of the pair of pendant phenyl groups gives rise to a more rigid polymer backbone as well as their strict alternation of monomers. Specific methyl derivatives of STMA are shown to enhance nanodisc solution behavior and homogeneity and represent an improved generation of polymers for maximizing structural resolution.
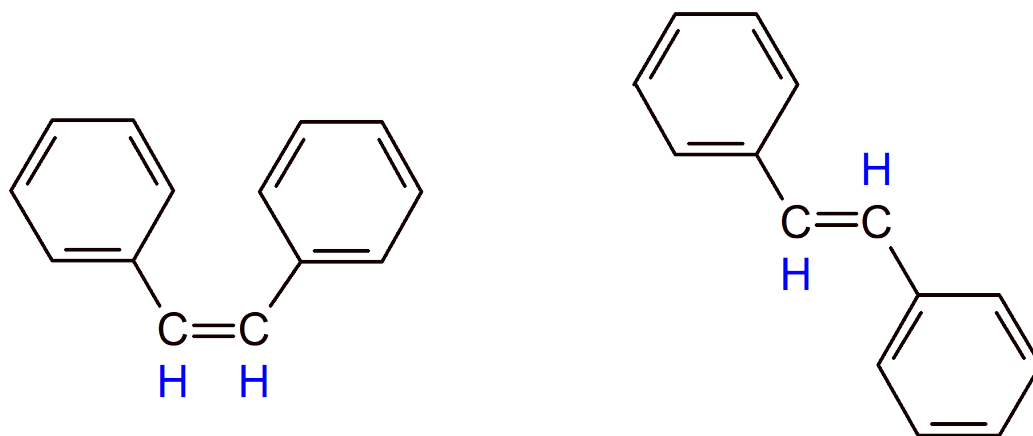
Figure 3.1. *Cis* (left) and *trans* (right) configurations of stilbene monomer.

3.3. Experimental section

3.3.1. Materials

SMA2000 (anhydride form) was purchased from Cray Valley (USA). Other reagents were obtained from Sigma-Aldrich unless stated otherwise.

3.3.2. Synthesis of polymers

All STMA polymers were synthesized in 2010 and shared with us in 2018 [10]. Please see Appendix 1 for detailed synthesis protocols.

3.3.3. Activation and characterization of stilbene-*alt*-maleic anhydride polymers

SMA2000 (anhydride form) and all stilbene-maleic anhydride polymers were acid hydrolyzed (in NaOH) and activated to maleic acid forms as described in reference [9]. Before lyophilization, the pH of each sample was adjusted to 8. Dried polymers were stored at room temperature. The conversion was verified using FT-IR.

3.3.4 Membrane isolation and preparation of native PagP in STMA nanodiscs

A His$_6$-PagP construct in pET21b vector was overexpressed in the outer membrane of *E. coli* BL21 (DE3) *pLysS* and the crude membrane and outer membrane were isolated used high-speed centrifugations according to previous reports. The crude membrane was used for solubilization assays and the outer membrane was further used for the preparation of STMA nanodiscs containing PagP.

The concentration of polymer was maintained at 0.5% w/v, while SMA2000 was used at a 1% w/v concentration based on previous reports. Para-methyl stilbene-maleic acid (**3**) and ortho-methyl stilbene-maleic acid (**4**) were incubated with 10 mL of ~80 mg/mL of outer membrane suspension (in Tris 10 mM, 100 mM NaCl, 5% v/v glycerol pH 8.0) for

30 min at 37° C followed by overnight incubation at cold room. The soluble fraction was next used for His-affinity batch purification using Ni-NTA HisPur resins. After washing the column with 10 and 30 mM imidazole (in 10 mM Tris and 100 mM NaCl), the protein was eluted with 250 mM imidazole. Fractions of each step of purification were collected, and the boiled samples in 2X sample buffer (Bio-Rad) were analyzed by SDS-PAGE (12% precast gel; Bio-Rad) and Western blot (PVDF membrane; Bio-Rad) probed with anti-His tag probe (Peirce).

Using Sephadex S200 10/300 GL (GE), PagP-stilbene-maleic acid nanodiscs were further purified according based on their size in Tris 10 mM, 100 mM NaCl, glycerol 5% (v/v) buffer. Fractions were used for TEM imaging.

3.3.5. Electron microscopy of PagP-stilbene MA nanodiscs

Samples containing PagP-stilbene maleic acid nanodiscs were directly (no concentration needed) used for negative staining electron microscopy. Sample was applied to glow-charged 400 nm-mesh carbon-coated copper grids (Electron Microscopy Science, USA) and let it absorb for 1 min. The grids were then washed three times with deionized water and stained with 2% (w/v) uranyl acetate (filtered, 0.45 μm). The grids were air-dried at least for two hours before imaging. The EM micrographs were collected using Tecnai G20 transmission electron microscope (FEI Eindhoven, NL; an acceleration voltage of 200 kV) equipped with an Eagle 4 k × 4 k CCD camera (FEI).

3.3.6. NMR data acquisition

Large unilamellar vesicle (LUV) of Dimyristoylphosphatidylcholine (DMPC) lipids (3.5 mM in Tris 10 mM, 100 mM NaCl) were incubated with 2% (w/v) of methyl stilbene- MA copolymers at 37 ºC and entirely clarified samples were used for data collection at 40 ºC.

^{1}H NMR and ^{31}P NMR spectra were acquired using a Varian VNMRS 600 MHz NMR spectrometer using 5 mm high-field indirect detection broadband PFG probe. Experiments were performed with 20 ms 90º pulse, broadband ^{1}H WALTZ decoupling, 1024 scans, and 1 s repetition delay were used in experiments. NMR spectra were referenced by setting ^{31}P chemical shift of 100% H_3PO_4 sample to 0 ppm. Spectra were collected in HEPES 10 mM, pH 8.0, 100 mM NaCl.

3.3.7. The Sensitivity of stilbene-maleic acid (MA) copolymers to pH and divalent cations

The concentration of polymers in each test was kept constant (0.5% w/v). All buffers were prepared according to reference 12**.** Briefly, sodium acetate (50 mM; pH 4 and 5) and tris buffer (50 mM; pH values of 6, 8, 10) were supplemented with 100 mM NaCl and used for pH sensitivity assays. The sensitivity of stilbene-MA (**3**) and (**4**) to divalent cations was tested in Tris buffer (pH 8.0, NaCl 100 mM) in the presence of increasing concentrations of $CaCl_2$ (2.5, 5, 7.5 and 10 mM).

3.4. Results and discussion

3.4.1. Synthesis and characterization of STMA polymers

The hydrophobic bulk of stilbenes is conducive to membrane insertion but limits water solubility. Hence the STMA polymers were synthesized by free-radical polymerization of

the substituted stilbene and maleic anhydride reactants [10] purified by size exclusion chromatography and then hydrolyzed into maleic acid forms. Five STMA polymers containing methyl or carboxylate substituents were activated by NaOH in aqueous solution, as was a control SMA2000 polymer that is known to form native nanodiscs [1] (Fig. 3.2). The conversion of maleic anhydride groups to maleic acids to form the water-soluble product was confirmed FT-IR (Fig. 3.3). All activated stilbene MA polymers were soluble at Tris 10 mM pH 8.0 [11, 12] and with 100 mM NaCl.
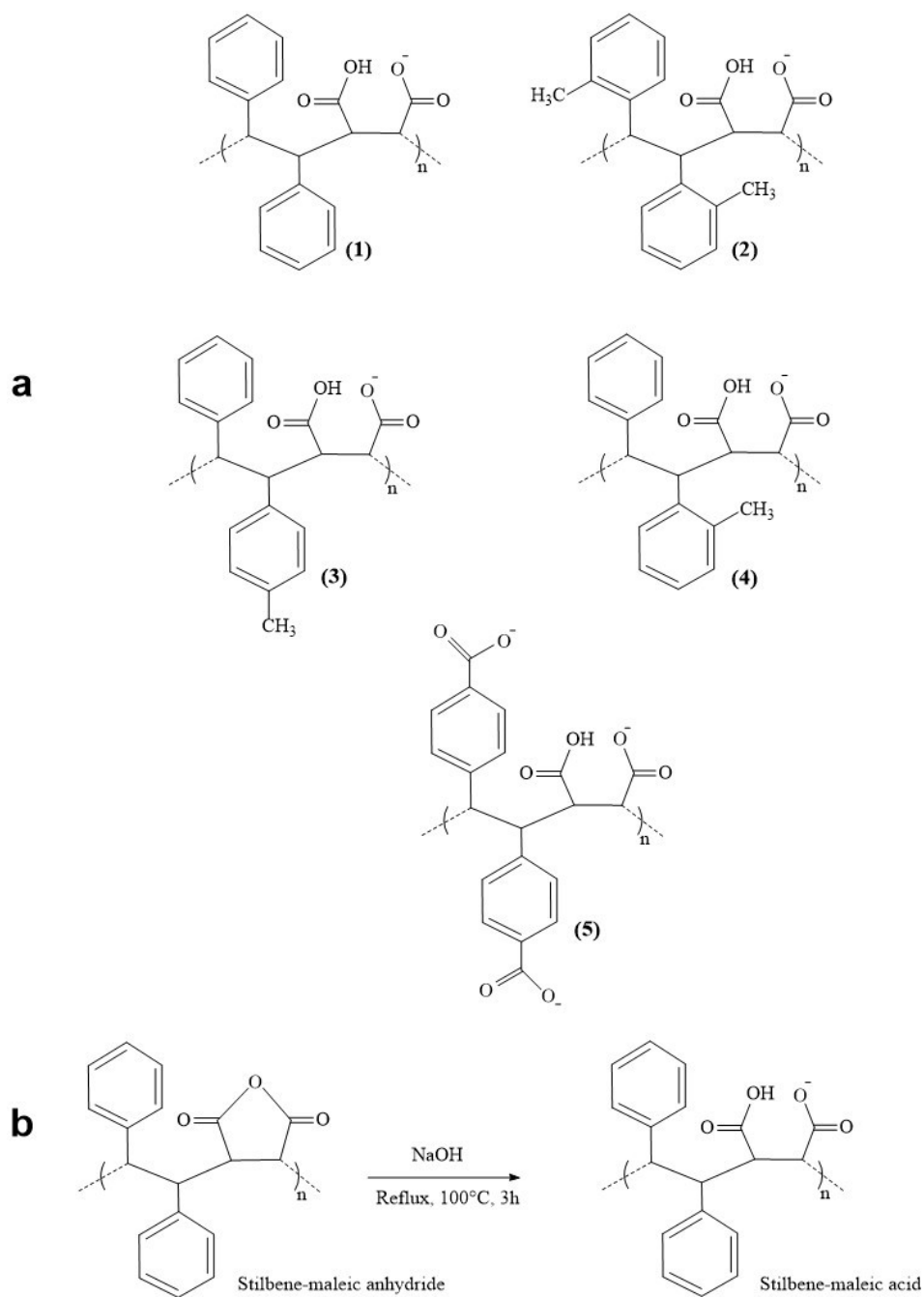
Figure 3.2. a. Chemical structures of different formulations of stilbene-maleic acid (**1**), methyl stilbene-*alt*-maleic acid in para (**3**), ortho (**2, 4**) configurations and dicarboxylate stilbene-maleic acid (**5**) polymers. b. The reaction for activating all the STMA polymers used here is shown.
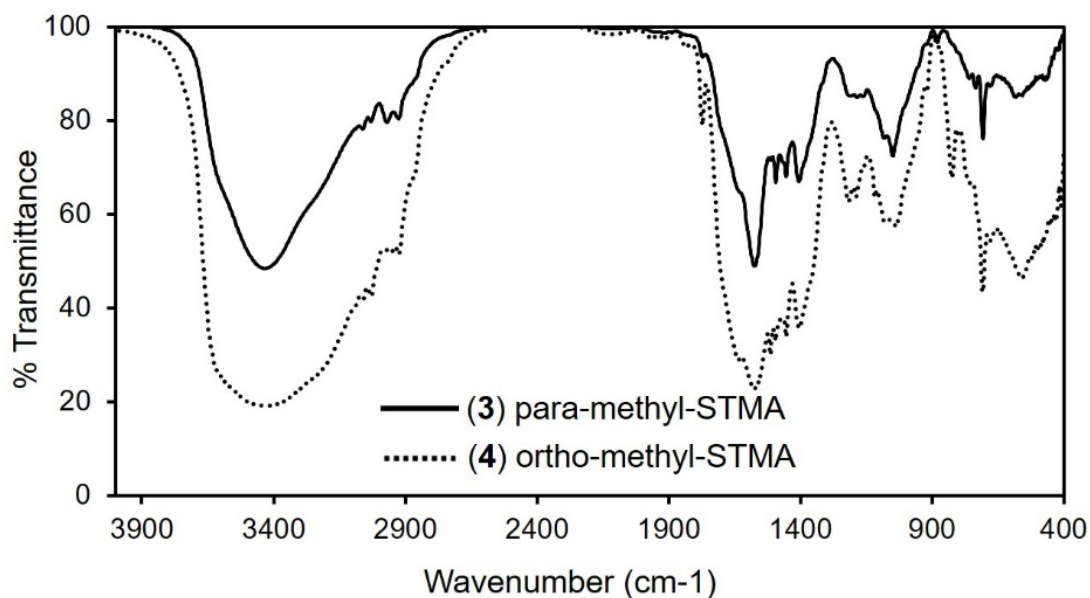
Figure 3.3. FT-IR spectra of 4-methylstilbene-*alt*-maleic (**3**) acid and 2-methylstilbene-*alt*-maleic acid (**4**).

The size of polymers ranges between 4-6 kDa, except dicarboxylate-stilbene-alt-maleic anhydride (**5**) (40 kDa) (Table 3.1). The *ortho*-methyl substituted stilbene-MA (**4**) copolymer is the most homogenous (PDI 1.1), while both methylated stilbene-MA derivatives (**3**) and (**2**) have similar PDIs (~1.5).

Polymer Number, Name, Abbreviation	M_n(kDa)	PDI
(**1**) stilbene-*alt*-maleic anhydride, STMA	nd	nd
(**2**) di-*ortho*-methyl-STMA, doMe-STMA	5.1	1.52
(**3**) *para*-methyl-STMA, pMe-SMTA	5.8	1.54
(**4**) *ortho*-methyl-SMTA, oMe-STMA	4.4	1.19
(**5**) di-*para*-carboxylate-STMA, CO2-STMA	40	1.43

*nd: Not determined.

Table 3.1. A list of some properties of different stilbene-maleic acid (MA) copolymers (**1-5**) that have been synthesized and tested for the formation of lipid-protein nanodiscs. Since (**1**) is insoluble in THF, Mn and PDI values were not determined.

To test whether STMA polymers spontaneously form nanodiscs from lipid bilayers, we examined whether they directly solubilized vesicles composed of dimyristoylphosphatidylcholine (DMPC). The polymer concentrations used were comparable to that of the widely used SMA2000 polymer (1-2% w/v). Surprisingly, only methyl-STMA compounds **3** and **4** could simultaneously disperse multilayer vesicles of DMPC (Fig. 3.4a). In contrast, di-*ortho* methyl-STMA **2** and di-*para*-carboxylate-STMA **5** were unable to solubilize DMPC vesicles and form nanodiscs. Due to their weak activity in and the anticipated challenge for solubilization of biological membrane, the latter polymers were not pursued further in subsequent assays.
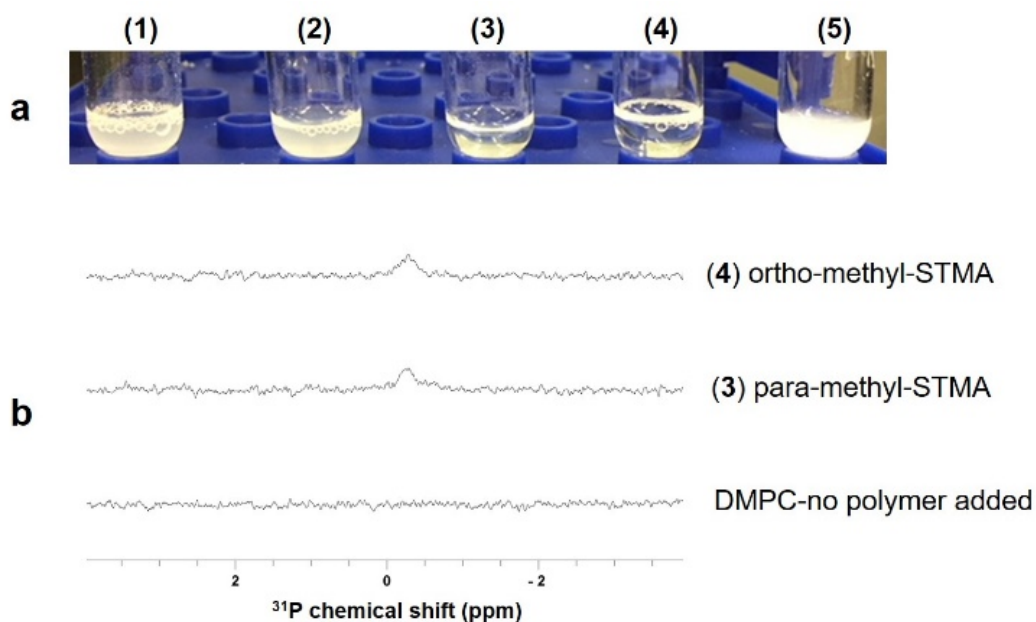
Figure 3.4. A. Solubilization of DMPC lipid vesicles by different stilbene maleic acid copolymers. Only *para*-methyl stilbene-MA (**3**) and *ortho*-stilbene-MA (**4**) could clarify the lipid suspension. B. The broad ^{31}P NMR signal of lipid vesicles composed of DMPC (5 mM) becomes resolvable upon the addition of polymers **3** and **4** at 2% w/v concentrations, indicating the formation of rapidly tumbling nanodiscs.

3.4.2. Solubilization of synthetic and biological membrane

The membrane solubilizing activity of STMA was validated by NMR spectroscopy. Large vesicles composed of DMPC phospholipid exhibit ^{31}P NMR signals that are broadened beyond detection, but upon addition of polymers **3** or **4,** the liposome suspensions clarify and reveal readily resolvable ^{31}P NMR signals (Fig. 3.4b). This indicates the formation of water-soluble nanodiscs in a manner that is similar to that reported of SMA2000 polymer with similar solubilization and saturation limits

3.4.3. Solution behavior of STMA polymers

The STMA polymers were expected to behave in solution similarly to SMA polymers due to the retention of maleic acid subunits. The pK_a values of maleic acid in aqueous solution are ~4.4 and ~9.0) [13], suggesting comparable charge distributions and pH-dependent solubility profiles, with SMA2000 being most water-soluble between pH 7 and 8. The polymer solubilities were tested over a wider range from pH 5 to 10. Surprisingly, compounds **3** and **4** were soluble from pH 5 to 10 (Fig. 3.5). This provides STMA polymers with broader utility across the biological range of pH values under which proteins operate, including in acidophiles, lysosomes, and endosomes. The increased pH solubility of STMA polymers is likely due at least in part to the lack of polystyrene elements, which can seed aggregation, as well as altered backbone dynamics in stilbenes, and give these polymers a practical advantage over SMA polymers. The sensitivity of SMA polymers to divalent cations is well known. As expected, due to the common cation-binding maleic acid subunits, both **3** and **4** show similar sensitivity to levels of Ca^{+2} that exceed 5 mM, where they begin to form visible precipitates (Fig. 3.5c) [14]. This does limit STMA utility

in functional assays that rely on high calcium levels. However, it also provides a way to coax membrane proteins from the STMA-based nanodiscs into liposomes or detergent phases by elevating polycation levels to drops the polymer out of solution.
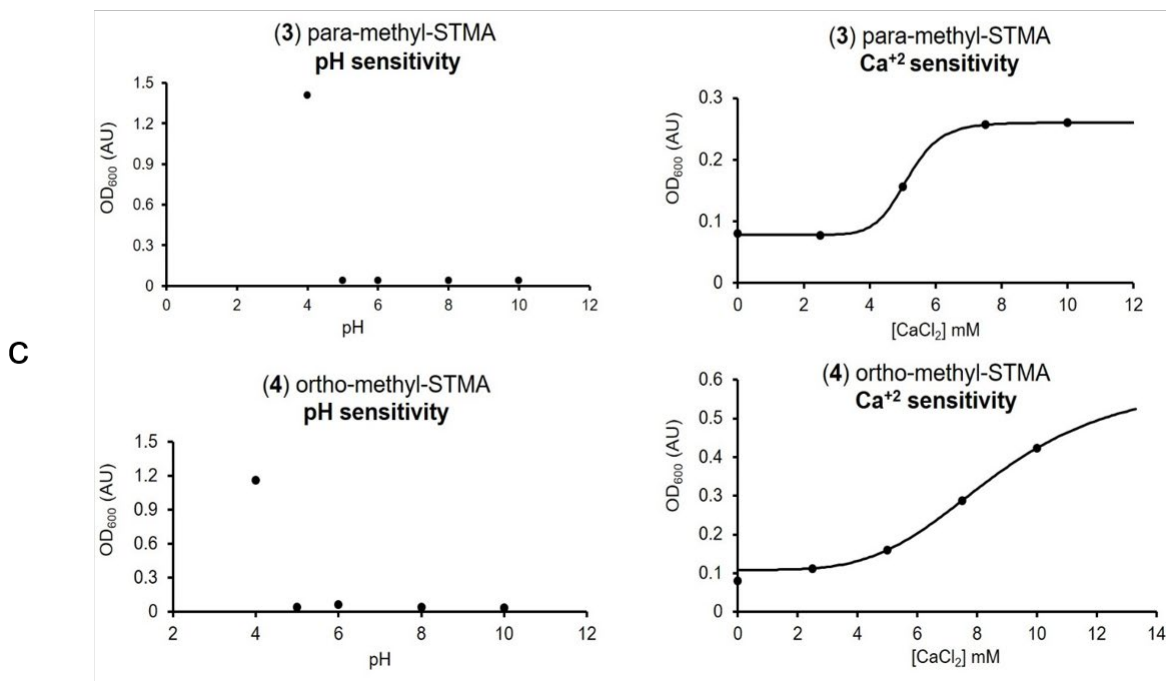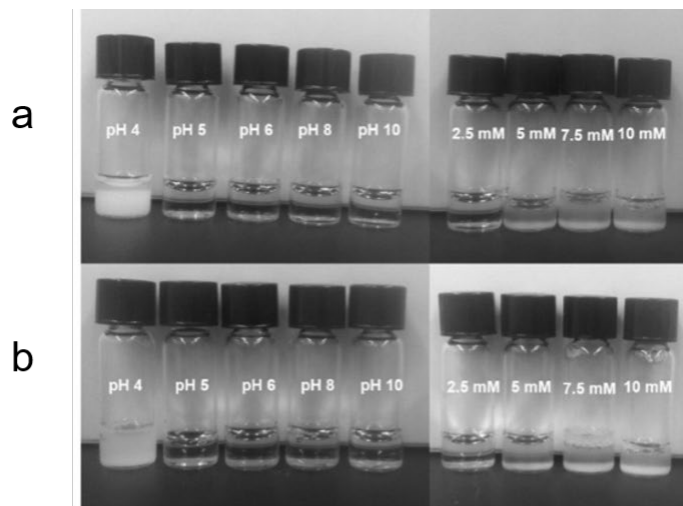
Figure 3.5. The pH sensitivity (left panel) and divalent cation (*i.e.*, Ca^{+2}, pH 8.0) tolerance (right panel) of pMe-STMA (**3**) (a) and oMe-STMA (**4**) (b). c.The turbidity of samples used

for calcium sensitivity and pH tolerance assays was measured at 600 nm. Tris buffer (10 mM, pH 8.0) was used as a reference.

The methyl STMA polymers were investigated for their ability to solubilize *E. coli* outer membranes, which are tightly packed with proteins and glycolipids. The palmitoyl transferase PagP was expressed into the outer membrane in order to test whether its physiologically relevant bilayer assembly could be purified and studied. Compounds **3** and **4** were added individually to raw outer membrane samples at a polymer concentration of 0.5% w/v, which is five times lower than the level generally recommended for SMA2000 polymer activity [13] as high polymer concentrations can induce large, undesirable aggregates. The yield of PagP monomers and dimers [15, 16] solubilized directly from the outer membrane into the supernatant was comparable to the levels of PagP extracted by SMA2000 at 1 w/v% concentration (Fig. 3.6). This suggests that **3** and **4** function like SMA2000 by releasing protein-lipid complexes directly from biological membranes into native nanodiscs and allows purification with common affinity tags. Moreover, STMA polymers work efficiently at lower concentrations and appear to preferentially stabilize protein dimers suggesting a gentler interaction with the memtein.
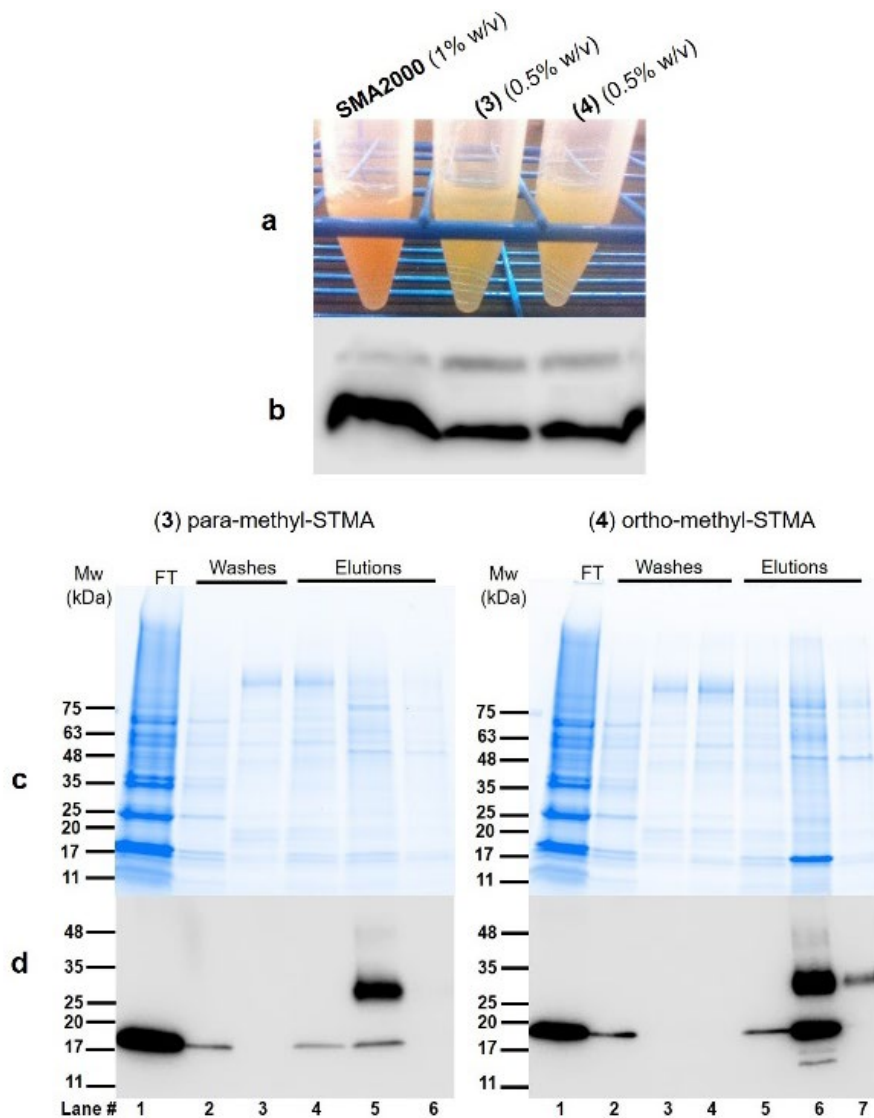
Figure 3.6. a. Solubilization of the total membrane of *E. coli* cultures expressing His₆-tagged PagP protein by STMA **3** and **4**. b. Western blot (probed against His-tag) compares the level of solubilization by **3** and **4** versus SMA2000. c.The Ni-NTA affinity purification stages of PagP-STMA nanodiscs from the outer membrane of *E. coli* include flow-through (FT), wash (with 10 mM imidazole) and elution (250 mM imidazole) fractions which were analyzed on stain-free gels and confirmed by Western blotting (d).

The nanodiscs containing His-tagged PagP protein were purified in a single step over a standard metal affinity resin. The stain-free SDS-PAGE gel displays a prominent band for **4** after elution (lane 6) with apparent molecular weights of 18 and 36 kDa, which

correspond to the monomeric unfolded and oligomeric states, respectively, of PagP following heat denaturation [17]. These states are less conspicuous in the PagP purification using 3 (panel c, lane 5). This indicates that the yield of purified monomer and dimer appears to be dependent on the particular STMA derivative used, with 4 generating a higher yield of purified protein overall. In both cases, PagP nanodiscs elute at the same retention volume (~15 mL) by size exclusion chromatography (Fig. 3.7), implying the similarity of sizes of nanodiscs. Negative stain TEM imaging of these fractions shows nanodiscs with diameters of approximately 20 nm, which are larger than the 10 nm PagP nanodiscs formed by SMA2000 polymer and provide significantly more carrying capacity (Fig. 3.8).
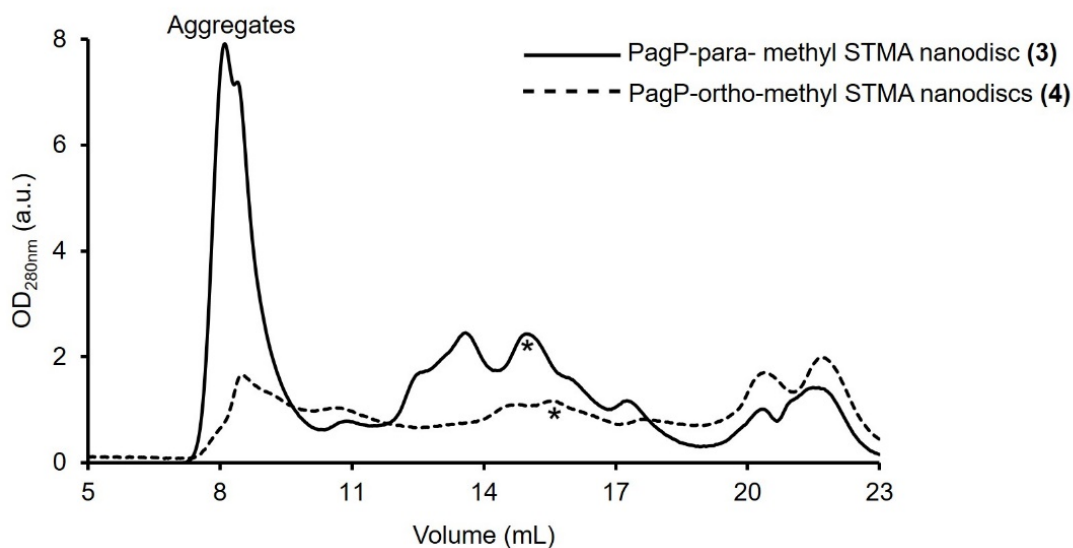
Figure 3.7. Size exclusion chromatography (SEC) profiles of PagP-methyl stilbene nanodiscs (using para-methyl STMA (**3**) and ortho-methyl STMA (**4**)) purified by nickel affinity column. Asterisks show fractions that contain a high amount of protein nanodiscs and used for TEM imaging.
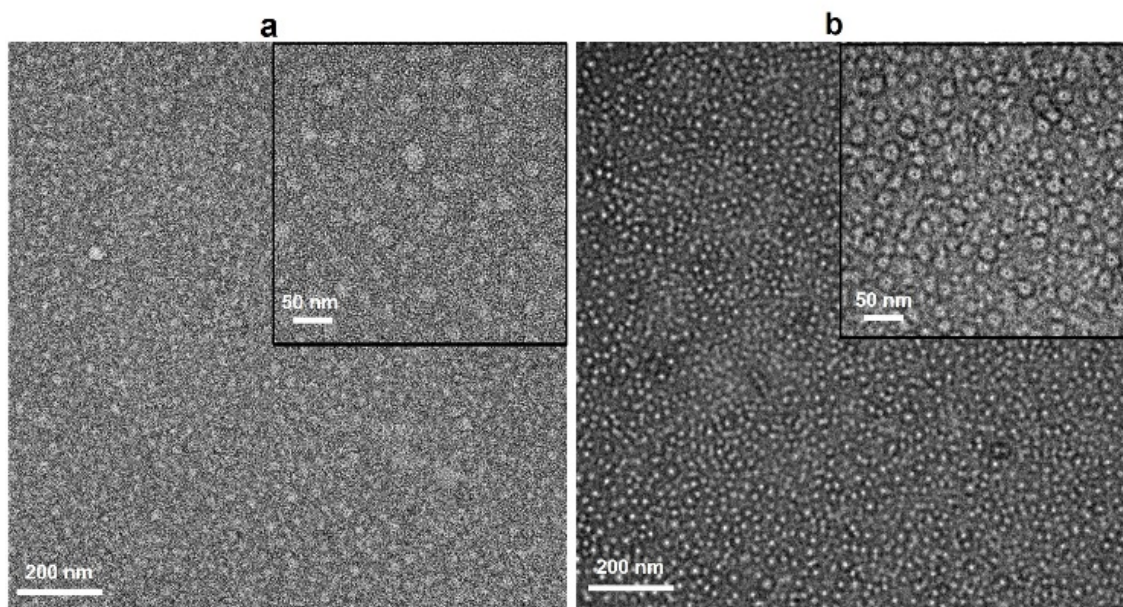
Figure 3.8. Negative stain EM images of native nanodiscs formed from outer membranes containing PagP using (a) pMe-STMA (**3**) and oMe-STMA (b) polymers.

In summary, we report that synthetic polymers with strictly alternating stilbene and maleimide-based subunits having minimal sequence and batch polydispersity can effectively solubilize biological membrane, including native bacterial membranes. Polymers 3 and 4 have less backbone flexibility than the styrene containing polymers yet are still capable of interacting with lipid bilayers and penetrating into biological membranes to excise nanodiscs which capture lipid-membrane protein complexes. The STMA polymers can be, therefore, utilized for detergent-free purification of membrane proteins, and add valuable diversity within the repertoire of amphipathic polymers available for native nanodisc production. The notable advantages of the methyl-substituted STMA over SMA is their ability to rigidify the polymer backbone, regularize the periodicity of sidechains, and enhance solubility over a wider range of pH values while generating large nanodiscs capable of holding multimeric protein assemblies.

Future improvements on the STMA series presented here can be envisaged. Different modifications can be accommodated by the maleic anhydride subunit [18-21] in order to improve the polycation tolerance and to add thiols or other moieties to incorporate affinity tags and fluorescent labels. Such additions would enhance the utility of methyl STMA copolymers and resulting nanodiscs further into the realm of large scale production of membrane protein targets and high throughput screening. The unique potential of this series for detailed biophysical and structural analysis bodes well for future studies that push the resolution of protein-lipid-polymer complexes to the atomic level.

3.5. References

[1] T.J. Knowles, R. Finka, C. Smith, Y.-P. Lin, T. Dafforn, M. Overduin, Membrane proteins solubilized intact in lipid-containing nanoparticles bounded by styrene-maleic acid copolymer, J. Am. Chem. Soc, 131 (2009) 7484-7485.

[2] M. Overduin, M. Esmaili, Memtein: The fundamental unit of membrane-protein structure and function, Chem Phys Lipids, 218 (2019) 73-84.

[3] M. Overduin, M. Esmaili, Structures and Interactions of Transmembrane Targets in Native Nanodiscs, SLAS Discov, (2019) 1-10.

[4] J.L. De la Fuente, E.L. Madruga, Homopolymerization of methyl methacrylate and styrene: Determination of the chain-transfer constant from the mayo equation and the number distribution for n-dodecanethiol, J Polym Sci Pol Chem, 38 (2000) 170-178.

[5] A.M. Savage, X. Zhou, J. Huang, S.R. Turner, A review of semi-rigid, stilbene-containing alternating copolymers, Appl Petrochem Res, 5 (2015) 27-33.

[6] C. Sun, S. Benlekbir, P. Venkatakrishnan, Y. Wang, S. Hong, J. Hosler, E. Tajkhorshid, J.L. Rubinstein, R.B. Gennis, Structure of the alternative complex III in a supercomplex with cytochrome oxidase, Nature, 557 (2018) 123-126.

[7] W. Qiu, Z. Fu, G.G. Xu, R.A. Grassucci, Y. Zhang, J. Frank, W.A. Hendrickson, Y. Guo, Structure and activity of lipid bilayer within a membrane-protein transporter, Proc Natl Acad Sci USA ,115 (2018) 12985-12990.

[8] M. Mao, C. Kim, S. Wi, S.R. Turner, Chain structure of substituted stilbene - Maleic anhydride alternating copolymer probed by solid-state NMR, Macromolecules, 41 (2008) 387-389.

[9] Y. Li, M.Q. Zhang, M. Mao, S.R. Turner, R.B. Moore, T.H. Mourey, L.A. Slater, J.R. Hauenstein, Chain Stiffness of Stilbene Containing Alternating Copolymers by SAXS and SEC, Macromolecules, 45 (2012) 1595-1601.

[10] Y. Li, S.R. Turner, Free radical copolymerization of methyl-substituted stilbenes with maleic anhydride, Eur Polym J, 46 (2010) 821-828.

[11] J. Huang, X. Geng, C. Peng, T.Z. Grove, S.R. Turner, Enhanced Fluorescence Properties of Stilbene-Containing Alternating Copolymers, Macromol Rapid Commun, 39 (2018)1-6.

[12] Beom Lim, Yong, M.C. E., K. Younghwan, T.W. B., R. Chongsuk, The inhibition of prions through blocking prion conversion by permanently charged branched polyamines of low cytotoxicity, Biomaterials, 31 (2010) 2025-2033.

[13] T.H. Haines, Anionic Lipid Headgroups as a Proton-Conducting Pathway Along the Surface of Membranes - a Hypothesis, Proc Natl Acad Sci, 80 (1983) 160-164.

[14] M.C. Fiori, Y. Jiang, G.A. Altenberg, H. Liang, Polymer-encased nanodiscs with improved buffer compatibility, Sci Rep, 7 (2017) 1-10.

[15] D.J.K. Swainsbury, S. Scheidelaar, N. Foster, R. van Grondelle, J.A. Killian, M.R. Jones, The effectiveness of styrene-maleic acid (SMA) copolymers for solubilization of integral membrane proteins from SMA-accessible and SMA-resistant membranes, Biochim Biophys Acta-Biomembranes, 1859 (2017) 2133-2143.

[16] M.M. Xue, L.S. Cheng, I. Faustino, W.L. Guo, S.J. Marrink, Molecular Mechanism of Lipid Nanodisk Formation by Styrene-Maleic Acid Copolymers, Biophys J, 115 (2018) 494-502.

[17] R.E. Bishop, H.S. Gibbons, T. Guina, M.S. Trent, S.I. Miller, C.R. Raetz, Transfer of palmitate from phospholipids to lipid A in outer membranes of Gram-negative bacteria, EMBO J, 19 (2000) 5071-5080.

[18] N.Z. Hardin, T. Ravula, G.D. Mauro, A. Ramamoorthy, Hydrophobic Functionalization of Polyacrylic Acid as a Versatile Platform for the Development of Polymer Lipid Nanodisks, Small, 15 (2019) 1-5.

[19] S. Lindhoud, V. Carvalho, J.W. Pronk, M.E. Aubin-Tam, SMA-SH: Modified Styrene-Maleic Acid Copolymer for Functionalization of Lipid Nanodiscs, Biomacromolecules, 17 (2016) 1516-1522.

[20] T. Ravula, N.Z. Hardin, S.K. Ramadugu, A. Ramamoorthy, PH Tunable and Divalent Metal Ion Tolerant Polymer Lipid Nanodiscs, Langmuir, 33 (2017) 10655-10662.

[21] K. Yasuhara, J. Arakida, T. Ravula, S.K. Ramadugu, B. Sahoo, J.I. Kikuchi, A. Ramamoorthy, Spontaneous Lipid Nanodisc Formation by Amphiphilic Polymethacrylate Copolymers, J Am Chem Soc, 139 (2017) 18657-18663.

Chapter 4

The Effect of Hydrophobic Alkyl Sidechains on Size and Solution Behaviors of Nanodiscs Formed by Alternative Styrene-Maleamic Copolymers

4.1. Significance

The development of amphipathic polymers, including various formulations of styrene-maleic acid (SMA) copolymers, has allowed the purification of increasing sizes and complexities of biological membrane protein assemblies in native nanodiscs. However, the factors determining the sizes and shapes of the resulting bio-nano particles remain unclear. Here, we show how grafting on short alkyl amine sidechains onto the polar residues leads to a broad set of nanoparticle sizes with improved solution behavior. The solubilization of lipid vesicles occurs over a wide range of pH levels and calcium concentrations, providing utility across the physiologically relevant range of solution conditions.

Furthermore, the active SMA derivatives contain alternating monomers, which have inherently lower sequence polydispersity. Pronounced differences in the shapes of native nanoparticles were formed from *Escherichia coli* bacterial outer membrane containing PagP protein using methyl, ethyl, and propylamine derivatives of styrene-maleic anhydride. In particular, the methylamine-substituted polymer forms smaller, monodispersed nanodiscs, while the longer alkyl derivatives form irregular nanostructures. Thus, the introduction of hydrophobicity onto the polar sidechains of amphipathic polymers has profound effects on the morphology of native nanodisc, with shorter methyl moieties offering more uniformity and utility for structural biology studies.

4.2. Introduction to polymer-based solubilization of biomembrane

The membrane bilayer is composed of a heterogeneous and dynamic population of different classes of membrane proteins and lipids and undergoes significant morphological changes, including tubulation, fusion and vesiculation events. As such, its

diverse states mediate and regulate vital cellular functions, including signaling and trafficking. Stabilization and visualization of the structures, functions and dynamics of the component system within the membrane environment remain at the heart of answering many fundamental questions in molecular biology.

Since the publication of the first atomic structure of membrane protein in the 1970s [1], many structures of membrane assemblies have been characterized in a variety of membrane mimics. These include micelles, bicelles, and nanodiscs bounds by amphipathic polymers such as amphipols or membrane scaffold proteins [2]. However, these systems dissociate the membrane proteins from their native bound lipids and still rely on the use of detergents. The discovery that SMA copolymers can be used for genuinely detergent-free solubilization of native biological membranes to directly and spontaneously form ~10 nm diameter discs [3] has opened up the new field of native nanodiscs. Unlike biopolymers such as DNA or protein, SMA polymers are synthesized chemically (in the absence of any parent templates) by polymerization of styrenes and maleic anhydride monomers into alternating or non-alternating products. Despite various formulations of amphipathic polymers designed for nanodiscs technology [4], conventional non-alternating SMA copolymers remain the most well-characterized, yet many not necessarily the most optimal, derivatives, with alternating SMA(1:1) not having yet been explored.

In the absence of hydrophobic ligands, amphipathic SMA copolymers display hypercoiling behavior such that styrene groups engage in the water-insoluble core and carboxylic acids stay on the surface, therefore increasing the viscosity of solutions in salt- and pH-dependent manner [5, 6]. The dynamic structures in SMA polymer cause the

formation of two hydrophobic and hydrophilic active surfaces (which highly resemble amphipathic helices of Apo-I proteins) [7] that can associate with lipid films and form nanometer-sized doughnut-shape particles. Encapsulation perturbs the membrane curvature (by creating a bulge) and planarity, allowing water molecules permeate in and, intriguingly, the distribution of Na^+ ions undergo remarkable changes [8]. MD models suggest that the relative abundance of maleic acid and styrene moieties in the polymer chain, their sequence and the length of SMA polymer may slightly change their behavior in association with DMPC lipid membrane. The net charge, length (≥1.4 kDa) and sequential polydispersity of SMA polymer (SSS≥3) are among other factors that influence the formation and stability of nanodiscs [9]. Ionic strength and pH of buffer (external factors) and abundance of carboxyl groups of MA monomers (pK_{a1} ~4 and pK_{a2} ~9) regulate the overall charge of SMA polymers, which in turn is detrimental to the formation of secondary structures along polymer chain; thus, to polymer solubility in solution and solubilization of lipid membrane [10].

Hydrophobic interactions and self-assembling processes are the driving force for the formation of SMALP nanoparticles. Here, we explored how the addition of hydrophobic aliphatic sidechains to alternating SMAn(1:1) derivatives influence self-assembly, solution behavior and application of purified native membrane proteins into nanodiscs for structural analyses. In this article, our model membrane protein PagP is a small outer membrane palmitate transferase β-barrel enzyme that is involved in lipopolysaccharide (LPS) remodeling [11], hence antimicrobial resistance in many pathogenic Gram-negative bacteria such as *Salmonella Typhimurium* [12].

4.3. Materials and Methods

4.3.1. Reagents

All reagents were from Sigma-Aldrich® unless specified otherwise. 1,2-dimyristoyl-sn-glycerol-3-phosphocholine (DMPC) was purchased from Avanti Polar Lipids, and alternating styrene-maleic anhydride (SMAn(1:1)) was from Total Cray Valley.

4.3.2. Polymer synthesis

As per each reaction, 9 millimoles of methylamine, ethylamine, and propylamine were diluted in H_2O and gradually added to SMAn(1:1) (5 g in DMF) at room temperature for 5 hours. The modified polymers were precipitated in excess diethyl ether three times and dried under vacuum. The powders were next dissolved in NaOH and again precipitated by hydrochloric acid (5 M) (pH 3.0). The polymer precipitants were collected and dissolved in 0.5 M NaOH. Before lyophilization, the pH of each solution was adjusted to 7.8-8.0. The FT-IR spectra of each sample collected to confirm the completion of the reaction.

4.3.3. Purification of PagP protein from native biomembrane

Recombinant (His)$_6$-tagged PagP was overexpressed in the outer membrane of *E.coli* BL21(DE3) *pLysS*, the outer membrane fraction was collected (from 6 L LB culture) and used for purification of PagP as described before [13]. The membrane fraction was incubated with 2% w/v concentration of each alkylamine polymers in Tris 10 mM, NaCl 100 mM and 5% v/v glycerol (buffer A) precisely according to reference [14]. Membrane lysates were further used for purification using a 5 mL HisTrap-HP column (GE). Buffer A supplemented with 10 mM and 30 mM imidazole were used as washing buffers 1 and 2, respectively, and PagP-nanodiscs were eluted with 250 mM imidazole (in buffer A). Samples from each step of purification were collected, mixed with sample buffer (2X, Bio-

Rad) and heated for 10 mins at 100 °C and then analyzed on a 12% precast stain-free SDS-PAGE (Bio-Rad). SDS-PAGE gels were imaged either after staining with Coomassie blue (SMA(1:1)-MA) or stain-free (SMA(1:1)-EtA and SMA(1:1)-PA) on a Gel Doc EZ system (Bio-Rad).

Fractions with the highest amount of PagP protein were used for size exclusion chromatography on a Superdex® 200 10/300 GL column (GE) in buffer A. Collected fractions were analyzed by Western blotting on a PVDF membrane (Bio-Rad) using His-Prob (Pierce). The bands were visualized using Clarity™-ECL substrate (Bio-Rad). Unheated (cold) samples refer to those incubated with sample buffer at room temperature for 10 min.

4.3.3. Solution behavior of alkylamine derivatives of SMA(1:1)

4.3.3.1. Calcium (divalent cation) tolerance assay

Buffers containing different millimolar concentrations of calcium chloride were prepared in Tris 10 mM, pH 8.0, and mixed with 0.5% w/v of each polymer. The mixtures were incubated at room temperature for 30 mins and the turbidity of samples was recorded at 600 nm.

4.3.3.2. pH tolerance assay

The pH sensitivity of 0.5% w/v of each polymer was tested over a pH range of 4-10, using citrate buffer (pH 4 and 5), phosphate buffer (pH 7) and Tris buffer (pH 8.0 and 10.0). All buffers contained 100 mM NaCl [15].

4.3.4. The size distribution of lipid nanodiscs

Unilamellar vesicles of DMPC (3.5 mM, 135 nm in diameter) were prepared in Tris 10 mM, NaCl 100 mM by sonication as described [16] and mixed with different amounts

of stock solution of polymers (in water, filtered) and incubated overnight at room temperature. The size distributions of lipid nanodiscs were analyzed by dynamic light scattering (DLS) on a Zetasizer Nano ZSP (Malvern Panalytical) using reusable 3 mm cuvettes. Each measurement was read three times (each with 12 scan average) and for at least three independent lipid-nanodiscs samples. Data were analyzed by Zetasizer software version 7.12.

4.3.5. Transmission electron microscopy (TEM) imaging

Microliter amounts of fresh size exclusion chromatography (SEC) fractions (M*, E** and P**) were loaded on carbon-coated copper grids (400 nm mesh, already glow charged for 30 sec), washed three times with deionized water and stained with uranyl acetate (2% w/v, filtered). Grids were dried for at least 2 hours before imaging on a Tecnai G20 transmission electron microscope (FEI Eindhoven, NL; an acceleration voltage of 200 kV), that is equipped with an Eagle 4 k × 4 k CCD camera (FEI).

4.4. Results and Discussion

The sequential polydispersity is defined as alternation of subunits along a polymer chain. Due to the propensity of styrene subunits to homopolymerization, the alternation of styrene and maleic acid subunits in SMA(1:1) is more homogenous than that in SMA polymers with 2:1 and 3:1 ratios of styrene: maleic anhydride. In other words, styrene and maleic acid comonomers in SMA(1:1) are more alternating than SMA(2:1) or SMA (3:1).

The relatively high number of maleic acid monomers in SMA(1:1), make it more water-soluble than SMA2000 or SMA3000. However, because of the sparsity of styrene subunits [17], the interaction of SMA(1:1) with biomembrane is relatively compromised. Hence, we added short alkylamine sidechains to increase membrane binding with small

decreases in the solubility of the polymer in solution. The length of the alkyl chain influences the kinetics of the reaction of alkylamines with anhydride groups. As such, methylamine is more reactive than both ethylamine and propylamine, hence requires careful control (Fig. 4.1).

The FT-IR spectra of each product (Fig. 4.2) shows no trace of anhydride band at 1780 cm^{-1}, which indicates all maleic anhydride subunits are grafted with alkylamine moieties. The broadband at 3000-3400 cm^{-1} and the strong band at 1560 cm^{-1} indicate the formation of carboxylic acids and amide bonds, respectively. At high concentration (~10% w/v, Tris pH 8.0), all polymers were as fully soluble and stable as source polymer SMA(1:1), showing no sign of turbidity or precipitation over time.

SMAn(1:1)

DMF, Et$_3$N

1. H$_2$N-CH$_3$
2. H$_2$N-CH$_2$-CH$_3$
3. H$_2$N-(CH$_2$)$_2$-CH$_3$

SMA(1:1)- methylamine**(1)**
SMA(1:1)-ethylamine**(2)**
SMA(1:1)-propylamine**(3)**
R: methyl, ethyl, propyl
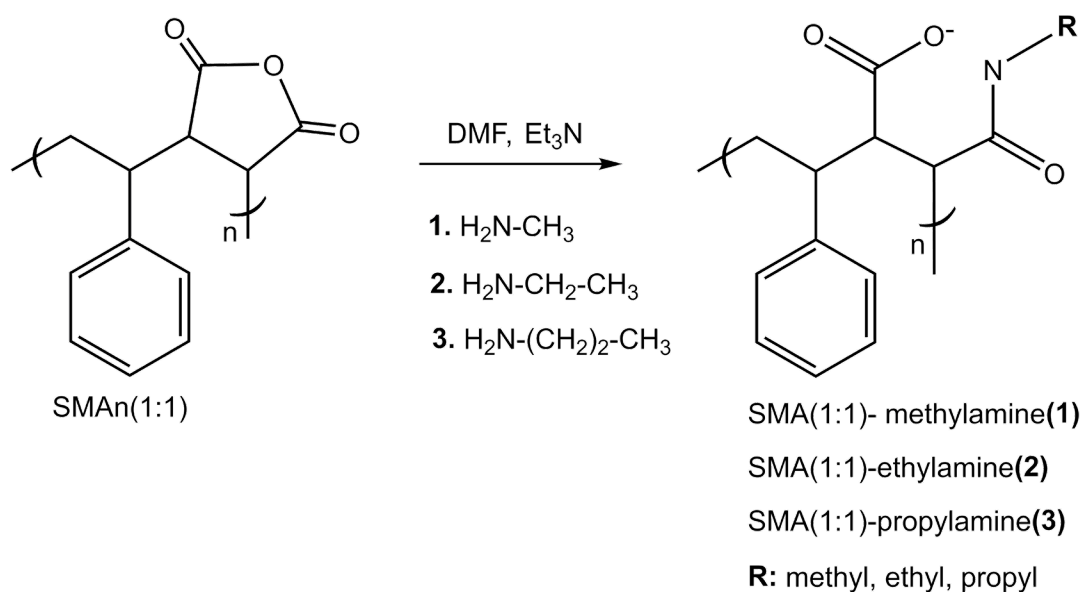
Figure 4.1. Synthesis of maleamic acid derivatives of SMAn(1:1) with methyl (1), ethyl (2) and propyl (3) amine sidechains. R indicates the alkyl sidechains and n denotes the alternative units in SMA(1:1) string.
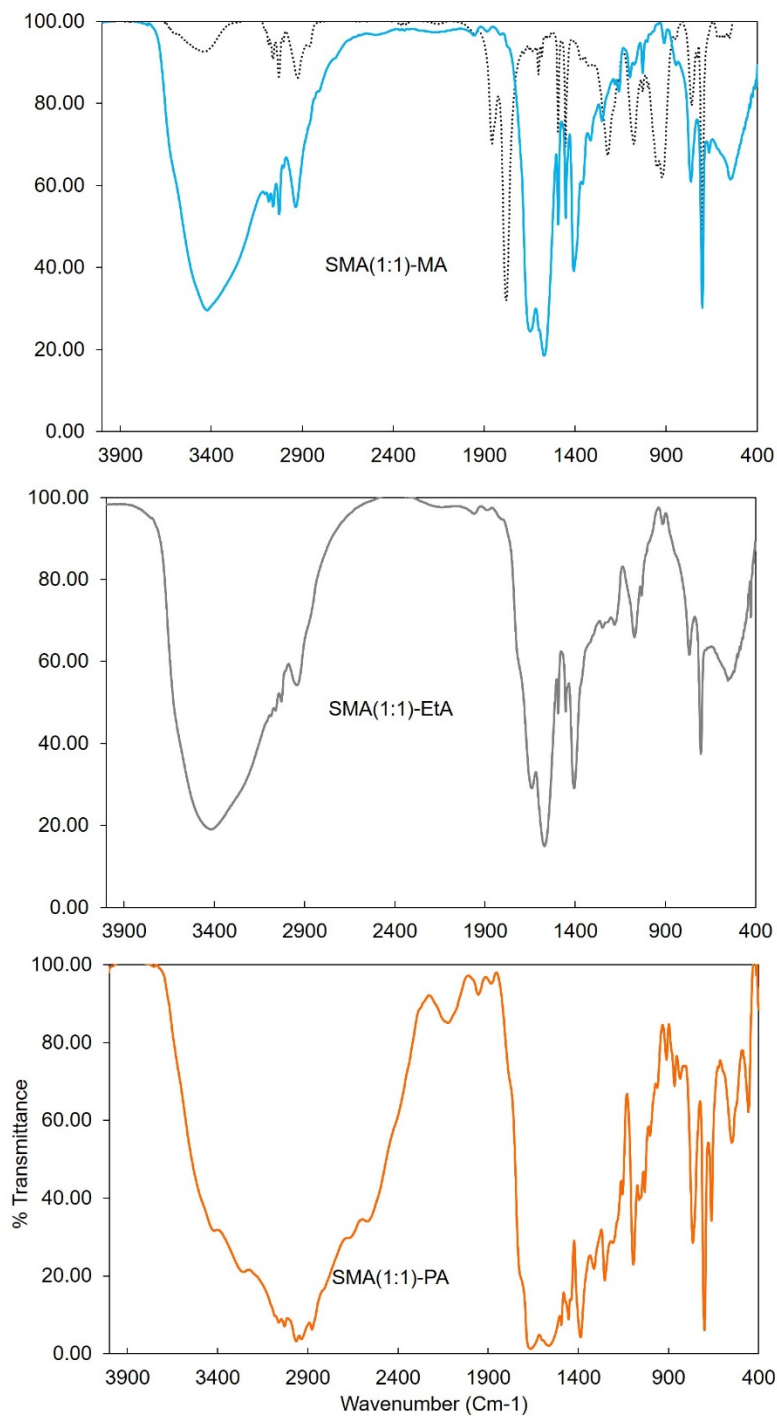
Figure 4.2. Fourier-transform infrared (FT-IR) spectra of KBr pellets of three alkylamine derivates of SMA(1:1) and SMAn(1:1) (dotted line) were recorded on Thermo Nicolet (Madison, WI, USA) instrument (model. Nicolet 8700).

For each series of polymers, dynamic light scattering data were collected at various lipid: polymer mass ratios. While SMA-EtA and SMA-PA at 0.2% (w/v) concentration were unable to clarify DMPC lipid suspension, SMA-MA thoroughly dispersed lipid vesicles to 40 nm diameter nanodiscs. This observation suggests that SMA(1:1) with short alkyl sidechains shows noticeably more detergent-like behavior than those with longer alkyl chains. In fact, at 1% w/v concentration of each polymer, SMA(1:1)-MA forms 14 nm discs while SMA(1:1)-EtA and -PA generate larger discs, respectively, with 25 and 32 nm. Hence, the addition of one methylene group dramatically increases the diameter of the resulting lipid nanodisc (Fig. 4.3 and Table 4.1).
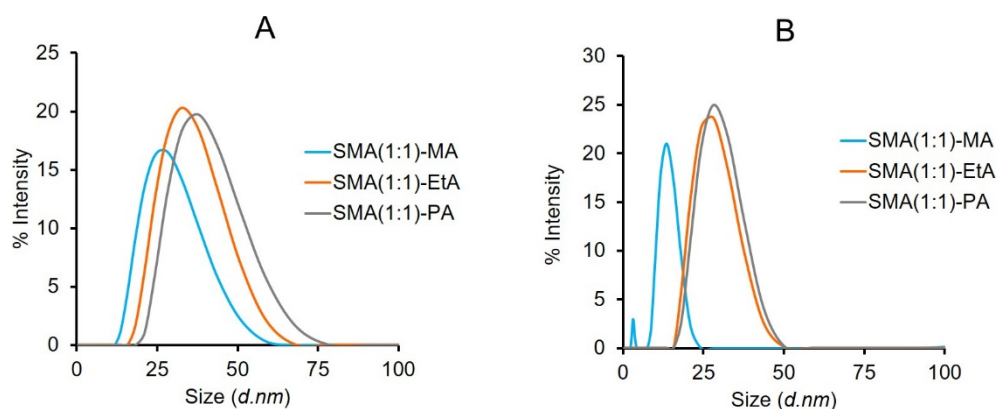
Figure 4.3. Size distribution of nanodiscs from DMPC (3.5 mM) and each alkylamine derivative of SMAn(1:1) at polymer concentrations of 0.6% w/v (A) and 1% w/v (B). Samples were incubated at room temperature overnight before measurement by DLS.

Polymer	SMA concentration (w/v)		
	0.2%	0.6%	1%
SMA(1:1)-MA	40.2±2.3	25.5±0.7	14.5±0.1
SMA(1:1)-EtA	Turbid	30.4±0.1	25±0.1
SMA(1:1)-PA	Turbid	37.3±2	32±3.3

Table 4.1. A summary of size distribution of DMPC (3.5 mM) nanodiscs formed at different concentrations of SMA(1:1)-MA, SMA(1:1)-EtA and SMA(1:1)-PA in Tris 10 mM, pH 8.0.

The results suggest that the diameter of nanodisc is significantly determined by the length and hydrophobicity of sidechains on maleamic acid subunits. SMA polymer with the longer hydrophobic sidechains tends to show more of worm-like micellar behavior with a higher propensity to aggregation, which is not necessarily desirable. However, to what extent is this effect beneficial for the purification of membrane proteins from native biomembranes? As shown in Fig. 4.4a, all alkylamine derivatives of SMA(1:1) (2% w/v) could purify PagP directly from the outer membrane of *E. coli*. However, the purified proteins display remarkably different size-exclusion chromatograms (Fig. 4.4b), which is consistent with the DLS data. PagP-(SMA)MA discs elute at ~15 mL, similar to the retention volume observed for PagP-SMA2000 discs. Conversely, in the PagP-(SMA)EtA chromatogram, two peaks are observed, a main peak 12.5 and a smaller peak at 15 mL. On the other hand, the SEC chromatogram of PagP-(SMA)PA discs displays only one small hump at 12.5 mL. According to the literature, PagP can form oligomeric species in the membrane [11]. Therefore, the larger species on SEC chromatograms are likely

oligomeric PagP. To evaluate this, we examined fractions at 15 mL, 12.5 mL and 8 mL (void volume) in heated (denatured) and unheated (native) forms on Western blots probed against the His-tag. As shown in Fig. 4.4c, PagP monomers are the only species in all major SEC fractions. This observation implies that the increased size of PagP nanodiscs is due to the encapsulation of more lipid molecules. Negative-stain electron micrographs of SEC fractions containing the highest amount of proteins support this notion (Fig. 4.4). The M* peak contains homogeneous populations of PagP-discs with roughly 15 nm diameter, whereas the E** and P** peaks consist mainly of a heterogeneous mixture of monomeric PagP discs and large aggregates. We also emphasize that in none of our SMALP preparation using alkyl-SMA(1:1), were we able to isolate homogenous dimeric PagP.

Alkylamine derivatives of SMA(1:1) polymers carry a similar negative charge and the same number of styrene subunits, yet they exhibit quite distinct behaviors in response to high concentration of calcium as well as acidic pH. These observations could reflect intermolecular polymer-polymer interactions. As shown in Fig. 4.5, SMA-MA can tolerate up to 8 mM $CaCl_2$. However, as for SMA-EtA and SMA-PA these values elevate up to 24 and 12.5 mM, respectively. In general, neutralization of negative charges on polymer by cations drives styrene-styrene interaction, hence, aggregation of polymers. We speculate that once SMA(1:1) polymers are grafted with alkyl sidechains and in the presence of calcium ions, both styrene moieties and alkyl sidechains could engage in hydrophobic interactions, causing the formation of microscopic aggregates rather than macroscopic precipitation.

We rationalize that the long and flexible propyl sidechains can branch out and become more accessible to hydrophobic interactions as compared with shorter ethyl sidechains. Therefore, SMA-PA would be more susceptible to precipitation by Ca^{+2} ions than SMA-EtA. The behavior of these polymers at acidic pH supports this view. SMA(1:1)-MA and SMA(1:1)-EtA are both soluble at pH range of 5-10, in contrast, SMA(1:1)-PA precipitates at pH 5 (so does SMA2000), which intriguingly suggests that the intermolecular hydrophobic interactions dominate in lower pH and drives aggregation of SMA-PA polymer (Fig. 4.6).

In contrast with our results on alkyl-derivatized SMA(1:1), N. Z. Hardin *et al.*, [18] have shown that short non-aromatic polyacrylic acid (PAA, 1.8 kDa) polymer functionalized with hydrophobic sidechains can convert DMPC lipid vesicles to nanodiscs with a diameter of ~9 nm (at polymer: lipid ratio of 1 w/w%) and they reported similarities in the TEM images for all series of nanodiscs. Interestingly, although pentyl, hexyl and neopentyl derivatives of PPA could solubilize complex cellular membranes, the butyl-derivative of PPA required more than 1:1 ratio of polymer: lipid to disperse DMPC vesicles.

Currently, there are no similar studies on alkyl-chain derivatives of non-aromatic amphipathic polymers such as diisobutylene-*alt*-maleic acid (DIBMA) [19] and polymethacrylate (PMA) [20] copolymers. Due to the relative similarity of DIBMA to SMA(1:1) in terms of the presence of alternating maleic acid moieties and charge distribution along the polymer chain, we speculate that the alkylamine derivatives of DIBMA follow the same behavior as alkylamine derivatives of SMA(1:1) under similar conditions. SMA-dA, SMA-EA (ethanolamine), SMA-ED and SMA-QA polymers, which

have been developed recently [21], differ significantly from our alkylamine SMA(1:1) derivatives, which offer longer and more regular backbone sequence, hence more regular side-chains and more homogenous populations of nanodiscs.
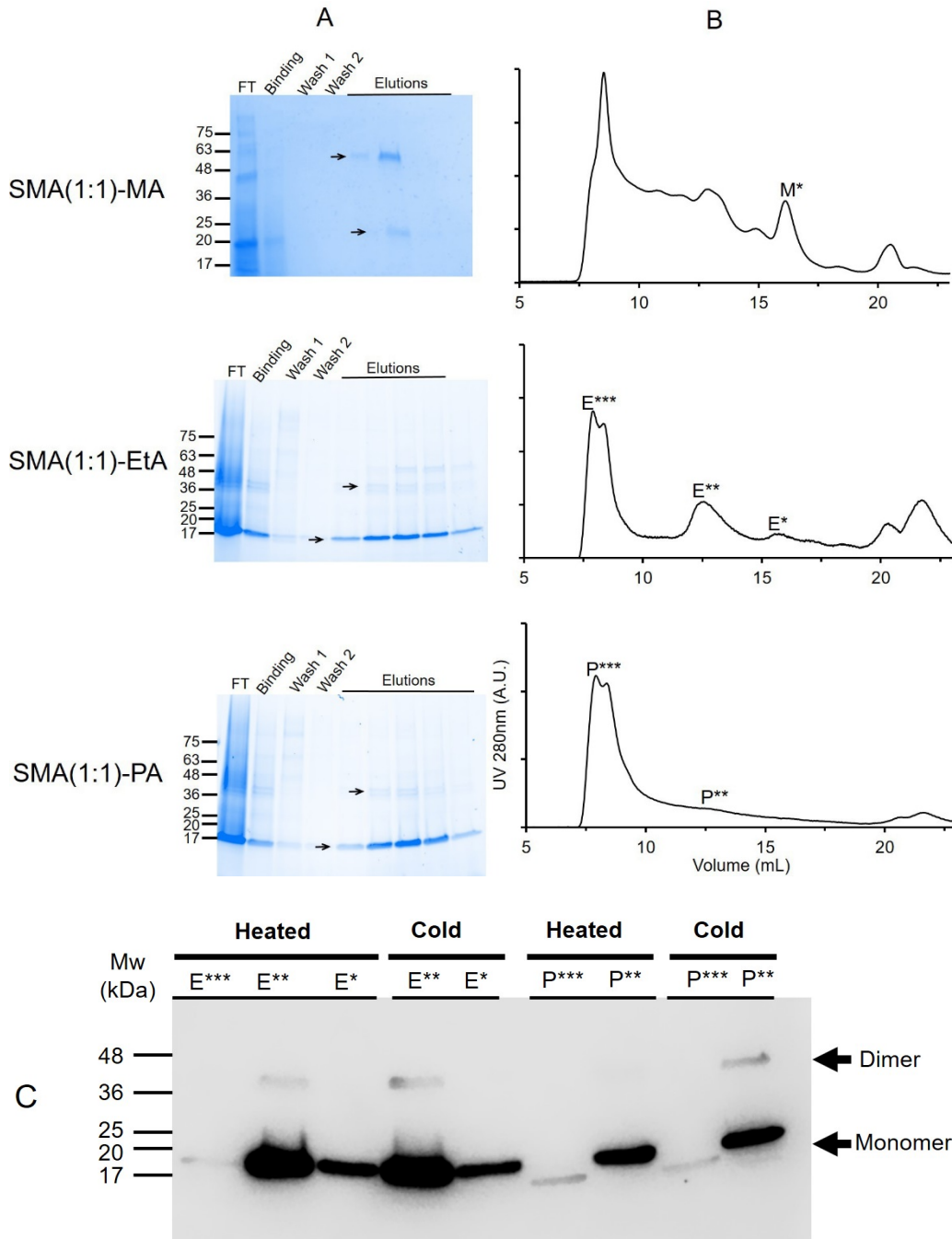
Figure 4.4. Purification of PagP using alkyl amine-substituted SMA(1:1). A. Metal affinity purification of PagP, a model bacterial β-barrel protein, directly from the outer membrane

of *E.coli* using nanodiscs formed by 1, 2, and 3. Arrows designate the location of monomer and dimer species on Coomassie blue-stained SAS-PAGE (1) and stain-free SDS-PAGE gels (2, 3). B. Different series of PagP-nanodiscs was further purified according to the size of particles on size exclusion chromatography. Peaks that may contain PagP-nanodiscs were labeled and analyzed by Western blots. C. To identify the oligomeric states of PagP in each fraction, Western blotting of the unheated (native) and heated (at 100 °C) SEC fractions (as marked on B) were compared.
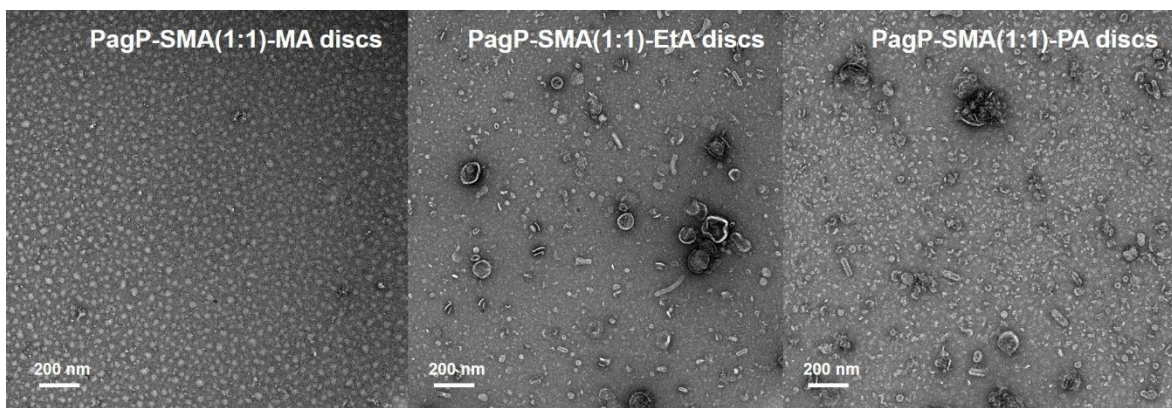
Figure 4.5. Transmittance electron micrographs of PagP native nanodiscs purified in M* (left), E** (middle), and P** (right) fractions of size exclusion chromatography. All fractions were used fresh and treated similarly for EM imaging.
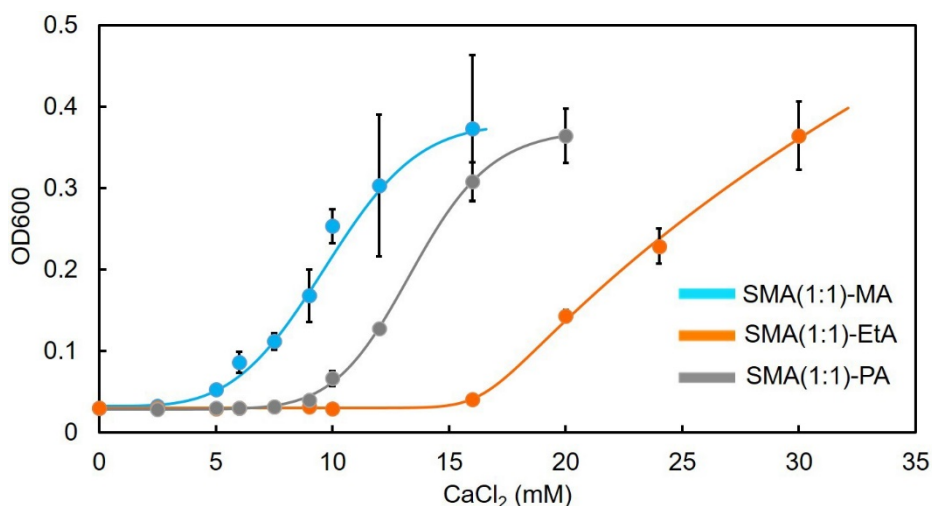
Figure 4.6. A comparative analysis of solubility of SMA(1:1)-MA, SMA(1:1)-EtA, and SMA(1:1)-PA polymers in various concentrations of Ca^{+2}. Each data point represents an

average of three independent measurements, and the curves were fitted to each data set using Prism8 software.
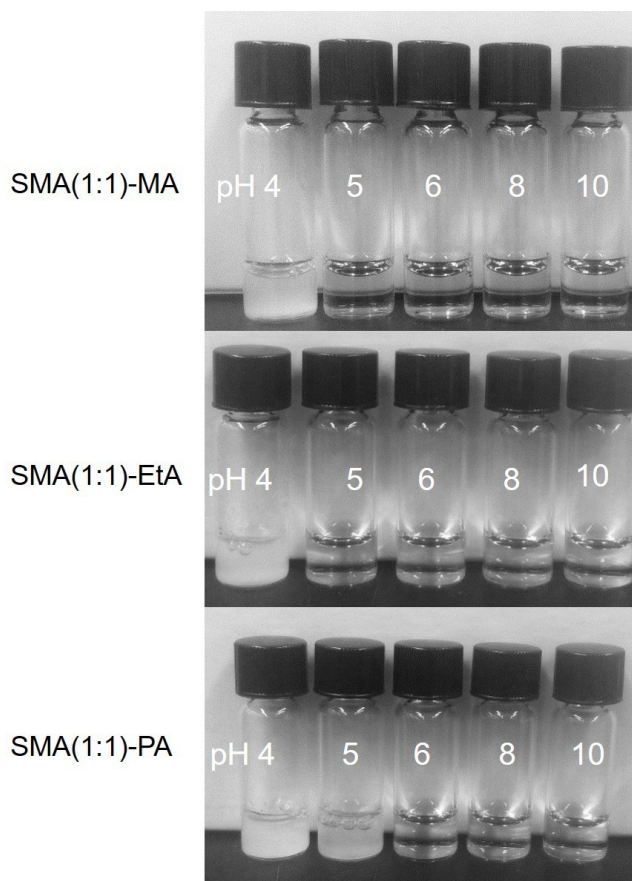
Figure 4.7. A visual and qualitative comparison between the pH tolerance (pH 4.0-10.0) profiles of equal concentrations of alkylamine derivatives of SMA(1:1).

4.5. Conclusions

Hydrophobic interactions and the self-assembling processes are two driving forces for the formation of SMALP nanoparticles. It's not surprising that polymer-polymer, polymer-lipid, protein-polymer interactions may compromise the yield, purity, and integrity of target proteins and, thus, downstream structural and functional analyses. Amphipathic polymers non-alternating SMAs can nonspecifically adsorb to hydrophobic patches of proteins (instead of acyl chains of lipids) or can become engaged in polymer-polymer

intramolecular interactions. Accordingly, the solubilization activity of alkylamine modified SMA(1:1) diminishes as the length of alkyl increases (SMA-MA> SMA-EtA> SMA-PA). We showed that hydrophobic sidechains could indeed increase the size of nanodiscs by forming discs, which accommodate more lipids. Collectively, however, the quality of SMALP nanodiscs formed by SMA-EtA and SMA-PA polymers appear to be less optimal for high-resolution imaging than those formed by SMA-MA polymer. Methylamine derivative of SMA(1:1) forms 14 nm discs, which are slightly larger than those made by SMA2000 [3] and could hold significantly larger memteins.

Novel formulations of SMA polymers (that reportedly form large and homogenous lipid nanodiscs) contain aliphatic sidechain capped with polar moieties (SH, OH, NH, N$^+$) [22-24]. According to our results, these polar groups are essential parts of side chains to induce more repulsive electrostatic interaction, hence limiting the excessive polymer-polymer interactions and aggregation.

4.6. References

[1] R. Henderson, P.N. Unwin, Three-dimensional model of purple membrane obtained by electron microscopy, Nature, 257 (1975) 28-32.

[2] L. Frey, N.A. Lakomek, R. Riek, S. Bibow, Micelles, Bicelles, and Nanodiscs: Comparing the Impact of Membrane Mimetics on Membrane Protein Backbone Dynamics, Angew Chem Int Edit, 56 (2017) 380-383.

[3] T.J. Knowles, R. Finka, C. Smith, Y.P. Lin, T. Dafforn, M. Overduin, Membrane proteins solubilized intact in lipid containing nanoparticles bounded by styrene-maleic acid copolymer, J. Am. Chem. Soc, 131 (2009) 7484-7485.

[4] M. Overduin, M. Esmaili, Memtein: The fundamental unit of membrane-protein structure and function, Chem Phys Lipids, 218 (2019) 73-84.

[5] W. Dannhauser, W.H. Glaze, R.L. Dueltgen, K. Ninomiya, Evidence from Intrinsic Viscosity and Sedimentation for Hypercoiled Configurations of Styrene-Maleic Acid Copolymer, J Phys Chem, 64 (1960) 954-955.

[6] S.R. Tonge, B.J. Tighe, Responsive hydrophobically associating polymers: A review of structure and properties, Adv. Drug Deliv. Rev, 53(2001)109-122.

[7] I.G. Denisov, Y.V. Grinkova, T.H. Bayburt, S.G. Sligar, Nanodiscs in Membrane Biochemistry and Biophysics, Chem Rev, 117 (2017) 4669-4713.

[8] J.D. Perlmutter, W.J. Drasler, 2nd, W. Xie, J. Gao, J.L. Popot, J.N. Sachs, All-atom and coarse-grained molecular dynamics simulations of a membrane protein stabilizing polymer, Langmuir, 27 (2011) 10523-10537.

[9] P.S. Orekhov, M.E. Bozdaganyan, N. Voskoboynikova, A.Y. Mulkidjanian, H.J. Steinhoff, K.V. Shaitan, Styrene/Maleic Acid Copolymers Form SMALPs by Pulling Lipid Patches out of the Lipid Bilayer, Langmuir, 35 (2019) 3748-3758.

[10] S. Scheidelaar, M.C. Koorengevel, J.D. Pardo, J.D. Meeldijk, E. Breukink, J.A. Killian, Molecular Model for the Solubilization of Membranes into Nanodisks by Styrene Maleic Acid Copolymers, Biophys J, 108 (2015) 279-290.

[11] C.R. Raetz, C.M. Reynolds, M.S. Trent, R.E. Bishop, Lipid A modification systems in gram-negative bacteria, Annu Rev Biochem, 76 (2007) 295-329.

[12] R. Goto, T. Miki, N. Nakamura, M. Fujimoto, N. Okada, Salmonella Typhimurium PagP- and UgtL-dependent resistance to antimicrobial peptides contribute to the gut colonization, PLoS One, 12 (2017) e0190095, 1-10.

[13] R.E. Bishop, H.S. Gibbons, T. Guina, M.S. Trent, S.I. Miller, C.R. Raetz, Transfer of palmitate from phospholipids to lipid A in outer membranes of gram-negative bacteria, EMBO J, 19 (2000) 5071-5080.

[14] S.C. Lee, T.J. Knowles, V.L.G. Postis, M. Jamshad, R.A. Parslow, Y.-p. Lin, A. Goldman, P. Sridhar, M. Overduin, S.P. Muench, T.R. Dafforn, A method for detergent-free isolation of membrane proteins in their local lipid environment, Nat Protoc, 11 (2016) 1149-1162.

[15] M.C. Fiori, Y. Jiang, G.A. Altenberg, H. Liang, Polymer-encased nanodiscs with improved buffer compatibility, Sci Rep, 7 (2017) 1-10.

[16] N.J. Cho, L.Y. Hwang, J.J.R. Solandt, C.W. Frank, Comparison of Extruded and Sonicated Vesicles for Planar Bilayer Self-Assembly, Materials, 6 (2013) 3294-3308.

[17] O. Korotych, J. Mondal, K.M. Asfura, J. Hendricks, B. D., J. Polym, Evaluation of commercially available styrene-co-maleic acid polymers for the extraction of membrane proteins from spinach chloroplast thylakoids, Europ Polym J, 114 (2018) 485-500.

[18] N.Z. Hardin, T. Ravula, G.D. Mauro, A. Ramamoorthy, Hydrophobic Functionalization of Polyacrylic Acid as a Versatile Platform for the Development of Polymer Lipid Nanodisks, Small, 15 (2019) 1-5.

[19] A.O. Oluwole, J. Klingler, B. Danielczak, J.O. Babalola, C. Vargas, G. Pabst, S. Keller, Formation of Lipid-Bilayer Nanodiscs by Diisobutylene/Maleic Acid (DIBMA) Copolymer, Langmuir, 33 (2017) 14378-14388.

[20] K. Yasuhara, J. Arakida, T. Ravula, S.K. Ramadugu, B. Sahoo, J.I. Kikuchi, A. Ramamoorthy, Spontaneous Lipid Nanodisc Formation by Amphiphilic Polymethacrylate Copolymers, J. Am. Chem. Soc, 139 (2017) 18657-18663.

[21] S. Lindhoud, V. Carvalho, J.W. Pronk, M.E. Aubin-Tam, SMA-SH: Modified Styrene-Maleic Acid Copolymer for Functionalization of Lipid Nanodiscs, Biomacromolecules, 17 (2016) 1516-1522.

[22] S.C.L. Hall, C. Tognoloni, J. Charlton, É.C. Bragginton, A.J. Rothnie, P. Sridhar, M. Wheatley, T.J. Knowles, T. Arnold, K.J. Edler, T.R. Dafforn, An acid-compatible co-polymer for the solubilization of membranes and proteins into lipid bilayer-containing nanoparticles, Nanoscale, 10 (2018) 10609-10619.

[23] M. Overduin, M. Esmaili, Native Nanodiscs and the Convergence of Lipidomics, Metabolomics, Interactomics and Proteomics, Appl Sci, 9 (2019) 1230-1245.

Chapter 5

Introduction to Cellular and Infectious

Prion Proteins

5.1. An overview of the history of prion diseases

Transmissible spongiform encephalopathies (TSEs) or prion diseases consist of a broad range of fatal neurological disorders affecting humans and animals. Contrary to Watson and Crick's 'central dogma', it is believed that prion diseases are caused by a protein, devoid of DNA involvement. The first reported prion disease was recorded in Marino sheep in the 18th century and was characterized by behaviors such as abnormal gait, excessive licking and pruritus that drives sheep to scrape themselves against the fences [1]. Later, human prion diseases, such as Kuru and Creutzfeldt–Jakob disease (CJD), were described in the early 20th century [2]. As a result of a wealth of interactive research by multiple groups, especially that of Stanley Prusiner, the "proteinaceous infectious particles" or "prion" hypothesis was established, a significant advancement in our understanding of biological systems, protein folding and infectious protein-misfolding diseases [3-7].

Briefly, the Prion hypothesis describes the templated misfolding of the native PrP protein, translated from *prn-p* gene, in TSE diseases. Interestingly, *prn-p*-knockout mice do not develop disease symptoms after inoculation with infectious protein, and yet infectious proteins can be produced *de novo* in bacteria [8-10]; these observations are among the most conclusive evidence of the exclusive role of "prion" protein in TSE diseases. Additional independent support for Prion hypothesis [11] was uncovered in 1994 when yeast prions such as Ure2p and Sup35 were discovered and demonstrated the same template-based misfolding of their folded isoforms. A year later, R.A. Bessen *et al.* replicated strain-specific PK- resistant PrP (PrP^{Sc}) in a cell-free system and proposed

a nucleation protein polymerization model for replication of the benign cellular isoform (PrP^C) to a disease-correlated isoform of PrP (also known as PrP <u>Sc</u>rapie, PrP^{Sc}) [12, 13].

Early biochemical and biophysical studies revealed that mammalian PrP^C [3] shows a 30-35 kDa band on SDS-PAGE as it can be post-translationally glycosylated at two asparagine residues and is sensitive to proteases [14]. Spectroscopic methods (Fourier-transform infrared (FT-IR) spectroscopy and circular dichroism (CD) and NMR spectroscopy revealed that the secondary structure of PrP^C contains three α helices (42%) and one β sheet (3%), a flexible disordered N-terminal domain, turns and a disulfide bond connecting helices 2 and 3 (Fig. 5.1) [15, 16]. Conversely, PrP^{Sc} contains a protease and detergent-resistant core of PrP^C (27-30 kDa) with a substantial increase in beta sheets (54%) [17]. The same biochemical characteristics are still used to identify different species of PrP^{Sc}, namely TME (in mink), CJD (in human), CWD (in cervids), and BSE (in cattle) [18]. Due to the significance of PrP in mammalian diseases, the metabolism (synthesis, trafficking and degradation) of PrP^C, as well as the structure of cellular PrP^C and PrP^{Sc} and the conversion between these two isoforms have been extensively studied.

Figure 5.1. One out of many solution NMR structures of the PrP domain of mouse PrP^C protein (121-231) (PDB 1AG2). α helices are shown in red, and β sheets and turns in green.

5.2. Synthesis, trafficking and degradation of PrP^C

PrP^C is expressed in the central nervous system, especially the neuronal cells of the brain, spinal cord, and, the glial cell, and, to a lesser extent, in the peripheral tissues. Nascent PrP receives a glycosyl-phosphatidylinositol (GPI) anchor at its C-terminus after synthesis in the endoplasmic reticulum (ER) and before transition to the Golgi. Further maturation of the glycan structures and GPI anchor occur in various segments of the Golgi apparatus, producing properly-folded PrP upon translocation to the outer leaflet of the plasma membrane [19]. This process, under normal condition, takes approximately 30 mins. The majority of PrP^C on the cell surface are localized in lipid rafts, and degradation of mature, cell-surface PrP occurs primarily via clathrin-based endocytosis and endosomal degradation (~3-4 hours) [20], which is also a standard route to recycle PrP back the plasma membrane [21, 22]. Defects in this pathway can generate low levels of aberrant PrP. For instance, ^{Ntm}PrP (N- terminus reversed PrP) is a product of inefficient

translocation through the Sec61 complex. Therefore, PrP remains transmembrane with reversed orientations of C- and N- termini (N-terminus inside cytosol and C-terminus inside the ER lumen), and ^{cyto}PrP entirely remains in the cytosol. Other machinery, such as the translocon-associated protein complex (TRAP) and the translocating chain associating membrane protein (TRAM), might influence the translocation process (Fig. 5.2) [23, 24]. This precise regulation of PrP biosynthesis and translocation suggests the importance of avoiding excess unfolded PrP in cells, especially during ER stress. The accumulation of misfolded species of PrP can lead to neurodegenerative disease and mutations on the signal sequence and hydrophobic domain (HD residues 112-135), which prevent the proper translocation of PrP, can lead to neurodegenerative disease in mice [25]. The damage through the accumulation of such defective species of PrP is cell-specific, which can lead to a neurodegenerative disease that, unlike prion diseases, is not transmissible [26, 27]. These observations challenge the link between the spontaneous formation of PrP^{Sc} and abnormal cellular species of PrP. Hypothetically, however, the accumulation of PrP^{Sc}, which is paired with lysosomal deficiency and increased ER stress, might decrease the degradation of aberrant species and trigger the downstream cytotoxicity and increase the formation of abnormal PrP.
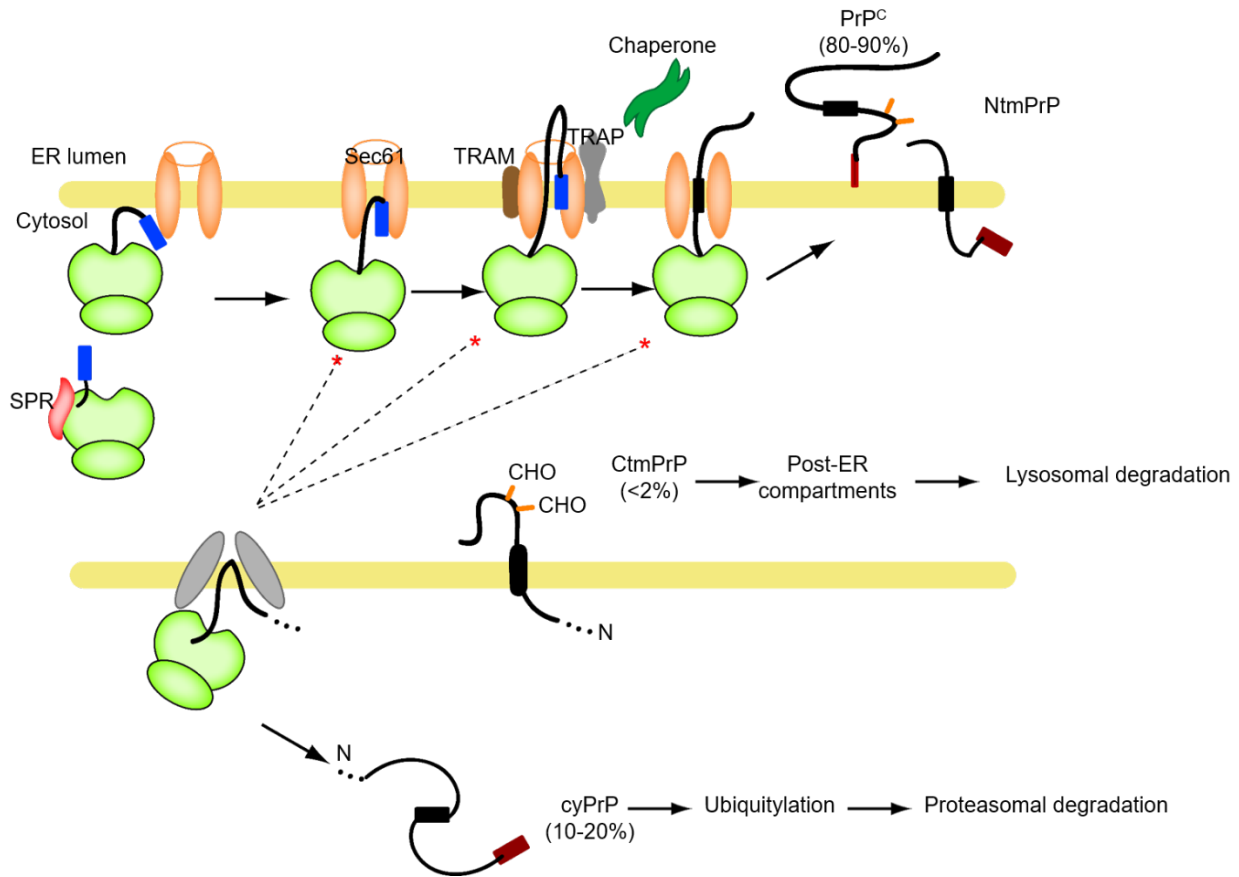
Figure 5.2. Schematic summary of the biosynthesis and trafficking of cellular PrP. Blue, red and black rectangles represent targeting sequence, the hydrophobic domain and GPI-anchor signal, respectively. CHOs indicate the N-glycan moieties.

A variety of clearance mechanisms exist to remove abnormal proteins. Unfolded or misfolded proteins might, either spontaneously or through chaperon-assisted processes, refold. Otherwise, they will be removed from the cytosol by the cell's degradation machinery or sequestered into organelles (*e.g.,* aggresome) that shield the unfolded species from exposure to other native proteins. Collectively, these strategies avoid the overwhelming saturation of chaperons and degradation compartments [28]. Aggregated species in inclusion bodies can go through ubiquitination and proteasomal degradation through the unfolded protein response (UPS) pathway. However,

experimental evidence of α.synuclein and N-terminal fragment of Huntington protein suggest that the ubiquitinated aggregates might block the proteasome or inhibit its function (Fig. 5.3) [29, 30]. Mis-localized PrP^C proteins experience different microenvironments, which may result in interacting with various partners (transcription factors, structural proteins, chaperons, autophagy factors) that, in turn, trigger or alter specific signaling pathways. This phenomenon is called the toxic sequestration model that has been used to explain other proteinopathies such as Alzheimer's, Huntington and Parkinson's diseases [31]. More insights on the cell biology and physiological function of normal PrP enhance our understanding of its disease-related isoform.
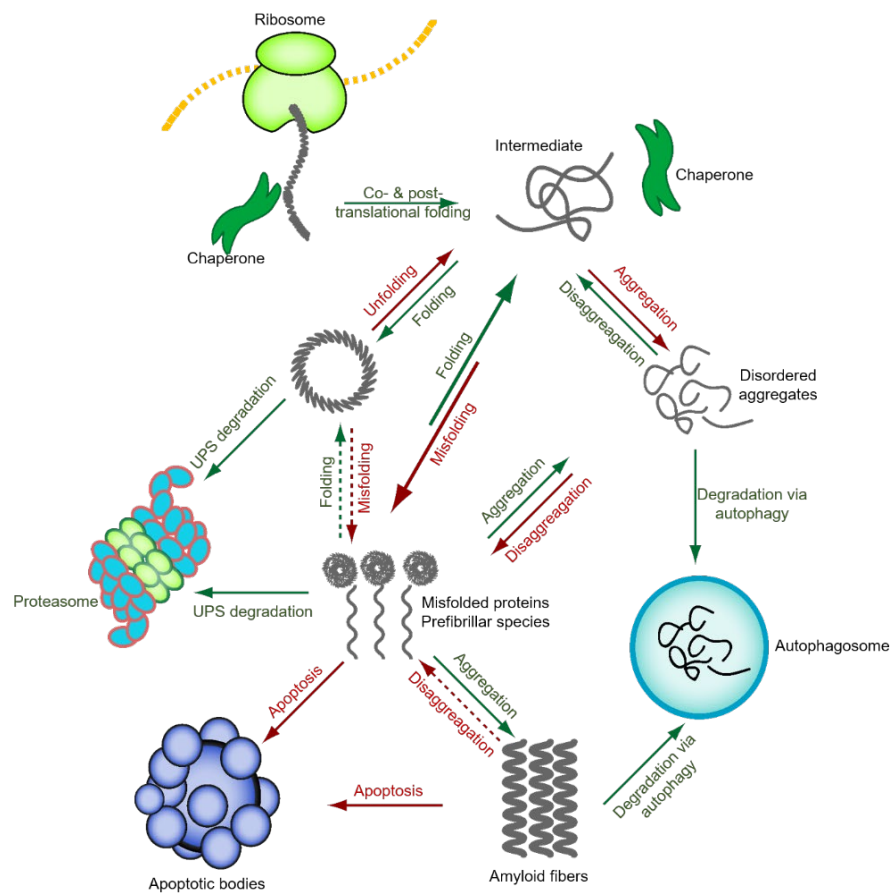
Figure 5.3. Cellular mechanisms to cope with unfolded and misfolded proteins. Chaperons assist the restoration of misfolded species. However, under certain

circumstances, misfolded/unfolded proteins undergo fibrillization and form pre-fibrillar oligomers, which if not degraded by proteasome and autophagosome, lead to amyloid fibers and eventually apoptotic cell death. Green and red arrows, respectively, mark how constructive and destructive these pathways are for the cells.

5.3. Physiological roles of PrP^C

In vivo and *in vitro* evidence suggests a cytoprotective role for PrP^C against apoptosis induced by Bax and Dpl as well as chronic oxidative stress, which have also been crucially important in other neurodegenerative diseases. However, the precise mechanism of this protection remains controversial. *Prnp*-knockout mice demonstrate higher susceptibility to oxidative stress-inducing chemicals and have significantly higher biochemical markers of oxidative stress (such as lipid peroxidation and carbonylated proteins). However, this does not narrow down the role of PrP, as any dysregulation in the cell, including-mitochondrial dysfunction, inflammation, impaired iron-metabolism, calcium signaling abnormalities, the elevated level of aggregate proteins, and altered proteasomal degradation pathways cause oxidative stress [33, 34]. Several proteins can interact with cell surface PrP^C, including laminin receptor precursor (LRP), NRAGE (Neurotrophin receptor-interacting MAGE homolog), and synapsin-1b, N-CAM. In many cases, the function of these interactions, particularly the cytoplasmic partners, remain elusive [35, 36].

Since PrP is a copper-binding protein, its role in copper metabolism has intrigued researchers. PrP^C contains four copper-binding sites located in residues 96,111 and histidines in the octa-repeat domain (Fig. 5.4) [37]. The binding of four copper ions to the octa-repeat domain is pH-dependent and negatively cooperative. Coordinating of Cu^{+2} to His96 and His111 induces the formation of beta-sheet, a significant conformational

change, inflexible N-terminal segment of PrP^C [38]. PrP^C is involved in cellular uptake of copper, which occurs through localization of PrP^C (from lipid raft) to clathrin-coated pits and, subsequently, endocytosis of PrP^C-copper complex to the cytosol [39]. Interestingly, the level of copper, yet not other heavy metals, decreases in *prn-p* knockout mice, supporting the crucial role of PrP^C in copper efflux. However, this pathway is not considered as a pivotal Cu^{+2} uptake route and may have additional regulatory functions [37].
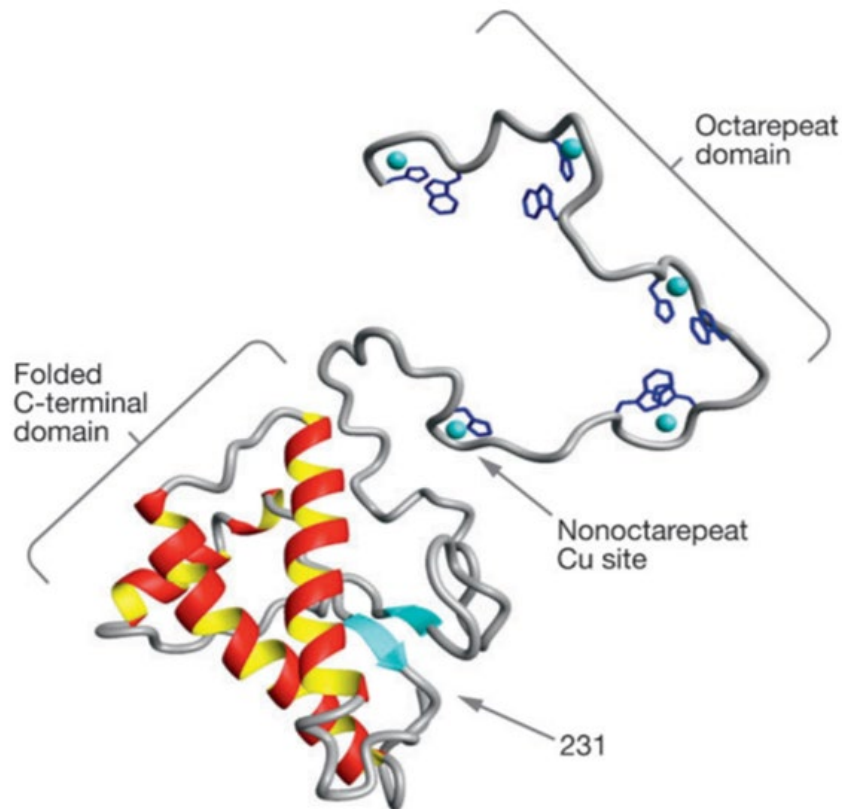
Figure 5.4. The copper-chelating capacity of PrP^C. Four copper ions coordinate with four distinct sites on the N-terminal part of cellular prion. Figure adapted with permission from ref [40].

PrP^C could also be involved in transmembrane signaling and, as a result, regulate neurotoxicity, neuronal survival, and axonal growth. Antibody-induced crosslinking [41] of

PrP^C on the cell surface revealed that elevated level of reactive oxygen species (ROS) and the downstream activation of Fyn tyrosine kinase, NADPH oxidase and extracellular-regulated kinases (ERKs), PI3/Akt and MAPK-dependent pathways contribute to the neuroprotective effects of PrP^C [42]. Further evidence supports the interaction between PrP^C and N-CAM in lipid rafts that promotes neurite outgrowth [43, 44]. Loss of synapses in prion disease implies the pivotal role of PrP^C in the formation of synapses and in the regulation of their proper function and structure. A considerable amount of evidence indicates the antegrade and retrograde transport of PrP^C in CNS and peripheral neurons [45]. Overall, it is unclear how the transformation of PrP^C to PrP^{Sc} triggers neurodegeneration, as the disease-associated isoform of PrP could either have its distinguished toxic function or impede the normal function of PrP^C in neurons (loss of function).

5.4. Overview of the structure and function of amyloids

There are numerous examples of proteinopathies (such as Parkinson's, Huntington's, Alzheimer's, Type II diabetes) caused by misfolded proteins that aggregate, form amyloids, and deposit either in peripheral tissues or in the central nervous system (CNS). Nevertheless, none of these share the transmissibility and infectivity of prion diseases. Cellular factors such as posttranslational modifications, degradation mechanisms and cell-surface accessibility are key elements that distinguish prion diseases from other types of proteinopathies [46].

Under a susceptible biochemical condition, any protein can form amyloid or amyloid-like structures. The presence of flexible disordered regions makes some amyloidogenic proteins more prone to build large and thermodynamically stable

aggregates. Aggregates show a low propensity for degradation and act as "seed" for the conversion of folded proteins and the propagation [47]. In prion diseases, PrP^{Sc} undergoes self-assembly via a nucleation-dependent polymerization mechanism and forms several quaternary structures [48]. This process (that resembles the crystallization process) begins with a nucleation step and follows by elongation steps, which are comprised the formation of oligomers, proto-fibrils, amorphous aggregates, and supermolecular fibers, and two-dimensional crystals that display another intriguing subassembly of truncated PrP^{Sc} [49, 50].

According to classical nucleation theory (CNT), the formation of nanoscale amyloid fibrils follows a sigmoid pattern, in which the lag and log phases represent a nucleation phase and incremental elongation of fibril length, respectively, and ends with a plateau phase. However, once the ratio of the log : lag phase enhances to 0.5 and above, the sigmoid shape turns to a hyperbolic curve. Nucleation can be either primary (from no seed in a reaction) or secondary (induced by breakage of fibrils); however, without a pre-formed fibril, the secondary nucleation seems implausible. A seed recruits more native protein (*e.g.,* PrP^{C}) and templates identical structures along the axis (replication). The growth of fiber depends on the availability of each soluble and aggregated proteins (reacting species) [48]. Inspired by this mechanism, scientists can replicate PrP^{Sc} species *in vitro* using misfolding cyclic amplification (PMCA) technique (Fig. 5.5) [51].
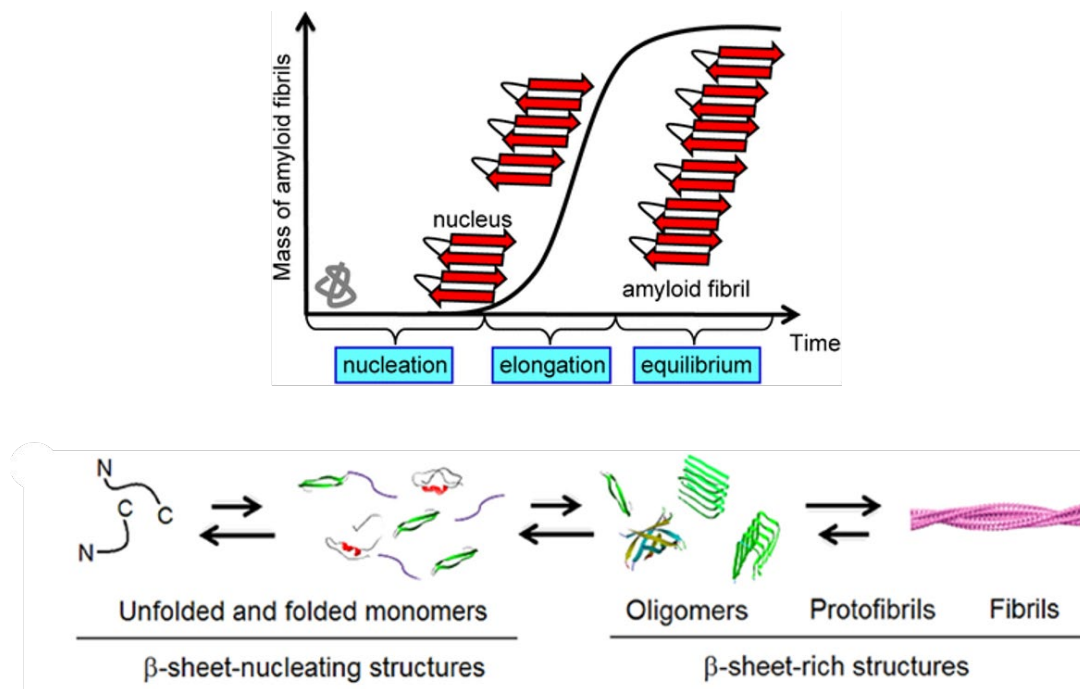
Figure 5.5. *In vitro* amplification of PrP^{Sc} follows a sigmoid plot (consisting of nucleation, elongation and equilibration phases) leads to formation of β-sheet-rich oligomers, protofilaments, and rod fibers. Figure reproduced from ref [48, 52].

The amyloid-beta structure is an evolutionary well-conserved structure from bacteria to mammals and is not necessarily pathologic. Current evidence exhibits functional amyloids responsible for such diverse actions as biofilm formation in bacteria (*e.g.,* curli fiber), cell regulation in yeast (such as PSI$^+$ and HET-s), and the synthesis of melanin and hemostasis in mammals (*e.g.,* Pmel and fibrin) [53]. Due to their resistance to proteolytic digestion and self-perpetuating capacities, amyloid structures can be considered as molecular memory [54, 55].

Amyloid fibers were first clinically observed as insoluble fibril deposits in over 40 deadly human diseases and could also be stained by Congo red, resulting in green, yellow, or red birefringence [56]. The standard X-ray diffraction pattern of amyloid fibril indicates a very ordered cross-β-structure, in which β-strands are stacked perpendicularly

123

to the Y-axis of the fiber and steric-zipper sidechain interaction (interdigitated β-sheets) that are arranged either in a Parallel-In-Register-β-Sheet (PIRIBS) or β-solenoid (βS) conformations (2-rung or four-rung βS) (Fig. 5.6) [57, 58]. Initial attempts using a library of motif-grafted antibodies revealed that residues within 23-33, 89-104 and 136-158 segments of PrP^C are three PrP^{Sc}-recognition motifs that serve at the interface between PrP^C and PrP^{Sc} and are necessary for this conversion [59, 60]. Furthermore, large truncations at both N- and C- terminal sequences of PrP^C hinder this reaction. Surface chemical labeling of lysine and tyrosine residues confirmed that the C terminus of PrP^C undergoes a tremendous conformation change during the transition to scrapie isoform [61]. Sequence-based statistical coupling analysis (SCA) implies that α2 and α3 helices are the initial segments that undergo transformation [62].

Interestingly, the differences in the amino acid sequence of PrP^C further translate into unique secondary structures (non-genetic conformational polymorphisms), which may explain differences in the interspecies barrier of prion structure and transmission of prion disease. For instance, *in vivo* and *in vitro* evidence suggest that the loop (L1), connecting β1 and α2, displays variable rigidity in different animals. Location of loops and turns that link β-sheets exhibit a vital role in the rise of different strains of prions, which explains why the use of different strains may lead to impeded nucleation polymerization of specific stain of PrP^{Sc}, hence imposes interspecies barrier for transmission of disease [63-66].

How a newly recruited PrP^C converts to nascent PrP^{Sc} and forms a new infectious isoform has remained a mystery until recently, when computational analysis (coarse-grained molecular dynamics simulation) using 4-rung β-solenoid structure as a working

124

model, shone a light on this template-based and mechanistically precise replicative complex [67].
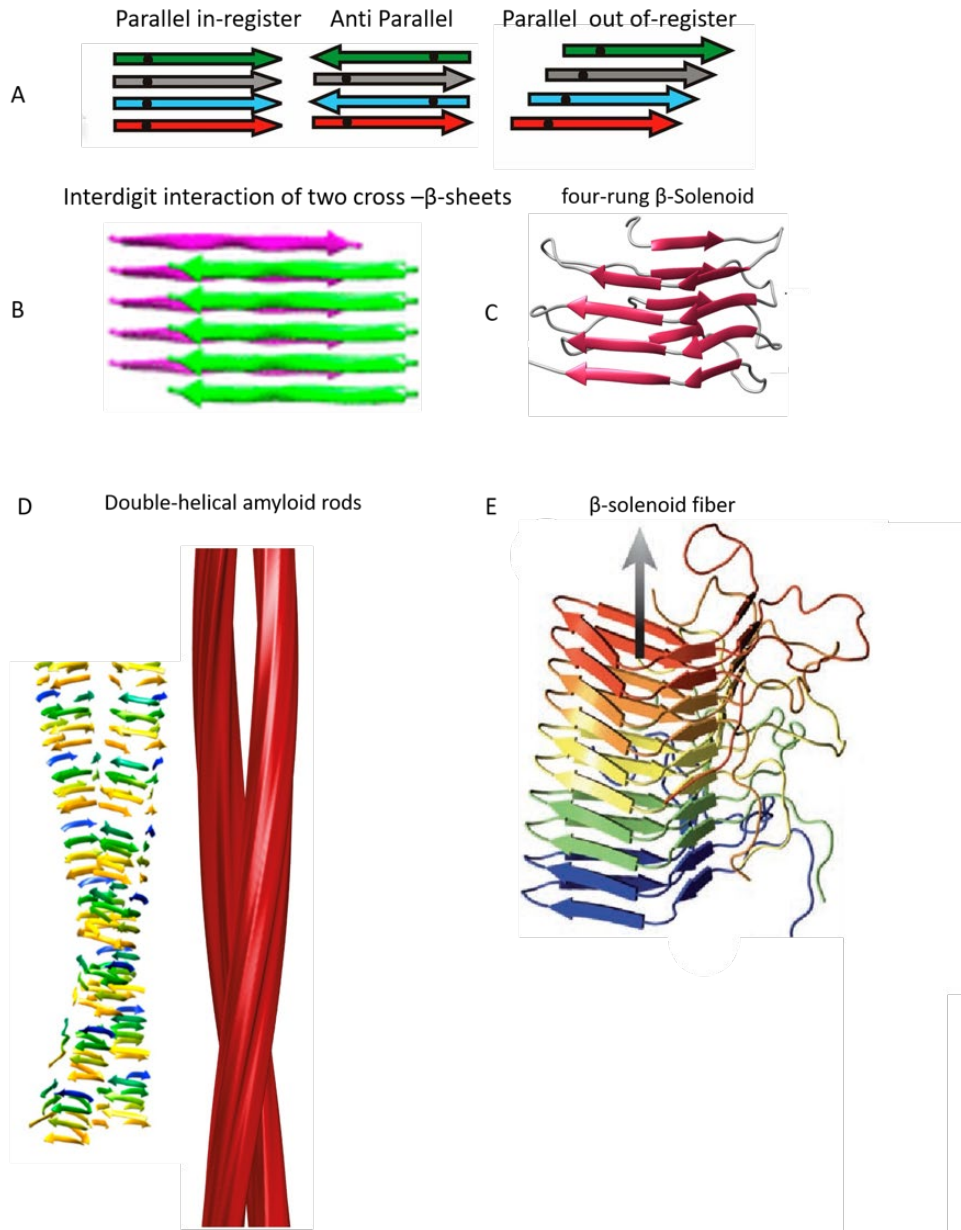
Figure 5.6. A. Schematic illustrations of some possible arrangements of β-sheets (adapted with permission from ref [68]) that lead to the formation of protofilaments with cross-β (B; adapted with permission from ref [69]) and arc 4-rung-β-solenoid structures (C; adapted with permission from ref [67]). D. Cryo-EM reconstitution of double-helical mammalian PrP^{Sc} rod (adapted with permission from ref [70]). E. The solid-state NMR

structure (PDB 2RNM) of amyloid fiber of HET-s (218-289) with β-solenoid structure (adapted with permission from ref [58]). Arrow indicates the fiber axis.

Atomic force microscopy (AFM) and electron microscopy (negative-stained), NMR, high-resolution cryo-electron microscopy, and X-ray crystallography of fibrillar proteins and peptides isolated from infected hosts or prepared *in vitro* unveiled that the quaternary structures of prion fibrils, as well as their constituent steric-zipper structures, are highly polymorphic [71]. The elements of structural polymorphism include fibril morphologies (such as helical and flat ribbon fibrils of α-synuclein and Tau), the degree of twist angle, the length and mass of each fibril, and the number of protofilament units per fibril (Fig. 5.7). Strong Van der Waals and electrostatic interactions in steric zippers (steric fit) and many hydrogen bonds along the fiber length stabilize the fiber structure. Due to the large variation in amyloid fibrillar structures, which occur even under the same controlled conditions and in tissues, there must be an unknown mechanism that controls such diversity [72]. Notably, *in vitro* bacterially-expressed fibrillar recombinant prions (rec-PrP) are not infectious (with $\geq 10^5$ times less infectivity) [73]. However, under a process termed "deformed templating", intracerebral injection of these rec-PrP fibers and multiple rounds of *in vivo* passages leads to the propagation of fully infectious PrP^{Sc} amyloid fibers [74].
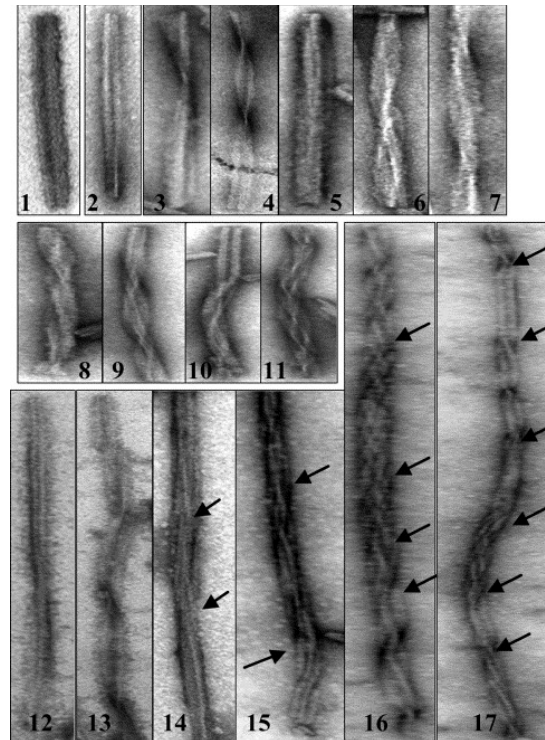
Figure 5.7. Negative-stained electron micrographs of amyloid fibers with different morphologies formed under the same *in vitro* condition. Arrows point to sites where changes in twisting take place. Figure adapted with permission from ref [71].

The self-assembly of amyloid rods is an evolutionarily conserved mechanism to form a long-lasting structure. The link between early molecular events leading to fibrilization of prions and the infectivity of these particles is not well known. A growing body of evidence supports the idea that small intermediate oligomers that form in the onset of the polymerization reaction are considerably more infectious than fibrillar superstructures [54]. Since the conception of the "protein-only" hypothesis, efforts have been made to isolate the high-titer infectious prion particles from the brains of terminally sick hosts as well as to over-express the PrP^{Sc} particles *in vitro* using cell-based assays [75]. The protease-resistant nature of PrP^{Sc} facilitates its purification from a pool of cellular proteins and the use of detergents (to remove copurified lipids) improved the purity of *ex*

vivo amyloid fibers, which were thought to be the artifact caused by purification conditions. Therefore, concurrently, many scientists sought to characterize smaller infectious oligomers (intermediate states of fibril formation), which show higher infectivity than rod fibrillar prions *in vivo* even independent from the endogenous expression of PrP^C [76, 77].

As demonstrated by domain-specific antibodies, granular oligomeric states expose a stretch of hydrophobic residues that drive their insertion into the membrane, hence explains their cellular toxicity [77]. Such particles also exhibit higher cellular uptake, which can trigger intracellular toxicity by the interaction of oligomers with mitochondrial membrane and the release of cytochrome c [78]. Soluble oligomeric particles, which are not proteinase K-sensitive, contain β-sheet enriched structure [50, 79]. Similarly, early oligomeric species are possible sources of cytotoxicity in other neurodegeneration-associated proteins such as Tau and α-synuclein. The level of apoptotic markers (such as BrdU) elevates more in oligomeric-infected tissues than in those infected with fibrillar PrP^{Sc}. Utilizing a combination of immunogold labeling and cryo-EM assures a high-resolution approach for the identification of these transition states [80]. Overall, the intermediate states of fibrilization promise to be more efficient targets for drug design and pharmaceutical intervention. However, due to protease sensitivity of these species, relatively low abundance in infected cells, heterogeneous structure, and the experimental challenges associated with the purification of oligomers, there is no high-resolution structure for them [81].

The most accurate *ex vivo* structure of mouse infectious prion (protease-treated and N-terminally-truncated PrP27-30) displays a fibrillar rod (20 nm in width) with two fibers each containing double-helical substructures (protofilaments) and are separated

with a gap (of 8-10 nm) filled with irregularly-structured and low-electron density material (mainly lipids, *N*-linked glycan) [82]. This structure suggests a β-solenoid structure for PrP^{Sc}. On the other hand, the fibrillar recombinant prions show a single fiber with 10 nm width that contains two helical protofilaments [70, 83]. Heterogeneity of isolated sample (glycan branches, and GPI anchor) from infected tissue is the most limiting factor in structural analysis of prions. Surprisingly, the cryo-EM structure of anchor-less mammalian prion 27-30 is also a β-solenoid structure and supports a head-to-head orientation of PrP^{Sc} monomer with each protofilament estimated to be approximately 3-6 nm in diameter [84]. Many β-helix structures (pectin methylesterase and β-barrels) follow a negative-design strategy to avoid edge-edge propagation of β-helical structure. Likewise, amyloid β-solenoid structures are capped by an α-helix or a strand to prevent unlimited amplification (and aggregation), and they follow a head-to-tail or head-to-head/tail-to-tail elongation pattern. Structural data, thus far, falls in favor of head-to-head/tail-to-tail rearrangement mechanism [70, 85].

Mass spectrometric analyses of PK-digested fragments derived from GPI-anchorless PrP^{Sc}, 263K PrP^{Sc} (from hamster), and DY PrP^{Sc} indicate that all these structures share a typical β-solenoid structure; however, this experiment requires that all glycans be cleaved off before analysis [86]. Many proteases don't have a cleavage site on PrP^{Sc}, and this property enables scientists to isolate and structurally analyze intact PrP^{Sc} proteins directly from tissues [87], disproving the speculation that amyloid structure is the result of protease digestion and use of detergents. In other words, intact PrP^{Sc} fibrils are actively present in infected tissues and the presence of lipid-dissociating reagents (such as detergents or phosphotungstic acid (PTA) perturbs the membrane environment

and increase the PrP^{Sc} self-assembly [88]. The "deformed templating" mechanism allows the generation of milligram amounts of full-length and ^{13}C and ^{15}N labeled recombinant PrP^{Sc} fibrils that can be analyzed by solid-state NMR spectroscopy. The results of such structural analyses agreed with the classic in-register-β-stack model, suggesting the recombinant-sourced prions differ from endogenous PrP^{Sc} fibers, yet the high-resolution structure of this infectious recPrP^{Sc} would reveal much about the enigmatic "deformed templating" mechanism [89]. Taken together, despite all discoveries in the field of prion, the high-resolution structure of PrP^{Sc} itself remains elusive due to the thermodynamically unstable nature of PrP^{Sc}.

5.5. Roles of cofactors in the transition of PrP^{C} to PrP^{Sc}

Co-factors such as anionic lipids (1-palmitoyl-2-oleoyl-sn-glycerol-3-phospho-glycerol; POPG) [90] and RNA molecules [73] can reportedly initiate the transition of PrP^{C} to the infectious PrP^{Sc} by inducing considerable structural rearrangements that result in the infectivity of recombinant PrP. Step-wise addition of POPG and RNA to rec-PrP cause the formation of two non-infectious intermediates, which after an *in vitro* PMCA amplification, resulting in the production of 100% fully infectious species [91]. Intriguingly, deuterium exchange mass spectrometry (DXMS) analysis on overlapping peptides derived from partial hydrolysis of the purified intermediates can track solvent accessibility of the backbone amides in rec-PrP-POPG and POPG-rec-PrP-RNA intermediates. Incubation with the lipid cofactor leads to dominant conformational changes in entire α-helices and β2, notably helix 1 and β strand 2 nearly unfold, while the α2-α3 loop becomes less accessible. CD and FT-IR experiment confirmed that they form a β-sheet. Besides, amino acids in N-terminus become less accessible by creating a secondary structure

(either α-helix or β-sheet). Hydrophobic interaction between POPG and segment 111–117 of PrP^C protects this area from proteolytic digestion. The immediate effect of RNA in exposing the N-terminal domain appears to be essential, particularly during PMCA amplification. In the absence of RNA, anionic lipids such as phosphatidylserine (PS), phosphatidyl inositol (PI), and phosphatidyl glycerol (PG) are unable to drive the transition of PrP^C to PrP^{Sc}. Yet, PE alone is sufficient to drive this reaction in all animal species [92]. RNA alone can stimulate (or catalyze) the pathological transformation only in a small number of species (sheep and hamster) [93, 94]. Experimental evidence indicates that cofactors such as RNA and lipids could be determining factors in differentiating prion strains. Nucleic acid sequence, length, and quaternary structures (for instance, quadruplex structure) can influence the binding affinity of cofactors to PrP^C and are critical for its conversion [95]. Further explorations have unveiled the catalytic role of small extracellular non-coding RNAs, DNAs [96] and sulfated glycosaminoglycans [97] in the transformation of PrP^C to PrP^{Sc} and PrP^{Sc}-like species in cholesterol-rich lipid raft membrane microdomains [98].

Among lipids, metabolism of cholesterol has been widely studied in many neurogenerative diseases, such as Niemann Pick Type C (NPC), Alzheimer's [99], prion diseases, as well as in protein misfolding diseases such as Tauopathies, and type II diabetes [100]. Regarding prions, plasma levels of cholesterol, carried mainly by apo-lipoproteins B, controls the propagation, and consequently infectivity, of prions in mice. *In vitro* studies demonstrate that during prion infection, the expression level of one of the cholesterol receptors (cholesterol efflux regulatory protein (CERP) or ATP-binding cassette transporter; ABCA1) elevates, although its abundance on the plasma membrane

decreases by 50%. Moreover, localization and internalization of ABCA1 receptor on lipid rafts are controlled by cell-surface PrP^{Sc}, which leads to the reduction in efflux of cholesterol. Lipid analysis of *in vitro* PrP^{Sc}-infected cells shows that cholesterol esters, free cholesterol, phosphatidylethanolamine (PE), and triglycerides were significantly increased without remarkable changes in level of other lipid classes [101].

5.6. References

[1] M.D. Zabel, C. Reid, A brief history of prions, Pathog Dis, 73 (2015).

[2] R.H. Wilkins, I.A. Brody, Creutzfeldt-Jakob disease, Arch Neurol, 25 (1971) 572-573.

[3] B. Oesch, D. Westaway, M. Walchli, M.P. McKinley, S.B. Kent, R. Aebersold, R.A. Barry, P. Tempst, D.B. Teplow, L.E. Hood, et al., A cellular gene encodes scrapie PrP 27-30 protein, Cell, 40 (1985) 735-746.

[4] G.D. Hunter, R.A. Gibbons, R.H. Kimberlin, G.C. Millson, Further Studies of Infectivity and Stability of Extracts and Homogenates Derived from Scrapie Affected Mouse Brains, J Comp Pathol, 79 (1969) 101-108.

[5] I.H. Pattison, Resistance of the Scrapie Agent to Formalin, J Comp Pathol, 75 (1965) 159-164.

[6] S.B. Prusiner, Novel proteinaceous infectious particles cause scrapie, Science, 216 (1982) 136-144.

[7] H.J. Cho, Requirement of a protein component for scrapie infectivity, Intervirology, 14 (1980) 213-216.

[8] Z.H. Zhang, Y. Zhang, F. Wang, X.H. Wang, Y.Y. Xu, H.Y. Yang, G.H. Yu, C.G. Yuan, J.Y. Ma, De novo generation of infectious prions with bacterially expressed recombinant prion protein, FASEB J, 27 (2013) 4768-4775.

[9] R.C. Moore, J. Hope, P.A. McBride, I. McConnell, J. Selfridge, D.W. Melton, J.C. Manson, Mice with gene targetted prion protein alterations show that Prnp, Sinc and Prni are congruent, Nat Genet, 18 (1998) 118-125.

[10] M.A. Barria, A. Mukherjee, D. Gonzalez-Romero, R. Morales, C. Soto, De Novo Generation of Infectious Prions In Vitro Produces a New Disease Phenotype, PLoS Pathog, 5 (2009).

[11] R.B. Wickner, [Ure3] as an Altered Ure2 Protein - Evidence for a Prion Analog in Saccharomyces-Cerevisiae, Science, 264 (1994) 566-569.

[12] R.A. Bessen, D.A. Kocisko, G.J. Raymond, S. Nandan, P.T. Lansbury, B. Caughey, Non-genetic propagation of strain-specific properties of the scrapie prion protein, Nature, 375 (1995) 698-700.

[13] J.H. Come, P.E. Fraser, P.T. Lansbury, A Kinetic-Model for Amyloid Formation in the Prion Diseases - Importance of Seeding, Proc Natl Acad Sci USA, 90 (1993) 5959-5963.

[14] D.C. Bolton, M.P. Mckinley, S.B. Prusiner, Identification of a Protein That Purifies with the Scrapie Prion, Science, 218 (1982) 1309-1311.

[15] R. Riek, S. Hornemann, G. Wider, M. Billeter, R. Glockshuber, K. Wuthrich, NMR structure of the mouse prion protein domain PrP(121-231), Nature, 382 (1996) 180-182.

[16] K.J. Knaus, M. Morillas, W. Swietnicki, M. Malone, W.K. Surewicz, V.C. Yee, Crystal structure of the human prion protein reveals a mechanism for oligomerization, Nat Struct Biol, 8 (2001) 770-774.

[17] L.M. Miller, M.W. Bourassa, R.J. Smith, FTIR spectroscopic imaging of protein aggregation in living cells, Biochim Biophys Acta-Biomembr, 1828 (2013) 2339-2346.

[18] M. Fiorini, M. Bongianni, S. Monaco, G. Zanusso, Biochemical Characterization of Prions, Prog Mol Biol Transl, 150 (2017) 389-407.

[19] O. Chakrabarti, A. Ashok, R.S. Hegde, Prion protein biosynthesis and its emerging role in neurodegeneration, Trends Biochem Sci, 34 (2009) 287-295.

[20] D.R. Borchelt, M. Scott, A. Taraboulos, N. Stahl, S.B. Prusiner, Scrapie and Cellular Prion Proteins Differ in Their Kinetics of Synthesis and Topology in Cultured-Cells, J Neuropath Exp Neur, 49 (1990) 743-752.

[21] C. Sunyach, A. Jen, J. Deng, K.T. Fitzgerald, Y. Frobert, J. Grassi, M.W. McCaffrey, R. Morris, The mechanism of internalization of glycosylphosphatidylinositol-anchored prion protein, EMBO J, 22 (2003) 3591-3601.

[22] B. Hay, R.A. Barry, I. Lieberburg, S.B. Prusiner, V.R. Lingappa, Biogenesis and Transmembrane Orientation of the Cellular Isoform of the Scrapie Prion Protein, Mol Cell Biol, 7 (1987) 914-920.

[23] S. Voigt, B. Jungnickel, E. Hartmann, T.A. Rapoport, Signal sequence-dependent function of the TRAM protein during early phases of protein transport across the endoplasmic reticulum membrane, J Cell Biol, 134 (1996) 25-35.

[24] R.D. Fons, B.A. Bogert, R.S. Hegde, Substrate-specific function of the translocon-associated protein complex during translocation across the ER membrane, J Cell Biol, 160 (2003) 529-539.

[25] R.S. Hegde, P. Tremblay, D. Groth, S.J. DeArmond, S.B. Prusiner, V.R. Lingappa, Transmissible and genetic prion diseases share a common pathway of neurodegeneration, Nature, 402 (1999) 822-826.

[26] G. Zanusso, R.B. Petersen, T.C. Jin, Y. Jing, R. Kanoush, S. Ferrari, P. Gambetti, N. Singh, Proteasomal degradation and N-terminal protease resistance of the codon 145 mutant prion protein, J Biol Chem, 274 (1999) 23396-23404.

[27] J. Heske, U. Heller, K.F. Winklhofer, J. Tatzelt, The C-terminal globular domain of the prion protein is necessary and sufficient for import into the endoplasmic reticulum, J Biol Chem, 279 (2004) 5435-5443.

[28] E. Cohen, A. Taraboulos, Scrapie-like prion protein accumulates in aggresomes of cyclosporin A-treated cells, EMBO J, 22 (2003) 404-417.

[29] M.S. Hipp, C.N. Patel, K. Bersuker, B.E. Riley, S.E. Kaiser, T.A. Shaler, M. Brandeis, R.R. Kopito, Indirect inhibition of 26S proteasome activity in a cellular model of Huntington's disease, J Cell Biol, 196 (2012) 573-587.

[30] T. Nonaka, M. Hasegawa, A Cellular Model To Monitor Proteasome Dysfunction by alpha-Synuclein, Biochemistry, 48 (2009) 8014-8022.

[31] G. Matsumoto, S. Kim, R.I. Morimoto, Huntingtin and mutant SOD1 form aggregate structures with distinct molecular properties in human cells, J Biol Chem, 281 (2006) 4477-4485.

[32] H. Olzscha, Posttranslational modifications and proteinopathies: how guardians of the proteome are defeated, Biol Chem, 400 (2019) 895-915.

[33] B.S. Wong, T. Liu, R.L. Li, T. Pan, R.B. Petersen, M.A. Smith, P. Gambetti, G. Perry, J.C. Manson, D.R. Brown, M.S. Sy, Increased levels of oxidative stress markers detected in the brains of mice devoid of prion protein, J Neurochem, 76 (2001) 565-572.

[34] F.R. Bertuchi, D.M.G. Bourgeon, M.C. Landemberger, V.R. Martins, G. Cerchiaro, PrPC displays an essential protective role from oxidative stress in an astrocyte cell line derived from PrPC knockout mice, Biochem Bioph Res Commun, 418 (2012) 27-32.

[35] L. Westergard, H.M. Christensen, D.A. Harris, The cellular prion protein (PrPC): Its physiological function and role in disease, Biochim Biophys Acta-Mol Basis Dis, 1772 (2007) 629-644.

[36] K.S. Lee, R. Linden, M.A.M. Prado, R.R. Brentani, V.R. Martins, Towards cellular receptors for prions, Rev Med Virol, 13 (2003) 399-408.

[37] D.R. Brown, K. Qin, J.W. Herms, A. Madlung, J. Manson, R. Strome, P.E. Fraser, T. Kruck, A. von Bohlen, W. Schulz-Schaeffer, A. Giese, D. Westaway, H. Kretzschmar, The cellular prion protein binds copper in vivo, Nature, 390 (1997) 684-687.

[38] C.E. Jones, S.R. Abdelraheim, D.R. Brown, J.H. Viles, Preferential Cu^{2+} coordination by His96 and His111 induces beta-sheet formation in the unstructured amyloidogenic region of the prion protein, J Biol Chem, 279 (2004) 32018-32027.

[39] P.C. Pauly, D.A. Harris, Copper stimulates endocytosis of the prion protein, J Biol Chem, 273 (1998) 33107-33110.

[40] G.L. Millhauser, Copper and the prion protein: Methods, structures, function, and disease, Annu Rev Phys Chem, 58 (2007) 299-320.

[41] R. Loertscher, P. Lavery, The role of glycosylphosphatidylinositol (GPI)-anchored cell surface proteins in T-cell activation, Transpl Immunol, 9 (2002) 93-96.

[42] L. Solforosi, J.R. Criado, D.B. McGavern, S. Wirz, M. Sanchez-Alavez, S. Sugama, L.A. DeGiorgio, B.T. Volpe, E. Wiseman, G. Abalos, E. Masliah, D. Gilden, M.B. Oldstone, B. Conti, R.A. Williamson, Cross-linking cellular prion protein triggers neuronal apoptosis in vivo, Science, 303 (2004) 1514-1516.

[43] A. Santuccione, V. Sytnyk, I. Leshchyns'ka, M. Schachner, Prion protein recruits its neuronal receptor NCAM to lipid rafts to activate p59fyn and to enhance neurite outgrowth, J Cell Biol, 169 (2005) 341-354.

[44] J. Kanaani, S.B. Prusiner, J. Diacovo, S. Baekkeskov, G. Legname, Recombinant prion protein induces rapid polarization and development of synapses in embryonic rat hippocampal neurons in vitro, J Neurochem, 95 (2005) 1373-1386.

[45] K.L. Moya, R. Hassig, C. Creminon, I. Laffont, L. Di Giamberardino, Enhanced detection and retrograde axonal transport of PrPc in peripheral nerve, J Neurochem, 88 (2004) 155-160.

[46] D.A. Harris, H.L. True, New insights into prion structure and toxicity, Neuron, 50 (2006) 353-357.

[47] F.U. Hartl, M. Hayer-Hartl, Converging concepts of protein folding in vitro and in vivo, Nat Struct Mol Biol, 16 (2009) 574-581.

[48] E. Chatani, N. Yamamoto, Recent progress on understanding the mechanisms of amyloid nucleation, Biophys Rev, 10 (2018) 527-534.

[49] Y. Goto, Revisiting supersaturation as a factor determining amyloid fibrillation, Prion, 10 (2016) 32-39.

[50] C. Govaerts, H. Wille, S.B. Prusiner, F.E. Cohen, Evidence for assembly of prions with left-handed beta-helices into trimers, Proc Natl Acad Sci USA, 101 (2004) 8342-8347.

[51] C. Soto, G.P. Saborio, L. Anderes, Cyclic amplification of protein misfolding: application to prion-related disorders and beyond, Trends Neurosci, 25 (2002) 390-394.

[52] E. Cerasoli, M.G. Ryadnov, B.M. Austen, The elusive nature and diagnostics of misfolded Abeta oligomers, Front Chem, 3 (2015) 17-23.

[53] C.P.J. Maury, The emerging concept of functional amyloid, J Intern Med, 265 (2009) 329-334.

[54] J.J. Wiltzius, M. Landau, R. Nelson, M.R. Sawaya, M.I. Apostol, L. Goldschmidt, A.B. Soriaga, D. Cascio, K. Rajashankar, D. Eisenberg, Molecular mechanisms for protein-encoded inheritance, Nat Struct Mol Biol, 16 (2009) 973-978.

[55] J. Shorter, S. Lindquist, Prions as adaptive conduits of memory and inheritance, Nat Rev Genet, 6 (2005) 435-450.

[56] J.D. Sipe, M.D. Benson, J.N. Buxbaum, S. Ikeda, G. Merlini, M.J.M. Saraiva, P. Westermark, Nomenclature 2014: Amyloid fibril proteins and clinical classification of the amyloidosis, Amyloid, 21 (2014) 221-224.

[57] B.R. Groveman, M.A. Dolan, L.M. Taubner, A. Kraus, R.B. Wickner, B. Caughey, Parallel In-register Intermolecular beta-Sheet Architectures for Prion-seeded Prion Protein (PrP) Amyloids, J Biol Chem, 289 (2014) 24129-24142.

[58] C. Wasmer, A. Lange, H. Van Melckebeke, A.B. Siemer, R. Riek, B.H. Meier, Amyloid fibrils of the HET-s(218-289) prion form a beta solenoid with a triangular hydrophobic core, Science, 319 (2008) 1523-1526.

[59] L. Solforosi, A. Bellon, M. Schaller, J.T. Cruite, G.C. Abalos, R.A. Williamson, Toward molecular dissection of PrPC-PrPSc interactions, J Biol Chem, 282 (2007) 7465-7471.

[60] G. Moroncini, N. Kanu, L. Solforosi, G. Abalos, G.C. Telling, M. Head, J. Ironside, J.P. Brockes, D.R. Burton, R.A. Williamson, Motif-grafted antibodies containing the replicative interface of cellular PrP are specific for PrPSc, Proc Natl Acad Sci USA, 101 (2004) 10404-10409.

[61] B.B. Gong, A. Ramos, E. Vazquez-Fernandez, C.J. Silva, J. Alonso, Z.S. Liu, J.R. Requena, Probing structural differences between PrPC and PrPSc by surface nitration and acetylation: evidence of conformational change in the C-terminus, Biochemistry, 50 (2011) 4963-4972.

[62] J. Chen, D. Thirumalai, Helices 2 and 3 are the initiation sites in the PrP(C) --> PrP(SC) transition, Biochemistry, 52 (2013) 310-319.

[63] A.D. Gossert, S. Bonjour, D.A. Lysek, F. Fiorito, K. Wuthrich, Prion protein NMR structures of elk and of mouse/elk hybrids, Proc Natl Acad Sci USA, 102 (2005) 646-650.

[64] T.D. Kurt, C. Bett, N. Fernandez-Borges, S. Joshi-Barr, S. Hornemann, T. Rulicke, J. Castilla, K. Wuthrich, A. Aguzzi, C.J. Sigurdson, Prion Transmission Prevented by Modifying the beta 2-alpha 2 Loop Structure of Host PrPC, J Neurosci, 34 (2014) 1022-1027.

[65] T.D. Kurt, G.C. Telling, M.D. Zabel, E.A. Hoover, Trans-species amplification of PrP(CWD) and correlation with rigid loop 170N, Virology, 387 (2009) 235-243.

[66] L.M. Kyle, T.R. John, R.V. Lewis, H.M. Schatzl, Introducing a rigid loop structure from deer into mouse prion protein increases its propensity for misfolding in vitro, Prion, 7 (2013) 88-89.

[67] G. Spagnolli, M. Rigoli, S. Orioli, A.M. Sevillano, P. Faccioli, H. Wille, E. Biasini, J.R. Requena, Full atomistic model of prion structure and conversion, PLoS Pathog, 15 (2019) 1-18.

[68] A. Gorkovskiy, K.R. Thurber, R. Tycko, R.B. Wickner, Locating folds of the in-register parallel beta-sheet of the Sup35p prion domain infectious amyloid, Proc Natl Acad Sci USA, 111 (2014) 4615-4622.

[69] A. Schmidt, K. Annamalai, M. Schmidt, N. Grigorieff, M. Fandrich, Cryo-EM reveals the steric zipper structure of a light chain-derived amyloid fibril, Proc Natl Acad Sci USA, 113 (2016) 6200-6205.

[70] E. Vazquez-Fernandez, M.R. Vos, P. Afanasyev, L. Cebey, A.M. Sevillano, E. Vidal, I. Rosa, L. Renault, A. Ramos, P.J. Peters, J.J. Fernandez, M. van Heel, H.S. Young, J.R. Requena, H. Wille, The Structural Architecture of an Infectious Mammalian Prion Using Electron Cryomicroscopy, PLoS Pathog, 12 (2016) 1-21.

[71] M. Anderson, O.V. Bocharova, N. Makarava, L. Breydo, V.V. Salnikov, I.V. Baskakov, Polymorphism and ultrastructural organization of prion protein amyloid fibrils: an insight from high-resolution atomic force microscopy, J Mol Biol, 358 (2006) 580-596.

[72] S. Zhang, M. Andreasen, J.T. Nielsen, L. Liu, E.H. Nielsen, J. Song, G. Ji, F. Sun, T. Skrydstrup, F. Besenbacher, N.C. Nielsen, D.E. Otzen, M. Dong, Coexistence of

ribbon and helical fibrils originating from hIAPP(20-29) revealed by quantitative nanomechanical atomic force microscopy, Proc Natl Acad Sci USA, 110 (2013) 2798-2803.

[73] F. Wang, X.H. Wang, C.G. Yuan, J.Y. Ma, Generating a Prion with Bacterially Expressed Recombinant Prion Protein, Science, 327 (2010) 1132-1135.

[74] J.K. Choi, I. Cali, K. Surewicz, Q. Kong, P. Gambetti, W.K. Surewicz, Amyloid fibrils from the N-terminal prion protein fragment are infectious, Proc Natl Acad Sci USA, 113 (2016) 13851-13856.

[75] P.C. Klohn, L. Stoltze, E. Flechsig, M. Enari, C. Weissmann, A quantitative, highly sensitive cell-based infectivity assay for mouse scrapie prions, Proc Natl Acad Sci USA, 100 (2003) 11666-11671.

[76] M.P. McKinley, R.K. Meyer, L. Kenaga, F. Rahbar, R. Cotter, A. Serban, S.B. Prusiner, Scrapie prion rod formation in vitro requires both detergent extraction and limited proteolysis, J Virol, 65 (1991) 1340-1351.

[77] H. Wille, W. Bian, M. McDonald, A. Kendall, D.W. Colby, L. Bloch, J. Ollesch, A.L. Borovinskiy, F.E. Cohen, S.B. Prusiner, G. Stubbs, Natural and synthetic prion structure from X-ray fiber diffraction, Proc Natl Acad Sci USA, 106 (2009) 16990-16995.

[78] M. Hashimoto, E. Rockenstein, L. Crews, E. Masliah, Role of protein aggregation in mitochondrial dysfunction and neurodegeneration in Alzheimer's and Parkinson's diseases, Neuromol Med, 4 (2003) 21-35.

[79] F. Sokolowski, A.J. Modler, R. Masuch, D. Zirwer, M. Baier, G. Lutsch, D.A. Moss, K. Gast, D. Naumann, Formation of critical oligomers is a key event during the

conformational transition of recombinant Syrian hamster prion protein, J Biol Chem, 278 (2003) 40481-40492.

[80] S.F. Godsave, H. Wille, P. Kujala, D. Latawiec, S.J. DeArmond, A. Serban, S.B. Prusiner, P.J. Peters, Cryo-Immunogold Electron Microscopy for Prions: Toward Identification of a Conversion Site, J Neurosci, 28 (2008) 12489-12499.

[81] K. Sasaki, H. Minaki, T. Iwaki, Development of oligomeric prion-protein aggregates in a mouse model of prion disease, J Pathol, 219 (2009) 123-130.

[82] C. Terry, R.L. Harniman, J. Sells, A. Wenborn, S. Joiner, H.R. Saibil, M.J. Miles, J. Collinge, J.D.F. Wadsworth, Structural features distinguishing infectious ex vivo mammalian prions from non-infectious fibrillar assemblies generated in vitro, Sci Rep, 9 (2019) 1-12.

[83] J. Collinge, Ex vivo mammalian prions are formed of paired double helical prion protein fibrils, Open Biol, 6 (2016)1-12.

[84] J.S. Richardson, D.C. Richardson, Natural beta-sheet proteins use negative design to avoid edge-to-edge aggregation, Proc Natl Acad Sci USA, 99 (2002) 2754-2759.

[85] A.W. Bryan, J.L. Starner-Kreinbrink, R. Hosur, P.L. Clark, B. Berger, Structure-based prediction reveals capping motifs that inhibit beta-helix aggregation, Proc Natl Acad Sci USA, 108 (2011) 11099-11104.

[86] E. Vazquez-Fernandez, J. Alonso, M.A. Pastrana, A. Ramos, L. Stitz, E. Vidal, I. Dynin, B. Petsch, C.J. Silva, J.R. Requena, Structural Organization of Mammalian Prions as Probed by Limited Proteolysis, PLoS One, 7 (2012) 1-8

[87] J.R. Requena, H. Wille, The Structure of the Infectious Prion Protein and Its Propagation, Prog Mol Biol Transl, 150 (2017) 341-359.

[88] D.J. Levine, J. Stöhr, L.E. Falese, J. Ollesch, H. Wille, S.B. Prusiner, J.R. Long, Mechanism of scrapie prion precipitation with phosphotungstate anions, Acs Chem Biol, 10 (2015) 1269-1277.

[89] J.J. Helmus, K. Surewicz, P.S. Nadaud, W.K. Surewicz, C.P. Jaroniec, Molecular conformation and dynamics of the Y145Stop variant of human prion protein in amyloid fibrils, Proc Natl Acad Sci USA, 105 (2008) 6284-6289.

[90] A.A. Zurawel, D.J. Walsh, S.M. Fortier, T. Chidawanyika, S. Sengupta, K. Zilm, S. Supattapone, Prion Nucleation Site Unmasked by Transient Interaction with Phospholipid Cofactor, Biochemistry, 53 (2014) 68-76.

[91] M.B. Miller, D.W. Wang, F. Wang, G.P. Noble, J.Y. Ma, V.L. Woods, S. Li, S. Supattapone, Cofactor Molecules Induce Structural Transformation during Infectious Prion Formation, Structure, 21 (2013) 2061-2068.

[92] N.R. Deleault, J.R. Piro, D.J. Walsh, F. Wang, J.Y. Ma, J.C. Geoghegan, S. Supattapone, Isolation of phosphatidylethanolamine as a solitary cofactor for prion formation in the absence of nucleic acids, Proc Natl Acad Sci USA, 109 (2012) 8546-8551.

[93] L. Thorne, L.A. Terry, In vitro amplification of PrPSc derived from the brain and blood of sheep infected with scrapie, J Gen Virol, 89 (2008) 3177-3184.

[94] N.R. Deleault, R.W. Lucassen, S. Supattapone, RNA molecules stimulate prion protein conversion, Nature, 425 (2003) 717-720.

[95] J.L. Silva, Y. Cordeiro, The "Jekyll and Hyde" Actions of Nucleic Acids on the Prion-like Aggregation of Proteins, J Biol Chem, 291 (2016) 15482-15490.

[96] P.K. Nandi, E. Leclerc, J.C. Nicole, M. Takahashi, DNA-induced partial unfolding of prion protein leads to its polymerization to amyloid, J Mol Biol, 322 (2002) 153-161.

[97] O. Ben-Zaken, S. Tzaban, Y. Tal, L. Horonchik, J.D. Esko, I. Vlodavsky, A. Taraboulos, Cellular heparan sulfate participates in the metabolism of prions, J Biol Chem, 278 (2003) 40041-40049.

[98] Taraboulos, Cholesterol Depletion and Modification of Cooh-Terminal Targeting Sequence of the Prion Protein Inhibit Formation of the Scrapie Isoform, J Cell Biol, 130 (1995) 121-132.

[99] A. Kuzyk, M. Kastyak, V. Agrawal, M. Gallant, G. Sivakumar, M. Rak, M.R. Del Bigio, D. Westaway, R. Julian, K.M. Gough, Association among amyloid plaque, lipid, and creatine in hippocampus of TgCRND8 mouse model for Alzheimer disease, J Biol Chem, 285 (2010) 31202-31207.

[100] H.H.L. Cui, B. Guo, B. Scicluna, B.M. Coleman, V.A. Lawson, L. Ellett, P.J. Meikle, M. Bukrinsky, N. Mukhamedova, D. Sviridov, A.F. Hill, Prion Infection Impairs Cholesterol Metabolism in Neuronal Cells, J Biol Chem, 289 (2014) 789-802.

[101] V. Perrier, T. Imberdis, P.A. Lafon, M. Cefis, Y. Wang, E. Huetter, J.D. Arnaud, T. Alvarez-Martinez, N. Le Guern, G. Maquart, L. Lagrost, C. Desrumaux, Plasma cholesterol level determines in vivo prion propagation, J Lipid Res, 58 (2017) 1950-1961.

Chapter 6

Infectious Lipid-bound Prion Multimers

in Custom Native Nanodiscs

6.1. Significance

Prion diseases are fatal and incurable neurodegenerative diseases that are driven by the propagation of pathological forms of prion proteins. It is well-established that prions are glycosylphosphatidylinositol (GPI)-linked and membrane-associated. However, the lipid-binding profiles and effects of lipids on infectivity and structure of prion proteins are not yet well understood. Native prion complexes have been isolated in nanodiscs for structural and functional studies that could enable the development of more specific diagnostic and therapeutic agents that target pathological lipid-bound multimeric states. The *in vivo* infectious activity and properties of brain-derived prion: lipid complexes in styrene-maleic acid-lipid particles (SMALPs) are compared, allowing the performances of a polymer series to be defined. These native nanodiscs offer a straightforward route for the production of physiologically relevant, homogeneous, and infectious prion particles. This opens up new avenues for clinical studies of agents and assays specific for the membrane assemblies driving neurodegenerative diseases.

6.2. Introduction

Neurodegenerative diseases, including Alzheimer's disease, Parkinson's disease and transmissible spongiform encephalopathies, involve pliable membrane-associated proteins that adopt multiple conformations. The critical role of the membrane is a confounding variable in mechanistic studies of these systems. Bound lipids are typically lost during membrane protein separation with known deleterious artifacts ensuing as these ligands usually stabilize otherwise labile structures and modulate sensitive functions [1]. Preserving the relevant target state is essential for developing accurate diagnostic assays and therapeutic agents, which are increasing priorities given the rising

incidence and socioeconomic impacts of these neurodegenerative conditions [2, 3]. There is a particular need to find alternatives for presenting and studying prions as the complexity of prion states (including monomers, multimers, protofibrils and fibrils) are modulated by various modifications, use of detergents, presence of ligands, and membrane bilayer surfaces. Native nanodiscs are increasingly used to prepare assemblies of the endogenous membrane: protein assemblies with biological lipids and modifications in their biologically intact states [1], but have limitations including excessive negative charge and polydispersity. Moreover, they not yet been used to tackle prions. Here, several polymer chemistries optimized for stabilizing and isolating memteins were tested and new polymers were developed to address the challenges presented by purifying and characterizing transient lipid-bound infectious prion multimers within a containment lab for pathogenic agents.

Infectious prion states are membrane-associated through GPI anchors, although their endogenous lipid complement is unclear. Prion analysis has relied on high concentrations of conventional detergents such as sarkosyl throughout preparations [4, 5]. Such detergents are known to alter the protease digestion profiles of prions [6] as well as their interactions with physiological partners, including heparin [7]. Moreover, detergent-based purification protocols cause excessive fibrilization of prions in Proteinase K (PK)- and phosphotungstic acid (PTA)-treated RML strain-infected mouse brain homogenates [8]. These studies prevail due to the lack of milder substitutes that could more gently release intact prion: lipid assemblies for analysis [9]. Alleviating this obstacle could potentially lead to resolving structural identities of the infectious prion forms and the mechanisms underlying their toxicity, lipid perturbations [10-13], GPI-anchoring and PK-

sensitive oligomerization during prion propagation [14]. Towards this end, we have developed and tested a novel series of SMA polymers for detergent-free isolation of infectious prions in native nanodiscs. These are used for in vitro structural and in vivo infectivity assays of PrPres assemblies from the brains of Hyper strain-infected hamsters (HY) and RML strain-infected FVB mice.

A novel polymer was designed here to overcome anticipated challenges with prions. Amphipathic polymers with statistical distributions of styrene and maleic acid monomers (in non-alternating ratios) can insert into virtually any cellular membrane, and spontaneously form native nanodiscs [15-17]. However, the heterogeneity of their sequences precludes resolution of the polymers or bound lipid headgroups in 3D structures [18, 19]. Alternating polymers are more homogenous due to their regular 1:1 repeating pattern of styrene and maleic acid subunits but are relatively ineffective at membrane solubilization [20-22]. To synthesize improved forms of SMA(1:1) that are more homodispersed and better suited for solubilization of metal-dependent proteins, including prions, we replaced the maleic acid groups with less charged maleamic derivative groups. Clusters of lipid-inserting styrenes can also mediate undesirable nonspecific interactions with fibrils. Hence the styrene ratio was halved with a compensatory methyl added onto the maleimide. Structural analyses would benefit from more regularized belts of polymer around nanodiscs that can encapsulate protein-phospholipid complexes. Hence, we incorporated thiol groups to offer hydrogen bonding and crosslinking potential. This custom approach is demonstrated for prions but has broad implications for biochemical, structural and lipidomic analyses of diverse membrane proteins, some of which remain intractable [23]. Here, we investigated the

strengths and weaknesses of using different formulations of SMA copolymers in vivo and in vitro as alternatives for detergents in the study of the infectious prions, with potential applicability to virtually any membrane-associated target.

6.3. Results and Discussion

6.3.1. Comparison of SMA polymers

In order to compare the effects of polymer charge and hydrophobicity on solubilization and infectivity of native prion, four series of SMA copolymers were synthesized. The SMA(2:1) and SMA(3:1) polymers contain non-alternating sequences with 2:1 and 3:1 ratios of styrene to maleic acid monomers, respectively. These two series offer distinct and established membrane interactions and solubilization profiles. SMA(2:1) and SMA(3:1) were synthesized by alkaline hydrolysis of the respective styrene-maleic anhydride forms (Fig. 6.1a) in alkaline solutions and subsequently used to assess prion solubilization and infectivity. A derivative with free thiol groups was synthesized by grafting cysteamine to SMA(2:1) polymer (Fig. 6.1b), with thiol groups in the resulting SMA-SH polymer [15] offering handles for cross-linking. A methylamine derivative, "SMA(1:1)ma" was synthesized because it offers less charge and relatively alternating sidechains (Fig. 6.1c). Thus it presents a concomitant increase in predicted metal compatibility, homogeneity as well as an enhanced potential for structural resolution.
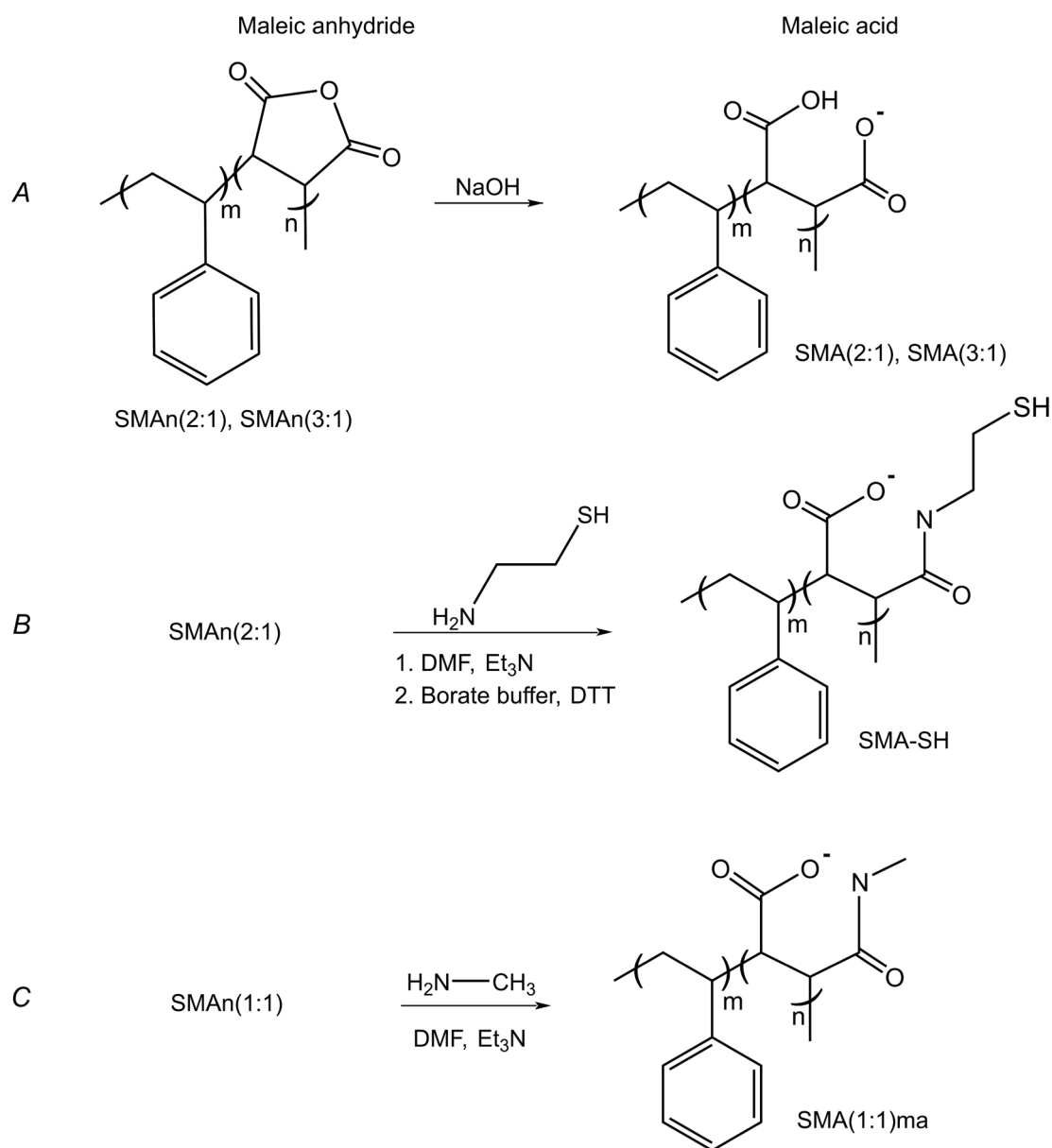
Figure 6. 1. Chemical structures and synthesis of the (A) SMA(2:1), SMA(3:1) (B) SMA-SH and (C) SMA(1:1)ma copolymers, which has average m:n ratios of styrene to maleic acid groups of 2:1, 3:1, 2:1 and 1:1, respectively.

Before proceeding to the solubilization of prions from the mammalian brain, we compared the abilities of the various polymers to solubilize multilayer vesicles (MLVs) composed of dimyristoyl phosphatidylcholine (DMPC) lipid. The SMA(1:1)ma form was able to solubilize membranes at a concentration of 1%, which is similar to the non-

alternating polymers, despite having a lower amount of membrane-binding styrene groups. This was expected due to the alkylamine derivatization reducing the net negative charge and increasing the overall polymer hydrophobicity, which is needed for efficient membrane insertion. Membranes were solubilized by SMA(1:1)ma at up to 10 mM calcium chloride, while SMA(2:1) precipitates above 5 mM; SMA(1:1) is active from pH 5 to 10 (Fig. 6.2), while other SMA polymers have narrower pH ranges and are optimal at pH 8.0. Thus SMA(1:1)ma has broader solution compatibility, less charge, sufficient hydrophobicity as well as lower sequencial heterogeneity while retaining comparable membrane solubilization activity. Hence it was included in our polymer panel to solubilize native-states of prion particles.
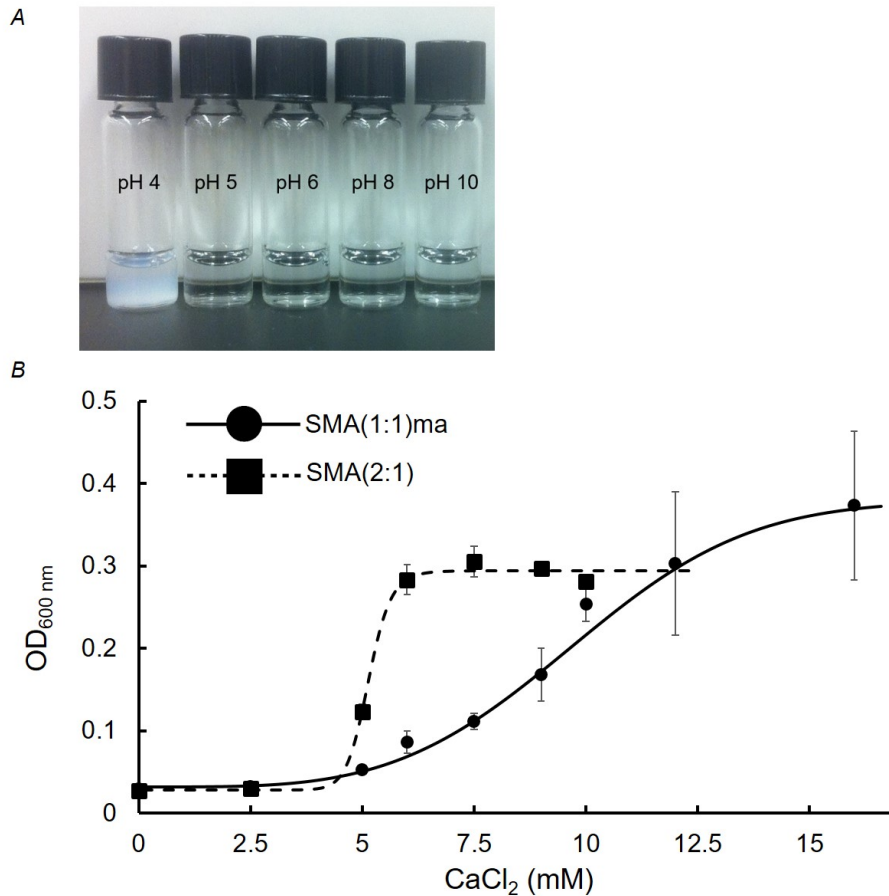
Figure 6.2. Membrane Solubilization by SMA(1:1)ma. A. The solubility of SMA(1:1)ma is shown by the clarity of solutions at pH values between 5-10 while it precipitates at pH 4. B. SMA(1:1)ma retains solubility at higher $CaCl_2$ concentrations than SMA(2:1) based on the turning points of 5 versus 10 mM.

6.3.2. Isolation and partial purification of protease-resistant PrP (PrP^{Sc}) using SMALP

Like established detergent-based prion purifications, the SMA-based approach also utilizes PTA to bind the endogenous PrP^{Sc} assemblies and separate them from other brain material. Optimization of the SMA protocol to achieve high recovery of multimeric PrP^{Sc} reduced the duration of incubation with PTA to one hour. Unlike detergents that are

maintained throughout the protocol, a minimal concentration of SMA polymer (1% w/v) was added only during the initial incubation with brain homogenate (Fig. 6.3) to reduce the heterogeneity of nanodiscs for fractionation and TEM imaging. Due to the stability of the SMALPs, no further polymer need be added downstream of the initial solubilization.
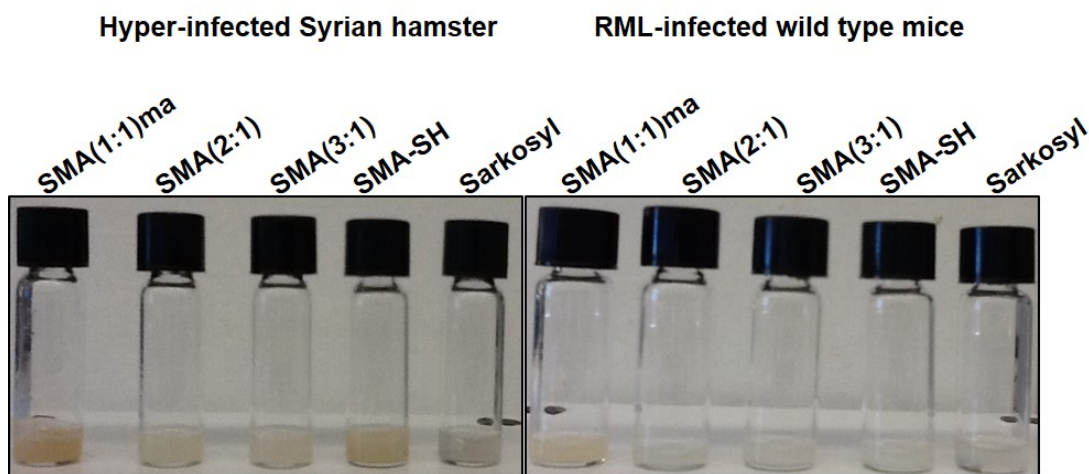
Figure 6.3. The physical appearance of PrP^{Sc} isolated from Hyper-infected Syrian hamsters and RML-infected wild-type mice using different SMA polymers. Sarkosyl-treated samples were shown for comparison.

Resistance to proteolytic digestion is a hallmark of prions found in tissues of organisms exhibiting transmissible spongiform encephalopathies. Both Proteinase K and Pronase E have been used for the isolation of the infectious prions. Pronase E retains the GPI-anchor moiety, which is required for stable interaction of prion with the plasma membrane [24]. Either of these proteases could be used to prepare PrP^{Sc} from the brain homogenate with similar results. However, the feasibility of finding PrP^{Sc} filaments in EM imaging from the Pronase E-treated samples was noticeably improved. Consequently, the PronaseE-resistant prion (hence PrP^{Sc}) was prioritized for preparation of membrane: prion assemblies in native SMA nanodiscs.

Native prion protein is variably glycosylated. It displays three characteristic bands on immunoblots corresponding to diglycosylated, monoglycosylated, and unglycosylated proteins. All the SMA-isolated PrP^{Sc} samples, whether isolated from Hyper strain-infected hamsters or RML strain-infected mice, share a similar profile of glycoforms with distinct molecular weights that match those of sarkosyl-purified PrP^{Sc} samples (Fig. 6.4b). However, the yield and purity of PrP^{Sc} extracts, as well as their physical appearances, differed between the various SMA-purified samples (Fig. 6.3). SMA(2:1) treated prions were the least turbid, whereas SMA(1:1)ma-purified prions appeared as a brown waxy pellet, which suggested the inclusion of more lipid or heme-containing proteins such as ferritin or cytoskeletal proteins like keratin (Fig. 6.3) [25]. Despite the digestion of nucleic acids by Benzonase nuclease [17] and using high-speed centrifugation, high molecular weight aggregates appeared in both SMA(1:1)ma and SMA(2:1) preparations. Immunoblotting experiments confirmed that the size of aggregates does not correlate with PrP^{Sc}. Due to the presence of apparent keratin fibers in EM images, we attributed the high molecular weight aggregates to cytoskeletal protein fibers.
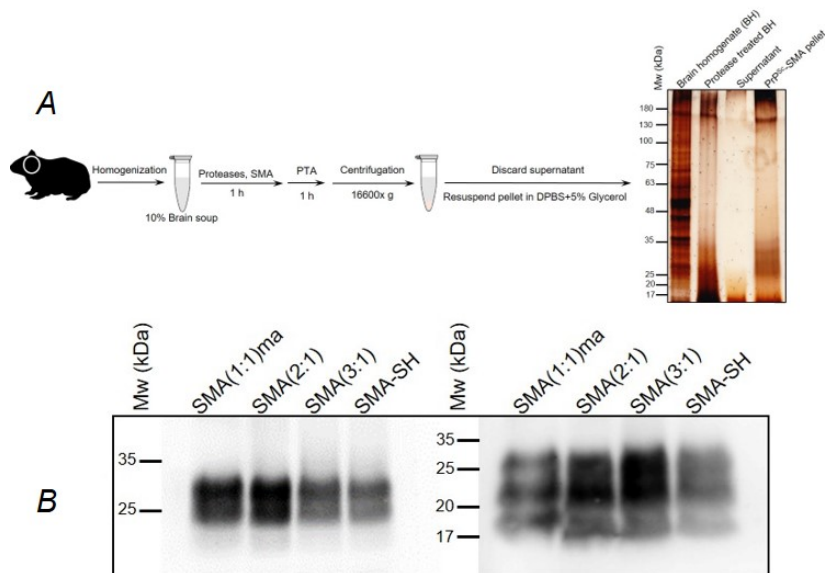
Figure 6.4. A. Schematic description of detergent-free isolation of protease (PK) resistant prion from the infected brain tissues. B. Immunoblots of SMA-purified PrP^{Sc} from Syrian Hyper hamsters and FVB-RML mice using an anti PrP^{Sc} primary antibody, showing similar molecular weights and glycosylation patterns for the SMA-purified PrP^{sc} preparation compared to samples purified with sarkosyl.

Given the mild membrane solubilization of intact native states by SMA polymers, we speculated more prion multimers to be extracted. The distribution of oligomeric states of SMA-purified PrP^{Sc} from hamster and mouse strains was examined via equilibrium sedimentation in step-wise sucrose density ultracentrifugations (Fig. 6.5). The majority of PrP^{Sc} protein extracted by SMA from Hyper hamster was buoyant and found in the top fraction, hence represented the lipid-associated states. At the same time, the levels of dense aggregates that sedimented out were relatively insignificant. However, treating PrP^{Sc} (derived from brains of Hyper (HY) and RML strains) with SMA(1:1)ma leads to a distribution of oligomeric states that localize at the interface of sedimentation sucrose gradients. This observation indicates that various SMA polymers preferentially solubilize the lipid: prion complexes and SMA(1:1)ma appears the best suited for solubilizing multimeric prion species.
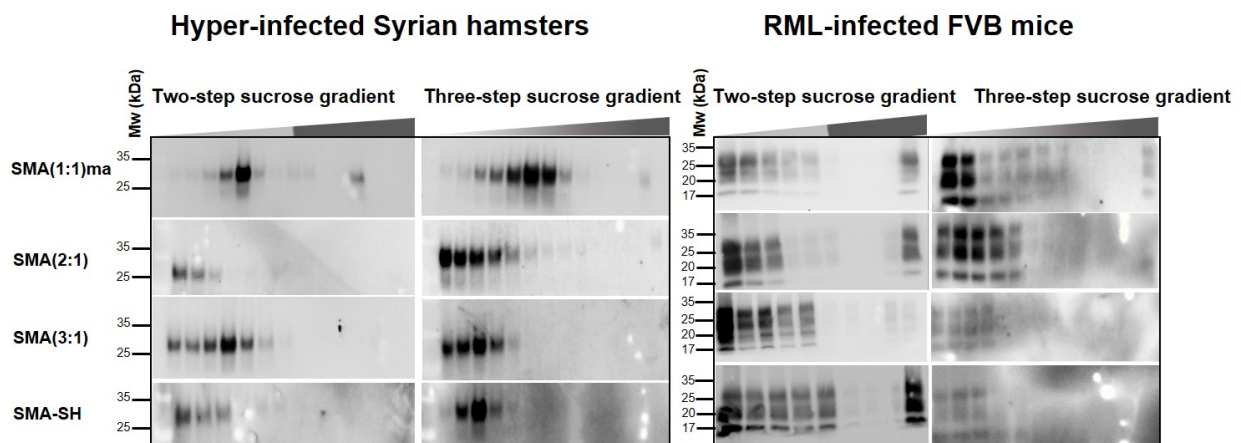
Figure 6.5. Protease treated SMA-PrP^{Sc} particles isolated from Syrian hamsters and FVB-RML mice were separated according to their densities using a two-step sucrose gradient (40 and 80%) and three-step (40, 55 and 80%) sucrose velocity ultracentrifugations, with fractions collected from the tops to the bottoms of tubes for immunoblotting. The majority of prion particles remained at the top layer of the gradient (40%), implying less aggregated, lipid-bound states of PrP^{Sc} in SMA nanodiscs.

6.3.3. Transmission electron microscopy of SMALP-isolated PrP^{Sc}

We investigated whether single or double prion filaments were obtained by SMA extraction from the brain, as these forms correspond to noninfectious and infectious states, respectively [26]. The SMA isolates of PrP^{Sc} are mainly in double-stranded filaments that have diameters of approximately 20 nm in negative stain electron microscopy images. At the same time, entangled long rods are observed in sarkosyl-treated samples (Fig. 6.6). Moreover, lipid vesicles are found in PrP^{Sc} preparations obtained with SMA and are particularly enriched in SMA(1:1)ma isolates, which show as protofilament: vesicle complexes. The lipid vesicles can be removed by treatment of SMA-PrP^{Sc} preparations with polyethylene glycol (PEG)6000 (4% w/v, 4 °C, overnight), which precipitates the PrP^{Sc} for EM analysis of the homogenous protein filaments. Large discs with diameters of 45 ± 5 nm containing 2D crystals of PrP^{Sc} can be obtained from PK- and SMA-SH treated Hyper strain brains (Fig. 6.7a), and are reminiscent of those seen in earlier studies [27]. The available thiols of SMA-SH and the higher prion yield from infected hamsters may both contribute to the formation of these PrP^{Sc} crystals, which are rarely seen in other SMA brain isolates. The top fractions of the sucrose gradients of SMA(2:1)- and SMA(1:1)ma HY PrP^{Sc} contain fibrils within the low-density lipid raft microdomains, which is consistent with native PrP^{Sc} filament association with the plasma membrane (Fig. 6.7b,c).
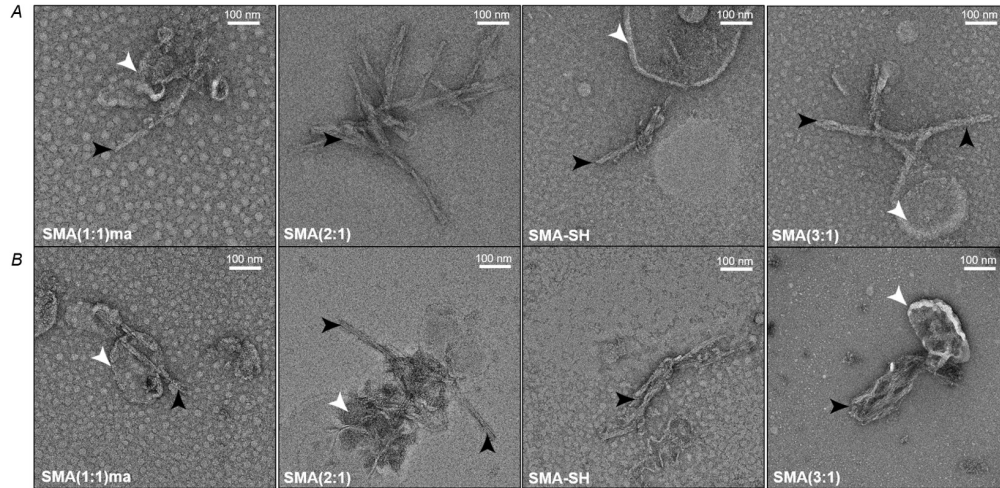
Figure 6.6. Negative stain electron micrographs of PrP^{Sc} fibrils from Syrian Hyper hamsters (A) and FVB-RML mice (B) using the indicated SMA copolymers. Black arrows point to isolated PrP^{Sc} double-helical microfilaments, and white arrows highlight the co-purified lipid vesicles.
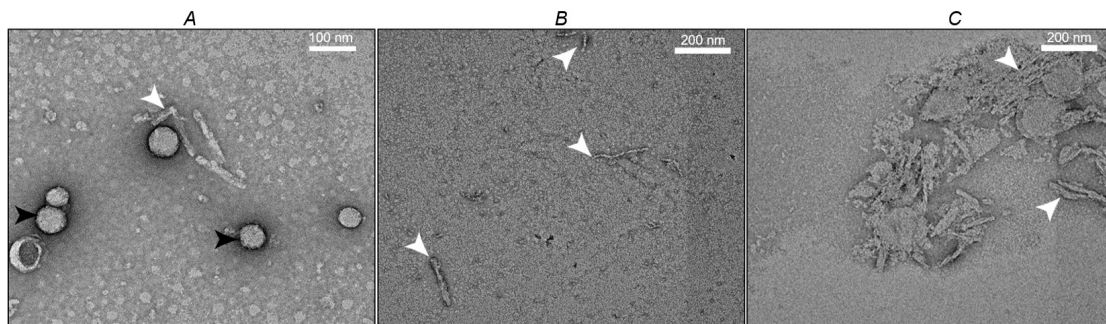
Figure 6.7. Negative-stained electron micrographs of (A) PrP^{Sc} fibrils (white arrow) and 2D crystals (black arrow) from Syrian Hyper hamster following SMA-SH and PK-treatment. Protofilaments and vesicles from the top-most fractions of sucrose gradients of SMA(2:1) (B) and SMA(1:1)ma (C)-treated Hyper hamster brain.

6.3.4. Lipid profile of the infectious PrP[Sc] in SMALPs versus sarkosyl

Co-purified lipids of PrP[Sc] are also crucial for transformation of cellular PrP to the scrapie isoform [11, 13, 28, 29]. Unlike some detergents that dissociate protein-bound lipids, SMA polymers are useful tools for studies of lipids bound to membrane proteins [30] and amyloids [14, 31]. In this regard, however, the use of detergents and the infectivity associated with high titer PrP[Sc] pellets have limited the investigation of the lipid profile of infectious prions from endogenous sources [32]. To address this deficiency, the infectivity of PrP[Sc] from different SMA copolymer and sarkosyl preparations was compared (Table 6.2). The lipids associated with PrP[Sc] assemblies extracted from brains of infected and healthy hamsters and mice were identified and quantified, allowing relative levels of eleven types of lipids to be compared (Fig. 6.8). An internal standard (batyl alcohol) was added to the sample during lipid extraction and the amount of lipids was calculated from HPLC chromatograms (Fig 6.9, Table 6.1). The findings demonstrate that SMA(1:1)ma discs provide the highest capacity for isolation of various types of lipids. This outcome is in accordance with the waxy appearance of PrP[Sc] pellet purified using this polymer. The next highest prion-associated lipid capacity are offered by SMA(2:1) and SMA-SH polymers, respectively.

Interestingly, HY hamster and RML strains have a relatively distinctive lipid profile; for instance, triglyceride (TG) is solely present in HY hamster samples. Also, the lipid profiles reveal the existence of critical signaling lipids, including cholesterol, phosphatidylinositol (PI) and sphingomyelin [33] near PrP[Sc] proteins. This result is consistent with similar reports of other misfolding diseases such as Alzheimer's and type 2-diabetes [34, 35].
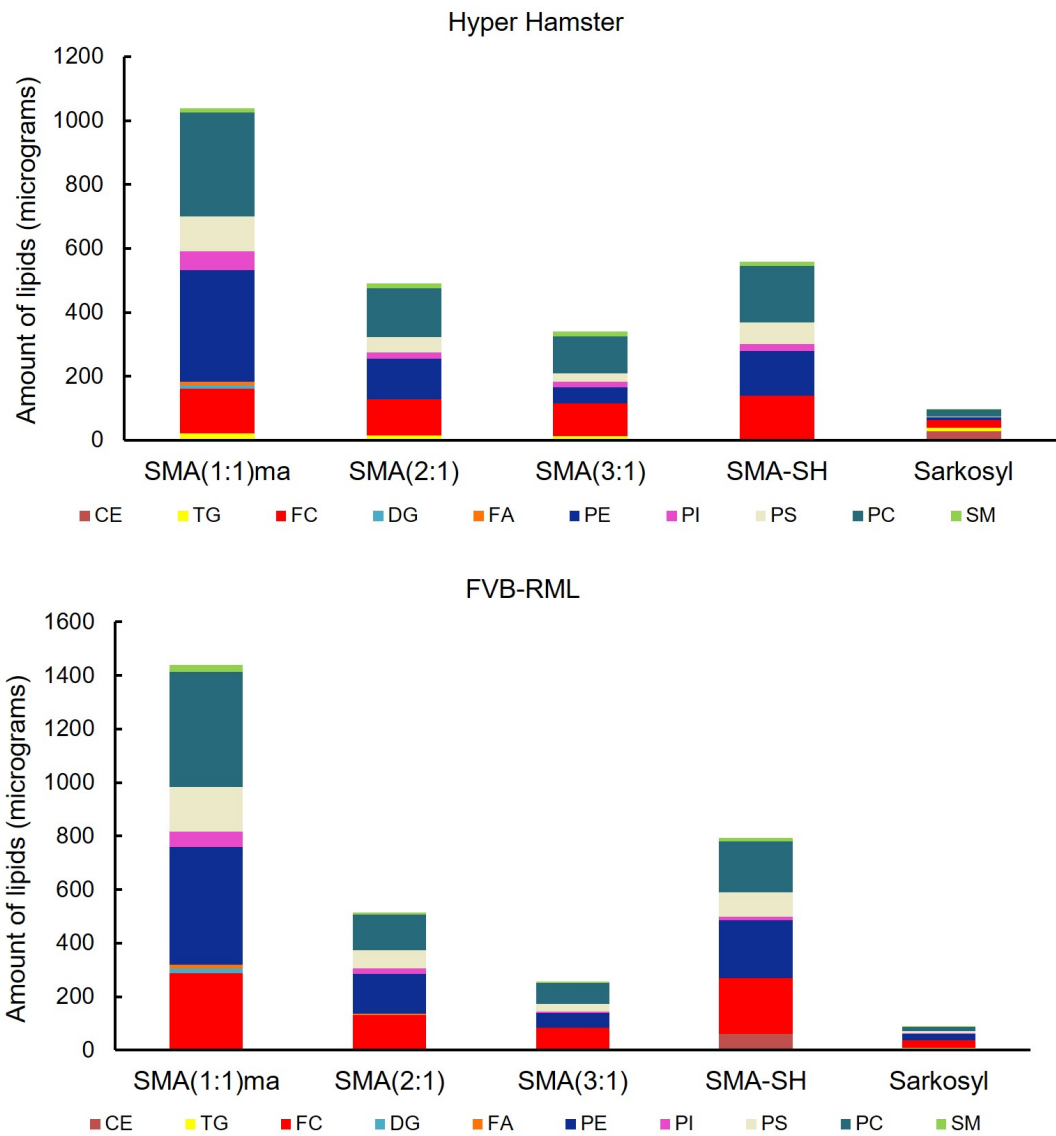
Figure 6.8. Different lipid species in each SMA isolated-PrP^{Sc} pellet from Hyper hamster (top) and FVB-RML mice (bottom) were quantified and their cumulative amounts were shown in stack plots including levels of cholesterol esters (CE), triglycerol (TG), free cholesterol (FC), sn-1,2-dipalmitoyl phosphatidylglycerol (DG), free fatty acid (FA), phosphatidylethanolamine (PE), phosphatidylinositol (PI), phosphatidylserine (PS), phosphatidylcholine (PC) and sphingomyelin (SM).
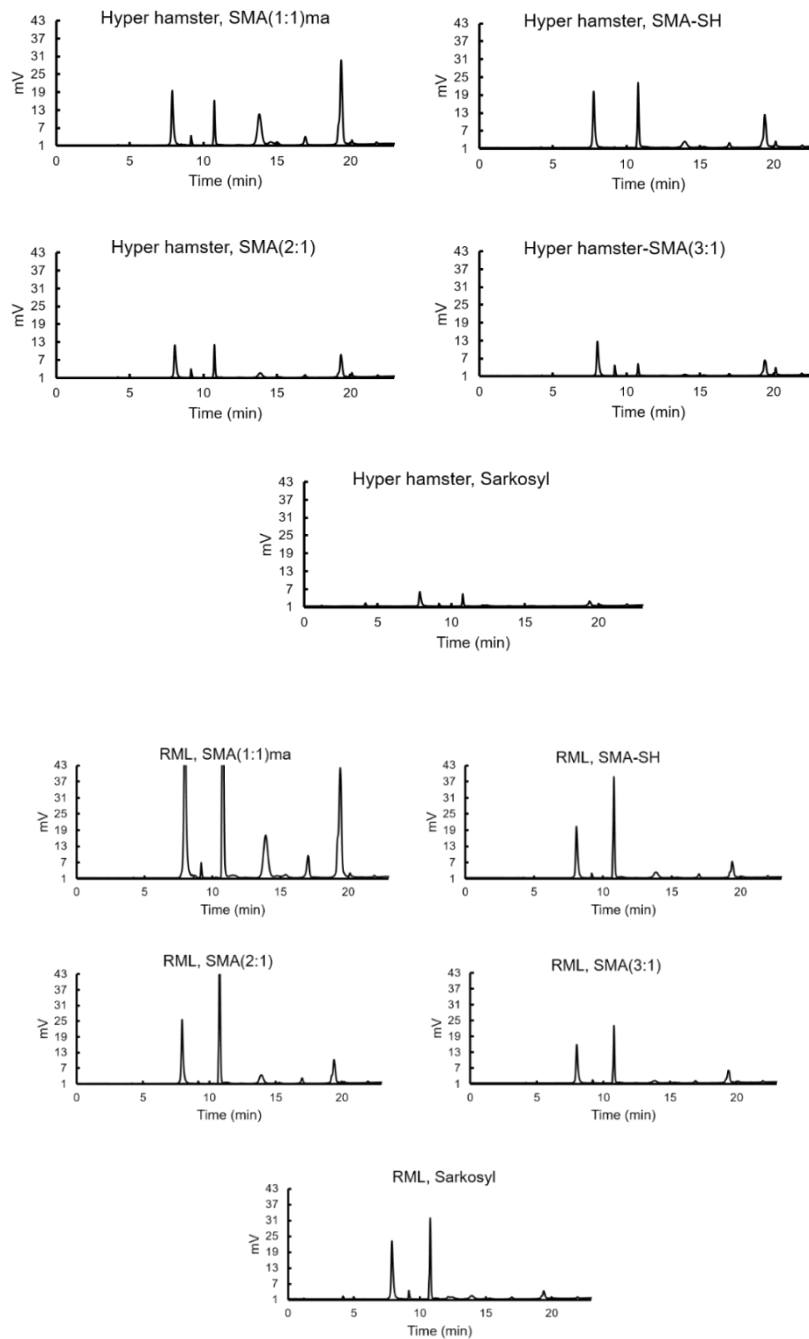
Figure 6.9. The HPLC chromatograms of isolated lipids from SMA-isolated PrP^{Sc} from HY hamster and RML mice infected brains.

Lipid type	Hyper-hamster					FVB-RML				
	SMA(1:1)ma	SMA(2:1)	SMA(3:1)	SMA-SH	Sarkosyl	SMA(1:1)ma	SMA(2:1)	SMA(3:1)	SMA-SH	Sarkosyl
CE	4.81	4.96	3.99	5.09	27.41	0	2.77	2.29	61.18	3.54
TG	17.18	11.13	9.31	0	11.09	0	0	0	0	4.29
FC	138.40	111.81	103.15	133.87	24.35	288.78	127.65	81.19	208.93	31.17
DG	11.22	0	0	0	0	17.92	0	0	0	0
FA	11.50	0	0	0	0	13.31	5.43	0	0	0
PE	348.21	128.07	49.66	139.50	8.57	437.60	148.81	56.82	215.55	21.83
PI	58.64	19.78	16.60	22.00	0	57.36	22.19	5.25	12.40	1.92
PS	108.67	47.86	27.39	67.89	2.23	166.50	66.76	27.70	90.77	8.05
PC	325.24	152.82	114.53	176.36	21.46	430.09	133.19	78.17	190.89	16.80
SM	14.59	13.35	15.13	14.81	3.12	28.07	8.13	6.18	13.40	1.58

Table 6.1. Summary of the type and amount of lipids (in micrograms) in all SMA-treated samples. Lipids include cholesterol esters (CE), triglycerides (TG), free cholesterol (FC), dipalmitoyl phosphatidylglycerol (DG), phosphatidylethanolamine (PE), phosphatidylinositol (PI), phosphatidylserine (PS), phosphatidylcholine (PC) and sphingomyelin (SM).

6.3.5. Bioassay of SMALP- PrP^{Sc} particles

The disease symptoms in animals inoculated with SMA- purified PrP^{Sc}, sarkosyl-purified PrP^{Sc} and brain homogenates were monitored and compared (Table 6.2). Prion disease presents as ataxia, scruffy coats, loss of gait, weight loss and head bobbing at the time of euthanization [36]. The average incubation times (from SMALP-PrP^{Sc} particle inoculation until terminal disease) were consistently around 85-90 days in Hyper hamsters, with SMA(1:1)ma, SMA(2:1) and purified PrP^{Sc} showing similar periods (Table 6.1a) as sarkosyl- purified PrP^{Sc}. In contrast, inoculation with SMA(3:1)- and SMA-SH purified PrP^{Sc} samples yielded the longest incubation times (significantly different from sarkosyl-treated samples and brain homogenate group), suggesting lower infectivity. As expected, inoculation with 1% prion 263K brain homogenate from infected animals was most lethal. Given the 153 days for average incubation time of RML strain in FVB mice, mice incubated with SMA-SH and SMA(3:1) purified PrP^{Sc} showed the shortest and

longest incubation times; 163 and 187 days, respectively (Table 6.2b). The infectivity of SMA(3:1)-purified PrP^{Sc} is significantly different from PrP^{Sc} in brain homogenate or sarkosyl-purified PrP^{Sc}. Despite the variability of the incubation period for different SMA-purified samples, animals in SMA(2:1), SMA(1:1)-methylamine, and SMA-SH groups show the same clinical symptoms. The second subsequent passage of the brain homogenates of animal (infected with SMALP- PrP^{Sc} particles in the first passage) to healthy hamsters (Table. 6.3) displays the same symptoms at the terminal stage as the first passage. The incubation period of SMA(3:1), SMA(1:1)ma and SMA-SH groups are significantly different from that in the 263K brain homogenate infected group. However, PK-digestion of postmortem brain tissues reveals that all animals, regardless of the incubation period and clinical symptoms, display the characteristic profile of PK-resistant PrP (Fig. 6.10). Differences in the phenotypes between the groups of SMALP-PrP^{Sc} treated animals suggests that the unique chemical properties of each type of SMA polymer could influence the microstructure of PrP^{Sc} protofilaments, hence modulating their infectivity.

A	Sample	Incubation period (days) ± SEM (N/N$_0$)
	1% 263K brain homogenate (control)	71±0.5 (4/4)
	treated with 1% Sarkosyl-PrP^{Sc} (control)	76±5 (12/12)
	treated with 1% SMA(1:1)ma-PrP^{Sc}	84±8 (12/12)
	treated with 1% SMA(2:1)-PrP^{Sc}	87±3 (12/12)
	treated with 1% SMA-SH-PrP^{Sc}	88±4 (12/12)*
	treated with 1% SMA(3:1)-PrP^{Sc}	94±3 (12/12)*

B	Sample	Incubation period (days) ± SEM (N/N$_0$)
	treated with 1% Sarkosyl-PrP^{Sc} (control)	158±19 (19/19)
	treated with 1% SMA(1:1)ma-PrP^{Sc}	174±27 (9/9)
	treated with 1% SMA(2:1)-PrP^{Sc}	172±21 (15/15)
	treated with 1% SMA-SH-PrP^{Sc}	163±15 (14/14)
	treated with 1% SMA(3:1)-PrP^{Sc}	187±33.5 (17/17)*

Table 6.2. A summary of bioinfectivity of SMA-treated PrP^{Sc} samples in Hyper hamster (A) and RML mice samples (B). In both cases, 1% brain homogenates and Sarkosyl purified PrP^{Sc} were used as controls. Asterisks indicate the significant difference (P-value < 0.001) between the incubation periods of SMA-treated samples and sarkosyl-purified PrP^{Sc}.

Re-inoculation Sample (Hamster)	Incubation period (days) ± SEM (N/N$_0$)
1% 263K brain homogenate (control)	71±0.5 (4/4)
treated with 1% SMA(1:1)ma-PrP^{Sc}	87±3 (10/10)*
treated with 1% SMA(2:1)-PrP^{Sc}	74±3 (6/6)
treated with 1% SMA-SH-PrP^{Sc}	97±2 (6/6)*
treated with 1% SMA(3:1)-PrP^{Sc}	115±0.5 (6/6)*

Table 6.3. The second passage of SMA isolates of Hyper PrP^{Sc} into healthy Syrian hamsters caused infectivity with a similar incubation period as in the first passage (Table 6.1). Asterisks indicate the significant difference (P-value < 0.001) between the incubation periods of SMA-treated samples and the control.
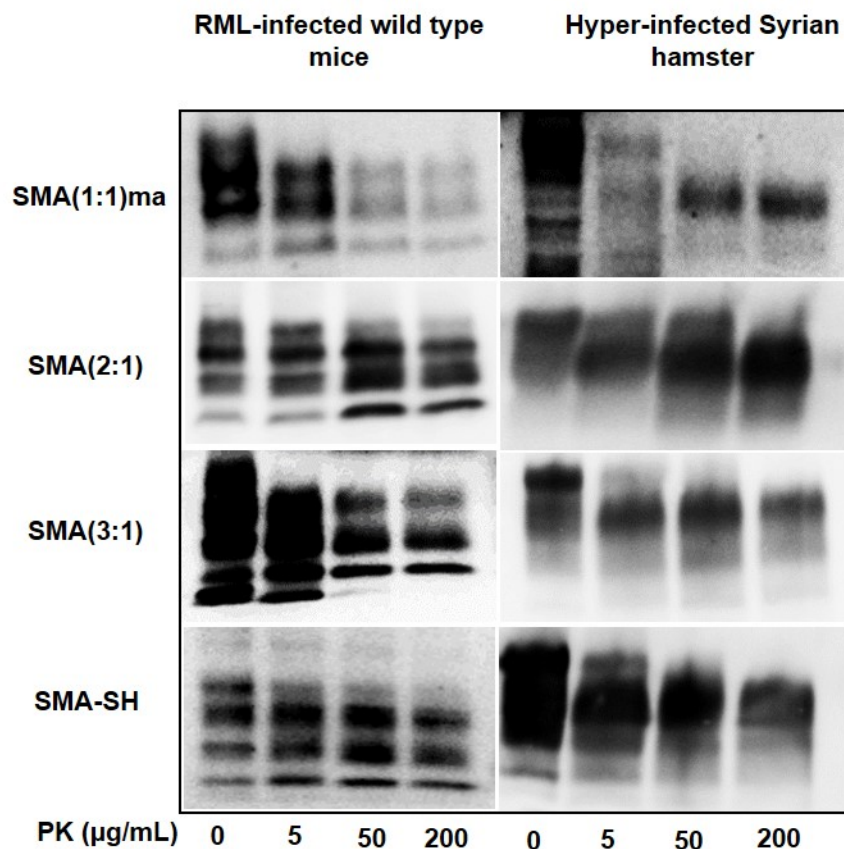
Figure 6.10. Post-mortem brains of SMA-PrP^{Sc} infected Syrian hamsters and SMA-PrP^{Sc} infected wild-type mice were treated with Proteinase K (PK). The PK-digestion patterns of all samples confirm the presence of protease-resistant prion protein.

6.4. Conclusions

We have shown that the SMA-based purification of PrP^{Sc} from infected rodent brains provides a viable detergent-free protocol with minimal exposure to PTA or added polymer. The density-based fractionation of the resulting particles yields the lipid-bound state of PrP^{Sc} protofilaments with least aggregation [8] and multimers that co-purify with SMALP-nanodiscs. The choice of protease is a crucial element in the isolation of non-fibrillar, membrane-bound and infectious PrP^{Sc}. To this end, the copolymer-based strategy in combination with high-performance proteases such as thermolysin [37] could

164

yield a gentle and minimal perturbing preparative approach for further structural analysis. Our data shows that the new protocol is fully compatible with protease types, including PK and PE, for isolation of truncated and intact PrP[Sc] assemblies. Structural investigation of GPI anchor-dependent propagation of PrP[Sc], hence its lipid raft related signaling would require the intact native assemblies of PrP[Sc]-lipids and, to this date, the amphipathic polymers are the only available tools for this purpose [38]. The fact that SMA(1:1)ma is particularly effective for isolation of membrane-bound prion provides an avenue for preparation of memtein with reduced nonspecific interactions, polydispersity and calcium sensitivity. It thus overcomes many limitations of other SMA polymers. Demonstration of the solubilization of the biologically active multimer prion protein with SMA(1:1)ma with a two-fold improvement in tolerance to cation and membrane binding capacity suggests a general utility for diverse membrane assemblies that are often cation and lipid dependent. SMA(1:1)ma demonstrates a superior potential for lipidomics and metabolomics analyses of highly infectious PrP[Sc] assemblies isolated from infected brains. This advancement represents a fundamental advantage over detergents which dissociate physiologically relevant lipid molecules or ligands, except those which are tightly bound and buried between core fibers, such as the unresolved hydrophobic ligands in cryo-EM studies of tau fibers [39]. Determination of lipid and ligand identities and accurate quantification of lipid ratios will allow replication of the native membrane environment for future mechanistic studies of the lipid-dependent transformation of prions from the normal cellular states to the scrapie form. This will rely on fractionation and time-resolved studies of the SMA-treated and ideally PTA-free RML brain homogenate. This separation of transient and irreversible states could be facilitated by differences in their hydrodynamic

sizes and conformations, which we speculate could be lipid-dependent. Stabilization and resolution of the intermediate state most critical for infectivity remain a non-trivial but increasingly feasible prospect. In addition to custom SMA forms developed here, examples of synthetic polymers such as cellulose ethers (CEs) and methylcellulose have been shown to prolong the incubation periods of PrP^{Sc} in prion disease animal models [40].

In addition to their utility for *in vitro* analysis of memteins, SMA polymers are well-known for their *in vivo* applications as drug delivery vehicles [41, 42]. Here we typically used a polymer concentration of 1% w/v, although even lower levels (0.5% w/v) are also effective in liberating the PrP-lipid complexes. SMA is added to the brain homogenate in only one initial step. sThe purified PrP^{Sc}-lipid assembly is injected into animals with little if any free SMA polymer present. The incubation periods of SMA-purified PrP^{Sc} can be explained in the light of previous studies on the anti-prion activity of positively and anionic modified charged dendrimers [43]; suggesting that polymer's surface charge does not correlate with the prolonged incubation period of PrP^{Sc}. Moreover, several studies confirmed that low toxicity polymers could resolve the PrP^{Sc} aggregation, thus giving rise to longer incubation time in murine models [44-46]. The application of SMA(1:1)ma would reduce the net charge and hydrophobic clusters of unmodified SMA polymers, thus allowing specific target interactions to be favored over non-specific electrostatic and hydrophobic interactions with off-targets.

6.5. Experimental section

6.5.1. Polymer synthesis.

SMA(2:1) and SMA(3:1) (Polyscope) were each modified to their corresponding acid forms by hydrolysis in 1M NaOH while refluxing at 70 °C for 3 hours (14) and dried under vacuum. A cysteamine-grafted derivative of SMA(2:1) (SMA-SH) was synthesized using established methods [47] and stored with 20 mM dithiothreitol (DTT). SMA(1:1)ma was synthesized from SMA(1:1), as described in Fig. 1. Stock solutions (8% w/v, pH 7.5) of each polymer were prepared in Dulbecco's phosphate-buffered saline (DPBS) with 5% glycerol (v/v). Fourier Transform InfraRed (FT-IR) spectra were collected (data not shown) and samples were stored frozen until use.

6.5.2. Prion isolation from brains.

Brain homogenates (20% w/v) were prepared from brains of clinically sick Hyper strain-infected hamsters and RML-infected FVB mice in DPBS+5% glycerol, mixed with 8% (w/v) SMA stock solution to a final concentration of 1% (w/v) and PronaseE (Sigma-Aldrich). Each mixture was then incubated at 37°C for 30 min after which the protease was inactivated by EDTA [48]. Then sodium phosphotungstic acid (PTA, 200 µL of 10% w/v, pH 7.2) was added and the mixture was incubated for one hour at 37°C. The solutions were centrifuged at 16,500×g, and the pellets were re-suspended in DPBS and 5% (v/v) glycerol and stored at -20°C for later assays.

6.5.3. Sucrose gradient ultracentrifugation.

Sucrose gradients in DPBS were prepared in 3.5 mL Beckman ultracentrifuge tubes to resolve prion multimers. Three independent sets of SMA-purified samples were

overlaid on top of each gradient and spun at 130,000×g in a SWTi55 swinging-bucket

rotor (Beckman Coulter) for at least 17 hours at 4°C. Fractions (200 µL) were collected

from the top to the bottom of tubes and 40 µL aliquots were mixed with an equal volume

of sample buffer (Bio-Rad) and heated for 10 min at 100°C as per Western blotting and

SDS-PAGE gels.

6.5.4. Negative-stain Transmission Electron Microscopy

Carbon coated copper grids with a 400 nm-mesh were charged using an EMS 100

x glow discharge unit (Electron Microscopy Sciences) for 30 seconds. Microliter amounts

of each SMA-purified prion sample were loaded on the grids and let to adsorb for 30

seconds. The grids were washed three times (3×50 µL) with ammonium acetate (100 mM

and 10 mM, pH 6.8), and stained with filtered 2% uranyl acetate. Excess dye was

removed using a filter paper and air-dried for at least 5 minutes before TEM

imaging. Micrographs were collected using a Tecnai G20 transmission electron

microscope equipped with an Eagle 4 k × 4 k CCD camera (FEI) with an acceleration

voltage of 200 kV.

6.5.5. Infectivity assays

The FVB mice came from in-house breeding, and 23 day old golden Syrian

hamsters were purchased from Envigo. The SMA-isolated PrP^{Sc} samples and controls

were serially diluted 100 times in DPBS. Diluted samples were then used to

intracerebrally inoculate three independent groups of animals, each with at least four

animals of healthy FVB mice (30 µL per animal) and Syrian hamsters (50 µL per animal).

Their behavior was monitored daily and after clinical diagnosis of prion disease, the brains

of sacrificed animals were isolated and stored at -80 °C for analysis. Data were analyzed using Student's t-test (SigmaPlot 14.0).

6.5.6. Immunoblotting and silver staining

Prion samples were mixed with an equal volume of 2× sample buffer containing 700 mM β-mercaptoethanol, and heated at 100 °C for 10 min. Before loading on pre-cast 10 or 12%, stain-free SDS-PAGE gels (Bio-Rad) samples were centrifuged for 2 min at 14,000×g. Electrophoresis was performed at 100 V for ~ 2 hours at room temperature. Proteins were electrotransferred to polyvinylidene difluoride (PVDF) membranes (Millipore) at 100 volts for one hour at room temperature in 25 mM Tris pH 8.3, 192 mM glycine, 20% methanol (v/v). Membranes were blocked in tris buffered saline (TBS) with 0.1% (v/v) Tween and 5% (w/v) bovine serum albumin (BSA) for one hour at room temperature, followed by incubation overnight at 4°C with an in-house mouse anti-prion antibody. The membrane was washed three times for 10 minutes in TBS with 0.1% Tween, and further incubated with secondary alkaline phosphatase (AP)-conjugated goat-anti-mouse antibody (Bio-Rad) for one hour. After three 10 minutes washes, the membrane was incubated with 1 mL of AP-Substrate (Bio-Rad) and immunoblots were imaged using ImageQuant (GE Life Science).

6.5.7. Proteinase K resistance assay

The brain tissue of each infected animal was removed post-mortem, and a brain homogenate (10% w/v) was prepared in DPBS with 5% glycerol. To assess the protease sensitivity of prions, 160 µL of 10% brain homogenate was incubated with varying concentrations of PK (0, 5, 50, 200 µg/mL) at 37°C for 60 minutes with constant agitation. PK was inactivated by adding 0.5 mM phenylmethylsulfonyl fluoride (PMSF) and samples

169

were mixed with 2X sample buffer, heated to 100 °C, run on SDS-PAGE and immunoblotted (using an in-house anti-PrP^{Sc} antibody). The Silver staining method [49] includes fixing and washing gels in ethanol to remove excess SDS. After treatment with Farmer's solution, gels were incubated with AgNiO$_3$ for 20 minutes and developed in formaldehyde sodium carbonate solution.

6.5.8. Lipid analysis

The total lipid was isolated from high titer PTA complexes of PrP^{Sc} solubilized in SMA polymer or sarkosyl according to established methods [50] using methanol: chloroform (1:2 v/v) in a BSL-2 lab biosafety cabinet following decontamination by incubation of PTA pellets with 5 M guanidinium thiocyanate for one hour at room temperature [51]. Total lipids were analyzed by HPLC according to the previous report [52], lipid species were identified according to their retention time, and the amount of each lipid was quantified using standard lipids.

6.6. References

[1] M. Overduin, M. Esmaili, Memtein: The fundamental unit of membrane-protein structure and function, Chem Phys Lipids, 218 (2019) 73-84.

[2] F. Chiti, C.M. Dobson, Protein misfolding, functional amyloid, and human disease, Annual review of biochemistry, 75 (2006) 333-366.

[3] K. Giles, A.L. Woerman, D.B. Berry, S.B. Prusiner, Bioassays and Inactivation of Prions, Cold Spring Harbor perspectives in biology, 9 (2017) DOI:10.1101/cshperspect.a023499.

[4] M.P. McKinley, A. Taraboulos, L. Kenaga, D. Serban, A. Stieber, S.J. DeArmond, S.B. Prusiner, N. Gonatas, Ultrastructural localization of scrapie prion proteins in cytoplasmic vesicles of infected cultured cells, Lab Invest, 65 (1991) 622-630.

[5] D. Riesner, Biochemistry and structure of PrP(C) and PrP(Sc), Br Med Bull, 66 (2003) 21-33.

[6] J. Breyer, W.M. Wemheuer, A. Wrede, C. Graham, S.L. Benestad, B. Brenig, J.A. Richt, W.J. Schulz-Schaeffer, Detergents modify proteinase K resistance of PrP Sc in different transmissible spongiform encephalopathies (TSEs), Vet Microbiol, 157 (2012) 23-31.

[7] Y. Shaked, R. Engelstein, R. Gabizon, The binding of prion proteins to serum components is affected by detergent extraction conditions, J Neurochem, 82 (2002) 1-5.

[8] D.J. Levine, J. Stöhr, L.E. Falese, J. Ollesch, H. Wille, S.B. Prusiner, J.R. Long, Mechanism of scrapie prion precipitation with phosphotungstate anions, ACS. Chem. Biol, 10 (2015) 1269-1277.

[9] J. Collinge, Ex vivo mammalian prions are formed of paired double helical prion protein fibrils, Open Biol 160035, 6 (2016)1-12.

[10] D.C. Bode, M. Freeley, J. Nield, M. Palma, J. H., Amyloid-β oligomers have a profound detergent-like effect on lipid membrane bilayers, imaged by atomic force and electron microscopy, J Biol Chem, 294 (2019) 7566-7572.

[11] O. Gursky, Role of lipids in protein misfolding, Adv Exp Med Biol, 855 (2015) 5-7.

[12] K.J. Korshavn, C. Satriano, Y. Lin, R. Zhang, M. Dulchavsky, A. Bhunia, M.I. Ivanova, Y.-H. Lee, C. La Rosa, M.H. Lim, A. Ramamoorthy, Reduced Lipid Bilayer

Thickness Regulates the Aggregation and Cytotoxicity of Amyloid-β, J Biol Chem, 292 (2017) 4638-4650.

[13] F. Wang, J. Ma, Role of lipid in forming an infectious prion?, Acta Biochim Biophys Sin, 45 (2013) 485-493.

[14] S. Ambadi Thody, M.K. Mathew, J.B. Udgaonkar, Mechanism of aggregation and membrane interactions of mammalian prion protein, Biochim Biophys Acta-Biomembr, 1860 (2018) 1927-1935.

[15] J.M. Dorr, S. Scheidelaar, M.C. Koorengevel, J.J. Dominguez, M. Schafer, C.A. van Walree, J.A. Killian, The styrene-maleic acid copolymer: a versatile tool in membrane research, Eur Biophys J, 45 (2016) 3-21.

[16] T.J. Knowles, A. Scott-Tucker, M. Overduin, I.R. Henderson, Membrane protein architects: the role of the BAM complex in outer membrane protein assembly, Nature reviews. Microbiology, 7 (2009) 206-214.

[17] S.C. Lee, T.J. Knowles, V.L.G. Postis, M. Jamshad, R.A. Parslow, Y.P. Lin, A. Goldman, P. Sridhar, M. Overduin, S.P. Muench, T.R. Dafforn, A method for detergent-free isolation of membrane proteins in their local lipid environment, Nat Protoc, 11 (2016) 1149-1162.

[18] W. Qiu, Structure and activity of lipid bilayer within a membrane-protein transporter, Proc Natl Acad Sci USA, 115 (2018) 12985-12990.

[19] C. Sun, S. Benlekbir, P. Venkatakrishnan, Y. Wang, S. Hong, J. Hosler, E. Tajkhorshid, J.L. Rubinstein, R.B. Gennis, Structure of the alternative complex III in a supercomplex with cytochrome oxidase, Nature, 557 (2018) 123-126.

[20] A. Grethen, A.O. Oluwole, B. Danielczak, C. Vargas, S. Keller, Thermodynamics of nanodisc formation mediated by styrene/maleic acid (2:1) copolymer, Sci Rep, 7 (2017) 11517-11531.

[21] O. Korotych, J. Mondal, K.M. Asfura, J. Hendricks, B. D., J. Polym, Evaluation of commercially available styrene-co-maleic acid polymers for the extraction of membrane proteins from spinach chloroplast thylakoids, Eur Polym J, 114 (2018) 485-500.

[22] K.A. Morrison, A. Akram, A. Mathews, Z.A. Khan, J.H. Patel, C. Zhou, D.J. Hardy, C. Moore-Kelly, R. Patel, V. Odiba, T.J. Knowles, M.-U.-H. Javed, N.P. Chmel, T.R. Dafforn, A.J. Rothnie, Membrane protein extraction and purification using styrene-maleic acid (SMA) copolymer: effect of variations in polymer structure, Biochem J, 473 (2016) 4349-4360.

[23] M. Overduin, M., Esmaili, Nanodiscs, and the Convergence of Lipidomics, Metabolomics, Interactomics, and Proteomics, Appl Sci, 9 (2019) 1230-1245.

[24] L. D'Castro, A. Wenborn, N. Gros, S. Joiner, S. Cronier, J. Collinge, J.D.F. Wadsworth, Isolation of proteinase K-sensitive prions using pronase E and phosphotungstic acid, PLoS One, 5 (2010) 1-7.

[25] S.A. Priola, K.L. McNally, The role of the prion protein membrane anchor in prion infection, Prion, 3 (2009) 134-138.

[26] C. Terry, R.L. Harniman, J. Sells, A. Wenborn, S. Joiner, H.R. Saibil, M.J. Miles, J. Collinge, J.D.F. Wadsworth, Structural features distinguishing infectious ex vivo mammalian prions from non-infectious fibrillar assemblies generated in vitro, Sci Rep, 9 (2019) 1-12.

[27] H. Wille, S.B. Prusiner, Ultrastructural studies on scrapie prion protein crystals obtained from reverse micellar solutions, Biophys J, 76 (1999) 1048-1062.

[28] J. Fantini, N. Garmy, R. Mahfoud, N. Yahi, Lipid rafts: structure, function and role in HIV, Alzheimer's and prion diseases, Expert Rev Mol Med, 4 (2002) 1-22.

[29] D.R. Taylor, N.M. Hooper, The prion protein and lipid rafts, Mol Membr Biol, 23 (2006) 89-99.

[30] M. Camargo, P. Intasqui Lopes, P.T. Del Giudice, V.M. Carvalho, K.H.M. Cardozo, C. Andreoni, R. Fraietta, R.P. Bertolla, Unbiased label-free quantitative proteomic profiling and enriched proteomic pathways in seminal plasma of adult men before and after varicocelectomy, Hum Reprod, 28 (2013) 33-46.

[31] M.F.M. Sciacca, C. Tempra, F. Scollo, L.R.C. Milardi D, Amyloid growth and membrane damage: Current themes and emerging perspectives from theory and experiments on Aβ and hIAPP, Biochim Biophys Acta-Biomembr, 1860 (2018) 1625-1638.

[32] Q. Bui, J. Sherma, J.K. Hines, Using High-Performance Thin-Layer Chromatography-Densitometry to Study the Influence of the Prion and Its Determinant Prion Protein Rnq1 on Yeast Lipid Profiles, Separations, 5 (2018) 1-6.

[33] K. Simons, D. Toomre, Lipid rafts, and signal transduction, Nature reviews. Mol Cell Biol, 1 (2000) 31-39.

[34] B.B. Guo, S.A. Bellingham, A.F. Hill, The neutral sphingomyelinase pathway regulates packaging of the prion protein into exosomes, J Biol Chem, 290 (2015) 3455-3467.

[35] Y.A. Hannun, L.M. Obeid, Principles of bioactive lipid signaling: lessons from sphingolipids, Nature reviews. Mol Cell Biol, 9 (2008) 139-150.

[36] D. Gonzalez-Romero, M.A. Barria, P. Leon, R. Morales, C. Soto, Detection of infectious prions in urine, FEBS Lett, 582 (2008) 3161-3166.

[37] S. Cronier, N. Gros, M.H. Tattum, G.S. Jackson, A.R. Clarke, J. Collinge, J.D.F. Wadsworth, Detection and characterization of proteinase K-sensitive disease-related prion protein with thermolysin, Biochem J, 416 (2008) 297-305.

[38] P. Angelisová, O. Ballek, J. Sýkora, O. Benada, T. Čajka, J. Pokorná, D. Pinkas, V. Hořejší, The use of styrene-maleic acid copolymer (SMA) for studies on T cell membrane rafts, Biochim Biophys Acta-Biomembr, 1861 (2019) 130-141.

[39] B. Falcon, J. Zivanov, W. Zhang, A.G. Murzin, H.J. Garringer, R. Vidal, R.A. Crowther, K.L. Newell, B. Ghetti, M. Goedert, S.H.W. Scheres, Novel tau filament fold in chronic traumatic encephalopathy encloses hydrophobic molecules, Nature, 568 (2019) 420-423.

[40] K. Teruya, A. Oguma, K. Nishizawa, M. Kawata, Y. Sakasegawa, H. Kamitakahara, K. Doh-Ura, A Single Subcutaneous Injection of Cellulose Ethers Administered Long before Infection Confers Sustained Protection against Prion Diseases in Rodents, PLoS pathogens, 12 (2016) 1-23.

[41] S.R. Tonge, B.J. Tighe, Responsive hydrophobically associating polymers: a review of structure and properties, Adv. Drug Deliv. Rev, 53(2001)109-122.

[42] K. Tsukigawa, L. Liao, H. Nakamura, J. Fang, K. Greish, M. Otagiri, H. Maeda, Synthesis, and therapeutic effect of styrene-maleic acid copolymer-conjugated pirarubicin, Cancer Sci, 106 (2015) 270-278.

[43] J.M. McCarthy, B. Rasines Moreno, D. Filippini, H. Komber, M. Maly, M. Cernescu, B. Brutschy, D. Appelhans, M.S. Rogers, Influence of surface groups on

poly(propylene imine) dendrimers anti-prion activity, Biomacromolecules, 14 (2013) 27-37.

[44] Beom Lim, Yong, M.C. E., K. Younghwan, T.W. B., R. Chongsuk, The inhibition of prions through blocking prion conversion by permanently charged branched polyamines of low cytotoxicity, Biomaterials, 31 (2010) 2025-2033.

[45] M. Fischer, D. Appelhans, S. Schwarz, B. Klajnert, M. Bryszewska, B. Voit, M. Rogers, Influence of surface functionality of poly(propylene imine) dendrimers on protease resistance and propagation of the scrapie prion protein, Biomacromolecules, 11 (2010) 1314-1325.

[46] S. Supattapone, H.O. Nguyen, F.E. Cohen, S.B. Prusiner, M.R. Scott, Elimination of prions by branched polyamines and implications for therapeutics, Proc Natl Acad Sci USA, 96 (1999) 14529-14534.

[47] S. Lindhoud, V. Carvalho, J.W. Pronk, M.E. Aubin-Tam, SMA-SH: Modified Styrene-Maleic Acid Copolymer for Functionalization of Lipid Nanodiscs, Biomacromolecules, 17 (2016) 1516-1522.

[48] A. Wenborn, C. Terry, N. Gros, S. Joiner, L. D'Castro, S. Panico, J. Sells, S. Cronier, J.M. Linehan, S. Brandner, H.R. Saibil, J. Collinge, J.D. Wadsworth, A novel and rapid method for obtaining high titer intact prion strains from the mammalian brain, Sci Rep, 5 (2015) 10062.

[49] H. Wille, M. Shanmugam, M. Murugesu, J. Ollesch, G. Stubbs, J.R. Long, J.G. Safar, S.B. Prusiner, Surface charge of polyoxometalates modulates polymerization of the scrapie prion protein, Proc Natl Acad Sci USA, 106 (2009) 3740-3745.

[50] J.M. Dorr, M.C. Koorengevel, M. Schafer, A.V. Prokofyev, S. Scheidelaar, E.A. van der Cruijsen, T.R. Dafforn, M. Baldus, J.A. Killian, Detergent-free isolation, characterization, and functional reconstitution of a tetrameric K+ channel: the power of native nanodiscs, Proc Natl Acad Sci USA, 111 (2014) 18607-18612.

[51] S. Botsios, S. Tittman, L. Manuelidis, Rapid chemical decontamination of infectious CJD and scrapie particles parallel treatments known to disrupt microbes and biofilms, Virulence, 6 (2015) 787-801.

[52] M. Graeve, D. Janssen, Improved separation and quantification of neutral and polar lipid classes by HPLC-ELSD using a monolithic silica phase: application to exceptional marine lipids, J Chromatogr B Analyt Technol Biomed Life Sci, 877 (2009) 1815-1819.

Chapter 7

Final Discussion, Conclusions

&

Future Directions

7.1. Final discussion

Multiple membrane mimic systems such as micelles, bicelles, amphipols, membrane scaffold proteins (MSP)-based nanodiscs and, more recently, polymer-based nanodiscs have been utilized for high-resolution structural determination of MPs (using X-ray diffraction and cryo-EM) and their functional analyses (drug design, ligand binding and screening assays).

Except for amphipathic polymers, the experimental preparation of all these membrane-like systems is detergent dependent, which consequently leads to dissociation of diverse natural lipid molecules, destabilization, or aggregation of proteins, hence in many cases compromising the activity and stability of target membrane proteins.

Amphipathic polymers are the only tool that can directly extract proteins along with their surrounding native lipid bilayer and form native nanodisc of target membrane proteins. Lipids are involved in many crucial biological roles such as lipid signaling, metabolism, enzymatic functions, and conformational regulation of membrane proteins [1]. So once lipids stripped away by detergent during sample preparation, the biologically relevant conformational states of membrane proteins undergo significant changes [2].

Styrene-maleic acid polymers are the first example of chemically synthesized polymers used for isolation of native nanodiscs of MP, and they have been constantly subjected to improvement to meet the need of the scientific community. Such efforts include limiting the non-specific interaction of polymer and target protein, tuning the size and homogeneity of membrane protein nanodisc, and improving the solubility of polymers at acidic pH and physiological concentration of divalent metal ions. To this end, chemical

179

modification of maleic anhydride comonomer with ethanolamine (SMA-EA) [3], quaternary amines (SMA-QA) [4], tertiary amine (SMI) [5] functional groups and zwitterionic PC moiety (zSMA) [6], diethylamine (SMA-ED) [7] result in various non-carboxylic acid sidechains, hence less charge density on the polymer. A list of SMA polymers with non-carboxylic sidechains are listed in Table 7.1. Most of these derivatives can solubilize synthetic lipid vesicle *in vitro* and do not precipitate at acidic pH and physiologic concentration of calcium and magnesium. However, their abilities to solubilize biological membranes has not been tested.

In chapters 2 and 3, I have shown that short alkyl sidechains and amphoteric moieties, such as aminoxide and imidazole, could be utilized to improve the behavior of SMA in buffer solutions and to rationally modulate the size of nanodiscs in order to accommodate larger protein complexes.

While the significance of styrene: maleic acid ratio for the solubilization of native membrane had been assessed prior to this research, I discovered that the sequential dispersity (random distribution) of phenyl rings along the polymer chain could affect the spectrophotometric characteristics of SMA polymers, regardless of the chemistry of sidechains. By grafting novel sidechains on a relatively less random backbone (SMA1:1), I could synthesize novel fluorescent styrene-maleamic polymers. Solution behavior of AO, His and MA/EtA/PA SMA(1:1) is comparable to that of previously reported polymers (with 1.3:1 S: MA ratio and RAFT SMA polymers, Table 7.1). Yet, their fluorescence at an excitation wavelength of 320 nm, distinguishes them from almost all other categories of amphipathic polymers reported thus far.

Methyl stilbene-maleic acid (methyl STMA) polymers are a unique series of aromatic amphipathic polymers that consist of methyl stilbene (methyl moiety at *para* and *meta* positions) and maleic acid comonomers and, to some extent, resemble SMA(2:1). Methyl STMA polymers show strict alternation of phenyl and maleic acid monomers along the polymer chain. Such alternation in 5 kDa polymer is very unprecedented for SMA (even through RAFT polymerization). Unlike SMA2000, methyl STMA polymers can solubilize native membranes into larger nanodiscs (~ 20 nm) and stay soluble in acidic pH. However, unlike SMA-EA, SMA-QA, SMI, MA/EtA/PA SMA(1:1), methyl STMA precipitate at 2.5 mM concentration of calcium. Thus far, the kinetics of the solubilization of MLV vesicles of DMPC and biomembrane by methyl STMA have not been fully addressed or compared with other amphipathic polymers. Nevertheless, we speculate, the relatively stiff backbone of stilbene-MA polymers may affect the thermodynamics, hence kinetics of membrane solubilization.

Aromatic amphipathic polymers still seem to attract more popularity than aliphatic amphipathic counterparts (DIBMA and PMA, Table 7.1) for structural studies of membrane proteins, specially using cryo-EM and lipid cubic phase crystallography. Conversely, aliphatic polymers contain less hydrophobic patches, hence demonstrate the least nonspecific interaction with target proteins. This phenomenon, therefore, makes DIBMA and PMA intensively desired for therapeutic target membrane proteins such as ion channels, GPCRs, proteases, kinases, nuclear hormone receptors with druggable sites accessible to the cell surface. Besides, due to lack of phenyl ring, DIBMA and PMA do not interfere with ultraviolet absorbance of proteins, thus fully compatible with

spectrophotometric analysis of membrane proteins using circular dichroism and UV-Vis spectroscopy [8,9].

The non-specific interaction of novel His, AO, and MA/EtA/PA SMA and methyl STMA polymers with protein surfaces have not been examined or compared with aliphatic polymers (DIBMA or PMA). Therefore, the suitability of these polymers for future drug screening projects remains to be investigated. For the ease of comparison, characteristics of various formulations of amphipathic polymers in the current literature and the novel polymers in this thesis are listed in Table 7.1.

7.2. Conclusions and future directions

The field of polymeric detergents or polymer-based nanodiscs is still in its infancy and requires interdisciplinary efforts to overcome the shortcomings of synthetic amphipathic polymers for applications related to the biological membranes. Over the past few years, my research has been focused on the optimization of SMA polymers for purification of membrane proteins, namely a bacterial membrane protein PagP and the infectious prion protein, and biophysical and biochemical analyses of the resulting SMALP particles.

In this thesis, I specifically focused on three major issues related to SMA polymers: (i) Spectroscopic interference of styrene-based polymers with proteins absorbance that limits detection and quantification of each component in solution; (ii) The sequential polydispersity of SMA that stems from radical polymerization of styrene and maleic anhydride subunits; and (iii) Aggregation of SMA polymers in acidic pH and high concentration of divalent cations, such as calcium.

The results demonstrated that the derivatization of maleic anhydride units with various functional sidechains, including zwitterionic moieties (*e.g.,* histamine and amine oxide) and hydrophobic alkylamine, shifts the pK_a of the polymer chains. This can lead to significant improvements in the buffer behavior of SMA(1:1) and SMA(2:1) polymers, to the extent that makes these series of polymers fully applicable for analysis of lipid-protein complex at pH 5.0 and up to at least 5 mM calcium chloride. One novel finding of my work was the synthesis of the maleamic acid and maleimide forms of the zwitterionic group-containing SMA polymers on a non-RAFT polymer backbone of SMA(1:1) (Mw 5.5 kDa). All derivatized SMA polymers were entirely compatible with negative-stain electron microscopy, which has significant future implications for single-particle electron microscopy. However, methyl and propylamine sidechains, if not capped with a polar group, such as hydroxyl, would drive the self-aggregation of polymer chains and ultimately undermine the detergent-like propensity of SMA(1:1). This effect would be even more pronounced for SMA(2:1) and SMA(3:1), which contain more percentage of styrene subunits.

Potentially, any modifications discussed here can be readily applied to other aromatic and aliphatic polymers that contain MA subunit. However, due to the complex and unpredictable behavior of polymers (unlike proteins) in solution, the ultimate effect of these sidechains on the performance on each polymer should be experimentally tested.

By grafting multiple sidechains (some not shown in this thesis) on different SMAn polymers, I discovered that the intrinsic fluorescence of styrene subunits is self-quenched in SMA(2:1) and (3:1). In addition to its relatively low sequential heterogeneity, SMA(1:1) initially promised to be an excellent candidate to formulate a fluorescent SMA polymer.

However, my preliminary results suggest that the fluorescence property of SMA(1:1) is quenched upon interaction with native bacterial membranes. Intriguingly, the maleimide version of the amine oxide derivative of SMA(1:1) (which is made by partial dehydration of maleamic form) has a stable fluorescence even after incubation with biomembranes, leading to a hypothesis that sidechains may play a pivotal role in permanent fluorescence of amphipathic polymer. This criterion should be considered and examined in future designs.

Histamine-grafted SMA polymers interact with Ni-NTA resins via imidazole moieties, and possibly with other Ni^{+2} active surfaces (such as Biacore SPR chips). This advantage expands the application of His-SMALP particles for drug and ligand discoveries. An array of imidazole molecules is required (minimum 3-4 imidazole moieties) to improve the binding affinity of His-polymer to Ni^{+2} surface. One series of novel SMA formulations that I developed (data not discussed) are amino acid-derivatized SMA (patent filed). Since amino acids, *per se*, are almost insoluble in organic solvents such as DMF, the decarboxylated or esterified amino acid derivatives should be used in synthesis reactions. In light of this, I extrapolate that commercially available short poly-histidine tags do not benefit this purpose unless esterified or decarboxylated. This approach, in theory, would lead to the birth of novel poly-His tagged SMA polymers.

My results suggested that methylated stilbene-*alt*-maleic acid copolymers resemble strictly alternating homologs of SMA(2:1) polymer with restricted backbone flexibility and well-defined sequence of each co-monomer. These characteristics may change the binding affinity of stilbene-based polymers to biomembrane and the kinetics of membrane fragmentation and solubilization. Due to the scarcity of methyl stilbene-MA

polymer samples, I was not able to cover these topics in my research; hence it remains to be addressed in the future.

The nonspecific interaction of different SMA polymers with protein surfaces (including antibodies) is still a significant drawback, as it may compromise the activity of target proteins and also shield the strategic binding cavities. This feature is mainly specific to phenyl-containing polymers such as SMA (and likely methyl STMA) and was truly reflected in infectivity assays of SMA-isolated PrP^{Sc} particles. My results confirmed that some types of SMA polymers (SZ2500 and SZ30010) present such a phenomenon more pronouncedly than others (SMA2000). The general notion is that increasing the ratio of S: MA would aggravate this effect. I speculate that electron- withdrawing moieties such as OH, Br, Cl, and NO$_2$ would decrease the electron clouds of the phenyl group and therefore mitigate the nonspecific binding. The hypothesis (patent filed) should be tested in future formulations of SMA polymers.

Covalently circularized MSP proteins have been used to encapsulate membrane proteins into circularized nanodiscs [10,11]. In principle, we can expand this concept to linear amphipathic polymers and come up with cyclic amphipathic polymers [12].

This approach may result in polymers with less polydispersity. However, the synthesis of cyclic polymers is a daunting task. Therefore, thus far, polymer chemists have not been able to synthesize cyclic variants of any amphipathic polymers for the solubilization of membrane protein.

The results from native ESI-MS analysis of PagP (appendix 2) in novel SMA polymers suggest that the behavior of these nanodiscs in the gas phase is dramatically

different from what is reported for SMA2000-based nanodiscs, in a sense that in most cases, even after applying maximum voltage, we were not able to release and detect PagP protein *in vacuo*. Therefore, the data was not shown or discussed in this thesis. An extensive analysis is required in the future to determine what factors define the behavior of various formulations of polymers, therefore the stability of related nanodiscs in the gas phase.

Polymer	Mw (kDa)	Sidechain on MA	PDI	Alternation	Calcium tolerance (mM)	Lowest pH tolerance	Styrene based?	RAFT?	Source polymer	Disc size (nm)†	Charge	Solubilizing biomembrane?
SMA2000, SZ30010	7.5-10	NA	~2.5	Random	2.5	~6	Yes	No	NA	~10 nm	-	Yes
DIBMA	`15.3	NA	NA	Relatively alternating	20	5	No	No	NA	~12 nm	-	Yes
SMA-EA	1.6	Ethanol amine	NA	Random	NA	5	Yes	No	~ 1.3:1	~60 nm	-	NA
SMA-ED	1.6	Diethylamine	NA	Random	40<	5	Yes	No	~ 1.3:1	~10 nm	-	NA
SMA-QA	1.6	2-(aminoethyl)trimethyl-ammonium	NA	Random	NA	5	Yes	No	~ 1.3:1	~30 nm	+	NA
SMI	7.5-10	dimethylaminopropylamine	NA	Random	100	5	Yes	No	2:1	~11	+/-	Yes
SMA-MA/EA*/PA	5.5	MA/EA*/PA	2.5	Relatively alternating	10/25/12	5/5/6	Yes	No	1:1	15/ 25/32 nm	-	Yes
Ortho, para methyl STMA	4.4, 5.8	NA	1.2, 1.5	Strictly alternating	2.5	5	No	No	STMA	~20 nm	-	Yes
AO-SMA	5.5	Amine oxide	~2.2	Relatively alternating	~6.5	5	Yes	No	1:1	~20 nm	-	Yes
His-SMA	5.5	Histidine	~2.2	Relatively alternating	~6	5	Yes	No	1:1	~24 nm	-	Yes
zSMA	<12	Phosphatidyl choline (PC)	1.1-1.2	Random	20	5	Yes	Yes	NA	NA	+/-	Yes
PMA	2-14	NA	NA	Random	NA	5	No	No	NA	~20 nm	-	Yes
SMA-SH	7.5	Cysteamine	~ 2.5	Random	NA	6	Yes	No	2:1	~12 nm	-	Yes

*Ethylamine; †Size varies depending on the mass ratio of polymer to lipid; **NA:** not applicable.

Table 7.1. An updated list of amphipathic polymers that can solubilize lipid vesicles and biomembranes, form native nanodiscs and some display improved solution behaviors.

References

[1] E. Fahy, D. Cotter, M. Sud, S. Subramaniam, Lipid classification, structures and tools, Biochim Biophys Acta, 1811 (2011) 637-647.

[2] Y. Sonntag, M. Musgaard, C. Olesen, B. Schiott, J.V. Moller, P. Nissen, L. Thogersen, Mutual adaptation of a membrane protein and its lipid bilayer during conformational changes, Nat Commun, 2 (2011) 304.

[3] T. Ravula, S.K. Ramadugu, G. Di Mauro, A. Ramamoorthy, Bioinspired, Size-Tunable Self-Assembly of Polymer-Lipid Bilayer Nanodiscs, Angew Chem Int Ed, 56 (2017) 11466-11470.

[4] T. Ravula, N.Z. Hardin, J. Bai, S.C. Im, L. Waskell, A. Ramamoorthy, Effect of polymer charge on functional reconstitution of membrane proteins in polymer nanodiscs, Chem Commun, 54 (2018) 9615-9618.

[5] S.C.L. Hall, C. Tognoloni, J. Charlton, É.C. Bragginton, A.J. Rothnie, P. Sridhar, M. Wheatley, T.J. Knowles, T. Arnold, K.J. Edler, T.R. Dafforn, An acid-compatible co-polymer for the solubilization of membranes and proteins into lipid bilayer-containing nanoparticles, Nanoscale, 10 (2018) 10609-10619.

[6] M.C. Fiori, Y. Jiang, G.A. Altenberg, H. Liang, Polymer-encased nanodiscs with improved buffer compatibility, Sci Rep, 7 (2017) 1-10.

[7] T. Ravula, N.Z. Hardin, S.K. Ramadugu, A. Ramamoorthy, PH Tunable and Divalent Metal Ion Tolerant Polymer Lipid Nanodiscs, Langmuir, 33 (2017) 10655-10662.

[8] A.O. Oluwole, B. Danielczak, A. Meister, J.O. Babalola, C. Vargas, S. Keller, Solubilization of Membrane Proteins into Functional Lipid-Bilayer Nanodiscs Using a Diisobutylene/Maleic Acid Copolymer, Angew Chem Int Edit, 56 (2017) 1919-1924.

[9] K. Yasuhara, J. Arakida, T. Ravula, S.K. Ramadugu, B. Sahoo, J. Kikuchi, A. Ramamoorthy, Spontaneous Lipid Nanodisc Fomation by Amphiphilic Polymethacrylate Copolymers, J Am Chem Soc, 139 (2017) 18657-18663.

[10] M.L. Nasr, G. Wagner, Covalently circularized nanodiscs; challenges and applications, Curr Opin Struct Biol, 51 (2018) 129-134.

[11] Y. Yusuf, J. Massiot, Y.T. Chang, P.H. Wu, V. Yeh, P.C. Kuo, J. Shiue, T.Y. Yu, Optimization of the Production of Covalently Circularized Nanodiscs and Their Characterization in Physiological Conditions, Langmuir, 34 (2018) 3525-3532.

[12] B.J. Ree, T. Satoh, T. Yamamoto, Micelle Structure Details and Stabilities of Cyclic Block Copolymer Amphiphile and Its Linear Analogues, Polymers, 11 (2019).

Bibliography

A. Das, J. Zhao, G.C. Schatz, S.G. Sligar, R.P. Van Duyne, Screening of Type I and II Drug Binding to Human Cytochrome P450-3A4 in Nanodiscs by Localized Surface Plasmon Resonance Spectroscopy, Anal Chem, 81 (2009) 3754-3759.

A. Dathe, T. Heitkamp, I. Perez, H. Sielaff, A. Westphal, S. Reuter, R. Mrowka, M. Borsch, Observing monomer-dimer transitions of neurotensin receptors 1 in single SMALPs by homoFRET and in an ABELtrap, Proc Spie, 10884 (2019)1-12.

A. Grethen, A.O. Oluwole, B. Danielczak, C. Vargas, S. Keller, Thermodynamics of nanodisc formation mediated by styrene/maleic acid (2:1) copolymer, Scie Rep, 7 (2017) 11517-11531.

A. Kuzyk, M. Kastyak, V. Agrawal, M. Gallant, G. Sivakumar, M. Rak, M.R. Del Bigio, D. Westaway, R. Julian, K.M. Gough, Association among amyloid plaque, lipid, and creatine in hippocampus of TgCRND8 mouse model for Alzheimer disease, J Biol Chem, 285 (2010) 31202-31207.

A. Santuccione, V. Sytnyk, I. Leshchyns'ka, M. Schachner, Prion protein recruits its neuronal receptor NCAM to lipid rafts to activate p59fyn and to enhance neurite outgrowth, J Cell Biol, 169 (2005) 341-354.

A. Wenborn, C. Terry, N. Gros, S. Joiner, L. D'Castro, S. Panico, J. Sells, S. Cronier, J.M. Linehan, S. Brandner, H.R. Saibil, J. Collinge, J.D. Wadsworth, A novel and rapid method for obtaining high titer intact prion strains from the mammalian brain, Sci Rep, 5 (2015) 10062.

A.A. Zurawel, D.J. Walsh, S.M. Fortier, T. Chidawanyika, S. Sengupta, K. Zilm, S. Supattapone, Prion Nucleation Site Unmasked by Transient Interaction with Phospholipid Cofactor, Biochemistry, 53 (2014) 68-76.

A.D. Gossert, S. Bonjour, D.A. Lysek, F. Fiorito, K. Wuthrich, Prion protein NMR structures of elk and of mouse/elk hybrids, Proc Natl Acad Sci USA, 102 (2005) 646-650.

A.K. Iyer, K. Greish, J. Fang, R. Murakami, H. Maeda, High-loading nanosized micelles of copoly(styrene-maleic acid)-zinc protoporphyrin for targeted delivery of a potent heme oxygenase inhibitor, Biomaterials, 28 (2007) 1871-1881.

A.M. Savage, X. Zhou, J. Huang, S.R. Turner, A review of semi-rigid, stilbene-containing alternating copolymers, Appl Petrochem Res, 5 (2015) 27-33.

A.O. Oluwole, A. Meister, J.O. Babalola, C. Vargas, S. Keller, Membrane Proteins Solubilization of Membrane Proteins into Functional Lipid-Bilayer Nanodiscs Using a Diisobutylene / Maleic Acid Copolymer, Angew.Chem.Int.Ed (2017) 1919-1924.

A.O. Oluwole, J. Klingler, B. Danielczak, J.O. Babalola, C. Vargas, G. Pabst, S. Keller, Formation of Lipid-Bilayer Nanodiscs by Diisobutylene/Maleic Acid (DIBMA) Copolymer, Langmuir, 33 (2017) 14378-14388.

A.P. Bali, I.D. Sahu, A.F. Craig, E.E. Clark, K.M. Burridge, M.T. Dolan, C. Dabney-Smith, D. Konkolewicz, G.A. Lorigan, Structural characterization of styrene-maleic acid copolymer-lipid nanoparticles (SMALPs) using EPR spectroscopy, Chem Phys Lipids, 220 (2019) 6-13.

A.S. Hauser, M.M. Attwood, M. Rask-Andersen, H.B. Schioth, D.E. Gloriam, Trends in GPCR drug discovery: new agents, targets and indications, Nat Rev Drug Discov, 16 (2017) 829-842.

A.W. Bryan, J.L. Starner-Kreinbrink, R. Hosur, P.L. Clark, B. Berger, Structure-based prediction reveals capping motifs that inhibit beta-helix aggregation, Proc Natl Acad Sci USA, 108 (2011) 11099-11104.

A.Y. Shih, P.L. Freddolino, A. Arkhipov, K. Schulten, Assembly of lipoprotein particles revealed by coarse-grained molecular dynamics simulations, J Struct Biol, 157 (2007) 579-592.

B. Danielczak, S. Keller, Collisional lipid exchange among DIBMA-encapsulated nanodiscs (DIBMALPs), Eur Polym J, 109 (2018) 206-213.

B. Falcon, J. Zivanov, W. Zhang, A.G. Murzin, H.J. Garringer, R. Vidal, R.A. Crowther, K.L. Newell, B. Ghetti, M. Goedert, S.H.W. Scheres, Novel tau filament fold in chronic traumatic encephalopathy encloses hydrophobic molecules, Nature, 568 (2019) 420-423.

B. Hay, R.A. Barry, I. Lieberburg, S.B. Prusiner, V.R. Lingappa, Biogenesis and Transmembrane Orientation of the Cellular Isoform of the Scrapie Prion Protein, Mol Cell Biol, 7 (1987) 914-920.

B. Oesch, D. Westaway, M. Walchli, M.P. McKinley, S.B. Kent, R. Aebersold, R.A. Barry, P. Tempst, D.B. Teplow, L.E. Hood, et al., A cellular gene encodes scrapie PrP 27-30 protein, Cell, 40 (1985) 735-746.

B.B. Gong, A. Ramos, E. Vazquez-Fernandez, C.J. Silva, J. Alonso, Z.S. Liu, J.R. Requena, Probing structural differences between PrPC and PrPSc by surface nitration and acetylation: evidence of conformational change in the C-terminus, Biochemistry, 50 (2011) 4963-4972.

B.B. Guo, S.A. Bellingham, A.F. Hill, The neutral sphingomyelinase pathway regulates packaging of the prion protein into exosomes, J Biol Chem, 290 (2015) 3455-3467.

B.J. Ree, T. Satoh, T. Yamamoto, Micelle Structure Details and Stabilities of Cyclic Block Copolymer Amphiphile and Its Linear Analogues, Polymers, 11 (2019).

B.R. Groveman, M.A. Dolan, L.M. Taubner, A. Kraus, R.B. Wickner, B. Caughey, Parallel In-register Intermolecular beta-Sheet Architectures for Prion-seeded Prion Protein (PrP) Amyloids, J Biol Chem, 289 (2014) 24129-24142.

B.S. Wong, T. Liu, R.L. Li, T. Pan, R.B. Petersen, M.A. Smith, P. Gambetti, G. Perry, J.C. Manson, D.R. Brown, M.S. Sy, Increased levels of oxidative stress markers detected in the brains of mice devoid of prion protein, J Neurochem, 76 (2001) 565-572.

Beom Lim, Yong, M.C. E., K. Younghwan, T.W. B., R. Chongsuk, The inhibition of prions through blocking prion conversion by permanently charged branched polyamines of low cytotoxicity, Biomaterials, 31 (2010) 2025-2033.

C. Govaerts, H. Wille, S.B. Prusiner, F.E. Cohen, Evidence for assembly of prions with left-handed beta-helices into trimers, Proc Natl Acad Sci USA, 101 (2004) 8342-8347.

C. Soto, G.P. Saborio, L. Anderes, Cyclic amplification of protein misfolding: application to prion-related disorders and beyond, Trends Neurosci, 25 (2002) 390-394.

C. Southan, J.L. Sharman, H.E. Benson, E. Faccenda, A.J. Pawson, S.P.H. Alexander, O.P. Buneman, A.P. Davenport, J.C. McGrath, J.A. Peters, M. Spedding, W.A. Catterall, D. Fabbro, J.A. Davies, Nc-Iuphar, The IUPHAR/BPS Guide to PHARMACOLOGY in 2016: towards curated quantitative interactions between 1300 protein targets and 6000 ligands, Nucleic Acids Res, 44 (2016) 1054-1068.

C. Sun, S. Benlekbir, P. Venkatakrishnan, Y. Wang, S. Hong, J. Hosler, E. Tajkhorshid, J.L. Rubinstein, R.B. Gennis, Structure of the alternative complex III in a supercomplex with cytochrome oxidase, Nature, 557 (2018) 123-126.

C. Sunyach, A. Jen, J. Deng, K.T. Fitzgerald, Y. Frobert, J. Grassi, M.W. McCaffrey, R. Morris, The mechanism of internalization of glycosylphosphatidylinositol-anchored prion protein, EMBO J, 22 (2003) 3591-3601.

C. Terry, R.L. Harniman, J. Sells, A. Wenborn, S. Joiner, H.R. Saibil, M.J. Miles, J. Collinge, J.D.F. Wadsworth, Structural features distinguishing infectious ex vivo mammalian prions from non-infectious fibrillar assemblies generated in vitro, Scie Rep, 9 (2019) 1-12.

C. Wasmer, A. Lange, H. Van Melckebeke, A.B. Siemer, R. Riek, B.H. Meier, Amyloid fibrils of the HET-s(218-289) prion form a beta solenoid with a triangular hydrophobic core, Science, 319 (2008) 1523-1526.

C. Wurth, M. Grabolle, J. Pauli, M. Spieles, U. Resch-Genger, Relative and absolute determination of fluorescence quantum yields of transparent samples, Nat Protoc, 8 (2013) 1535-1550.

C.E. Carney, I.L. Lenov, C.J. Baker, K.W. MacRenaris, A.L. Eckermann, S.G. Sligar, T.J. Meade, Nanodiscs as a Modular Platform for Multimodal MR-Optical Imaging, Bioconjugate Chem, 26 (2015) 899-905.

C.E. Jones, S.R. Abdelraheim, D.R. Brown, J.H. Viles, Preferential Cu2+ coordination by His96 and His111 induces beta-sheet formation in the unstructured amyloidogenic region of the prion protein, J Biol Chem, 279 (2004) 32018-32027.

C.P. Wong, P.J. Miller, Vibrational spectroscopic studies of alane, J Energ Mater, 23 (2005) 169-181.

C.P.J. Maury, The emerging concept of functional amyloid, J Intern Med, 265 (2009) 329-334.

C.R. Raetz, C.M. Reynolds, M.S. Trent, R.E. Bishop, Lipid A modification systems in gram-negative bacteria, Annu Rev Biochem, 76 (2007) 295-329.

C.V. Robinson, Mass spectrometry: From plasma proteins to mitochondrial membranes, Proc Natl Acad Sci USA, 116 (2019) 2814-2820.

D. Gonzalez-Romero, M.A. Barria, P. Leon, R. Morales, C. Soto, Detection of infectious prions in urine, FEBS Lett, 582 (2008) 3161-3166.

D. Li, V.E. Pye, M. Caffrey, Experimental phasing for structure determination using membrane-protein crystals grown by the lipid cubic phase method, Acta Crystallogr D Biol Crystallogr, 71 (2015) 104-122.

D. Riesner, Biochemistry and structure of PrP(C) and PrP(Sc), Br Med Bull, 66 (2003) 21-33.

D. Xia, C.A. Yu, H. Kim, J.Z. Xia, A.M. Kachurin, L. Zhang, L. Yu, J. Deisenhofer, Crystal structure of the cytochrome bc1 complex from bovine heart mitochondria, Science, 277 (1997) 60-66.

D.A. Harris, H.L. True, New insights into prion structure and toxicity, Neuron, 50 (2006) 353-357.

D.C. Bode, M. Freeley, J. Nield, M. Palma, J. H., Amyloid-β oligomers have a profound detergent-like effect on lipid membrane bilayers, imaged by atomic force and electron microscopy, J Biol Chem, 294 (2019) 7566-7572.

D.C. Bolton, M.P. Mckinley, S.B. Prusiner, Identification of a Protein That Purifies with the Scrapie Prion, Science, 218 (1982) 1309-1311.

D.J. Levine, J. Stöhr, L.E. Falese, J. Ollesch, H. Wille, S.B. Prusiner, J.R. Long, Mechanism of scrapie prion precipitation with phosphotungstate anions, Acs Chem Biol, 10 (2015) 1269-1277.

D.J. Rader, Molecular regulation of HDL metabolism and function: implications for novel therapies, J Clin Invest, 116 (2006) 3090-3100.

D.J.K. Swainsbury, S. Scheidelaar, N. Foster, R. van Grondelle, J.A. Killian, M.R. Jones, The effectiveness of styrene-maleic acid (SMA) copolymers for solubilization of integral membrane proteins from SMA-accessible and SMA-resistant membranes, Biochim Biophys Acta-Biomembr, 1859 (2017) 2133-2143.

D.R. Borchelt, M. Scott, A. Taraboulos, N. Stahl, S.B. Prusiner, Scrapie and Cellular Prion Proteins Differ in Their Kinetics of Synthesis and Topology in Cultured-Cells, J Neuropath Exp Neur, 49 (1990) 311-311.

D.R. Brown, K. Qin, J.W. Herms, A. Madlung, J. Manson, R. Strome, P.E. Fraser, T. Kruck, A. von Bohlen, W. Schulz-Schaeffer, A. Giese, D. Westaway, H. Kretzschmar, The cellular prion protein binds copper in vivo, Nature, 390 (1997) 684-687.

D.R. Taylor, N.M. Hooper, The prion protein and lipid rafts, Mol Membr Biol, 23 (2006) 89-99.

E. Chatani, N. Yamamoto, Recent progress on understanding the mechanisms of amyloid nucleation, Biophys Rev, 10 (2018) 527-534.

E. Cohen, A. Taraboulos, Scrapie-like prion protein accumulates in aggresomes of cyclosporin A-treated cells, EMBO J, 22 (2003) 404-417.

E. Fahy, D. Cotter, M. Sud, S. Subramaniam, Lipid classification, structures and tools, Biochim Biophys Acta, 1811 (2011) 637-647.

E. Vazquez-Fernandez, J. Alonso, M.A. Pastrana, A. Ramos, L. Stitz, E. Vidal, I. Dynin, B. Petsch, C.J. Silva, J.R. Requena, Structural Organization of Mammalian Prions as Probed by Limited Proteolysis, PLoS One, 7 (2012) 1-8.

E. Vazquez-Fernandez, M.R. Vos, P. Afanasyev, L. Cebey, A.M. Sevillano, E. Vidal, I. Rosa, L. Renault, A. Ramos, P.J. Peters, J.J. Fernandez, M. van Heel, H.S. Young, J.R. Requena, H. Wille, The Structural Architecture of an Infectious Mammalian Prion Using Electron Cryomicroscopy, PLoS Pathog, 12 (2016) 1-21.

E.B. Martin Jakubec, Samuel Furse, Morten L. Govasli, Vinnit George, Diana Turcu, Igor Iashchishyn, Ludmilla Morozova-Roche, Øyvind Halskau, Cholesterol is a strong promotor of an α-Synuclein membrane binding mode that accelerates oligomerization, BioRxiv DOI: 10.1101/725762, (2019).

E.W. Yu, G. McDermott, H.I. Zgurskaya, H. Nikaido, D.E. Koshland, Jr., Structural basis of multiple drug-binding capacity of the AcrB multidrug efflux pump, Science, 300 (2003) 976-980.

F. Chiti, C.M. Dobson, Protein misfolding, functional amyloid, and human disease, Annu rev Biochem, 75 (2006) 333-366.

F. Sokolowski, A.J. Modler, R. Masuch, D. Zirwer, M. Baier, G. Lutsch, D.A. Moss, K. Gast, D. Naumann, Formation of critical oligomers is a key event during the conformational transition of recombinant Syrian hamster prion protein, J Biol Chem, 278 (2003) 40481-40492.

F. Wang, J. Ma, Role of lipid in forming an infectious prion?, Acta Biochim Biophys, 45 (2013) 485-493.

F. Wang, X.H. Wang, C.G. Yuan, J.Y. Ma, Generating a Prion with Bacterially Expressed Recombinant Prion Protein, Science, 327 (2010) 1132-1135.J.K. Choi, I. Cali,

K. Surewicz, Q. Kong, P. Gambetti, W.K. Surewicz, Amyloid fibrils from the N-terminal prion protein fragment are infectious, Proc Natl Acad Sci USA, 113 (2016) 13851-13856.

F.R. Bertuchi, D.M.G. Bourgeon, M.C. Landemberger, V.R. Martins, G. Cerchiaro, PrPC displays an essential protective role from oxidative stress in an astrocyte cell line derived from PrPC knockout mice, Biochem Bioph Res Commun, 418 (2012) 27-32.

F.U. Hartl, M. Hayer-Hartl, Converging concepts of protein folding in vitro and in vivo, Nat Struct Mol Biol, 16 (2009) 574-581.

G. Matsumoto, S. Kim, R.I. Morimoto, Huntingtin and mutant SOD1 form aggregate structures with distinct molecular properties in human cells, J Biol Chem, 281 (2006) 4477-4485.

G. Moroncini, N. Kanu, L. Solforosi, G. Abalos, G.C. Telling, M. Head, J. Ironside, J.P. Brockes, D.R. Burton, R.A. Williamson, Motif-grafted antibodies containing the replicative interface of cellular PrP are specific for PrPSc, Proc Natl Acad Sci USA, 101 (2004) 10404-10409.

G. Spagnolli, M. Rigoli, S. Orioli, A.M. Sevillano, P. Faccioli, H. Wille, E. Biasini, J.R. Requena, Full atomistic model of prion structure and conversion, PLoS Pathog, 15 (2019)1-18.

G. Zanusso, R.B. Petersen, T.C. Jin, Y. Jing, R. Kanoush, S. Ferrari, P. Gambetti, N. Singh, Proteasomal degradation and N-terminal protease resistance of the codon 145 mutant prion protein, J Biol Chem, 274 (1999) 23396-23404.

G.D. Hunter, R.A. Gibbons, R.H. Kimberlin, G.C. Millson, Further Studies of Infectivity and Stability of Extracts and Homogenates Derived from Scrapie Affected Mouse Brains, J Comp Pathol, 79 (1969) 101-108.

G.H.M. Huysmans, S.E. Radford, D.J. Brockwell, S.A. Baldwin, The N-terminal helix is a post-assembly clamp in the bacterial outer membrane protein PagP, J Mol Biol, 373 (2007) 529-540.

G.L.K. Hoh, D.O. Barlow, A.F. Chadwick, D.B. Lake, S.R. Sheeran, Hydrogen Peroxide Oxidation of Tertiary Amines, J Am Oil Chem Soc, 40 (1963) 268-271.

H. Lee, R.G. Larson, Coarse-grained molecular dynamics studies of the concentration and size dependence of fifth- and seventh-generation PAMAM dendrimers on pore formation in DMPC bilayer, J Phys Chem B, 112 (2008) 7778-7784.

H. Wille, M. Shanmugam, M. Murugesu, J. Ollesch, G. Stubbs, J.R. Long, J.G. Safar, S.B. Prusiner, Surface charge of polyoxometalates modulates polymerization of the scrapie prion protein, Proc Natl Acad Sci USA, 106 (2009) 3740-3745.

H. Wille, S.B. Prusiner, Ultrastructural studies on scrapie prion protein crystals obtained from reverse micellar solutions, Biophys J, 76 (1999) 1048-1062.

H. Wille, W. Bian, M. McDonald, A. Kendall, D.W. Colby, L. Bloch, J. Ollesch, A.L. Borovinskiy, F.E. Cohen, S.B. Prusiner, G. Stubbs, Natural and synthetic prion structure from X-ray fiber diffraction, Proc Natl Acad Sci USA, 106 (2009) 16990-16995.

H.H.L. Cui, B. Guo, B. Scicluna, B.M. Coleman, V.A. Lawson, L. Ellett, P.J. Meikle, M. Bukrinsky, N. Mukhamedova, D. Sviridov, A.F. Hill, Prion Infection Impairs Cholesterol Metabolism in Neuronal Cells, J Biol Chem, 289 (2014) 789-802.

H.J. Cho, Requirement of a protein component for scrapie infectivity, Intervirology, 14 (1980) 213-216.

Hashimoto, E. Rockenstein, L. Crews, E. Masliah, Role of protein aggregation in mitochondrial dysfunction and neurodegeneration in Alzheimer's and Parkinson's diseases, Neuromol Med, 4 (2003) 21-35.

I.G. Denisov, Y.V. Grinkova, T.H. Bayburt, S.G. Sligar,Nanodiscs in Membrane Biochemistry and Biophysics. Chem Rev. 117(2017) 4669-4713.

I.G. Denisov, Y.V. Grinkova, A.A. Lazarides, S.G. Sligar, Directed self-assembly of monodisperse phospholipid bilayer nanodiscs with controlled size, J Am Chem Soc, 126 (2004) 3477-3487.

I.H. Pattison, Resistance of the Scrapie Agent to Formalin, J Comp Pathol, 75 (1965) 159-164.

J. Breyer, W.M. Wemheuer, A. Wrede, C. Graham, S.L. Benestad, B. Brenig, J.A. Richt, W.J. Schulz-Schaeffer, Detergents modify proteinase K resistance of PrP Sc in different transmissible spongiform encephalopathies (TSEs), Vet Microbiol, 157 (2012) 23-31.

J. Broecker, B.T. Eger, O.P. Ernst, Crystallogenesis of Membrane Proteins Mediated by Polymer-Bounded Lipid Nanodiscs, Structure, 25 (2017) 384-392.

J. Chen, D. Thirumalai, Helices 2 and 3 are the initiation sites in the PrP(C) --> PrP(SC) transition, Biochemistry, 52 (2013) 310-319.

J. Coates, Interpretation of infrared spectra, a practical approach, Encyclopedia of analytical chemistry: applications, theory and instrumentation, (2006) 1-23.

J. Collinge, Ex vivo mammalian prions are formed of paired double helical prion protein fibrils, Open Biol 160035, 6 (2016) 1-12.

J. Fantini, N. Garmy, R. Mahfoud, N. Yahi, Lipid rafts: structure, function and role in HIV, Alzheimer's and prion diseases, Expert Rev Mol Med, 4 (2002) 1-22.

J. Heske, U. Heller, K.F. Winklhofer, J. Tatzelt, The C-terminal globular domain of the prion protein is necessary and sufficient for import into the endoplasmic reticulum, J Biol Chem, 279 (2004) 5435-5443.

J. Huang, S.R. Turner, Recent advances in alternating copolymers: The synthesis, modification, and applications of precision polymers, Polymer, 116 (2017) 572-586.

J. Huang, X. Geng, C. Peng, T.Z. Grove, S.R. Turner, Enhanced Fluorescence Properties of Stilbene-Containing Alternating Copolymers, Macromol Rapid Commun, 39 (2018)1-6.

J. Kanaani, S.B. Prusiner, J. Diacovo, S. Baekkeskov, G. Legname, Recombinant prion protein induces rapid polarization and development of synapses in embryonic rat hippocampal neurons in vitro, J Neurochem, 95 (2005) 1373-1386.

J. Shorter, S. Lindquist, Prions as adaptive conduits of memory and inheritance, Nat Rev Genet, 6 (2005) 435-450.

J. Yang, C.-C. Dong, X.-L. Chen, X. Sun, J.-Y. Wei, J.-F. Xiang, J.L. Sessler, H.-Y. Gong, Excimer Disaggregation Enhanced Emission: A Fluorescence "Turn-On" Approach to Oxoanion Recognition, J Am Chem Soc, 141(2019) 4597-4612.

J.D. Perlmutter, W.J. Drasler, 2nd, W. Xie, J. Gao, J.L. Popot, J.N. Sachs, All-atom and coarse-grained molecular dynamics simulations of a membrane protein stabilizing polymer, Langmuir, 27 (2011) 10523-10537.

J.D. Sipe, M.D. Benson, J.N. Buxbaum, S. Ikeda, G. Merlini, M.J.M. Saraiva, P. Westermark, Nomenclature 2014: Amyloid fibril proteins and clinical classification of the amyloidosis, Amyloid, 21 (2014) 221-224.

J.H. Come, P.E. Fraser, P.T. Lansbury, A Kinetic-Model for Amyloid Formation in the Prion Diseases - Importance of Seeding, Proc Natl Acad Sci USA, 90 (1993) 5959-5963.

J.J. Helmus, K. Surewicz, P.S. Nadaud, W.K. Surewicz, C.P. Jaroniec, Molecular conformation and dynamics of the Y145 Stop variant of human prion protein in amyloid fibrils, Proc Natl Acad Sci USA, 105 (2008) 6284-6289.

J.J. Wiltzius, M. Landau, R. Nelson, M.R. Sawaya, M.I. Apostol, L. Goldschmidt, A.B. Soriaga, D. Cascio, K. Rajashankar, D. Eisenberg, Molecular mechanisms for protein-encoded inheritance, Nat Struct Mol Biol, 16 (2009) 973-978.

J.L. De la Fuente, E.L. Madruga, Homopolymerization of methyl methacrylate and styrene: Determination of the chain-transfer constant from the mayo equation and the number distribution for n-dodecanethiol, J Polym Sci Pol Chem, 38 (2000) 170-178.

J.L. Popot, T. Althoff, D. Bagnard, J.L. Baneres, P. Bazzacco, E. Billon-Denis, L.J. Catoire, P. Champeil, D. Charvolin, M.J. Cocco, G. Cremel, T. Dahmane, L.M. de la Maza, C. Ebel, F. Gabel, F. Giusti, Y. Gohon, E. Goormaghtigh, E. Guittet, J.H. Kleinschmidt, W. Kuhlbrandt, C. Le Bon, K.L. Martinez, M. Picard, B. Pucci, J.N. Sachs, C. Tribet, C. van Heijenoort, F. Wien, F. Zito, M. Zoonens, Amphipols from A to Z, Annu Rev Biophys, 40 (2011) 379-408.

J.L. Silva, Y. Cordeiro, The "Jekyll and Hyde" Actions of Nucleic Acids on the Prion-like Aggregation of Proteins, J Biol Chem, 291 (2016) 15482-15490.

J.M. Dorr, M.C. Koorengevel, M. Schafer, A.V. Prokofyev, S. Scheidelaar, E.A. van der Cruijsen, T.R. Dafforn, M. Baldus, J.A. Killian, Detergent-free isolation, characterization, and functional reconstitution of a tetrameric K^+ channel: the power of native nanodiscs, Proc Natl Acad Sci USA, 111 (2014) 18607-18612.

J.M. Dorr, S. Scheidelaar, M.C. Koorengevel, J.J. Dominguez, M. Schafer, C.A. van Walree, J.A. Killian, The styrene-maleic acid copolymer: a versatile tool in membrane research, Eur Biophys J, 45 (2016) 3-21.

J.M. McCarthy, B. Rasines Moreno, D. Filippini, H. Komber, M. Maly, M. Cernescu, B. Brutschy, D. Appelhans, M.S. Rogers, Influence of surface groups on poly(propylene imine) dendrimers anti-prion activity, Biomacromolecules, 14 (2013) 27-37.

J.R. Requena, H. Wille, The Structure of the Infectious Prion Protein and Its Propagation, Prog Mol Biol Transl, 150 (2017) 341-359.

J.S. McDowall, I. Ntai, J. Hake, P.R. Whitley, J.M. Mason, C.R. Pudney, D.R. Brown, Steady-State Kinetics of a-synuclein Ferrireductase Activity Identifies the Catalytically Competent Species, Biochemistry, 56 (2017) 2497-2505.

J.S. Richardson, D.C. Richardson, Natural beta-sheet proteins use negative design to avoid edge-to-edge aggregation, Proc Natl Acad Sci USA, 99 (2002) 2754-2759.

K. Giles, A.L. Woerman, D.B. Berry, S.B. Prusiner, Bioassays and Inactivation of Prions, Cold Spring Harbor perspectives in biology, 9 (2017) DOI:10.1101/cshperspect.a023499.

K. Greish, A. Nagamitsu, J. Fang, H. Maeda, Copoly(styrene-maleic acid) - Pirarubicin micelles: High tumor-targeting efficiency with little toxicity, Bioconjugate Chem, 16 (2005) 230-236.

K. Greish, T. Sawa, J. Fang, T. Akaike, H. Maeda, SMA-doxorubicin, a new polymeric micellar drug for effective targeting to solid tumors, J Control Release, 97 (2004) 219-230.

K. Kanonenberg, J. Royes, A. Kedrov, G. Poschmann, F. Angius, A. Solgadi, O. Spitz, D. Kleinschrodt, K. Stuhler, B. Miroux, L. Schmitt, Shaping the lipid composition of bacterial membranes for membrane protein production, Microb Cell Fact, 18 (2019) 131.

K. Sasaki, H. Minaki, T. Iwaki, Development of oligomeric prion-protein aggregates in a mouse model of prion disease, J Pathol, 219 (2009) 123-130.

K. Simons, D. Toomre, Lipid rafts and signal transduction, Nature reviews. Mol Cell Biol, 1 (2000) 31-39.

K. Teruya, A. Oguma, K. Nishizawa, M. Kawata, Y. Sakasegawa, H. Kamitakahara, K. Doh-Ura, A Single Subcutaneous Injection of Cellulose Ethers Administered Long before Infection Confers Sustained Protection against Prion Diseases in Rodents, PLoS Pathog, 12 (2016) e1006045.

K. Tsukigawa, L. Liao, H. Nakamura, J. Fang, K. Greish, M. Otagiri, H. Maeda, Synthesis and therapeutic effect of styrene-maleic acid copolymer-conjugated pirarubicin, Cancer Sci, 106 (2015) 270-278.

K. Yasuhara, J. Arakida, T. Ravula, S.K. Ramadugu, B. Sahoo, J.I. Kikuchi, A. Ramamoorthy, Spontaneous Lipid Nanodisc Formation by Amphiphilic Polymethacrylate Copolymers, J Am Chem Soc, 139 (2017) 18657-18663.

K.A. Morrison, A. Akram, A. Mathews, Z.A. Khan, J.H. Patel, C. Zhou, D.J. Hardy, C. Moore-Kelly, R. Patel, V. Odiba, T.J. Knowles, M.U. Javed, N.P. Chmel, T.R. Dafforn, A.J. Rothnie, Membrane protein extraction and purification using styrene-maleic acid (SMA) copolymer: effect of variations in polymer structure, Biochem J, 473 (2016) 4349-4360.

K.J. Knaus, M. Morillas, W. Swietnicki, M. Malone, W.K. Surewicz, V.C. Yee, Crystal structure of the human prion protein reveals a mechanism for oligomerization, Nat Struct Biol, 8 (2001) 770-774.

K.J. Korshavn, C. Satriano, Y. Lin, R. Zhang, M. Dulchavsky, A. Bhunia, M.I. Ivanova, Y.-H. Lee, C. La Rosa, M.H. Lim, A. Ramamoorthy, Reduced Lipid Bilayer

Thickness Regulates the Aggregation and Cytotoxicity of Amyloid-β, J Biol Chem, 292 (2017) 4638-4650.

K.J. Laurie, A. Dave, T. Straga, E. Souzeau, T. Chataway, M.J. Sykes, T. Casey, T. Teo, J. Pater, J.E. Craig, S. Sharma, K.P. Burdon, Identification of a novel oligomerization disrupting mutation in CRYAlphaA associated with congenital cataract in a South Australian family, Hum Mutat, 34 (2013) 435-438.

K.L. Moya, R. Hassig, C. Creminon, I. Laffont, L. Di Giamberardino, Enhanced detection and retrograde axonal transport of PrPc in peripheral nerve, J Neurochem, 88 (2004) 155-160.

K.M. Pos, A. Schiefner, M.A. Seeger, K. Diederichs, Crystallographic analysis of AcrB, FEBS Lett, 564 (2004) 333-339.

K.S. Lee, R. Linden, M.A.M. Prado, R.R. Brentani, V.R. Martins, Towards cellular receptors for prions, Rev Med Virol, 13 (2003) 399-408.

L. Conley, Y. Tao, A. Henry, E. Koepf, D. Cecchini, J. Pieracci, S. Ghose, Evaluation of eco-friendly zwitterionic detergents for enveloped virus inactivation, Biotechnol Bioeng, 114 (2017) 813-820.

L. D'Castro, A. Wenborn, N. Gros, S. Joiner, S. Cronier, J. Collinge, J.D.F. Wadsworth, Isolation of proteinase K-sensitive prions using pronase E and phosphotungstic acid, PLoS One, 5 (2010) 1-7.

L. Frey, N.A. Lakomek, R. Riek, S. Bibow, Micelles, Bicelles, and Nanodiscs: Comparing the Impact of Membrane Mimetics on Membrane Protein Backbone Dynamics, Angew. Chem. Int. Edit, 56 (2017) 380-383.

L. Hou, H. Zhang, H. Chen, Q. Xia, D. Huang, L. Meng, X. Liu, Synthesis and surface properties of N, N-dimethyl-N-dodecyl polyoxyethylene amine-based surfactants: Amine oxide, betaine and sulfobetaine, J Surfactants Deterg, 17 (2014) 403-408.

L. Solforosi, A. Bellon, M. Schaller, J.T. Cruite, G.C. Abalos, R.A. Williamson, Toward molecular dissection of PrPC-PrPSc interactions, J Biol Chem, 282 (2007) 7465-7471.

L. Solforosi, J.R. Criado, D.B. McGavern, S. Wirz, M. Sanchez-Alavez, S. Sugama, L.A. DeGiorgio, B.T. Volpe, E. Wiseman, G. Abalos, E. Masliah, D. Gilden, M.B. Oldstone, B. Conti, R.A. Williamson, Cross-linking cellular prion protein triggers neuronal apoptosis in vivo, Science, 303 (2004) 1514-1516.

L. Thorne, L.A. Terry, In vitro amplification of PrPSc derived from the brain and blood of sheep infected with scrapie, J Gen Virol, 89 (2008) 3177-3184.

L. Westergard, H.M. Christensen, D.A. Harris, The cellular prion protein (PrPC): Its physiological function and role in disease, Biochim Biophys Acta-Mol Basis Dis, 1772 (2007) 629-644.

L.M. Kyle, T.R. John, R.V. Lewis, H.M. Schatzl, Introducing a rigid loop structure from deer into mouse prion protein increases its propensity for misfolding in vitro, Prion, 7 (2013) 88-89.

L.M. Miller, M.W. Bourassa, R.J. Smith, FTIR spectroscopic imaging of protein aggregation in living cells, Biochim Biophys Acta-Biomembr, 1828 (2013) 2339-2346.

M. Alami, K. Dalal, B. Lelj-Garolla, S.G. Sligar, F. Duong, Nanodiscs unravel the interaction between the SecYEG channel and its cytosolic partner SecA, EMBO J, 26 (2007) 1995-2004.

M. Anderson, O.V. Bocharova, N. Makarava, L. Breydo, V.V. Salnikov, I.V. Baskakov, Polymorphism and ultrastructural organization of prion protein amyloid fibrils: an insight from high-resolution atomic force microscopy, J Mol Biol, 358 (2006) 580-596.

M. Caffrey, A comprehensive review of the lipid cubic phase or in meso method for crystallizing membrane and soluble proteins and complexes, Acta Crystallogr F, 71 (2015) 3-18.

M. Camargo, P. Intasqui Lopes, P.T. Del Giudice, V.M. Carvalho, K.H.M. Cardozo, C. Andreoni, R. Fraietta, R.P. Bertolla, Unbiased label-free quantitative proteomic profiling and enriched proteomic pathways in seminal plasma of adult men before and after varicocelectomy, Hum Reprod, 28 (2013) 33-46.

M. Fiorini, M. Bongianni, S. Monaco, G. Zanusso, Biochemical Characterization of Prions, Prog Mol Biol Transl, 150 (2017) 389-407.

M. Fischer, D. Appelhans, S. Schwarz, B. Klajnert, M. Bryszewska, B. Voit, M. Rogers, Influence of surface functionality of poly(propylene imine) dendrimers on protease resistance and propagation of the scrapie prion protein, Biomacromolecules, 11 (2010) 1314-1325.

M. Graeve, D. Janssen, Improved separation and quantification of neutral and polar lipid classes by HPLC-ELSD using a monolithic silica phase: application to exceptional marine lipids, J Chromatogr B Analyt Technol Biomed Life Sci, 877 (2009) 1815-1819.

M.L. Nasr, G. Wagner, Covalently circularized nanodiscs; challenges and applications, Curr Opin Struct Biol, 51 (2018) 129-134.

M. Mao, C. Kim, S. Wi, S.R. Turner, Chain structure of substituted stilbene - Maleic anhydride alternating copolymer probed by solid-state NMR, Macromolecules, 41 (2008) 387-389.

M. Overduin, B. Klumperman, Advancing membrane biology with poly(styrene-co-maleic acid)-based native nanodiscs., Eur Polymer J., 110 (2018) 63-68.

M. Overduin, M. Esmaili, Memtein: The fundamental unit of membrane-protein structure and function, Chem Phys Lipids, 218 (2019) 73-84.

M. Overduin, M. Esmaili, Native Nanodiscs and the Convergence of Lipidomics, Metabolomics, Interactomics and Proteomics, Appl Sci, 9 (2019) 1230-1245.

M. Overduin, M. Esmaili, Structures and Interactions of Transmembrane Targets in Native Nanodiscs, SLAS Discov, (2019) 1-10.

M.A. Barria, A. Mukherjee, D. Gonzalez-Romero, R. Morales, C. Soto, De Novo Generation of Infectious Prions In Vitro Produces a New Disease Phenotype, PLoS Pathog, 5 (2009).

M.A. McLean, M.C. Gregory, S.G. Sligar, Nanodiscs: A Controlled Bilayer Surface for the Study of Membrane Proteins, Annu Rev Biophys, 47(2018) 107-124.

M.A. Schuler, I.G. Denisov, S.G. Sligar, Nanodiscs as a new tool to examine lipid-protein interactions, Methods Mol Biol, 974 (2013) 415-433.

M.A. Seeger, A. Schiefner, T. Eicher, F. Verrey, K. Diederichs, K.M. Pos, Structural asymmetry of AcrB trimer suggests a peristaltic pump mechanism, Science, 313 (2006) 1295-1298.

M.B. Miller, D.W. Wang, F. Wang, G.P. Noble, J.Y. Ma, V.L. Woods, S. Li, S. Supattapone, Cofactor Molecules Induce Structural Transformation during Infectious Prion Formation, Structure, 21 (2013) 2061-2068.

M.C. Fiori, Y. Jiang, G.A. Altenberg, H. Liang, Polymer-encased nanodiscs with improved buffer compatibility, Sci Rep, 7 (2017) 1-10.

M.C. Orwick, P.J. Judge, J. Procek, L. Lindholm, A. Graziadei, A. Engel, G. Grobner, A. Watts, Detergent-free formation and physicochemical characterization of nanosized lipid-polymer complexes: Lipodisq, Angew Chem Int Ed, 51 (2012) 4653-4657.

M.D. Zabel, C. Reid, A brief history of prions, Pathog Dis, 73 (2015).

M.F.M. Sciacca, C. Tempra, F. Scollo, L.R.C. Milardi D, Amyloid growth and membrane damage: Current themes and emerging perspectives from theory and experiments on Aβ and hIAPP, Biochim Biophys Acta-Biomembr, 1860 (2018) 1625-1638.

M.K. Trivedi, A.B. Dahryn Trivedi, G.N. Gunin Saikia, Physical and Structural Characterization of Biofield Treated Imidazole Derivatives, Nat Prod Res 03 (2015).

M.M. Xue, L.S. Cheng, I. Faustino, W.L. Guo, S.J. Marrink, Molecular Mechanism of Lipid Nanodisk Formation by Styrene-Maleic Acid Copolymers, Biophys J, 115 (2018) 494-502.

M.P. McKinley, A. Taraboulos, L. Kenaga, D. Serban, A. Stieber, S.J. DeArmond, S.B. Prusiner, N. Gonatas, Ultrastructural localization of scrapie prion proteins in cytoplasmic vesicles of infected cultured cells, Lab Invest, 65 (1991) 622-630.

M.P. McKinley, R.K. Meyer, L. Kenaga, F. Rahbar, R. Cotter, A. Serban, S.B. Prusiner, Scrapie prion rod formation in vitro requires both detergent extraction and limited proteolysis, J Virol, 65 (1991) 1340-1351.

M.S. Hipp, C.N. Patel, K. Bersuker, B.E. Riley, S.E. Kaiser, T.A. Shaler, M. Brandeis, R.R. Kopito, Indirect inhibition of 26S proteasome activity in a cellular model of Huntington's disease, J Cell Biol, 196 (2012) 573-587.

N. Kielland, M. Vendrell, R. Lavilla, Y.T. Chang, Imaging histamine in live basophils and macrophages with a fluorescent mesoionic acid fluoride, Chem Commun, 48 (2012) 7401-7403.

N.J. Cho, L.Y. Hwang, J.J.R. Solandt, C.W. Frank, Comparison of Extruded and Sonicated Vesicles for Planar Bilayer Self-Assembly, Materials, 6 (2013) 3294-3308.

N.R. Deleault, J.R. Piro, D.J. Walsh, F. Wang, J.Y. Ma, J.C. Geoghegan, S. Supattapone, Isolation of phosphatidylethanolamine as a solitary cofactor for prion

formation in the absence of nucleic acids, Proc Natl Acad Sci USA, 109 (2012) 8546-8551.

N.R. Deleault, R.W. Lucassen, S. Supattapone, RNA molecules stimulate prion protein conversion, Nature, 425 (2003) 717-720.

N.Z. Hardin, T. Ravula, G.D. Mauro, A. Ramamoorthy, Hydrophobic Functionalization of Polyacrylic Acid as a Versatile Platform for the Development of Polymer Lipid Nanodisks, Small, 15 (2019) 1-5.

O. Ben-Zaken, S. Tzaban, Y. Tal, L. Horonchik, J.D. Esko, I. Vlodavsky, A. Taraboulos, Cellular heparan sulfate participates in the metabolism of prions, J Biol Chem, 278 (2003) 40041-40049.

O. Chakrabarti, A. Ashok, R.S. Hegde, Prion protein biosynthesis and its emerging role in neurodegeneration, Trends Biochem Sci, 34 (2009) 287-295.

O. Gursky, Role of lipids in protein misfolding, Adv Exp Med Biol, 855 (2015) 5-7.

O. Korotych, J. Mondal, K.M. Gattas-Asfura, J. Hendricks, B.D. Bruce, Evaluation of commercially available styrene-co-maleic acid polymers for the extraction of membrane proteins from spinach chloroplast thylakoids, Eur Polym J, 114 (2019) 485-500.

P. Angelisová, O. Ballek, J. Sýkora, O. Benada, T. Čajka, J. Pokorná, D. Pinkas, V. Hořejší, The use of styrene-maleic acid copolymer (SMA) for studies on T cell membrane rafts, Biochim Biophys Acta-Biomembr, 1861 (2019) 130-141.

P.C. Klohn, L. Stoltze, E. Flechsig, M. Enari, C. Weissmann, A quantitative, highly sensitive cell-based infectivity assay for mouse scrapie prions, Proc Natl Acad Sci USA, 100 (2003) 11666-11671.

P.C. Pauly, D.A. Harris, Copper stimulates endocytosis of the prion protein, J Biol Chem, 273 (1998) 33107-33110.

P.J. Loll, Membrane proteins, detergents and crystals: what is the state of the art?, Acta Crystallogr F Struct Biol Commun, 70 (2014) 1576-1583.

P.K. Nandi, E. Leclerc, J.C. Nicole, M. Takahashi, DNA-induced partial unfolding of prion protein leads to its polymerization to amyloid, J Mol Biol, 322 (2002) 153-161.

P.M. Hwang, W.Y. Choy, E.I. Lo, L. Chen, J.D. Forman-Kay, C.R. Raetz, G.G. Prive, R.E. Bishop, L.E. Kay, Solution structure and dynamics of the outer membrane enzyme PagP by NMR, Proc Natl Acad Sci USA, 99 (2002) 13560-13565.

P.S. Orekhov, M.E. Bozdaganyan, N. Voskoboynikova, A.Y. Mulkidjanian, H.J. Steinhoff, K.V. Shaitan, Styrene/Maleic Acid Copolymers Form SMALPs by Pulling Lipid Patches out of the Lipid Bilayer, Langmuir, 35 (2019) 3748-3758.

Q. Bui, J. Sherma, J.K. Hines, Using High-Performance Thin-Layer Chromatography-Densitometry to Study the Influence of the Prion and Its Determinant Prion Protein Rnq1 on Yeast Lipid Profiles, Separations, 5 (2018) 1-6.

R. Friedel, Polymer Pioneers - a Popular History of the Science and Technology of Large Molecules - Morris, Pjt, ISIS, 78 (1987) 275-276.

R. Goto, T. Miki, N. Nakamura, M. Fujimoto, N. Okada, Salmonella Typhimurium PagP- and UgtL-dependent resistance to antimicrobial peptides contribute to the gut colonization, PLoS One, 12 (2017) e0190095, 1-10.

R. Henderson, P.N. Unwin, Three-dimensional model of purple membrane obtained by electron microscopy, Nature, 257 (1975) 28-32.

R. Loertscher, P. Lavery, The role of glycosyl phosphatidylinositol (GPI)-anchored cell-surface proteins in T-cell activation, Transpl Immunol, 9 (2002) 93-96.

R. Riek, S. Hornemann, G. Wider, M. Billeter, R. Glockshuber, K. Wuthrich, NMR structure of the mouse prion protein domain PrP(121-231), Nature, 382 (1996) 180-182.

R.A. Bessen, D.A. Kocisko, G.J. Raymond, S. Nandan, P.T. Lansbury, B. Caughey, Non-genetic propagation of strain-specific properties of scrapie prion protein, Nature, 375 (1995) 698-700.

R.B. Wickner, [Ure3] as an Altered Ure2 Protein - Evidence for a Prion Analog in Saccharomyces-Cerevisiae, Science, 264 (1994) 566-569.

R.C. Moore, J. Hope, P.A. McBride, I. McConnell, J. Selfridge, D.W. Melton, J.C. Manson, Mice with gene targetted prion protein alterations show that Prnp, Sinc and Prni are congruent, Nat Genet, 18 (1998) 118-125.

R.D. Fons, B.A. Bogert, R.S. Hegde, Substrate-specific function of the translocon-associated protein complex during translocation across the ER membrane, J Cell Biol, 160 (2003) 529-539.

R.E. Bishop, H.S. Gibbons, T. Guina, M.S. Trent, S.I. Miller, C.R. Raetz, Transfer of palmitate from phospholipids to lipid A in outer membranes of Gram-negative bacteria, EMBO J, 19 (2000) 5071-5080.

R.E. Bishop, Structural biology of membrane-intrinsic beta-barrel enzymes: sentinels of the bacterial outer membrane, Biochim Biophys Acta, 1778 (2008) 1881-1896.

R.E. Bishop, The lipid A palmitoyltransferase PagP: molecular mechanisms and role in bacterial pathogenesis, Mol Microbiol, 57 (2005) 900-912.

R.H. Wilkins, I.A. Brody, Creutzfeldt-Jakob disease, Arch Neurol, 25 (1971) 572-573.

R.K. Hite, Z. Li, T. Walz, Principles of membrane protein interactions with annular lipids deduced from aquaporin-0 2D crystals, EMBO J, 29 (2010) 1652-1658.

R.S. Hegde, P. Tremblay, D. Groth, S.J. DeArmond, S.B. Prusiner, V.R. Lingappa, Transmissible and genetic prion diseases share a common pathway of neurodegeneration, Nature, 402 (1999) 822-826.

S. Ambadi Thody, M.K. Mathew, J.B. Udgaonkar, Mechanism of aggregation and membrane interactions of mammalian prion protein, Biochim Biophys Acta-Biomembr, 1860 (2018) 1927-1935.

S. Botsios, S. Tittman, L. Manuelidis, Rapid chemical decontamination of infectious CJD and scrapie particles parallel treatments known to disrupt microbes and biofilms, Virulence, 6 (2015) 787-801.

S. Cronier, N. Gros, M.H. Tattum, G.S. Jackson, A.R. Clarke, J. Collinge, J.D.F. Wadsworth, Detection and characterization of proteinase K-sensitive disease-related prion protein with thermolysin, Biochem J, 416 (2008) 297-305.

S. Hall, C. Tognoloni, J. Charlton, É. Bragginton, A. Rothnie, P. Sridhar, M. Wheatley, T. Knowles, T. Arnold, K. Edler, D. TR., An acid-compatible co-polymer for the solubilization of membranes and proteins into lipid bilayer-containing nanoparticles., Nanoscale, 10 (2018) 10609-10619.

S. Lindhoud, V. Carvalho, J.W. Pronk, M.E. Aubin-Tam, SMA-SH: Modified Styrene-Maleic Acid Copolymer for Functionalization of Lipid Nanodiscs, Biomacromolecules, 17 (2016) 1516-1522.

S. Murakami, R. Nakashima, E. Yamashita, A. Yamaguchi, Crystal structure of bacterial multidrug efflux transporter AcrB, Nature, 419 (2002) 587-593.

S. Murakami, R. Nakashima, E. Yamashita, T. Matsumoto, A. Yamaguchi, Crystal structures of a multidrug transporter reveal a functionally rotating mechanism, Nature, 443 (2006) 173-179.

S. Scheidelaar, M.C. Koorengevel, C.A. van Walree, J.J. Dominguez, J.M. Dorr, J.A. Killian, Effect of Polymer Composition and pH on Membrane Solubilization by Styrene-Maleic Acid Copolymers, Biophys J, 111 (2016) 1974-1986.

S. Scheidelaar, M.C. Koorengevel, J.D. Pardo, J.D. Meeldijk, E. Breukink, J.A. Killian, Molecular Model for the Solubilization of Membranes into Nanodisks by Styrene Maleic Acid Copolymers, Biophys J, 108 (2015) 279-290.

S. Supattapone, H.O. Nguyen, F.E. Cohen, S.B. Prusiner, M.R. Scott, Elimination of prions by branched polyamines and implications for therapeutics, Proc Natl Acad Sci USA, 96 (1999) 14529-14534.

S. Voigt, B. Jungnickel, E. Hartmann, T.A. Rapoport, Signal sequence-dependent function of the TRAM protein during early phases of protein transport across the endoplasmic reticulum membrane, J Cell Biol, 134 (1996) 25-35.

S. Zhang, M. Andreasen, J.T. Nielsen, L. Liu, E.H. Nielsen, J. Song, G. Ji, F. Sun, T. Skrydstrup, F. Besenbacher, N.C. Nielsen, D.E. Otzen, M. Dong, Coexistence of ribbon and helical fibrils originating from hIAPP(20-29) revealed by quantitative nanomechanical atomic force microscopy, Proc Natl Acad Sci USA, 110 (2013) 2798-2803.

S.A. Priola, K.L. McNally, The role of the prion protein membrane anchor in prion infection, Prion, 3 (2009) 134-138.

S.B. Prusiner, Novel proteinaceous infectious particles cause scrapie, Science, 216 (1982) 136-144.

S.C. Lee, T.J. Knowles, V.L.G. Postis, M. Jamshad, R.A. Parslow, Y.-p. Lin, A. Goldman, P. Sridhar, M. Overduin, S.P. Muench, T.R. Dafforn, A method for detergent-free isolation of membrane proteins in their local lipid environment, Nat Prots, 11 (2016) 1149-1162.

S.C.L. Hall, C. Tognoloni, G.J. Price, B. Klumperman, K.J. Edler, T.R. Dafforn, T. Arnold, Influence of Poly(styrene- co-maleic acid) Copolymer Structure on the Properties and Self-Assembly of SMALP Nanodiscs, Biomacromolecules, 19 (2018) 761-772.

S.C.L. Hall, C. Tognoloni, J. Charlton, É.C. Bragginton, A.J. Rothnie, P. Sridhar, M. Wheatley, T.J. Knowles, T. Arnold, K.J. Edler, T.R. Dafforn, An acid-compatible co-polymer for the solubilization of membranes and proteins into lipid bilayer-containing nanoparticles, Nanoscale, 10 (2018) 10609-10619.

S.F. Godsave, H. Wille, P. Kujala, D. Latawiec, S.J. DeArmond, A. Serban, S.B. Prusiner, P.J. Peters, Cryo-Immunogold Electron Microscopy for Prions: Toward Identification of a Conversion Site, J Neurosci, 28 (2008) 12489-12499.

S.R. Tonge, B.J. Tighe, Responsive hydrophobically associating polymers: a review of structure and properties, Adv Drug Deliver Rev, 53 (2001) 109-122.

T. Boldog, S. Grimme, M.S. Li, S.G. Sligar, G.L. Hazelbauer, Nanodiscs separate chemoreceptor oligomeric states and reveal their signaling properties, Proc Natl Acad Sci USA, 103 (2006) 11509-11514.

T. Eicher, H.J. Cha, M.A. Seeger, L. Brandstatter, J. El-Delik, J.A. Bohnert, W.V. Kern, F. Verrey, M.G. Grutter, K. Diederichs, K.M. Pos, Transport of drugs by the multidrug transporter AcrB involves an access and a deep binding pocket that are separated by a switch-loop, Proc Natl Acad Sci USA, 109 (2012) 5687-5692.

T. Gonen, Y. Cheng, P. Sliz, Y. Hiroaki, Y. Fujiyoshi, S.C. Harrison, T. Walz, Lipid-protein interactions in double-layered two-dimensional AQP0 crystals, Nature, 438 (2005) 633-638.

T. Laursen, J. Borch, C. Knudsen, K. Bavishi, F. Torta, H.J. Martens, D. Silvestro, N.S. Hatzakis, M.R. Wenk, T.R. Dafforn, C.E. Olsen, M.S. Motawia, B. Hamberger, B.L.

Møller, J.E. Bassard, Characterization of a dynamic metabolon producing the defense compound dhurrin in sorghum, Science, 354 (2016) 890-893.

T. Nonaka, M. Hasegawa, A Cellular Model To Monitor Proteasome Dysfunction by alpha-Synuclein, Biochemistry, 48 (2009) 8014-8022.

T. Ravula, N.Z. Hardin, S.K. Ramadugu, A. Ramamoorthy, PH Tunable and Divalent Metal Ion Tolerant Polymer Lipid Nanodiscs, Langmuir, 33 (2017) 10655-10662.

T. Ravula, N.Z. Hardin, S.K. Ramadugu, S.J. Cox, A. Ramamoorthy, Formation of pH-Resistant Monodispersed Polymer-Lipid Nanodiscs, Angew Chem Int Ed, 57 (2018) 1342-1345.

T. Ravula, S.K. Ramadugu, G. Di Mauro, A. Ramamoorthy, Bioinspired, Size-Tunable Self-Assembly of Polymer–Lipid Bilayer Nanodiscs, Angew Chem Int Ed, 56 (2017) 11466-11470.

T.D. Kurt, C. Bett, N. Fernandez-Borges, S. Joshi-Barr, S. Hornemann, T. Rulicke, J. Castilla, K. Wuthrich, A. Aguzzi, C.J. Sigurdson, Prion Transmission Prevented by Modifying the beta 2-alpha 2 Loop Structure of Host PrPC, J Neurosci, 34 (2014) 1022-1027.

T.D. Kurt, G.C. Telling, M.D. Zabel, E.A. Hoover, Trans-species amplification of PrP(CWD) and correlation with rigid loop 170N, Virology, 387 (2009) 235-243.

T.H. Bayburt, Y.V. Grinkova, S.G. Sligar, Assembly of single bacteriorhodopsin trimers in bilayer nanodiscs, Arch Biochem Biophys, 450 (2006) 215-222.

T.H. Haines, Anionic Lipid Headgroups as a Proton-Conducting Pathway Along the Surface of Membranes - a Hypothesis, Proc Natl Acad Sci, 80 (1983) 160-164.

T.J. Knowles, A. Scott-Tucker, M. Overduin, I.R. Henderson, Membrane protein architects: the role of the BAM complex in outer membrane protein assembly, Nature reviews. Microbiology, 7 (2009) 206-214.

T.J. Knowles, R. Finka, C. Smith, Y.P. Lin, T. Dafforn, M. Overduin, Membrane proteins solubilized intact in lipid-containing nanoparticles bounded by styrene-maleic acid copolymer, J Am Chem Soc, 131 (2009) 7484-7485.

Taraboulos, Cholesterol Depletion and Modification of Cooh-Terminal Targeting Sequence of the Prion Protein Inhibit Formation of the Scrapie Isoform, J Cell Biol, 130 (1995) 121-132.

U. Adhikari, A. Goliaei, L. Tsereteli, M.L. Berkowitz, Properties of Poloxamer Molecules and Poloxamer Micelles Dissolved in Water and Next to Lipid Bilayers: Results from Computer Simulations, J Phys Chem B, 120 (2016) 5823-5830.

V. Perrier, T. Imberdis, P.A. Lafon, M. Cefis, Y. Wang, E. Huetter, J.D. Arnaud, T. Alvarez-Martinez, N. Le Guern, G. Maquart, L. Lagrost, C. Desrumaux, Plasma cholesterol level determines in vivo prion propagation, J Lipid Res, 58 (2017) 1950-1961.

V.E. Ahn, E.I. Lo, C.K. Engel, L. Chen, P.M. Hwang, L.E. Kay, R.E. Bishop, G.G. Prive, A hydrocarbon ruler measures palmitate in the enzymatic acylation of endotoxin, EMBO J, 23 (2004) 2931-2941.

W. Dannhauser, W.H. Glaze, R.L. Dueltgen, K. Ninomiya, Evidence from Intrinsic Viscosity and Sedimentation for Hypercoiled Configurations of Styrene-Maleic Acid Copolymer, J Phys Chem, 64 (1960) 954-955.

W. Qiu, Z. Fu, G.G. Xu, R.A. Grassucci, Y. Zhang, J. Frank, W.A. Hendrickson, Y. Guo, Structure and activity of lipid bilayer within a membrane-protein transporter, Proc Natl Acad Sci USA,115 (2018)12985-12990.

W.B. Liechty, D.R. Kryscio, B.V. Slaughter, N.A. Peppas, Polymers for Drug Delivery Systems, Annu Rev Chem Biomol, 1 (2010) 149-173.

Y. Goto, Revisiting supersaturation as a factor determining amyloid fibrillation, Prion, 10 (2016) 32-39.

Y. Li, M.Q. Zhang, M. Mao, S.R. Turner, R.B. Moore, T.H. Mourey, L.A. Slater, J.R. Hauenstein, Chain Stiffness of Stilbene Containing Alternating Copolymers by SAXS and SEC, Macromolecules, 45 (2012) 1595-1601.

Y. Li, S.R. Turner, Free radical copolymerization of methyl-substituted stilbenes with maleic anhydride, Eur Polym J, 46 (2010) 821-828.

Y. Shaked, R. Engelstein, R. Gabizon, The binding of prion proteins to serum components is affected by detergent extraction conditions, J Neurochem, 82 (2002) 1-5.

Y.A. Hannun, L.M. Obeid, Principles of bioactive lipid signaling: lessons from sphingolipids, Nature reviews. Mol Cell Biol, 9 (2008) 139-150.

Y.b. Lim, C.E. Mays, Y. Kim, W.B. Titlow, C. Ryou, The inhibition of prions through blocking prion conversion by permanently charged branched polyamines of low cytotoxicity, Biomaterials, 31 (2010) 2025-2033.

Y. Sonntag, M. Musgaard, C. Olesen, B. Schiott, J.V. Moller, P. Nissen, L. Thogersen, Mutual adaptation of a membrane protein and its lipid bilayer during conformational changes, Nat Commun, 2 (2011) 304.

Y. Yusuf, J. Massiot, Y.T. Chang, P.H. Wu, V. Yeh, P.C. Kuo, J. Shiue, T.Y. Yu, Optimization of the Production of Covalently Circularized Nanodiscs and Their Characterization in Physiological Conditions, Langmuir, 34 (2018) 3525-3532.

Z.H. Zhang, Y. Zhang, F. Wang, X.H. Wang, Y.Y. Xu, H.Y. Yang, G.H. Yu, C.G. Yuan, J.Y. Ma, De novo generation of infectious prions with bacterially expressed recombinant prion protein, FASEB J, 27 (2013) 4768-4775.

Appendix 1.

Synthesis of methyl stilbene-maleic acid polymers

1. Materials for synthesis of methyl stilbene-maleic acid polymers.

(E)-Stilbene (EMS-I, Aldrich, 96%), maleic anhydride (MAH, Aldrich, P99.0%), 2-methylbenzyl chloride (Aldrich,99%), 4-methylbenzyl chloride (Aldrich, 98%),o-tolualdehyde (Aldrich, 97%), benzaldehyde (Aldrich,P99%), potassium tert-butoxide solution 1.0 M in tetrahydrofuran(KOtBu, Aldrich), triethylphosphite (Aldrich, 98%), 2,20-azobisisobutyronitrile (AIBN, Aldrich, 98%) were all purchased from Aldrich and used as received. Tetrahydrofuran (THF, Fisher, HPLC grade) and hexane (Fisher, HPLC grade)and methylene chloride (Fisher, HPLC grade) were used as received. Water was deionized before use. Copolymers 1 and 5 were prepared according to the literature [1,2].

2. Synthesis of (E)-methyl stilbenes

(*E*)-2,2′-dimethylstilbene. Diethyl (2-methylbenzyl)phosphonate (20.25 g, 83.59 mmol), 2-methylbenzaldehyde (10.18 g, 84.74 mmol) and dry THF (35 mL) were added to a 250-mL round bottom flask with a stir bar and an addition funnel sealed with a septum. The apparatus was flushed with N_2 and chilled in an ice bath for 30 min. Potassium *tert*-butoxide (~1.0 M in THF, 100 mL, ~100 mmol) was added dropwise over 1 hour. During the addition, the reaction mixture changed from a pale yellow liquid to a yellow slurry. The ice bath was removed. The reaction mixture was allowed to warm to room temperature while stirring. After 24 hours, the orange gelatinous liquid was poured into deionized water (800 mL). A brown liquid layer appeared above the liquid. The solution was stirred with a spatula for ~5 min and allowed to sit at room temperature for 1 hour. A precipitate formed,

which was collected by filtration, washed with MeOH and dried *in vacuo* overnight to yield a white solid (11.79 g, 68%).

^{1}H NMR (CDCl$_3$, 400 MHz) δ ppm: 7.61 (t, 2H), 7.22 (m, 8H), 2.45 (s, 3H), 2.44 (s, 3H).

^{13}C NMR (CDCl$_3$, 100 MHz) δ ppm: 136.8, 135.83, 130.39, 130.38, 128.7, 128.01, 128.00, 127.54, 127.52, 126.6, 126.20, 126.18, 125.56, 125.54, 19.97, 19.96. IR: 968, cm^{-1}. mp: 82.0–82.4 °C; Lit. mp: 82–84 °C [1].

Synthesis of (E)-4-methylstilbene. Diethyl benzyl phosphonate (17.62 g, 77.21 mmol) and 4-methylbenzaldehyde (9.28 g, 77.2 mmol) and dry THF (31 mL) were added to a 250-mL round bottom flask with a stir bar and an addition funnel sealed with a septum. The apparatus was flushed with N$_2$ and chilled in an ice bath for 40 min. Potassium *tert*-butoxide (~1.0 M in THF, 93 mL, ~93 mmol) was added to the pale yellow solution dropwise over 1.5 h. During the addition, the reaction mixture changed from a light yellow liquid to an orange slurry. The ice bath was removed. The slurry was allowed to warm to room temperature while stirring. After 25 hours, the orange slurry was poured into MeOH (200 mL). Deionized water (400 mL) was added to the solution, resulting in a white precipitate (~5 g), which was filtered. Adding CH$_2$Cl$_2$ (~200 mL) to the filtrate gave two layers. After separation, hexanes (~100 mL) was added to the yellow organic layer; no change occurred other than dilution. Then aq saturated NH$_4$Cl (400 mL) was added to this organic layer resulting in a suspension of white solid, which was filtered and washed with MeOH. The solids were combined, dissolved in CH$_2$Cl$_2$ (~15 mL), and placed in a dry ice–acetone bath. A solid precipitated from the solution, collected by filtration, washed with MeOH, and dried *in vacuo* overnight to yield a white solid (11.02 g, 73%).

^{1}H NMR (CDCl$_3$, 400 MHz) δ ppm: 7.49 (dd, 2H), 7.41 (d, 2H), 7.34 (t, 2H), 7.23 (tt, ^{1}H), 7.16 (d, 2H), 7.09 (d, ^{1}H, J$_{app}$ = 16 Hz), 7.05 (d, ^{1}H, J$_{app}$ = 16 Hz), 2.35 (s, 3H). ^{13}C NMR (CDCl$_3$, 100 MHz) δ ppm: 137.49, 137.47, 137.5, 129.4, 128.62, 128.58, 127.7, 127.4, 126.39, 126.35, 21.2. mp: 118.5–119.0 °C; Lit. mp: 118–120 °C [1].

Synthesis of (*E*)-2-methylstilbene. Diethyl benzylphosphonate (13.74 g, 60.21 mmol), 2-methylbenzaldehyde (7.23 g, 60.21 mmol), and dry THF (17 mL) were added to a 250-mL round bottom flask equipped with a stir bar and an addition funnel sealed with a septum. The apparatus was flushed with N$_2$ and chilled in an ice bath for 40 min. Potassium *tert*-butoxide (~1.0 M in THF, 72 mL, ~72 mmol) was added to the pale yellow solution dropwise over 1 hour. During the addition, the reaction mixture changed from a pale yellow liquid to a yellow slurry. After the addition, the ice bath was removed. The reaction mixture was allowed to warm to room temperature while stirring. After 60 h, the reaction mixture was an orange gelatinous liquid. This liquid was poured into aq saturated NH$_4$Cl (600 mL); an oil formed above the aqueous layer. Adding CH$_2$Cl$_2$ (150 mL) gave two layers, which were separated. The aqueous layer was extracted with CH$_2$Cl$_2$ (1 $\times$ 150 mL, 1 $\times$ 100 mL). The organic layers were combined and washed with deionized water (300 mL), resulting in a cloudy emulsion. Aq saturated NH$_4$Cl (~50 mL) was added, resulting in clear organic and aqueous layers. The organic layer was separated and concentrated by rotary evaporation, resulting in orange oil. The oil was dissolved in hexanes (~5 mL). With a pipette, the resulting solution was carefully spread on top of a column (8 $\times$ 4 cm) of wet-packed (hexanes) silica gel. Hexanes (200 mL) were pushed through the column with modest air pressure. The concentration of the hexanes solution yielded a clear oil. MeOH (~10 mL) was added to the oil, resulting in the formation of a

white solid. The mixture was placed in a freezer overnight. The liquid above the solid The concentration, and the solid was dried under vacuum overnight. (8.02 g, 68 %).

^{1}H NMR (CDCl$_3$, 400 MHz) δ ppm: 7.59 (d, ^{1}H), 7.50 (d, 2H), 7.28 (m, 7H), 7.00 (d, ^{1}H), 2.43 (s, 3H). ^{13}C NMR (CDCl$_3$, 125 MHz) δ ppm: 137.7, 136.4, 135.8, 130.4, 130.0, 128.7, 127.57, 127.53, 126.54, 126.52, 126.2, 125.3, 19.92. IR: 97 cm^{-1}. The concentration: 32.4–33.2 °C. Lit. mp: 30 °C [3].

3. Polymer Synthesis:

Free-radical Copolymerization of (*E*)-4-Methylstilbene and Maleic Anhydride.

(*E*)-4-Methylstilbene (0.99 g, 5.1 mmol), recrystallized maleic anhydride (0.50 g, 5.1 mmol), and AIBN (0.015 g, 1 wt%) were added to a 50 mL round bottom flask equipped with a stir bar and sealed with a septum. THF (7 mL) was added to the flask via syringe. The yellow reaction mixture was sparged with argon for 10 min and was allowed to stir for 16 h at 60 °C. The reaction solution was then precipitated into hexanes by slow addition via pipette. The white precipitate was re-dissolved in THF and then precipitated into hexanes. The white solid was collected by filtration and placed under vacuum for 16 h at 60 °C. (1.45 g, 73.1%, M_n = 5.4 kDa, PDI = 1.54)

Free-radical Copolymerization of(*E*)-2,2'-Dimethylstilbene and Maleic Anhydride.

(*E*)-2,2-dimethylstilbene (1.03 g, 5.0 mmol), maleic anhydride (0.5 g, 5 mmol), and dicumyl peroxide (0.015 g, 1 wt%) were added to a 50 mL round bottom flask equipped with a stir bar and sealed with a septum. Anhydrous chlorobenzene (10 mL) was added to the flask via a syringe. The reaction mixture was sparged with argon for 10 min and

was allowed to stir for 24 h at 110 °C. The reaction solution was then precipitated into hexanes by slow addition via pipette. The precipitate was re-dissolved in THF and then precipitated into hexanes. The white solid was collected by filtration and placed under vacuum for 24 h at 60 °C. (0.74 g, 48.7%, M_n = 5.1 kDa, PDI = 1.52)

Free-radical Copolymerization of (_E_)-2-Methylstilbene and Maleic anhydride.

(_E_)-2-Methylstilbene (0.99 g, 5.0 mmol), maleic anhydride (0.5 g, 5 mmol), and dicumyl peroxide (0.015 g, 1 wt%) were added to a 50 mL round bottom flask equipped with a stir bar and sealed with a septum. Anhydrous chlorobenzene (10 mL) was added to the flask via a syringe. The reaction mixture was sparged with argon for 10 min and was allowed to stir for 24 h at 110 °C.

The reaction solution was then precipitated into hexanes by slow addition via pipette. The precipitate was re-dissolved in THF and then precipitated into hexanes. The white solid was collected by filtration and placed under vacuum for 24 h at 60 °C. (0.56 g, 37.6%, M_n = 4.4 kDa, PDI = 1.19).

References.

[1] J. R. Ebdon, B. J. Hunt, S. Hussein, _Br. Polym. J._ **1987,** 19 (3-4) 337-7.

[2] Y. Li, M. Mao, L. Matyolyak, S. R. Turner, _ACS MacroLett._ **2012,** 1, 257-A. Buquet, A. Couture, A. Lablachecombier, J Org Chem **1979**, _44_, 2300-2303

[3] G. Cahiez, O. Gager, F. Lecomte, _Org Lett_ **2008**, _10_, 5255-5256.

Appendix 2.

1. Expression constructs for wild type and mutant forms PagP

Wild type (His)$_6$-tagged PagP with N-terminal signal peptide in pET21a construct was a gift from Dr. Russell Bishop. Single mutants Ser77Ala and Tyr87Phe, and double mutant Ser77Ala-Tyr87Phe forms were prepared using the Q5® Site-Directed Mutagenesis Kit (NEB). The mutagenesis primers are listed in Table S2.1. The DNA sequence of each construct was confirmed before proceeding to expression.

Primers	Ser77Ala	Tyr87Phe
Forward primer	5'GCATTTAAGGACGCTTGGAACAAATGG3'	5'GCCATTGCCGGATTTGGATGGGAAAGT3'
Reverse primer	5'CCATTTGTTCCAAGCGTCCTTAAATGC3'	5'GATCTTTCCCATCCAAATCCGGCAATCGG3'

**Table S2.1.** List of primers used for creating single and double mutants of PagP.

Wild type and mutant PagP proteins were overexpressed in the outer membrane of *E. coli* BL21(DE3) *pLysE* and purified as described in Chapter 2. Briefly, after lysing the cells by French press at 10,000 psi, cell debris was removed at 8500 rpm centrifugation, and the supernatant was subjected to ultracentrifugation at 45000 rpm for one hour. The total membrane was resuspended in Tris 10 mM, pH 8.0 and subjected to 50% sucrose cushion (prepared in Tris 10 mM, pH 8.0) and centrifugation at 40000 rpm (SWi45) for 3 hours. The outer membrane pellet was incubated with 2% w/v SMA2000 solution in Tris 10 mM, 200 mM NaCl for 20 mins at room temperature. Membrane lysate was centrifuged at 40,000 rpm for 30 mins, and the supernatant was applied to HisPur Ni-NTA column pre-equilibrated with the same buffer as solubilization buffer with 10 mM imidazole. After

washing the column with wash buffers A and B (each containing Tris 10 mM, 250 mM NaCl and 20 and 40 mM imidazole, respectively). PagP nanodiscs were eluted in elution buffers (Tris 10 mM pH 8.0, 250 mM NaCl, 150 mM and 200 mM imidazole). The purity of each sample was assessed on 10% pre-cast SDS-PAGE (Bio-Rad) stained with Coomassie blue (**Fig S2.3**). Detergent-purified PagP from the outer membrane and the refolded PagP (from inclusion bodies) in detergents (DPC, LDAO) were used to set up the procedure and to ensure the accuracy of the data from the native SMALP samples.

The samples were dialyzed against ammonium acetate (200 mM) pH 6.8 and pH 8.0, and submitted for native-ESI MS analysis. The lipid profile of folded and unfolded released proteins were analyzed and compared. The commercially available *E. coli* total lipid (Avanti) was used as control. Alternatively, the total lipid of each SMALP nanodiscs was isolated in organic solvents and submitted to MS/MS analysis.
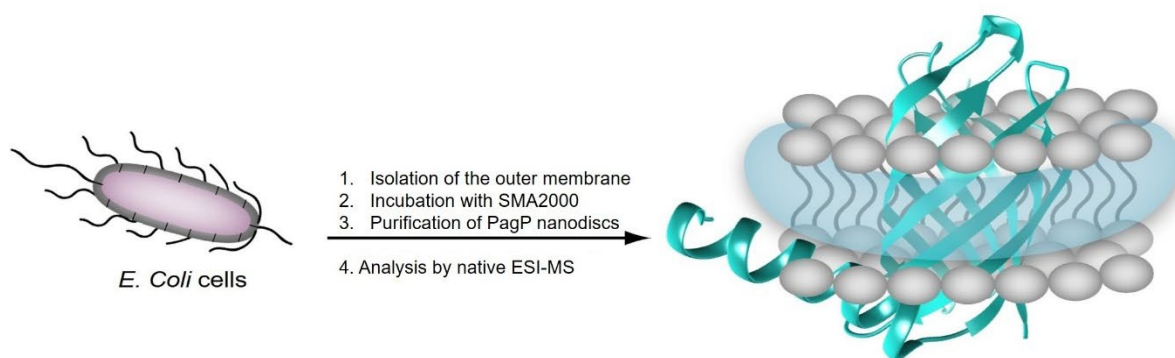
Figure S2.1. Schematic diagram of the preparation of SMALP nanodiscs of wild type and mutant PagP proteins directly from the outer membrane of *E. coli* and identification of bound lipids by native-ESI-MS.
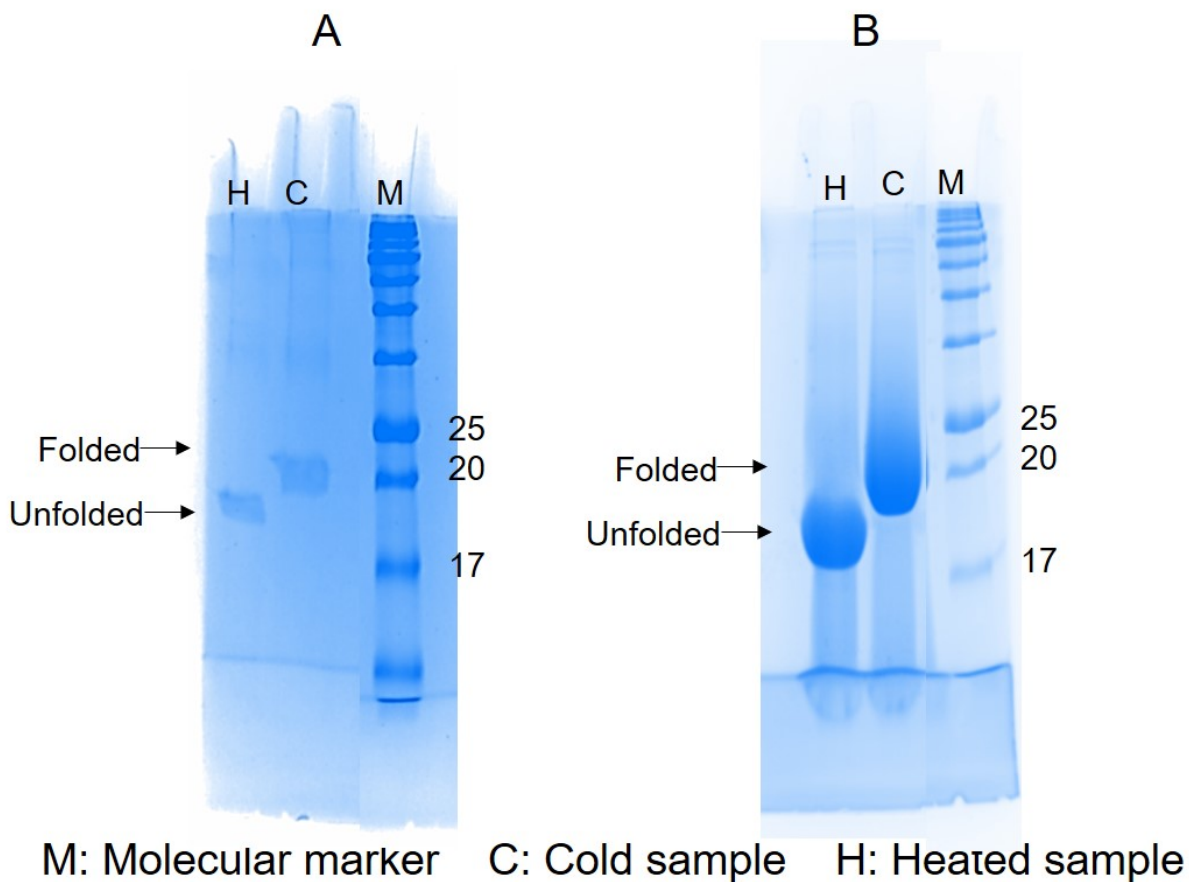
Figure S2.2. The cold SDS-PAGEs (15%) of LDAO-purified (A) and SMA2000- purified PagP (B) from the outer membrane of *E. coli* confirm that both samples are fully folded.


2. Native-ESI-MS

The ESI-MS measurements were carried out using a Synapt G2S quadrupole-ion mobility separation-time-of-flight (Q-IMS-TOF) mass spectrometer (Waters, Manchester, UK) equipped with a nanoESI source. The direct ESI-MS assay was implemented in positive ion mode. All the measurements involving the quantification of phospholipids was performed in the negative mode because of the ease of detecting the deprotonated phospholipid ions. A platinum wire was inserted into the nanoESI tip, produced from borosilicate capillary (1.0 mm o.d., 0.68 mm i.d.) using a P-1000 micropipette puller

(Sutter Instruments, Novato, CA), and a voltage of ~1.0 kV (positive ion mode) or ~ -1.0 kV (negative ion mode) was applied to carry out ESI. The source temperature was set to 60 °C using a cone voltage of 30 V. The trap and transfer voltages of 5 V and 2 V, respectively, were used for ESI-MS analysis. To release membrane protein, PagP from detergent micelles or SMALP particles, collision-induced dissociation (CID) was carried out in the trap region at voltages of 5 to 150 V. The released lipid ions were identified based on their measured MWs. Ion mobility separation (IMS) was used to separate the released membrane protein ions from detergent micelle or SMALP ions. For the IMS measurements, a wave height of 40 V and a wave velocity of 650 m s^{-1} were used and the helium and nitrogen gas flow rates were 190 mL min^{-1} and 80 mL min^{-1}, respectively. All data were processed using MassLynx software (version 4.1) and Driftscope $v.$2.5 (Waters, Manchester, UK).
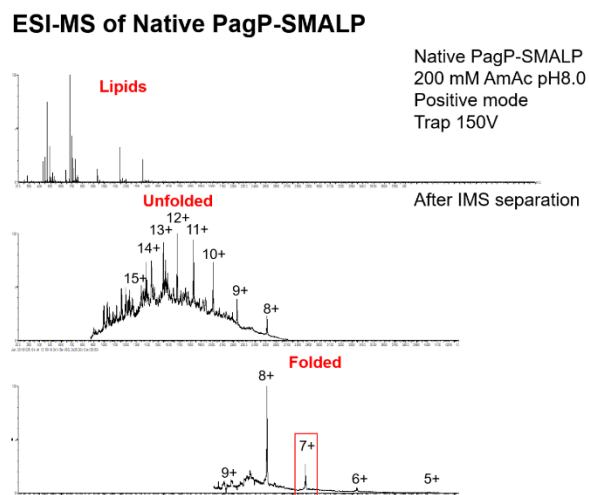
Figure S2.3. An example of separation of lipids, folded and unfolded PagP protein in the gas phase using nano IMS-ESI-MS.
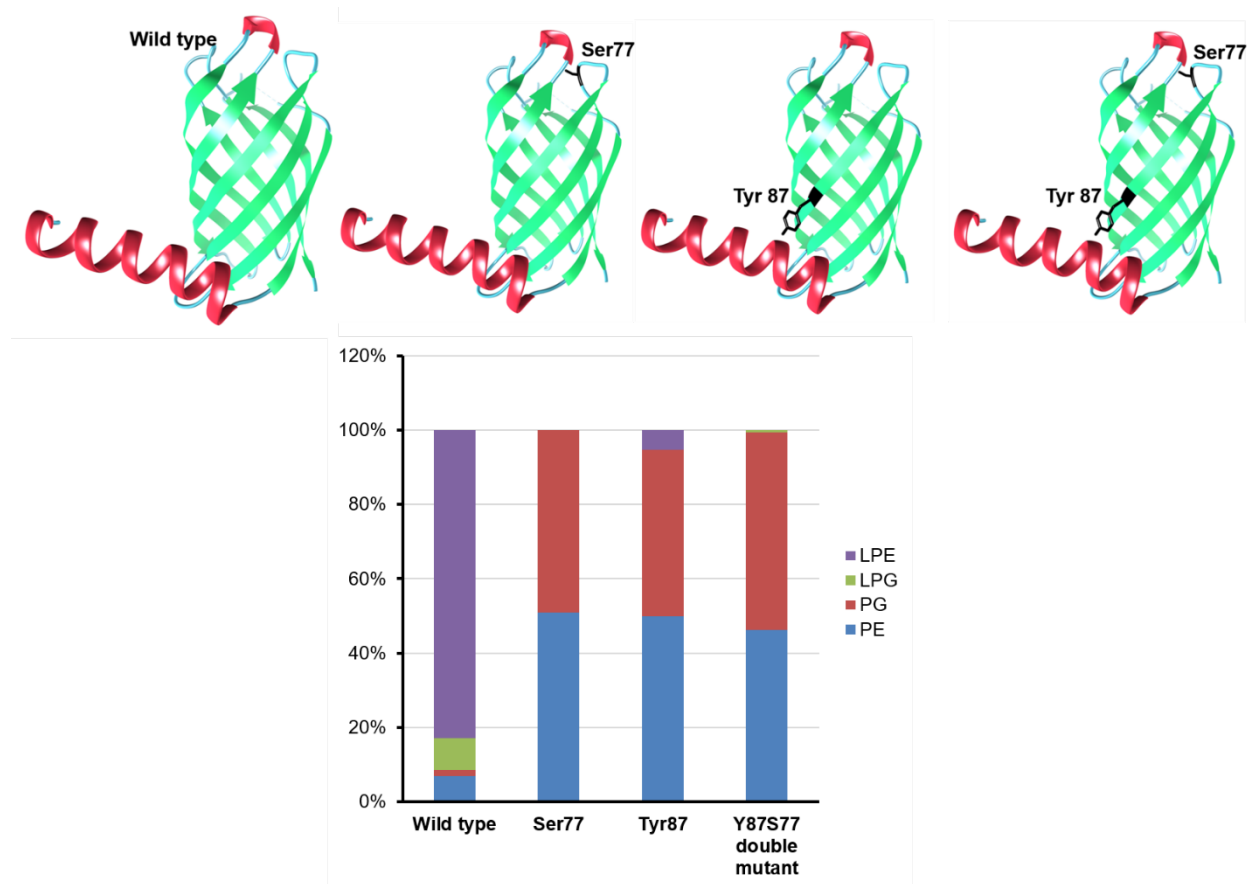
Figure S2.4. A summary of different lipid molecules copurified with native nanodiscs of wild-type and PagP mutants. The mutations on either Ser77 or Tyr87 deactivates the phospholipase activity of PagP in the membrane, verifying the existence of two active sites for the enzymatic function of PagP.

PagP Type Mw (Da)	Lipids pH 6.8	Lipids pH 8.0	Protein released pH 6.8	Protein released pH 8.0
Ser77Ala Mw: 20030 Da	LPE, LPG, PE, PG LPE and LPG: 1%	PE, PG	No protein released	Folded protein released
Wild type Mw: 20047 Da	LPE, LPG, PE, PG LPE and LPG: 90%	LPE, LPG, PE, PG LPE and LPG: 90%	Yes, unfolded	Yes, folded
Tyr87Phe Mw: 20030 Da	PE, PG	PE, PG	Yes, unfolded	No protein released
Double mutant Mw: 20013 Da	LPG, PE, PG LPG: 1.35%	LPE, PE, PG LPE: 0.1%	Yes, folded	Yes, folded

Table S2.2. A summary of lipid and protein species released in the gas phase. pH affects the folding stability of protein nanodiscs in vacuum.

Appendix 3.
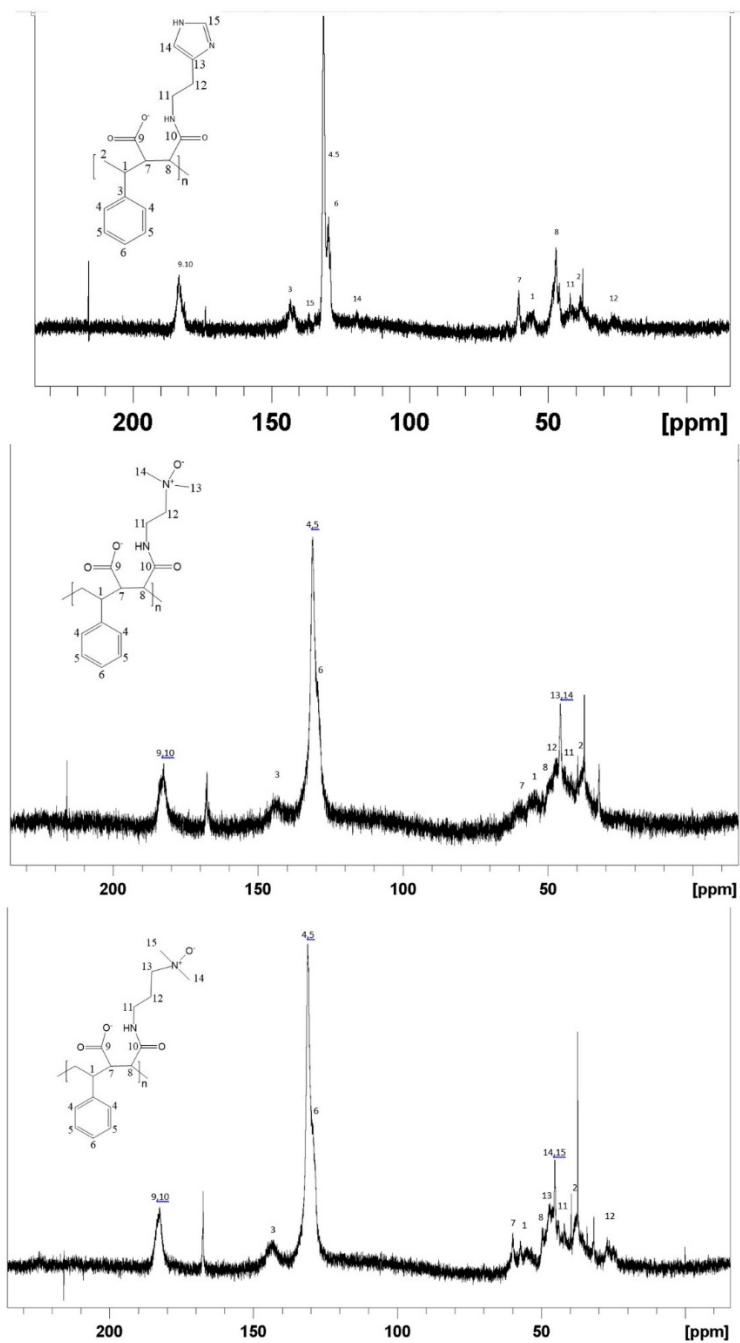
Figure S3.1. The ^{13}C NMR spectra of His-SMA, AO2-SMA (**4**) and AO3-SMA (**5**) in water. The spectra of polymers were recorded at 25 °C with a total of 36000 transients of 64k

data points and an acquisition time of 0.865 sec, 90° pulse width of 14.5 µs, 1-sec inter-pulse delay, a spectral width of 250 ppm, and WALTZ-16 ^{1}H decoupling. Line broadening of 2.0 Hz was applied before Fourier transformation. The residual methyl peak of DMF (37.54 ppm) was used for ^{13}C chemical shift calibration.